Super-fine Powdered Activated Carbon for the Removal of Microcystin-LR from Drinking Water

by

Mohammadsina Golchi

A thesis

presented to the University of Waterloo

in fulfillment of the

thesis requirement for the degree of

Master of Applied Science

in

Civil Engineering (Water)

Waterloo, Ontario, Canada, 2021

Author's Declaration

I hereby declare that I am the sole author of this thesis. This is a true copy of the thesis, including any required final revisions, as accepted by my examiners.

I understand that my thesis may be made electronically available to the public.

Abstract

Harmful algal blooms are potential threats to drinking water quality. During drinking water treatment, suspended and dissolved materials must be removed and treated, and in the case of cyanobacteria, these are intact cells and extracellular cyanotoxins. Cyanotoxins produced by different species of cyanobacteria are a major issue in drinking water treatment (Westrick et al., 2010). Microcystin-LR is among the most commonly detected and studied cyanotoxins. Microcystin-LR (MC-LR) is an hepatotoxin, which can cause irreversible damage to liver cells and cause chronic liver and kidney diseases and Health Canada's guidelines proposes a maximum acceptable concentration of 1.5 µg/L in drinking water. Powdered activated carbon can remove extracellular cyanotoxins from drinking water and is also often implemented for control of seasonal taste and odor issues. Newly developed super-fine powdered activated carbons (SPAC) have particles sizes around 1 µm, and they have been shown to have faster adsorption kinetics and similar or even higher capacities than conventional powdered activated carbon (PAC) for organics. Most of the SPAC studies to date focus on SPAC as a pre-treatment for microfiltration membranes. Only a few studies evaluated the use of SPAC in association with conventional treatment processes like coagulation, flocculation, sedimentation (CFS) and rapid media filtration. These more recent studies introduced the idea that it may be possible to implement SPAC in conventional drinking water treatment plants (DWTPs). The main focus of this study was to investigate the applicability of SPAC for the removal of microcystin-LR as an alternative to PAC in conventional DWTPs.

Three SPACs were prepared by pulverization of three commercially available PACs (wood-based BG-HHM (Calgon Carbon), coconut-based WPC (Calgon Carbon), and coal-based COL-PL60-800 (Activated Carbon Corp.)). These PACs were chosen since an earlier study has evaluated the adsorption of MC-LR onto these PACs (Liu, 2017). A method based on scanning electron microscope (SEM) imaging and static image analysis (SIA) was then developed and validated before it was used to determine the particle size distribution of the prepared SPACs. The median sizes of prepared SPACs ranged from 1.2 to 1.3 µm which classifies them as SPAC. The adsorption of MC-LR via the prepared SPACs was initially evaluated in buffered ultrapure water (pH 7.2) to establish baseline adsorption rates and capacities. The SPACs were dosed as dry powder in experiments in the ultrapure water. The WPC (coconut-based) SPAC had the highest adsorption rate for MC-LR, followed by the BG-HHM (wood-based) and COL-PL60-800 (coal-based) SPACs. The adsorption capacities of SPACs for MC-

LR were evaluated at both equilibrium and non-equilibrium (i.e. short contact times relevant to practice in DWTPs). At the short contact times in range of 5 to 120 min, the coconut-based SPAC had the highest capacity due it's faster adsorption rate, followed by the wood-based and coal-based SPACs. However, the dry powdered dosing method caused problems with dispersion of SPACs, so a prewetted slurry dosing method was used in experiments at equilibrium and all the later experiments in this study including those done in Lake Erie water. At equilibrium the SPACs were dosed as prewetted slurry and under those conditions, the BG-HHM (wood-based) SPAC had the highest capacity, while the WPC (coconut-based) SPAC had the least capacity in ultrapure water. The performance of SPACs at both equilibrium and short contact times for adsorption of MC-LR was compared with the performance of parent PACs reported by Liu (2017). All three prepared wood-based, coal-based, and coconut-based SPACs outperformed their parent PACs in terms of adsorption rate and capacities in both equilibrium and non-equilibrium conditions.

The adsorption of MC-LR via the prepared SPACs was also evaluated in Lake Erie water, which was sampled after pH adjustment to the target pH of 7.2. The SPACs were dosed as prewetted slurry in all of the experiments in Lake Erie water. In terms of adsorption rate, The BG-HHM (wood-based) SPAC adsorbed the MC-LR the fastest in Lake Erie water whereas the WPC (coconut-based) SPAC was the slowest. At short contact times (non-equilibrium), the BG-HHM (wood-based) SPAC exhibited the highest capacity for MC-LR followed by the COL-PL60-800 (coal-based) and WPC (coconut-based) SPACs. At equilibrium, the order of capacities was the same as one for the short contact times. The simplified equivalent compound model (SEBCM) was applied to the adsorption data of SPACs in Lake Erie water to describe the competitive adsorption of dissolved natural organic matter (NOM) and MC-LR at the short contact times in range of 5 to 30 minutes representing the relevant contact times in practice. The SEBCM model was proved successful in prediction of the required SPAC doses for reduction of a range of MC-LR influent concentrations to a target effluent concentration. Based on the SEBCM results all three SPACs can be reasonably dosed in range of 1 to 25 mg/L to reduce MC-LR concentration as high as 100 µg/L to below the strictest of the regulated drinking water concentrations (i.e. 0.4 µg/L set by USEPA for bottle-fed infants) in Canada, however, the 1.5 µg/L MAC is in effect. The predicted doses of SPACs were also compared with those of the parent PACs (Liu 2017), and the required doses for SPACs were several degrees of magnitude lower compared to the parent PACs.

The removal of SPACs from the Lake Erie water was evaluated with a series of jar tests, simulating typical CFS processes in DWTPs. The addition of SPACs to the low turbidity (2 NTU) Lake Erie water

increased its turbidity substantially. However, the results from the CFS experiments showed that the SPACs can be removed via conventional CFS using aluminum sulfate (alum) as a coagulant. Alum doses as low as 10 mg/L were sufficient for reduction of turbidity in Lake Erie water without addition of SPAC and also the water dosed with the BG-HHM (wood-based) SPAC to below 1 NTU. The water dosed with COL-PL60-800 (coal-based) SPAC required 15 mg/L of alum to achieve the same level of turbidity removal. The WPC (coconut-based) SPAC increased the turbidity of the Lake Erie by the most (>100 NTU) and required at least 30 mg/L of alum to achieve a residual turbidity below 1 NTU.

Overall, SPAC as a treatment method for removal of MC-LR from drinking water is a promising alternative to PAC. The benefits of SPAC, including the faster adsorption rate and higher short contact time capacities are essential to conventional DWTPs in terms of managing seasonal MC-LR presence in source waters. Further studies are required to evaluate the adsorption of other cyanotoxins via SPAC and to assess the removal of spent SPAC residual particles during rapid media filtration. With experimental commercial SPAC products slowly being developed it is necessary to assess the performance of SPAC for removal of variety of cyanotoxins in surface water under various conditions.

Acknowledgements

First and foremost, I would like to thank my supervisors Dr. Sigrid Peldszus and Dr. Peter Huck for their expert advice and guidance over the course of this study. They continued to encourage me during the challenging times and giving me hope, especially during the tough times of COVID-19 lockdowns which delayed the experimental phase of this study. I am grateful for their counsel, constant support, and professional advice. I also would like to extend my thanks to the readers of my thesis, Dr. William Anderson and Dr. Lei Xu.

I am grateful for the exceptional support from my colleagues at NSERC Chair in Water Treatment, special thanks to Kimia Aghasadeghi and Patrick King for their help with training and getting started in the lab. Thanks to Kasia Jaszczyszyn for her help and counsel during my experimental work in the lab. Thanks to Kirti Nemani for helping with LC-OCD analysis of the raw water. I would like to extend my thanks to my great colleagues and friends at NSERC Chair in Water Treatment, Lin Shen, Katrine Led, Patrick King, Kirti Nemani, Kasia Jaszczyszyn, Mahmoud Badawi, Hemant Arora, and Noshin Nawar Reza; it has been a great pleasure working with you all.

Thanks to Yanting Liu for explaining and clarifying her methods in her Master's thesis. This study is building on Yanting Liu's Master's thesis entitled "Treatment of the Cyanotoxins Cylindrospermopsin, Microcystin-LR, and Anatoxin-a by Activated Carbon in Drinking Water", which provided baseline performance data for powdered activated carbon utilized in in the current study for comparison.

Profound thanks to Seyfollah Gilak for his help with optimization of the LC-MS/MS method and troubleshooting the instrument. Thanks to Andrea Marrocco for her advice on PAC pulverization. Thanks to Shuhuan Li and Marianne Vandergriendt at Ecohydrology research group for providing assistance with the micronizing mill. Special thanks to Andrew Kacheff at chemical engineering department for his help with preliminary particle size distribution analysis and for BET analysis of the prepared SPACs.

Special thanks to Andrew Kacheff at Nanotechnology and Chemical engineering department at University of Waterloo for BET analysis of prepared SPAC samples. Thanks to Oluchi Okoro at Polytechnique Montréal University for help with determination of particle size distribution of "as received" PACs. Thanks to Steven Ngo at the Water STP group at University of Waterloo for TOC and DOC analysis for Lake Erie raw water samples. Great thanks to Matthew John Linehan, undergraduate

Table of Contents

ix

List of Figures

List of Tables

List of Acronyms

BET – Brunauer, Emmett, and Teller

c(RADfV) – Cyclo-(Arg-Ala-Asp-D-Phe-Val)

CCL – candidate contaminant list

DFT – density function theory

DOC – dissolved organic carbon

EBC – equivalent background compound

GAC – granular activated carbon

IAST – ideal adsorbed solution theory

JCR – joint confidence region

LC-MS – liquid chromatography mass spectrometry

LC-MS/MS – liquid chromatography tandem mass spectrometry

MAC – maximum acceptable concentration

MC-LR – microcystin-LR

MCs – microcystins

MDL – method detection limit

2MIB – 2-methylisoborneol

MRM – multiple reaction monitoring

NOM – natural organic matter

PAC – powdered activated carbon

pH$_{pzc}$ – pH at point of net zero surface charge

pKa – acid dissociation constant

PSD – particle size distribution

SEBCM – simplified equivalent background compound model

SEM – scanning electron microscope

SIA – static image analysis

SUVA – specific ultraviolet adsorption

SPAC – super-fine powdered activated carbon

TOC – total organic carbon

USEPA – United States Environmental Protection Agency

UV$_{254}$ – Ultraviolet absorbance at 254 nm

Disclaimer

In several instances in this study, commercial products and/or trade names were mentioned. The use of commercial names does not constitute endorsement or recommendation of these products and/or instruments by the authors.

Chapter 1

Introduction

1.1 Problem statement

Cyanobacteria are nitrogen-fixing photosynthetic bacteria that formerly were mistakenly identified as blue-green algae; cyanobacteria can grow exponentially to cover the surface of waterbodies, which is often known as a cyanobacterial bloom (Szlag et al., 2015). Blooms are more frequent as the result of nutrient loading and climate change; it has also been shown that higher temperatures can affect the intensity of the bloom and its longevity (Davis et al., 2009; Richardson et al., 2018).

Various species of cyanobacteria can produce potent toxins as secondary metabolites, known as cyanotoxins, which can be both contained inside the cells or excreted as an extracellular toxin. These toxins even at low concentrations in $\mu g/L$ could be considered a significant threat to mammal's health, including humans. Cyanotoxins, can find their way into the human body via several pathways, including but not limited to ingestion, often through water, inhalation, and skin contact (Svrcek & Smith, 2004) However, the most likely way of exposure would remain to be through drinking cyanotoxin-contaminated water. Unfortunately, through the past decade, several cases of animal and human intoxications with cyanotoxins were reported (Roegner et al., 2013). Cyanobacterial blooms can impact many types of water, including freshwater lakes, rivers, sea water, and brackish water (Paerl & Huisman, 2009). Temperate lakes, which are often used as sources for drinking water, are not an exception and are often impacted during the warm seasons by cyanobacterial blooms. Many of the fresh lakes are sources for drinking water, and there can be a high risk of contamination of source water with both cyanobacterial cells and extracellular toxins.

A clear example that demonstrates the possible severity of source water contamination with cyanotoxins, in this case Lake Erie, would be the 3 days " do not drink or boil" advisory issued as a result of detection of a potent cyanotoxin known as microcystin-LR (MC-LR) in treated drinking water in the City of Toledo, Ohio on August of 2014 (USEPA, 2015). The fact that prediction of whether a bloom contains toxic cyanobacteria species is almost impossible at the moment also elevates the risk and importance of source water monitoring (Davis et al., 2009)

MC-LR is one of the most detected and most studied among cyanotoxins (Merel et al., 2013). Microcystins (MCs) are widely detected in North America; concentrations ranging from no detection to around 30,000 µg/L were detected (Fristachi et al., 2008). Canada's drinking water treatment plants (DWTPs) raw water intakes were not immune from MC-LR contamination, concentrations of MC-LR were detected in DWTPs in Alberta, Manitoba, Ontario, and Quebec (Carrière et al., 2009).

To address these risks, health advisories and regulations were put in place by different authorities. To begin with, UEPA's very first contaminant candidate list (CCL1) included "cyanobacteria and their toxins" in 1998. Since the second contaminant candidate list (CCL2), cyanotoxins were a permanent member of the lists, including the latest CCL 5 This means that cyanotoxins, including the MCs, should be further studied in order to determine maximum contaminant levels (MCLs) for these cyanotoxins (USEPA, 2016). In 2015, USEPA issued health advisories for cyanotoxins, cylindrospermopsin (CYL), and total MCs (USEPA, 2015). Health advisories for total MCs are as follows: for children under the age of 6, the concentrations should be less than 0.3 µg/L, and for the other age groups, concentrations should be kept under 1.6 µg/L. Canada has regulated MCs in the form of a federal guideline with a maximum acceptable concentration (MAC) of 1.5 µg/L (Health Canada, 2017) which needs to be implemented by the provinces by corresponding regulations. The guideline applied only to MC-LR in the beginning. However, it was reviewed and has been applied to total MCs since 2018 (Health Canada, 2018). The province of Ontario has also adopted a MAC of 1.5 µg/L, although this is applied only to MC-LR in the latest iteration of the regulations (O. Reg. 169/03, 2020). Since the concerns about the presence of cyanotoxins, including MCs in drinking water, have been elevated through the past decades, investigation of effective treatment methods for the removal of cyanotoxins has gained more importance.

Activated carbon has been proven to be effective for the removal of taste and odor compounds such as geosmin and 2-methylisoborneol (2MIB), which can also be produced by cyanobacterial and algal blooms, and other micropollutants like pharmaceutical and organic contaminants (Westrick et al., 2010). It has been demonstrated that activated carbon can be implemented as an efficient treatment for extracellular cyanotoxins. Powdered activated carbon (PAC) was investigated widely for removal of cyanotoxins, specifically MC-LR, and has shown promising results. PAC used for removal of MC-LR has shown removals ranging from 60% to 98% (Kumar et al., 2018). Although, competitive adsorption with natural organic matter (NOM) and algogenic organic matter (AOM) highly impacts the performance of PAC (Zoschke et al., 2011). Providing a longer contact time for PAC could be a significantly challenging task for DWTP operators and may require redesigning and modification of the treatment train. Also, studies showed that PAC contact times employed in WTPs are usually shorter than the times required to reach equilibrium and therefore maximum removal. Liu (2017) showed that shorter contact times employed at WTPs combined with background organics competition for adsorption sites would significantly impact PACs performance in the removal of cyanotoxins.

Recently a new type of PAC known as super-fine powdered activated carbon (SPAC) is being developed and studied. SPAC, also known as micro-ground PAC, will share the same activation method with currently commercially available PAC but differs in the pulverization method, which allows the activated carbon

particles to reach a substantially smaller size of ~ 1 μm compared to the corresponding PAC which have median particle sizes in range of 20-40 μm. SPACs have been produced at bench-scale by pulverizing commercially available PACs via bead milling to decrease particle sizes to slightly below 1 μm, decreasing the original median particle sizes by an average of 30 folds. It is proven that a decrease in the particle size of adsorbent material speeds up the adsorption kinetics (Najm et al., 1990).

Studies done on SPAC at bench-scale showed significant improvement in adsorption rate for a variety of compounds and pollutants, and also increased capacity for large molecules like NOM. In one study performance of SPAC (0.8 μm) was compared with the corresponding as-received PAC (33 μm) for adsorption of NOM with a high UV_{254} absorbance (i.e. aromatic large molecules). Micrometer-sized SPAC reached equilibrium in less than a minute of contact time, and the dose required to achieve the same levels of NOM removal was decreased 10-fold compared to the as-received PAC (Matsui et al., 2004). For adsorption of geosmin (taste and odor agent produced by cyanobacteria), replacing normal-sized PAC with SPAC increased the removal rate from 65% to 96%. It was determined that a 2 mg/L dose of SPAC was equivalent to a normal-sized PAC dose of more than 20 mg/L (Matsui, Aizawa, Suzuki, et al., 2007). All of the studies on SPAC have proven that it is superior to PAC in terms of adsorption rate and required dose at time frames typical for WTP applications. However, the performance of SPAC for the removal of extracellular cyanotoxins has not yet been published.

1.2 Objectives

The main objective of this research is to investigate the potential of SPAC to remove the cyanotoxin MC-LR as a seasonal treatment under conditions representative of typical drinking water treatment practice. This main objective breaks into several sub-objectives as described below:

1) Production of SPAC and characterization of size distribution and other properties

   a) Sourcing of 3 commercially available PAC products: coal-based COL-PL60-800 (Carbon Activated Corporation), wood-based BG-HHM (Calgon Carbon), and coconut-based WPC® (Calgon Carbon). Results of this research are comparable to the ones reported by Liu (2017), since she used the same PACs for her research

   b) Selecting a commercially available milling method to pulverize PAC to a median particle size around 1 μg/L

   c) Studying the effect of milling time and method on particle size distribution of the SPAC

   d) Developing an scanning electron microscope (SEM) imaging method for determination of particle size distribution of SPAC

2) Evaluation of the performance of the produced SPACs for removal of MC-LR from ultra-pure water

   a) Determine the adsorption kinetics of cyanotoxin, MC-LR onto the three different SPACs (made from different base materials).

   b) Determine the adsorption isotherms of MC-LR onto the SPACs in ultrapure water.

   c) Determine the short contact time (non-equilibrium) adsorption capacities of MC-LR onto the SPACs in ultrapure water.

3) Evaluation of the performance of the produced SPACs for removal of MC-LR from surface water

   a) Determine the adsorption kinetics of cyanotoxin, MC-LR onto the three different SPACs (made from different base materials).

   b) Determine the adsorption isotherms of MC-LR onto the SPACs in natural surface water.

   c) Determine the short contact time (non-equilibrium) adsorption capacities of MC-LR onto the SPACs in natural surface water.

   d) Investigate the effects of NOM competition on cyanotoxin adsorption by comparing results from ultrapure water and surface water investigations.

4) Estimating the required dose for MC-LR reduction

   a) Estimate SPAC dosages needed to treat MC-LR by applying the simplified equivalent background compound model (SEBCM) to equilibrium isotherms and non-equilibrium loading data obtained for the adsorption of cyanotoxins onto each selected SPAC product in natural surface water.

5) Evaluate the removal of SPAC from surface water via conventional coagulation, flocculation, and sedimentation (CFS).

   a) Assess the removal of SPAC from surface water by simulating the CFS process via jar tests.

   b) Estimating the required dose of alum for removal of SPACs at the maximum dose required for treatment of MC-LR laden surface water.

1.3 Thesis Structure

The thesis includes 7 chapters (Figure 1.1). Chapter 1 includes a brief introduction on cyanotoxins and their treatment methods and describing the objectives of this study. Chapter 2 consists of a literature review covering the findings and results of previous studies on the adsorption of cyanotoxins onto activated carbon, especially PAC. It also provides an overview of SPAC research including, the pulverization methods,

particle size distribution analysis, and current applications in drinking water treatment. Chapter 3 reports on the base activated carbons used in this study and covers the pulverization procedure via a bead mill, the approaches for the determination of particle size distribution, and the characterization of the produced SPAC. Chapter 4 evaluates the adsorption kinetics, capacities, and isotherms of MC-LR onto the produced SPACs in ultrapure water. Chapter 5 covers the same evaluations in natural surface water to study the background interference of natural organic matter. Chapter 6 includes the results of jar tests involving selected SPAC and conventional commercially available coagulant to evaluate the efficiency of conventional coagulation methods in the removal of SPAC. Chapter 7 provides a summary of findings from this study and provides suggestions for future research in this field.
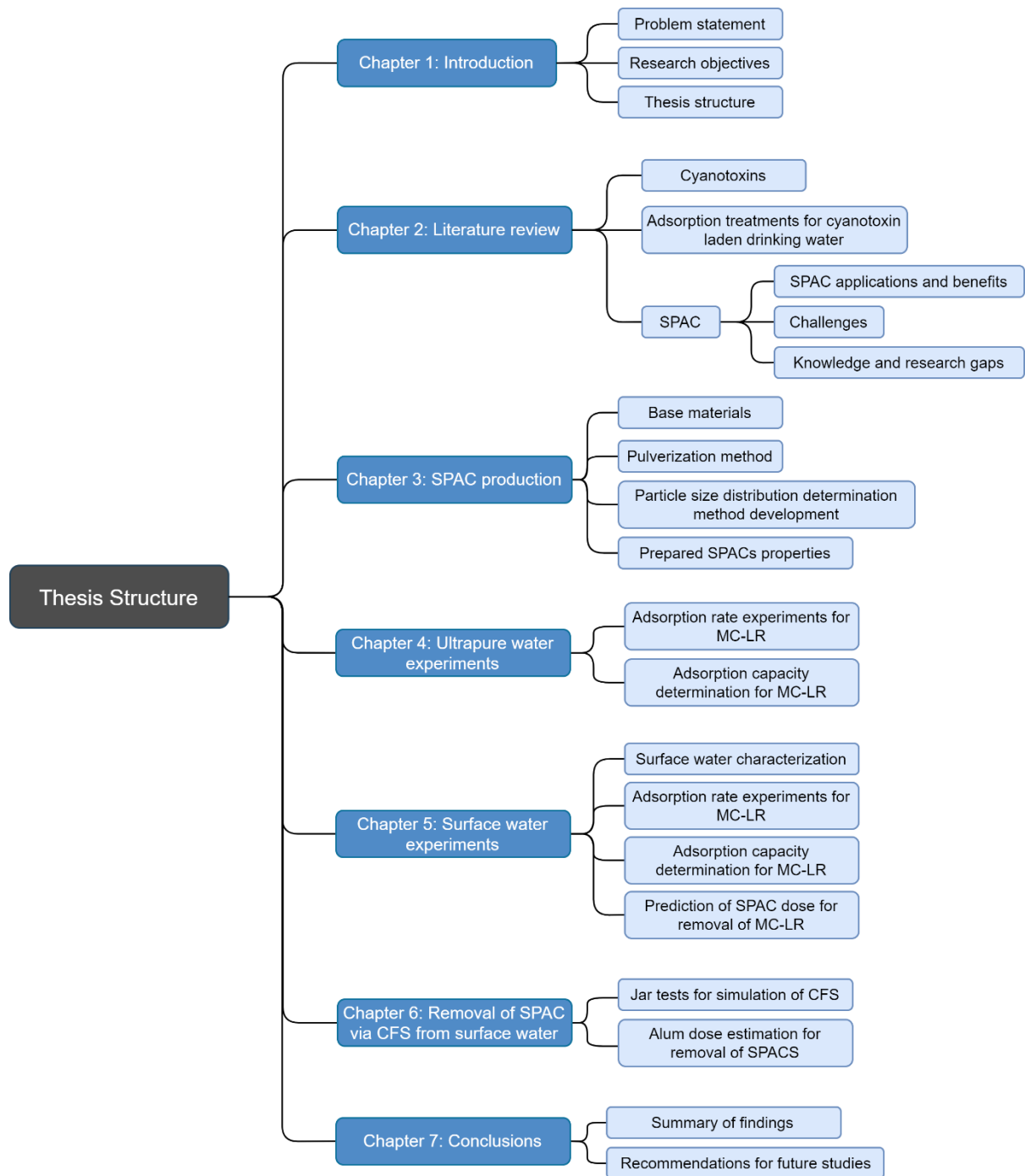
Figure 1.1 Thesis structure

Chapter 2

Literature review

2.1 Cyanotoxins

Cyanobacteria are known to be one of the earliest species that existed on the surface of the earth. It is believed that they are in existence for more than 3.5 billion years, and more than 2600 cyanobacteria species have been discovered so far (Du et al., 2019). Cyanotoxins are secondary metabolites of cyanobacteria and are produced by a variety of cyanobacteria genera (Westrick et al., 2010). Managing the risk of cyanotoxins can be very complicated since both toxin-producing and non-toxin-producing strains of cyanobacteria could coexist in a bloom. Another added level of complexity is the difficulty in the determination of whether a toxin-producing strain will be producing toxins under a given bloom condition (Merel et al., 2013). Cyanotoxins are categorized by both structure and type of toxicity. From a structural aspect, cyanotoxins can be divided into three categories, cyclic peptides and alkaloids, and lipopolysaccharides (LPSs). In terms of toxicity, there are two categories, hepatotoxins, and neurotoxins. Hepatotoxins affect the liver and can cause irreversible damage. Neurotoxins are known to interfere with the nervous system and can cause muscle paralysis.

Table 2.1 demonstrates how different cyanotoxins fall into these categories. Cyanotoxins are produced intracellularly and will be excreted gradually during the lifecycle of the cell, although a large amount of the intracellular matter including cyanotoxins will be released upon death of the cell when the cell structure is ruptured, which is also referred to as cell lysis (Pantelić et al., 2013) (Figure 2.1). Cell lysis is also caused by external stressors, including treatment processes like oxidation.

Table 2.1 Structure and toxicity type of cyanotoxins

Structure\Toxicity	Hepatotoxic	Neurotoxic
Cyclic peptides	microcystins and nodularins	-
Alkaloids	cylindrospermopsins	anatoxin-a and saxitoxins

7
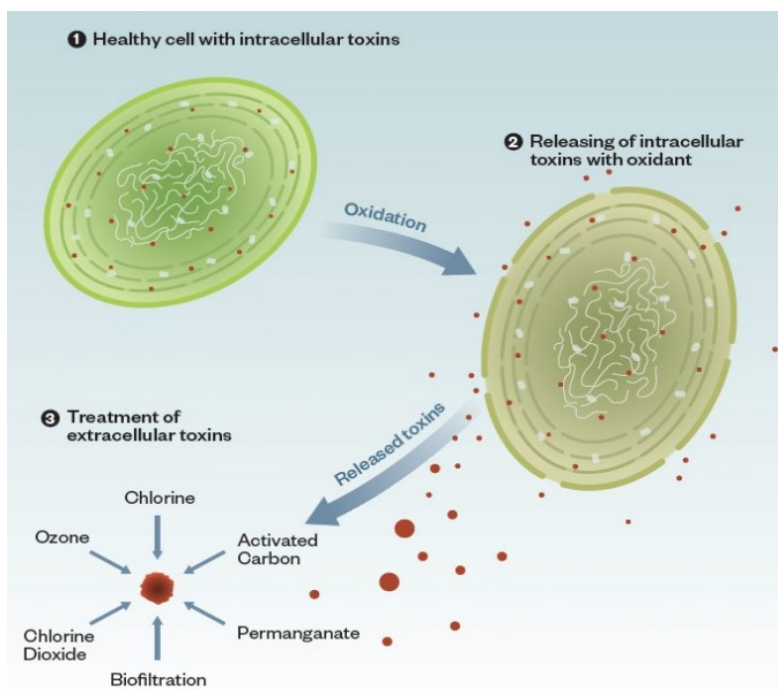
Figure 2.1 Lysis of cyanobacterial cells due to oxidation

(Reprinted with permission from Hazen and Sawyer)

2.1.1 Microcystins

Microcystins (MCs) are produced by a wide variety of cyanobacteria genera, including but not limited to *Microcystis, Nostoc, Anabaena, Dolichospermum, Leptolyngbya* and *Synechococcus* (Salmaso et al., 2016). Microcystins are cyclic peptides with a general structure of cyclo-(D-alanine-*X*-D-MeAsp-*Z*-Adda-D-glutamate-Mdha) in which *X* and *Y* are the places in the structure where the variable L amino acids sit (Figure 2.2) (Apeldoorn et al., 2007). The variable L amino acids distinguish the different microcystin congeners. The other variation factor would be methylation and demethylation at the specific sites on the cyclic peptide structure. The Adda amino acid (2S,3S,8S,9S)-3-amino-9-methoxy-2,6,8-trimethyl-10-phenyldeca-4,6-dienoic acid is deemed to be responsible for the toxicity of MCs. It is known that changes to the Adda region and acylation of glutamate can reduce the toxicity of MCs or render them completely nontoxic (Apeldoorn et al., 2007). The most common route of exposure to cyanotoxins, including microcystins and MC-LR, would remain to be through contaminated drinking water, yet skin contact and contaminated food supplements can be as probable.

8
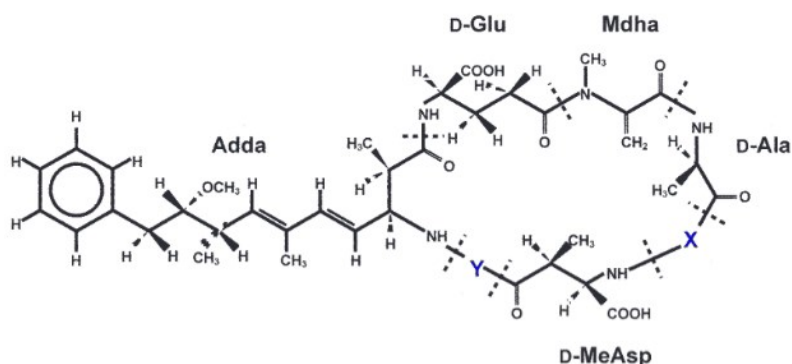
Figure 2.2 Structure of microcystins (Duy et al., 2000)

MCs mainly impact the liver in terms of toxicity, which is proven to be cumulative by forming an irreversible covalent bond with protein phosphates (Falconer, 1993). Microcystins can find their way to the liver through portal vein circulation and get adsorbed on hepatocytes via organic anion transporting peptides and the bile acid transport system (Massey et al., 2018). In order for the liver to recover, it needs to regrow hepatocytes (Chorus et al., 2000). Intoxication of the liver with microcystins can cause a variety of lethal damages, including hepatocyte necrosis, liver cancer, rounding of cells, cell blebbing, cell fragmentation, cell separation, and glycogen depletion (Batista et al., 2003). A combination of these damages can lead to the liver's failure in detoxifying and metabolizing endogenous and exogenous toxicants, which can eventually lead to blood accumulation in the liver resulting in an increase in liver size; this is also known as hepatocellular swelling (Massey et al., 2018). There are also reports on the effects of microcystins on microRNAs (miRNAs) in the liver. The exposure can cause alterations in miRNAs and result in liver injury and liver tumor promotion (Yang et al., 2017). The oral median lethal dose (LD_{50}) of MC-LR in mice is determined to be 10.9 mg/kg , and an intraperitoneal (i.p) LD_{50} of 50 µg/kg (Roegner et al., 2013).

MC-LR, alongside MC-RR and MC-YR (Figure 2.2), are the most detected microcystins. MC-LR is the most studied of MCs with leucine (L) and arginine (R) at the X and Y positions in the structure and a molecular weight of around 995 Da. MC-LR contains two ionizable carboxyl groups as well as an ionizable amino group (Maagd et al., 1999). The pK_a for these groups are 2.09, 2.19, and 12.48, respectively (Maagd et al., 1999). According to these pK_a values, specific species of MC-LR will be dominant in different pH ranges; $(COOH)_2(NH_2^+)$ at pH < 2, $(COO^-)(NH_2^+)$ at 2 < pH < 5.5 and $(COO^-)_2(NH_2^+)$ at pH > 5.5 (Liang et al., 2011). According to these pH ranges, MC-LR will maintain one negatively charged group in the neutral pH range. Microcystins are highly soluble in water, methanol, and ethanol. However, it is insoluble

in organic solvents such as acetone, benzene, chloroform, and ether (Apeldoorn et al., 2007). Microcystins are significantly more stable molecules compared to other cyanotoxins due to their cyclic peptide structure. Microcystins can endure several hours of boiling; therefore, boiling contaminated water will only result in further concentration of the toxin. In terms of chemical hydrolysis, even at 40°C and at high or low pH, very slow hydrolysis was reported. To achieve degradation of >90% of toxin in an acidic environment (pH 1), approximately 10 weeks were required. In basic environments (pH 9), the required time for breakdown surpassed 12 weeks (Apeldoorn et al., 2007). It is reported that microcystins are highly resistant to hydrolysis and oxidation in temperatures and pH values (near neutral) in typical surface water and drinking water reservoirs and maintain a half-life of approximately 10 weeks (Harada et al., 1996).

Cyanobacterial blooms are abundant in fresh surface waters of temperate regions during summer and late fall, and the Great Lakes in North America are no exception (Merel et al., 2010). Microcystins, including MC-LR, are the most detected cyanotoxins worldwide and in North America. In Canada, MC-LR has been detected in both western and eastern waterbodies. In the west, concentrations of microcystins were detected in 28 water bodies in Manitoba (Kotak & Zurawell, 2007). Sampling lake waters during the summer of 1995 in British Columbia revealed concentrations of MC-LR ranging from 31 to 1363 µg/L (Kotak & Zurawell, 2007). In the east, microcystins were detected in 22 lake water samples in southern Quebec in the summer of 2001 (Giani et al., 2005). In Ontario, MC-LR was also detected in several waterbodies throughout the last decades; examples would be multiple detections in the Lake of the Woods (Zastepa et al., 2017) Lake Erie is also known for having toxic *Microcystis* blooms of varying magnitude in the western basin during late summers such as the one caused the temporary shutdown of the Toledo, Ohio area water intake facility in August of 2014 (Müller et al., 2017). Lake Ontario is not immune to cyanobacterial blooms, and concentrations as high as 400 µg/L were observed during the peak of blooms at Hamilton Harbour (Murphy et al., 2003). In the US, microcystins were detected in ambient waters in several states, including New York, Nebraska, New Hampshire, and Florida (Fristachi et al., 2008).
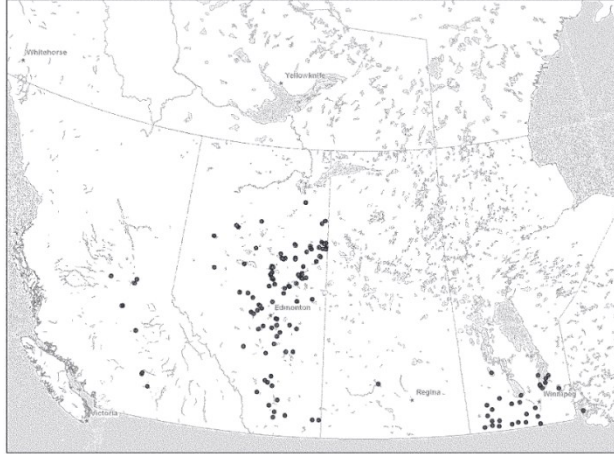
Figure 2.3 Waterbody locations in western Canada where microcystins have been detected (Kotak & Zurawell, 2007)

In response to these issues, regulations were put in place. WHO has issued a guideline on MC-LR requiring a maximum concentration of 1 μg/L in 2003 (World Health Organization, 2020), which was eventually adapted by several governments across the world. Health Canada also issued a federal guideline requiring a maximum acceptable concentration (MAC) of 1.5 μg/L for MC-LR (Health Canada, 2017). In the latest iteration of Health Canada's guideline, this MAC is applied to total microcystins (Health Canada, 2018), and provincial governments are required to implement this guidelines through issuing regulations which are at least as stringent as the provided guideline. USEPA has issued a health advisory in 2015, requiring MC-LR concentrations to be as low as 0.3 μg/L for infants and 1.6 μg/L for other age groups (USEPA, 2015).

Regarding the toxicity of cyanotoxins and the risks associated with contamination of drinking water with these toxins, utilities have to select proper treatment methods in order to be able to follow the aforementioned advisories and guidelines.

2.2 Activated carbon treatment for cyanotoxin laden drinking water

Adsorption is considered one of the reliable treatment processes for the removal of chemical contaminants from drinking water. Although there were several studies focusing on alternative adsorbents such as bentonites and attempts to modify their surface in order to achieve low cost and efficient adsorbents (Alexander et al., 2018; Sukenik et al., 2017), activated carbons are most common as the primary choice for contaminant removal in water treatment applications. Activated carbon as a conventional drinking water treatment mainly appears as a form of granular activated carbon (GAC) and powdered activated carbon (PAC). GAC is mainly loaded into a fixed bed contactor in the treatment process or used as a filter layer in rapid filtration. The particle size of GACs typically ranges from 0.4-3.4 mm (Drogui et al., 2012). PAC

comes in much smaller sizes ranging from 10 to 80 µm, and usually can be directedly injected into the front end of the treatment train, therefore, providing more flexibility. Activated carbon is generally sourced from coal, wood, and coconut. However, there have been efforts through the past decade to source activated carbon from alternative sustainable materials, including waste tire (Mashile et al., 2018, 2019). The activation process is done via various activation methods, in which the simplest is steam activation to create pores of appropriate sizes and activated sites for adsorption. While activated carbon adsorption is proven to be an effective method for the removal of extracellular cyanotoxins (dissolved cyanotoxins), they have absolutely no effect on intracellular toxins, since these toxins are contained within the cell walls (Merel et al., 2013).

2.2.1 Granular activated carbon

GAC is a popular adsorbent for the removal of synthetic organic chemicals (SOCs), including volatile organic chemicals (VOCs), pesticides, and herbicides. GAC can be loaded into fixed beds due to its large particle size. This type of application has inherent advantages, including lower carbon consumption and a simple regeneration process for the spent carbon (Najm, Snoeyink, Lykins, et al., 1991).

As mentioned earlier, GAC can be both used as a filter medium in dual media rapid filtration or as a standalone process in a fixed bed contactor. While the material used in both configurations is the same (GAC), there are significant differences in performance and maintenance. GAC as a filter medium is deemed to be suitable for the removal of particulates, partially adsorbing chemicals, and biodegrade organic contaminates (Westrick et al., 2010). Colonization of GAC with a microbiological film during treatment leads to biofiltration, which can accelerate the biodegradation of certain compounds (Hallé et al., 2015). On the other hand, GAC adsorbers are designed to only adsorb organic contaminants. In terms of maintenance and longevity of the treatments, GAC as filter medium can stay in service for up to 7 years when backwashed properly, though adsorption performance declines substantially usually within a year depending on carbon loading. On the contrary, GAC as an adsorber should be refreshed or properly regenerated once total organic carbon (TOC) breakthroughs reach the determined threshold (Westrick et al., 2010).

A study by Newcombe (2002) on a GAC column showed that the column lost its ability to remove microcystin at 80% TOC breakthrough. This might be evidence that GAC columns with long service life without regeneration would be an unreliable treatment method for cyanotoxins, and in order for GAC treatment to be effective in cyanotoxin removal, the column should be regenerated frequently (Westrick et al., 2010). Wang et al. (2007) investigated the effect of biofilm growth on the surface of GAC on MC-LR adsorption which showed that the growth of biofilm on the surface of GAC could prevent MC-LR from accessing adsorption sites of GAC. The study showed that biofilm was successful in biodegrading MC-LR,

although these results are highly dependent on the temperature and initial bacterial density and require longer contact time. Furthermore, it is worthy of mentioning that Wang et al. (2007) performed this study in Australia which has an overall warmer climate and experiencing harmful algal blooms year-round. Therefore, results of biofiltration experiments from this specific study are not directly applicable to temperate regions such as Great Lakes in North America, in which microcystin producing algal blooms are seasonal. Overall, GAC is reported to be suitable for the removal of MC-LR provided it is not exhausted, and regenerated when necessary (Westrick et al., 2010).

2.2.2 Powdered activated carbon

PAC and GAC are considered as the best treatment methods for the removal of dissolved contaminants, particularly seasonal issues including cyanotoxins, taste and odor compounds, and heightened levels of NOM and AOM. PAC is advantageous over GAC due to its lower cost, and the fact that it does not require a fixed bed contactor makes PAC treatment a generally more flexible practice. PAC can be applied to different parts of the treatment train, including plant intake, rapid mix, and rapid filtration influent (Najm et al., 1991). However, the preferred location would be at plant intake, this would provide the maximum contact time, and the following stages in the treatment, including coagulation, flocculation, sedimentation, and rapid filtration, would facilitate the removal of carbon particles without need of an additional process. In the case that there is not enough contact time available before the coagulant addition step, Najm et al. (1991) suggested using a continuous flow slurry contactor prior to rapid mixing in order to allow proper mixing, prevent interference from coagulants, and lengthen contact time.

While PAC is capable of removing SOCs and other micropollutants, regarding the flexibility of its application. PAC could be considered as an ideal treatment for seasonal issues including taste and odor (T&O) compounds like geosmin and 2-methylisoborneol (2-MIB) responsible for musty and earthy smell in drinking water which are also a side effect of seasonal cyanobacterial blooms. PAC is also widely studied for the removal of natural organic matter (NOM) and algal organic matter (AOM), which increases during warm seasons. PAC is proven to be an effective seasonal treatment method for T&O compounds, though the type of PAC used (source material) and required dose must be chosen carefully based on the characteristics of the adsorbent and contact time available to PAC at the treatment plant (Lalezary-Craig et al., 1988).

Lately, PAC was the center of attention for the removal of extracellular cyanotoxins, including MC-LR, due to the fact that it can be applied when needed. Being compared to GAC, PAC costs significantly less and does not require specialized infrastructure for implementation. Furthermore, PAC does not suffer from a performance drop due to pre-loading, as is the case for GAC, since it does not remain in service or is

reused (Vlad et al., 2014). However, PAC performance can also get impacted by organic background competition from NOM and AOM, which will be discussed in detail further in Section 2.2.3.

Several studies have investigated the removal of MC-LR via PAC in both pure water and natural surface waters, as summarized in Table 2.2. One of the earliest studies focused on the removal of MC-LR using 8 different PACs produced from the different source materials. The main finding of this study was that PACs with a higher mesopore volume (pores with diameters ranging from 2-50 nm) are the most effective for removal of MC-LR (Donati et al., 1994). This theory was also confirmed by Park et al. (2017) by establishing a relationship between mesoporous pore volume of PAC and its maximum capacity for MC-LR. These studies and others have shown that wood-based PACs have a larger mesoporous volume compared to coal-based and coconut-based PACs, thus, providing more efficient removal for MC-LR. Liu (2017) also investigated the performances of a wood-based, a coal-based, and a coconut-based PAC and also found that the wood-based PAC is the most efficient for removal of MC-LR.

Table 2.2 Performance of PAC for removal of MC-LR reported in the literature (Adapted from Park et al. (2017) with permission and expanded, * marks the recently added references)

Type of PAC	Initial MC-LR concentration (µg/L)	Adsorption capacity (µg/g)	Contact time	Dose of PAC (mg/L)	Reference
8 types of PACs	2500	11,000-250,000	72 h	2.5-200	(Donati et al., 1994)
Wood-based PAC	14	606.67	60 min	15	(Cook & Newcombe, 2002)
Wood-based PAC	17.4	552	60 min	15	(Newcombe & Nicholson, 2004)
Wood-based PAC	10.6	699.6	72 h	15	(Cook & Newcombe, 2008)
PAC	8.5	273-380	21 min	5, 10, 15	(Campinas & Rosa, 2012)
Coal-based PAC	10	150-160	30 min	10, 25, 50	(L. Ho et al., 2011)
Coal-based PAC	22	190-275	15 min	40-100	(Drogui et al., 2012)
Coal-based PAC	10	303.33	60 min	30	(Sam, 2012)
Wood-based PAC	33.5	33.47	60 min	1000	(Stoquart et al., 2016)
Wood-based PAC	10	600	60 min	10	(Cook & Newcombe, 2002)
4 types of PACs*	50	~3,700-8,800	4 – 24 h	5	(Bajracharya et al., 2018)
Tire-based PAC*	25	357 (max)	5-60 min	2,000-10,000	(Mashile et al., 2018)
3 types of PACs*	100	1400-7000	0.5 – 6 h	5-50	(Liu, 2017)

2.2.3 Effect of background organic matter on PAC treatment for MC-LR

Activated carbon adsorbents can be a very effective method for the removal of organic contaminants, including cyanotoxins. However, this type of treatment can get complicated and expensive depending on the amount and characteristics of target contaminants and the presence of background organics which are indicated by TOC. These compounds will also absorb onto activated carbon, reducing the capacity for the target compound and resulting in an increase of required adsorbent dose, thus, increasing the overall cost of treatment (Huck & Sozanski, 2011).

As mentioned earlier, a wide range of pollutants and organic material can be adsorbed onto activated carbon, these compounds, while present, can compete with target pollutants - in this case, cyanotoxins - for adsorption sites. To understand the nature of these competitions, it is necessary to review the mass transfer mechanism that governs adsorption of compounds onto adsorbent. This mechanism consists of four consecutive steps: 1) breaching of hydrodynamic boundary layer, in this step, the adsorbate is transported across the hydrodynamic boundary located around the adsorbent particle. 2) film diffusion, in this step, the adsorbate will diffuse through the boundary layer to reach the surface of the adsorbate; this step is also known as external diffusion. 3) once at the surface, the adsorbate will diffuse into the liquid inside the pores (pore diffusion); this phenomenon is known as intraparticle or internal diffusion. 4) at this final step, the adsorbate will bind to the final adsorption sites as a result of energetic interactions (Worch, 2012).

Background organic matter such as NOM can hinder adsorption of MC-LR onto activated carbon through two different mechanisms; NOM molecules with lower molecular weight (MW) ranging from 1.1 to 2.4 kDa can directly compete with MC-LR molecules for adsorption sites (step 4 of adsorption), since microcystin MW is in the same range (Campinas et al., 2013). The second mechanism is consisting of high MW NOM molecules blocking pore entries and preventing MC-LR molecules from reaching the adsorption sites (step 3 of adsorption). These mechanisms might suggest that pore size distribution of activated carbon and molecular weight of NOM can be the influential factors in the competition of NOM with MC-LR in adsorption onto PAC (Bajracharya et al., 2018). Although Matsui et al. (2003) suggested that due to limited contact time in the PAC applications, the direct competition mechanism is more probable over pore blockage. For the GAC applications, on the other hand, it is suggested that due to the preloading of carbon with NOM for a longer duration of time in contactors, the pore blockage mechanism is more dominant (Knappe et al., 1999).

The impact of NOM on adsorption of MC-LR onto activated carbons is inevitable, and it is accepted that removal efficiency of MC-LR by PAC is reduced in the presence of NOM (Bajracharya et al., 2018). Therefore, lots of effort has been put into modeling the interference of background organics with the adsorption of pollutants. Relying on ideal adsorbed solution theory (IAST) and Freundlich isotherm model,

Najm, Snoeyink, & Richard (1991) introduced the concept of equivalent background compound (EBC). EBC represents the portion of NOM directly competing with the target pollutant for adsorption sites. While using this model, all parameters for the EBC (initial concentration and isotherms parameters) are unknown and should be retrieved by fitting based on IAST, although, soon it was realized that fitting results are not unique and different sets of parameters impact the fitting quality (Graham et al., 2000). To address this, the EBC model was simplified by applying the same Freundlich parameters determined for the pollutant to the EBC (Najm, Snoeyink, & Richard, 1991). This model was further simplified by Qi et al. (2007) by adding the assumption that EBC is present at much higher concentrations than the pollutant; this approach is known as the simplified equivalent background compound model (SEBCM) (Worch, 2012). The SEBCM was further tested in a study by Zoschke et al. (2011) to model the adsorption of 2-MIB and geosmin in the presence of NOM under both equilibrium and non-equilibrium conditions. Liu (2017) also applied SEBCM to describe the adsorption of MC-LR onto PAC in natural waters for both equilibrium and shorter contact times. The success in describing the adsorption of algal metabolites and cyanotoxins onto PAC in the presence of NOM makes SEBCM a suitable approach for estimating the dose of PAC required to achieve adequate removal of cyanotoxins in natural waters.

2.3 Super-fine powdered activated carbon (SPAC)

Although, PAC treatment does not have the same level of efficiency in all treatment trains due to differences in contact time and water quality parameters between different plants. The typical PAC-water contact time in treatment plants is under 2 hours, which is significantly shorter than the time required for PAC to reach its equilibrium capacity for the aforementioned contaminants (Matsui et al., 2004). This could be addressed by optimizing the injection location of PAC in the treatment train or providing a dedicated slurry contactor before the rapid mix in the treatment train, though these solutions are not always practical, especially considering the seasonality of PAC treatment.

It is known that a reduction in particle size will increase the kinetic rates in activated carbon. This is mainly due to the increased external surface area of activated carbon. Early studies showed that PACs with smaller particle sizes had better performance in the removal of natural and synthetic organic matter in a given contact time (Najm et al., 1990; Weber et al., 1983). This improvement is also evident when comparing the kinetics of GAC and PAC and the equilibrium times for these carbons. In theory, reducing the particle size of PAC furthermore by pulverization should result in faster kinetics and eventually shorter equilibrium times. Matsui et al. (2004) tested this theory by pulverizing a commercially available PAC with a median size of 33 μm to a sub-micrometer median size of 0.8 μm and compared the performance of the pulverized PAC and the as-received PAC for the removal of NOM. This study found that reducing the particle size of the PAC decreased the equilibrium time from days to under an hour, more specifically the produced $0.8\ \mu m$

sized SPAC reach 80% of its equilibrium capacity for NOM (reported in UV_{260}) at 1 minute contact time while the 33 μm sized PAC reach only 35% of its equilibrium capacity at 60 minutes. The SPAC also presented increased capacity for high molecular weight NOM in range of 1400 to 3500 Da. Matsui et al. (2004) hypothesized that grinding the PAC causes ink-bottle-type constrictions in pores to fracture resulting in an increase in the mesoporous surface of carbon, which might be an explanation for the higher capacity for NOM. Pulverization of PAC can also affect pore size distribution and cause changes in internal surface properties by exposing previously inaccessible surfaces to new oxygen and hydrogen-containing functional groups (Partlan et al., 2016).

These results translate to significantly shorter contact times and lower doses required for removal of the target adsorbates at a given contact time, since the total adsorption capacity of the carbon will be available in a shorter contact time. Several studies have since evaluated the performance of micro-ground PAC for the removal of different pollutants, which are summarized in Table 2.3. Micro-ground PAC today is more commonly referred to as super-fine powdered activated carbon (SPAC) in the literature, which is generally referred to as PAC with a median particle size of around 1 μm.

Table 2.3 Summary of studies on the potential of SPAC for drinking and wastewater treatment

Type of source material	Type of application	Target adsorbate	As received PAC size (d50)	PAC dose (mg/L)	As received PAC performance	Pulverized PAC (SPAC) size (d50)	SPAC dose (mg/L)	SPAC performance	Reference
Wood-based PAC	Batch	NOM	33 μm	40	52% of eq. at 300 min	0.8 μm	4	80% of eq. at 1 min	(Matsui et al., 2004)
Wood-based PAC	Batch	NOM	33 μm and 18 μm			0.8 μm and 0.6 μm, respectively			(Matsui et al., 2005)
Wood-based PAC	Microfiltration pre-treatment	geosmin	7.6 μm	20	65% removal	0.65 μm	2	Reduced the concentration below 1 ng/L detection limit	(Matsui, Aizawa, Kanda, et al., 2007)
Wood-based PAC	Batch	geosmin	14 μm	0.6	43% removal in 60 min	0.74 μm	0.6	90% removal in 30 min	(Matsui, Ando, et al., 2009)
PAC	Batch	polystyrene sulfonates (PSSs)	10 μm	500	68% removal in 60 min	0.72 μm	100	86% Removal in 60 min	(Matsui et al., 2011)
Wood-based PAC	Batch	2-MIB and NOM	13.5 μm 8.12 μm	-	Freundlich isotherm: $$K_{2MIB}\frac{\left(\frac{nmol}{mg}\right)}{\left(\frac{nmol}{L}\right)^{1/n_{2MIB}}}=$$ 3.53 and 4.36, respectively $\frac{1}{n_{2MIB}}=0.466\ and\ 5.42,$ respectively	0.86 μm 0.66 μm	-	Freundlich isotherm: $K_m\frac{\left(\frac{nmol}{mg}\right)}{\left(\frac{nmol}{L}\right)^{1/n_m}}=4.44$ and 5.42, respectively $\frac{1}{n_{2MIB}}=0.451\ and\ 4.36,$ respectively	(Matsui et al., 2012)
Wood-based PAC	Batch	2-MIB, geosmin, and NOM	13.5 μm	For MIB: 10 For geosmin: 3	60% MIB removal in 3 min 68% geosmin removal in 10 minutes	0.86 μm	For MIB: 5 For geosmin: 0.5	96% MIB removal in 3 min 70% geosmin removal in 10 minutes	(Matsui et al., 2013)

11 types of PAC (wood-based, coconut-based, and coal-based)	Batch	Virus (Qβ and MS2)	13.2 μm (wood-based) 19.13 μm (coconut-based)	20	1.4 log virus removal in 8 hours	0.69 μm (wood-based) 0.65 μm (coconut-based) 0.67 μm (coal-based)	20	4.08 log virus removal in 8 hours	(Matsushita et al., 2013)
Wood-based PAC	Batch	2-MIB	27.5 μm	3	36% removal in 10 minutes	1.21 μm	3	99% removal in 10 minutes	(Pan et al., 2016)
3 types of PAC (two bituminous and a wood-based)	Batch	Wastewater micropollutants (ten pharmaceuticals and pesticides)	17 μm	3.8-22.5 depending on the pollutant	80% removal in 12h	0.96 μm	3.2-20.6 depending on the pollutant	80% removal in 10 minutes	(Bonvin et al., 2016)
Manufacturer provided Wood-based SPAC	Microfiltration pre-treatment	Per- and polyfluoroalkyl substances (PFASs)	-	-	-	0.88 μm	100-500	Capacity of 11 $\mu g/g$ of total PFAAs compared to 6.2 $\mu g/g$ for F400 GAC	(Murray et al., 2018)
3 types of GAC	AgCl-SPAC composite	bromide and iodide	-	-	-	1.68 μm, 1.58 μm, 1.35 μm (mean sizes) used for AgCl-SPAC production	10 mg/L of AgCl-SPAC	Selectively removed bromide and iodide in the presence of background organics	(Ateia et al., 2019)
7 types of PAC (three bituminous coal, two lignite coal, one coconut shell, one wood-based)	Batch	SOCs (Phenanthrene, Biphenyl, 2-Phenylphenol)	11.3 μm – 13.6 μm	1	Capacity of 50 to 150 mg of adsorbate per g of adsorbent in 1 hour	0.169 μm – 0.441 μm	1	Capacity of 140 to 250 mg of adsorbate per g of adsorbent in 1 hour	(Partlan et al., 2020)

2.3.1 SPAC applications and benefits

The most advantageous aspect of the SPAC application would be its faster adsorption kinetics. It is reported that SPAC generally presents faster adsorption kinetics compared to its corresponding source PAC. These reports are based on batch experiments evaluating adsorption of T&O compounds (2-MIB and geosmin) (Pan et al., 2016), NOM (Matsui et al., 2004, 2005), SOCs (Partlan et al., 2020), disinfection by-product (DBP) precursors (Ateia et al., 2019), pharmaceuticals (Bonvin et al., 2016), and virus surrogates (Matsushita et al., 2013). This faster kinetics not only results in shorter contact times to achieve a certain removal, it also has the potential to reduce the effects of background competition by NOM and AOM during adsorption of target adsorbates like SOCs (Partlan et al., 2020). It was also mentioned earlier that SPAC had shown a higher capacity for high MW organic matter with higher specific ultraviolet adsorption (SUVA), which was suggested to be linked with the increase in the mesoporous volume of activated carbon due to elimination of ink-bottle-effect at pore entries and the overall increase in active surface area (Bonvin et al., 2016; Matsui et al., 2004).

Pilot-scale studies are mainly focused on the application of SPAC as a pre-treatment for microfiltration (MF). MF and ultrafiltration setups are highly efficient for the removal of suspended particles and bacteria. However, they are unable to remove dissolved substances such as taste and odor compounds and SOCs. Membrane filtration setups also suffer from fouling caused by organic matter, biological growth, and fine suspended particles, which results in the reduction of permeability and a long-term trans-membrane pressure (TMP) increase despite periodic backwashes. Coupling microfiltration with activated carbon pre-treatment has several advantages, including promotion of larger floc formation after coagulation step and adequate removal of aforementioned dissolved substance (Matsui, Aizawa, Suzuki, et al., 2007). As mentioned earlier, adsorption of dissolved micropollutants, DBP precursors, and taste and odor compounds onto PAC is relatively slow and requires long contact times to reach its equilibrium capacity, especially in the presence of background organics like NOM and AOM. Hence, microfiltration setups are often known and deemed advantageous for their smaller footprints, the PAC contact times are often short in such setups. Therefore, PACs rarely reach their equilibrium capacity in MF setups and therefore a higher dose of PAC should be applied. A pilot-scale study by Matsui et al. (2007) showed that by replacing PAC with SPAC as a pre-treatment to microfiltration for removal of geosmin, a dose reduction of up to 90% could be achieved, and long-term TMP increase was substantially reduced by the addition of SPAC. The authors also found that SPAC performed better compared to PAC while exposed to the excessive AOM released by algae more efficiently compared to the parent PAC. Another pilot-scale study on ceramic microfiltration coupled with SPAC pre-treatment for removal of per- and polyfluoroalkyl substances (PFASs) showed that this novel

combination was 480 times more efficient than conventional GAC treatment in adsorption of PFASs based on the given contact time, activated carbon dose, and influent concentration in the pilot studies (Murray et al., 2018).

Although the application of SPAC is most practical while coupled with microfiltration due to adequate removal of SPAC particles via membranes, recent studies such as (Nakazawa et al., 2018a, 2018b) suggest that SPAC could be a replacement for PAC, when applied during conventional treatments; relying on coagulation, flocculation, sedimentation, and rapid filtration for the removal of SPAC particles, which is further discussed in Section 2.3.2.

2.3.2 Challenges associated with SPAC treatment

2.3.2.1 Removal of SPAC from water

As described in Section 2.3.1., SPAC treatment was originally proposed as a pre-treatment for membrane filtration procedures such as MF and ultrafiltration, since it was proven to decrease the fouling rate in such technologies. Also, the higher adsorption rate of SPAC results in achieving removals close to equilibrium capacity in relatively shorter contact times which makes it highly compatible with the small footprint of such filtration procedures. However, the use of SPAC as seasonal treatment in other treatment trains, which lack a membrane filtration step, might raise some concerns as the removal of smaller SPAC particles may be less efficient via conventional solid-liquid separations processes such as coagulation, sedimentation, and rapid media filtration compared to conventional PAC particles. These concerns are valid since even with the use of conventional PACs, there were incidents of breach of PAC particles into filtrate and resulted in customer complaints (Ando et al. 2010). In an attempt to address these concerns, Nakazawa et al. (2018a) studied the retention of SPAC particles after conventional treatment, including coagulation, sedimentation, and sand filtration. The results showed that the use of SPAC with conventional treatment methods does not significantly increase the risk of small particles being detected in the treated water. The same authors also proposed that applying simple modifications to coagulation procedure such as increasing the flash mixing intensity and use of high basicity coagulants can minimize the residual SPAC particles in finished treated water (Nakazawa et al., 2018a).

2.3.2.2 Production of SPAC

Another challenge associated with the SPAC treatment would be the production of SPAC itself. At the time of writing, SPACs are not commercially available, and a bead mill is required for pulverizing the commercially available PACs in order to produce the finer particles. The bead mills are limited to bench-scale studies and are required to run wet for maximum efficiency; this means that the final product will be

in the form of a slurry. The produced slurry can be dried, although it is not recommended since it is a time-consuming and inefficient task on an industrial scale, and there will be a higher chance of dispersion of dry fine particles during production and applications, which could be a health hazard. Furthermore, Pan et al. (2016) studied the adsorption of 2-MIB onto both wet-milled and dry-milled SPAC, which showed that wet-milled SPAC had a higher capacity for 2-MIB and presented improved characteristics, which is thoroughly discussed in chapter 3.

2.4 Knowledge gaps and research needs

Cyanotoxins remain a serious threat to the safety of drinking water due to an increase in the frequency of cyanobacterial blooms because of increased nutrient loading in lakes and climate change. With regulatory limits being updated and becoming more stringent, drinking water treatment plants continue to reassess the reliability of their technologies in order to be prepared for longer and more intense cyanobacterial blooms and the possible presence of cyanotoxins in their source water. It has been shown that PAC is an efficient treatment for cyanotoxin-laden water. More recently SPAC has received lots of attention due to its superiority to PAC, most prominently its faster kinetics which result in high removals at shorter contact time than with PAC. SPAC was also shown to have higher equilibrium capacities than the corresponding PACs' for certain natural and synthetic organic compounds. Although several studies evaluated the performance of SPAC for removal of taste and odor compounds produced by cyanobacteria and occasionally organic matter present in cyanobacteria-laden water (Matsui et al., 2007), at the time of writing, there was no study evaluating the application of SPAC for the removal of extracellular cyanotoxins for example MC-LR from surface water used for drinking water production.

Chapter 3
SPAC Production and Characterization

3.1 Summary

Three different commercially available PACs (with different base materials: coconut, wood, and coal) were pulverized via bead milling. An SEM imaging and SIA method was developed and successfully used to determine particle size distribution (PSD) of the pulverized PACs. The bead milling effectively reduced the median particle sizes (d50) of activated carbons to around $1\ \mu m$, classifying the produced materials as SPAC. The BET surface area and DFT pore size distribution analyses were performed on both as-received PACs and SPACs. The results showed that pulverization did not have a drastic effect on the BET internal surface area of the coconut-based (WPC) SPAC, while the internal surface area of wood-based (BG-HHM) and coal-based (COL-PL60-800) SPACs were slightly reduced. The DFT analysis also showed that the total pore volume of the SPACs was also reduced slightly after pulverization except for the coconut-based (WPC) SPAC. Despite the reduction in total pore volume after milling, the wood-based (BG-HHM) PAC and SPAC had the highest pore volume among the original PACs and the produced SPACs. The DFT analysis also showed minimal changes in the pore size distribution after pulverization of the PACs. The high percentage of mesopore volumes of the wood-based (BG-HHM) and coal-based (COL-PL60-800) SPACs could indicate that they may have an inherent advantage over coconut-based (WPC) SPAC in adsorbing MC-LR, which due to its large molecular size can only access mesopores.

3.2 Introduction

Activated carbon adsorption is widely used in drinking water treatment in the forms of PAC and GAC. However, both technologies have certain limitations; GAC requires a fixed bed contactor and, requires a substantial contact time to reach its maximum capacity for target adsorbate. GAC contactor efficiencies can also get impacted by preloading and long service times (Westrick et al., 2010). PAC, on the other hand, provides a more flexible treatment method since it does not necessarily require specialized infrastructure and theoretically can be applied directly at any point of the treatment provided that there is a particle removal step following PAC application (Najm, Snoeyink, & Richard, 1991). However, with short PAC-water contact times, the full capacity of PAC for target adsorbates will remain unused. Furthermore, competition of background organics such as natural organic matter (NOM) and algal organic matter (AOM) during algal blooms decreases the adsorption rates and capacity of PAC for target adsorbates as well (Huck & Sozanski, 2011).

In the past decade, several studies attempted to further decrease the particle size of PAC in order to achieve faster adsorption rates to overcome the aforementioned limitations. These attempts resulted in the development of a new type of activated carbon known as super-fine PAC or SPAC. SPAC median size (d50) is typically within 0.6-1.2 µm (Partlan et al., 2016), such small sizes provide substantially faster kinetics compared to PAC, which made SPAC a promising experimental adsorbent for removal of a variety of micropollutants including synthetics organic compounds (SOCs) (Partlan et al., 2020), NOM (Matsui et al., 2004), taste and odor compounds (Matsui et al., 2012, 2013; Pan et al., 2016), and micropollutants such as pharmaceuticals (Bonvin et al., 2016). SPAC also presented higher capacities for high molecular weight (MW) organic matter (Ando et al., 2010). These improvements attracted a lot of attention to SPAC and motivated researchers to study the potential of SPAC as a replacement for conventional PAC in water treatment processes.

SPACs are not currently commercially available; thus, they are produced by pulverization of commercially available PACs. This process typically relies on a mill as the means of pulverization. Unfortunately, there is no current standard procedure available for the milling of activated carbon. However, several studies were done on SPAC over the past decade; therefore, limited information is available on milling methods through these studies (Ando et al., 2010; Matsui et al., 2004, 2013). These studies typically used a wet bead mill to achieve the desired level of pulverization; bead milling consists of intense and high-velocity interaction between grinding material and the product material (Partlan et al., 2016). Wet bead milling introduces a carrier fluid that enhances pulverization by suspending the product material and provides improved contact between grinding and product materials. Using a carrier fluid can also improve product material recovery rates from the mill and protect the material from overheating during milling. The grinding material can also come in different materials, sizes, and shapes. Unfortunately, not many studies have specifically described the milling process being used for SPAC production and simply reported that pulverization was done via a wet bead mill (Partlan et al., 2016). Few studies have described their milling apparatus briefly and reported using a wet bead mill equipped with a recirculation system (Amaral et al., 2016; Partlan et al., 2016). There was also an occasion that a custom-built bead mill was used (Matsui et al., 2004). However, most studies reported using zirconium oxide as grinding material in the form of beads or balls and ultrapure water as the carrier fluid (Amaral et al., 2016; Matsui, Aizawa, Kanda, et al., 2007; Matsui et al., 2006; Partlan et al., 2016).

Dry milling was also evaluated for pulverization of PAC, dry milling systems use gas or steam as the carrier fluid and provide faster grinding rates, and storage footprint, and lower the chance of product contamination by the grinding material (Pan et al., 2016). However, the same study found that the wet-milled SPAC was

superior to dry-milled SPAC in terms of adsorption rate and capacity for taste and odor compounds (geosmin and 2-MIB). The lower capacity of dry-milled SPAC is postulated to be from the fact that activated carbon is more prone to oxidation during the dry milling process. Furthermore, from the production and storage aspect, the dry-milled SPAC showed more aggregation compared to wet-milled SPAC during production. The dry fine SPAC particles could also become airborne and pose a health hazard as particulate matter. Furthermore, at large scale dried powdered activated carbon could adsorb oxygen in a fast rate and pose the risk of suffocation in confined storage conditions.

In the absence of a standard procedure and the difficulty of accessing specialized equipment, the determining parameters would be milling intensity/speed and time. Some milling systems allow the adjustment of milling intensity, although these adjustments are not standardized among different types of mills. Thus, it would be easier to set the intensity to maximum and determine the optimum milling time via trial and error to achieve the desired particle size distribution (PSD). The determined milling time will be unique to each type of as received PAC, since the initial PSD and abrasion resistance is different between different PACs. Abrasion resistance is an index for the hardness of particles and directly affects particle breakdown rate during milling (Partlan et al., 2016).

In theory, reducing the particle size of activated carbon could improve adsorption rates as a result of increased active external surface area (Najm et al., 1990). Several studies have successfully achieved significantly improved adsorption rates by reducing the particle size of commercially available PACs to 0.6 to 1.2 µm range (Amaral et al., 2016; Ando et al., 2010; Bonvin et al., 2016; Heijman et al., 2012; Matsui et al., 2004, 2005). These studies pulverized the as received PACs with median sizes ranging from 10 to 33 µm; the produced SPACs' median size ranged from 0.6 to 1.21 µm. The robust bench-scale bead mills combined with a recirculation system allow even further pulverization to particle sizes as small as 0.14 µm, which is referred to as sub-micron SPAC (SSPAC) (Pan et al., 2017). However, studies that produced and evaluated SSPACs found that over pulverization of activated carbon particles can have adverse effects on their capacity for certain compounds (Pan et al., 2017). Takaesu et al. (2019) successfully increased the capacity of as received PACs by reducing the median diameter of particles to 0.8-1 µm (SPAC size) for 2-MIB and geosmin by almost 40%. However, the capacities decreased after further reduction of the median particle size to 0.14 to 0.3 µm (SSPAC size). The authors established a correlation between the capacity of activated carbon and the presence of oxygenated and acidic functional groups on the surface of PAC particles. The study suggests that long milling times and over pulverization of activated carbon to SSPAC increases the oxygen content of activated carbon and hence decreases its capacity for certain hydrophobic compounds due to a decrease in hydrophobicity of the activated carbon surface. Pan et al. (2017) also

reported that SSPAC with a median size of 0.14 μm has a lower 2-MIB capacity compared to the SPAC with particle sizes around 1 μm due to surface oxidation during micro-milling. Thus, it can be concluded from past studies (summarized in Table 2.2) that a median particle size of 0.8 to 1.2 μm seems to be a candidate optimum size; since this size range provides maximum capacity and kinetic rates for a large variety of adsorbates and is also reasonably achievable by a variety of available milling technologies. In this study, the target median SPAC size was set to approximately 1 μm.

Dynamic light scattering (DLS) is widely adopted in the literature for analyzing the particle size distribution of the pulverized and as received PACs. DLS uses a temporal autocorrelation function of scattered light or laser signals over time to calculate the size distribution of the particles. These signals are the result of the interaction of each particle with its surrounding particles caused by its Brownian motion (Coe et al., 2015). Scanning electron microscopy (SEM) is also used in the literature to study the morphology of the particles, analyzing pore structure, and occasionally determining particle size distribution as an alternative to DLS.

Although, the dynamic light/laser scattering and diffraction methods are widely used for PSD analysis of PAC and SPAC in the literature, these methods have some known shortcomings when it comes to PSD analysis of certain materials, a few examples are that the (1) size distribution calculations using the Brownian motion monitoring of the particles are based on the assumption that all particles are perfect spheres which is only the case for the manufactured reference material and not true for pulverized PAC particles, (2) many of the DLS instruments are designed for analysis of specially manufactured nanomaterials in narrow size ranges from 0.1 to 10 microns and are not suitable for samples with wider size distributions such as PAC and SPAC. There are specialized instruments (such as Malvern Mastersizer) which are able to analyse samples with wider size distribution by combining both light scattering and laser-diffraction methods. But these instruments are not always easily accessible. (3) Particles are prone to agglomeration while suspended in the carrier fluid, and this agglomeration can remain undetected in light scattering and diffraction methods and can alter the results of the analysis. Furthermore, fast industry standard methods such as laser diffraction are not always readily available for determination of PSD of powdered material such as PAC and SPAC. Optical and scanning electron microscopes on the other hand can be often found as standard instruments in research and academic setups. SEM imaging could be a very accurate method since it can scan the particles at different magnifications, and their actual diameter can be measured. Agglomerated particles can also be detected and excluded from the results. Optical microscopes and SEM combined with static image analysis (SIA) can be very useful in terms morphology analysis of the particles in addition to particle counting and measuring (Tinke et al., 2005). However, determining the settings during the SEM imaging (i.e. magnification, type of image, and contrast) and the details of the SIA

method should be tailored to the material being analysed. The implementation of SEM imaging combined with SIA is specific to the type and size of material along with the type of images used, and the quality of the images generated by the instrument. Therefore, there is no "one suits all" methodology available when it comes to PSD determination of various powdered materials. SIA is a general methodology for analysis of images acquired by different means (i.e. optical or electron microscopy, normal photography, etc.) for detection, counting, and characterization of the objects in images. Consequently, a specific method must be developed by applying SIA principles for determination of particle sizes of SPAC that is PAC particles after pulverization using SEM images. The developed method must determine the optimum magnification for imaging the samples and hence the lower and higher limit of range the analysis.

..

Considering the advantages and disadvantages of the methods mentioned above and the availability of instruments at the time when the research was conducted, the SEM imaging method along with SIA was chosen as the PSD analysis method for this research. The objectives and subobjectives of this study are therefore as below:

1) Prepare SPACs by wet milling of commercially available PACs
   a) Prepare SPACs by pulverizing commercially available wood-based, coal-based and coconut-based PACs via wet bead-milling (preferentially using a commercially available mill without modifications).
2) Determine particle size distribution of the prepared SPACs
   a) Develop a method to prepare SPAC samples for SEM analysis (i.e. determination of suspension fluid, additives, and base material for fixation of samples for imaging)
   b) Develop a method to determine the appropriate magnification for imaging
   c) Develop and finetune a static image analysis method for obtaining particle size distributions by analysing SEM images.
3) Determine the physiochemical properties of SPACs
   a) Measure internal surface area and determine the pore size distributions of prepared SPACs via Brunner-Emmett-Teller (BET) and density function theory (DFT) methods, respectively.
   b) Determine the zero point of charge of SPAC samples via mass titration method.

3.3 Materials and methods

3.3.1 PACs and pulverization procedure

BG-HHM (wood-based) and WPC (coconut-based) powdered activated carbons were donated by Calgon Carbon (PA, USA) at no charge. COL-PL60-800 (coal-based) PAC was provided by Activated Carbon Corporation (NY, USA). A McCrone micronizing mill (Glen Creston, London, UK) with agate grinding materials was used for pulverization of the as received PACs in the Earth Sciences Department at the University of Waterloo.
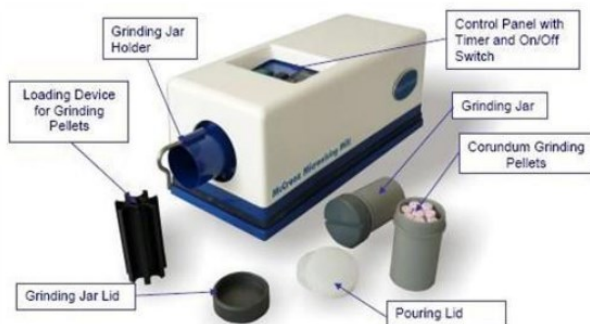
Figure 3.1 McCrone micronizing mill

Figure 3.2 Agate grinding material used in this study

The pulverization procedure was as follows: 100 milligrams of each carbon were diluted into 5 mL of Milli-Q water in the milling jar prior to pulverization. The McCrone micronizing mill came with constant milling intensity; thus, the only controlling parameter in the final size distribution of carbon particles was the milling time. Each PAC sample was pulverized for 60 minutes; after pulverization, the slurries were poured out of the milling jar into a vial, and the jar was washed out with an additional 20 mL of Milli-Q water which was also added to the vial to maximize recovery. The final nominal slurry concentration for each carbon was 0.1 mg of carbon in 25 mL of Milli-Q water. However, the actual concentration was probably substantially less, since the carbon particles can easily get trapped inside the jar and in between milling rods and was not recoverable.

3.3.2 Particle size distribution

SEM image analysis was chosen as the main method of PSD determination during the development of SPACs, mainly because of its availability and because other specialized instrumentation were either not available or, in the case of DLS, did not cover the required particle size range. The development of this

method is thoroughly discussed in Section 3.4.1, and the finalized method is explained in the remainder of Section 3.3.2.

3.3.2.1 Particle size distribution determination of parent PACs via laser diffraction

The parent PACs seem to have a broad size distribution based on the preliminary SEM images. The attempts to determine the PSD of PACs showed that the SEM imaging method could be laborious and time-consuming due to the very high number of particles that should be measured to achieve a distribution with 95% confidence for such broad distributions. Therefore, the PSD of the as-received PACs were determined by laser diffraction via Malvern Mastersizer 3000 (Malvern Panalytical, Spectris, United Kingdom) at an external lab at a later time during this study.

3.3.2.2 Sample preparation for SEM analysis

The sample preparation method adapted from Mazzoli & Favoni (2012) is described as follows. Samples were prepared by diluting 1 mL of slurry in 20 ml of isopropanol alcohol followed by the addition of 50 µL of Triton X-100 (Sigma Aldrich, USA) as a surfactant. Next, the suspension was placed in a sonification bath for up to 30 minutes to prevent agglomeration. Next, 2 ml of the prepared solution was filtered through an Isopore™ polycarbonate membrane with a pore size of 0.45 µm (MilliporeSigma) and left in a case at room temperature until completely dried. The Isopore membranes have a smooth glossy surface designed for both optical and electron microscopic imaging, which makes them suitable for this type of analysis. The prepared membranes were then cut and placed on stubs and gold-coated prior to loading them into the SEM vacuum chamber for analysis.

3.3.2.3 SEM analysis

FEI Quanta FEG 250 ESEM was used for analyzing samples at WATlab, University of Waterloo. High vacuum mode was used for analysis since PAC samples were sufficiently conductive after gold coating. A beam voltage of 20 kV was used for analysis, and the beam spot was set to 3.5. The magnification chosen for pulverized PACs was 2000x. This magnification was chosen using criteria, which were developed based on ISO 13322-1 (ISO 13322-1, 2014). The sample stub was divided into multiple zones based on the magnification, and the images for both secondary electrons (SE) and backscattered electrons (BSE) were saved for morphological analysis and sizing purposes, respectively. The BSE images were taken with maximum contrast to facilitate image analysis later. The developed method for sample preparation, the determination of suitable magnification, sample sub-zones for imaging and particle counting, and diameter measurement is thoroughly discussed in the next Section.

3.3.2.4 Image processing and analysis

Images were analyzed using the open-source image processing software ImageJ (Rueden et al., 2017). Images were calibrated using the scale bar, and particles were measured automatically using the thresholding method and occasionally manually for result confirmation. The automatic image analysis method was developed based on the recommendations and criteria provided in ISO 13322-1 (ISO 13322-1, 2014).

The BSE images were first preprocessed by ImageJ software, starting by adjusting the contrast and brightness to ensure that captured particle images stand out from the background. Next, the images were calibrated using the scale bar produced by the SEM instrument, so that pixels can be converted to μm. For this purpose, the "set scale" function from the "Analyse" toolbox was used. The scale bar is measured in pixels via the measuring tool and the known distance is entered for the number of measured pixels thus converting the pixels to SI units, which in this study is microns. For the images to be analysed by the image analysis methods, they should be segmented. Segmentation is a process to determine the pixels in the image that belong to the foreground objects, in this case carbon particles (ISO 13322-1, 2014). In order to achieve segmentation, the thresholding method was used over edge detection. The thresholding method assigns (grey-value) intensities to pixels in a greyscale image. All the pixels with intensities below the set threshold will be considered as background pixels and the pixels with intensities above the threshold will be considered as foreground objects. The ImageJ adjust threshold function requires a binary image thus all images were converted to 16-bit grayscale images prior to adjusting the pixel thresholds. Next the threshold was adjusted via "adjust threshold" function of ImageJ (Figure 3.3).

31
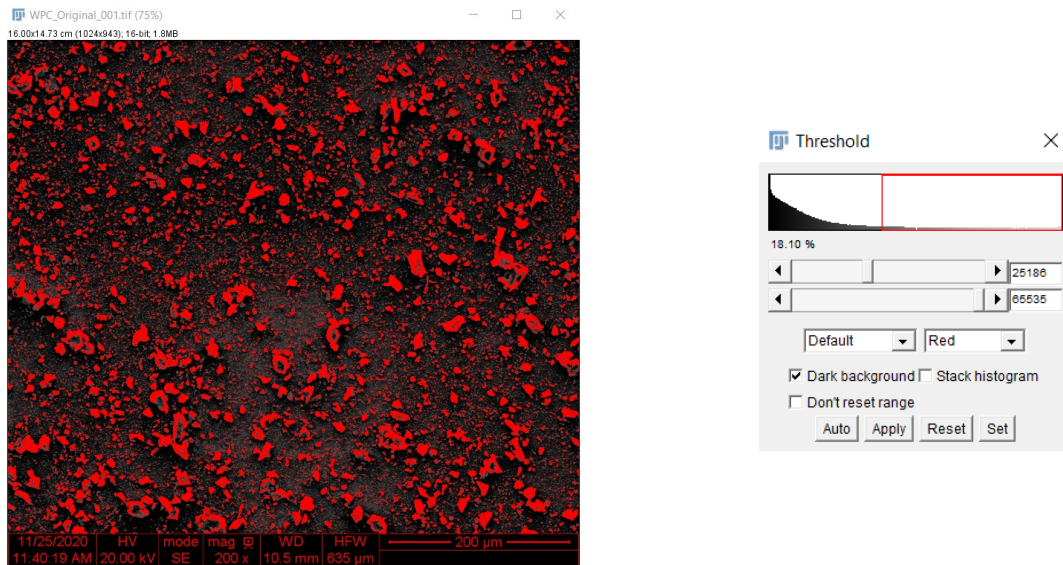
Figure 3.3 Adjusting threshold for segmentation of pulverized coconut-based SPAC

Next, the "Analyze particle" feature of ImageJ was used for the measurement of the particles in each image. The options "include holes" and "exclude edges" were used to ensure inclusion of all whole particles and excluding the particles that are cut-off by the edges of the frame (Figure 3.4). The results were saved for each processed image.
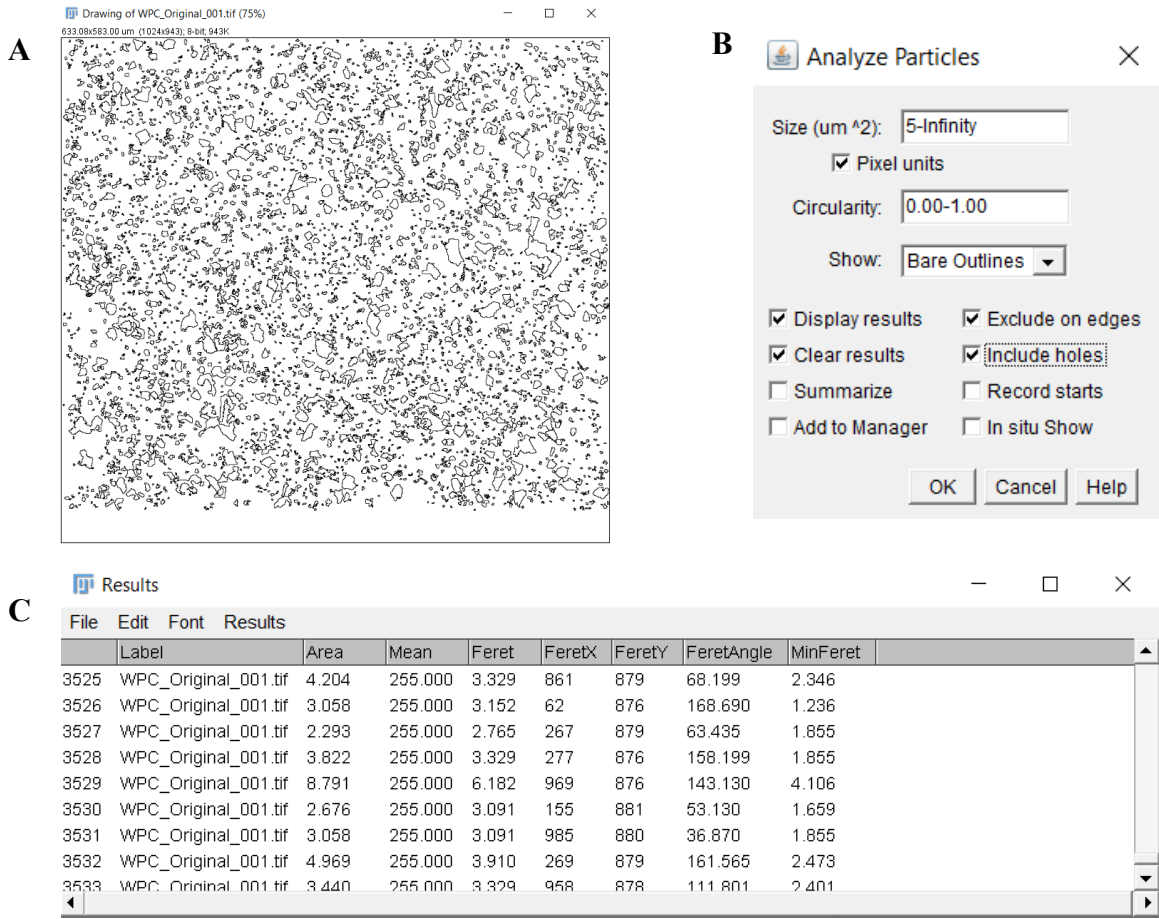
Figure 3.4 Analysing particle via ImageJ; (A) the analysed image (particles are outlined) (B) algorithm variables for analysing particles (i.e. size range in terms of pixels, circularity index, excluding particles on edge, etc.)

The resulting data were processed to determine the median of the length of all detected particles, which would translate to d50 of the sample, and cumulative distributions plots were produced by the Seaborn module (Waskom, 2021) in Python.

3.3.2.4.1 Determining the optimum magnification

In order to determine the proper magnification an image with the lowest magnification possible, providing that the largest particle in the sample fits in the frame, was taken from the sample. Next, the image was calibrated via the scale bar of the image, and the Feret diameter (distance between two parallel tangents on opposite sides of the image of a particle) of the largest visible particle was measured. After determining the largest particle diameter in the sample, the magnification of the image was adjusted to set the dimensions of the field of view (width and height of the image) 6 times larger than the maximum diameter to ensure that the largest particles of the samples are included in the analysis (Figure 3.5).

According to ISO 13322-1 the theoretical limit to the number of pixels per particle is one pixel. However, since the uncertainty of particle sizes will increase with low resolutions, the lower size threshold of the analysis should be adjusted such that the smallest particles included in the analysis has a projected area with a sufficient number of pixels (Figure 3.6). A limit of 6 pixels per particle is set as the lower limit of sizes detected. The 6 pixels will assure that the shape of the particle can be defined properly (Figure 3.6). Once the pixels are converted to SI units, the lower limits is reported in microns. The detected particles/objects with sizes below 6 pixels are considered as noise and omitted. Though it is worthy to mention that if the magnification is not correctly adjusted a substantial number of valid particles might be omitted as noise.
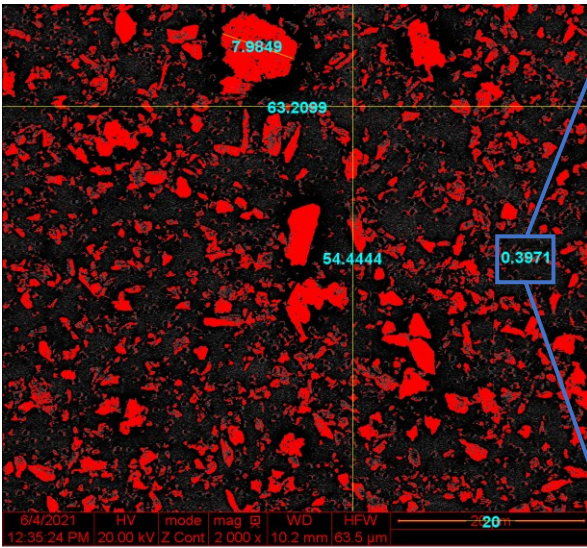
Figure 3.5 Determining largest particle in the sample and adjust the field of view at least 6 times larger: $6 \times 7.9 = 47.4 \leq 63.2 \ \& \ 54.4$
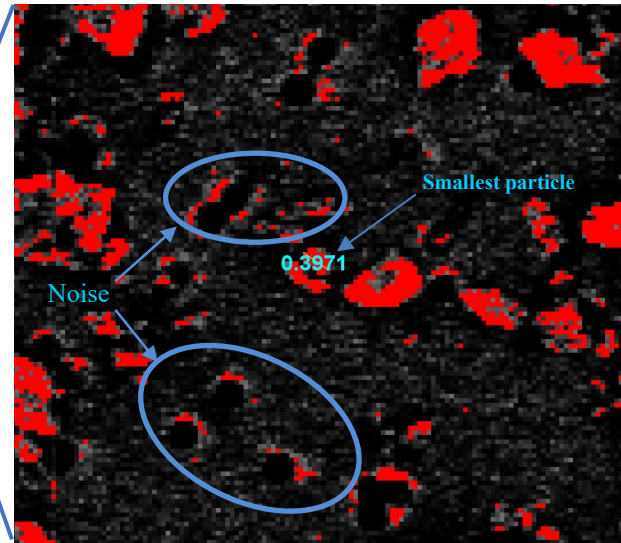
Figure 3.6 Determining the smallest particle in the sample with a sufficient number of pixels effectively setting a lower threshold to 0.397 μm

Based on the criteria above and the preliminary SEM images, the magnification of 2000x was chosen to analyse the SPACs in this study which would set the lower and higher boundary of the particle size ranges provided by this method to 0.4 and 40 μm, respectively. However, this magnification is specific to the material prepared in this study (SPACs), and determination of the optimum magnification for other type of material with different size ranges using the criteria provided and preliminary imaging is strongly recommended.

3.3.2.4.2 Number of particles to be counted for sufficient accuracy

To achieve an adequately accurate particle size distribution within defined levels of accuracy and confidence intervals, it is necessary to estimate the minimum number of particles to be counted and

measured. Therefore, such a method was developed by Masuda & Gotoh (1999), Wedd (2001) and Yoshida et al. (2009), and adapted by ISO 13322-1 (2014) and was used in this study to estimate the number of particles that need to be measured to achieve a size distribution with a specific confidence. The number of particles (n^*), is the estimated number of particles that should be sampled to achieve a mean diameter measurement within δ relative error with probability of P. Masuda & Gotoh (1999) have described a method for calculating the minimum number of particles to be counted n^* for the cases that relative error δ and probability P are given. The method uses an intermediate parameter u defined by the probability P:

$$\Phi(-|u|) = \frac{1 - P}{2} \qquad (Equation\ 3.1)$$

where Φ is a cumulative distribution function of the standard normal distribution. The values of u for most common probabilities P are given in Table 3.1.

Table 3.1 u(P) for some typical probability values above P = 50 %
(Values below 50 % are too low for the confidence level) adopted from ISO 13322-1

$P(\%)$	50	68.3	75	80	90	95	97.5	99	99.5	99.8	99.9
u	0.67	1.00	1.15	1.28	1.64	1.96	2.24	2.58	2.81	3.09	3.29

In the next step, the standard deviation (s) of the population diameters is needed. Assuming log-number distribution by number, it can be derived from 84th and 50th sample percentile diameters via Equation 3.2 below:

$$s = ln(s_g) = ln(x_{84.0}) - ln(x_{50.0}) \qquad (Equation\ 3.2)$$

The parameter s_g represents the geometric standard deviation of the sample, which characterizes the width for log-normal distributions independent on the weighting method for the diameter and ln is the natural logarithm.

With the standard deviation, s, calculated and value of u for the given probability from Table 3-1 (e.g. $u = 1.96$ for the $P = 95\%$ probability level), the interim parameter ω can be calculated via Equation 3.3:

$$\omega = u^2 \alpha^2 s^2 (2c^2 s^2 + 1) \qquad (Equation\ 3.3)$$

while

$$c = \beta + \frac{\alpha}{2}$$

Where α, β are constants defined based on the type of the mean diameter to be measured and they can be found in table 3-2. In this study the mean volume diameter with $\alpha = 3$ and $\beta = 0$ was chosen for calculation of $n *$.

Table 3.2 Parameters α and β for different diameter types (adapted from ISO 13322-1)

Type	α	β
Mass median diameter	6	0
Sauter diameter (mean volume-surface diameter)	5	0
Mean volume diameter	3	0

With all of the parameters determined it is now possible to substitute ω and the relative error δ (e.g. $\delta = 0.0316$ for 3.16% relative error)

$$n^* = \omega\delta^{-2}$$

(*Equation* 3.4)

For this study, since the log-normal distribution of the samples are unknown at the beginning, an iterative approach was taken. About 60 images were taken and analysed for each sample to establish a preliminary log normal distribution and to calculate 84th and 50th percentile diameters, next the number of particles, n^*, was calculated for each population. Additional samples were prepared based on the new n^* until a satisfactory number of particles, i.e. exceeding the minimum calculated value, were measured.

3.3.2.4.3 Flow chart describing the image analysis procedure in this study

```
                         ┌─────────────────┐
                         │      Start      │
                         └─────────────────┘
                                  │
                                  ▼
                         ┌─────────────────┐
                         │ Determine the   │
                         │ optimum         │
                         │ magnification   │
                         │ via preliminary │
                         │ images          │
                         └─────────────────┘
                                  │
                                  ▼
                         ┌─────────────────┐◄──────────────┐
                         │ Diluting sample │               │
                         │ in the          │               │
                         │ suspending      │               │
                         │ liquid          │               │
                         └─────────────────┘               │
                                  │                         │
                                  ▼                         │
                         ┌─────────────────┐                │
                         │    Sonication   │                │
                         └─────────────────┘                │
                                  │                         │
                                  ▼                  ┌──────────────┐
                         ┌─────────────────┐         │ Increase     │
              ┌─────────►│ Filtration and  │         │ suspending   │
              │          │ drying of       │         │ volume to    │
              │          │ sample fixed on │         │ dry sample   │
              │          │ membrane        │         │ ratio        │
              │          └─────────────────┘         └──────────────┘
              │                   │                         ▲
              │                   ▼                         │
              │          ┌─────────────────┐                │
              │          │ Divide sample   │                │
              │          │ into zones and  │                │
              │          │ take one SEM    │                │
              │          │ image per zone  │                │
              │          └─────────────────┘                │
              │                   │                         │
              │                   ▼                         │
              │              ◇─────────◇                    │
              │            ◇ Number of   ◇   Yes            │
              │           ◇ touching      ◇──────────────────┘
              │           ◇ particles are ◇
              │            ◇ more than 20% ◇
       ┌──────────────┐     ◇ of total   ◇
       │ Include more │       ◇─────────◇
       │ zones per    │            │
       │ samples -    │            ▼
       │ possibly     │     ┌─────────────────┐
       │ prepare      │     │ • Process images│
       │ additional   │     │   and measure   │
       │ samples to   │     │   particles     │
       │ cover more   │     │ • Determine     │
       │ particles    │     │   number of     │
       └──────────────┘     │   particles (n) │
              ▲             └─────────────────┘
              │                      │
              │                      ▼
              │             ┌─────────────────┐
              │             │ Calculate the   │
              │             │ number of       │
              │             │ particles needed│
              │             │ for accurate    │
              │             │ size distribution│
              │             │ analysis (n*)   │
              │             │ from the log-   │
              │             │ normal distrib. │
              │             └─────────────────┘
              │                      │
              │                      ▼
              │                 ◇─────────◇
              │         Yes    ◇  n << n*  ◇
              └────────────────◇           ◇
                                ◇─────────◇
                                     │ No
                                     ▼
                            ┌─────────────────┐
                            │ Store results   │
                            │ and establish   │
                            │ the log-normal  │
                            │ distribution    │
                            └─────────────────┘
```

3.3.3 Internal surface area and pore size distribution

The internal surface areas of PACs and SPACs were measured via Breuner-Emmette-Teller (BET) method at McGill University and the Nanotechnology department at the University of Waterloo, respectively. Pore size distribution and volumes were also determined by the density functional theory (DFT) method. The calculations for the DFT method were done via the PyGAPS module (Iacomi & Llewellyn, 2019) in the Python programming language.

3.3.4 Determination of zero point of charge

The method for determination of zero point of charge (pH_{pzc}) of parent PACs are adopted from Fiol & Villaescusa (2009). The method consists of dosing the PACs into a 0.03 M KNO_3 solution in concentrations in the range of 5 to 100 g/L in 30 mL vials. The vials were then agitated on an orbital shaker at 250 rpm for 24 h in order for the pH of the solutions to reach equilibrium. The equilibrium pH of the solution in each vial was then measured and plotted against the concentration of the PAC. The pH_{pzc} is the pH at which a plateau is reached in the equilibrium pH curve. However, the mass titration method requires a significant amount of activated carbon per titration, and only a limited amount of each SPAC was produced by bead milling due to the low capacity of the mill jar and the time required for each milling session (production of 1g of each SPAC took approximately 10 hours (100 mg per milling session)). Therefore, zero point of charge could not be determined for the produced SPACs.

3.4 Results and Discussion

3.4.1 Method development for determination of particle size distribution via SEM imaging

3.4.1.1 Sample dispersion method and support material

In the first attempt to determine PSD of SPAC samples via SEM, the SPAC slurries were dried at 105°C and the powder was fixed onto conductive carbon adhesive by dipping the adhesive onto dry powder and remove the excess sample by shaking so a layer of powder would form on the adhesive. The activated carbon is also a relatively conductive material; therefore, gold coating was not required for this method. An example of images acquired by this sample preparation method is presented in Figure 3.7A. Although the quality of the produced images is high and sizes of the visible particles can be measured manually, there is substantial particle overlap and touching as result of direct fixation of SPAC particles onto the carbon adhesive, and the resulting overlapping of particles makes automatic image analysis impossible. Furthermore, the surface of the carbon adhesive is highly porous, and particles were trapped within these

pores thus making the distinction of the background (carbon adhesive) and individual particles difficult. This makes the image processing with SIA inaccurate. According to ISO 13322-1 (2014), less than 20% of the particles in single image should be touching/overlapping for the SIA to be accurate.

In order to address the particle overlapping and background distinction issue, a dilute slurry was made by dispersing 4 mg of SPAC powder in 30 ml of ultrapure water under constant mixing and sonication, 50 µL of Triton X-100 was also added to the solution as surfactant to prevent particles from further agglomeration. A drop of the dilute slurry was added to the surface of a clean silicon wafer as the sample support material. Silicon wafers have a very smooth surface and are highly conductive, therefore, it facilitates the visual distinction of background (in this case silicon wafer) and SPAC particles. Although, this sample preparation method provided higher image clarity and quality (Figure 3.7B) over the direct fixation of particles onto carbon adhesive, and the number of touching particles were significantly reduced as the result of sonication and presence of a surfactant, larger particles still tended to agglomerate, which caused a substantial overestimation of particle sizes, when automatic SIA processes such as thresholding were performed on the images. Furthermore, the back scattered electron (BSE) images, which are more suitable for SIA via thresholding due to their higher contrast, were not very clear and led to problems with the thresholding algorithm due to a halo effect around the particles. The halo effect is caused by the substantial difference in atomic number of silicon and activated carbon, the material with higher atomic numbers appear brighter in BSE images whereas the material with lower atomic number appear darker. In this case silicon has a higher atomic number compared to carbon, which caused the background to appear brighter than SPAC particles in BSE images (Figure 3.7B*)*.

After further research, a sample preparation method was adapted from Mazzoli & Favoni (2012) which was used by the authors to prepare airborne dust particles of wood for SEM imaging and PSD determination. The method consists of dispersion of the particles in isopropanol alcohol (IPA) as a suspending liquid followed by vacuum filtration of the solution through 0.45 micron Isopore™ polycarbonate membranes which is described in detail in Section 3.3.2.2. The Isopore membrane features a smooth and glossy surface making it suitable for optical and electron microscopy purposes. The vacuum filtration process also ensures proper dispersion of the particles and evaporates the IPA quickly, reducing the drying time substantially. The polycarbonate membrane is non-conductive; blocking the path to ground, therefore, the samples needed to be gold-coated prior to analysis to ensure proper image quality. This sample preparation method provided satisfactory results in terms of particle dispersion and adequate contrast in BSE images (Figure 3.7C) and was used for PSD determination of SPACs in this study.
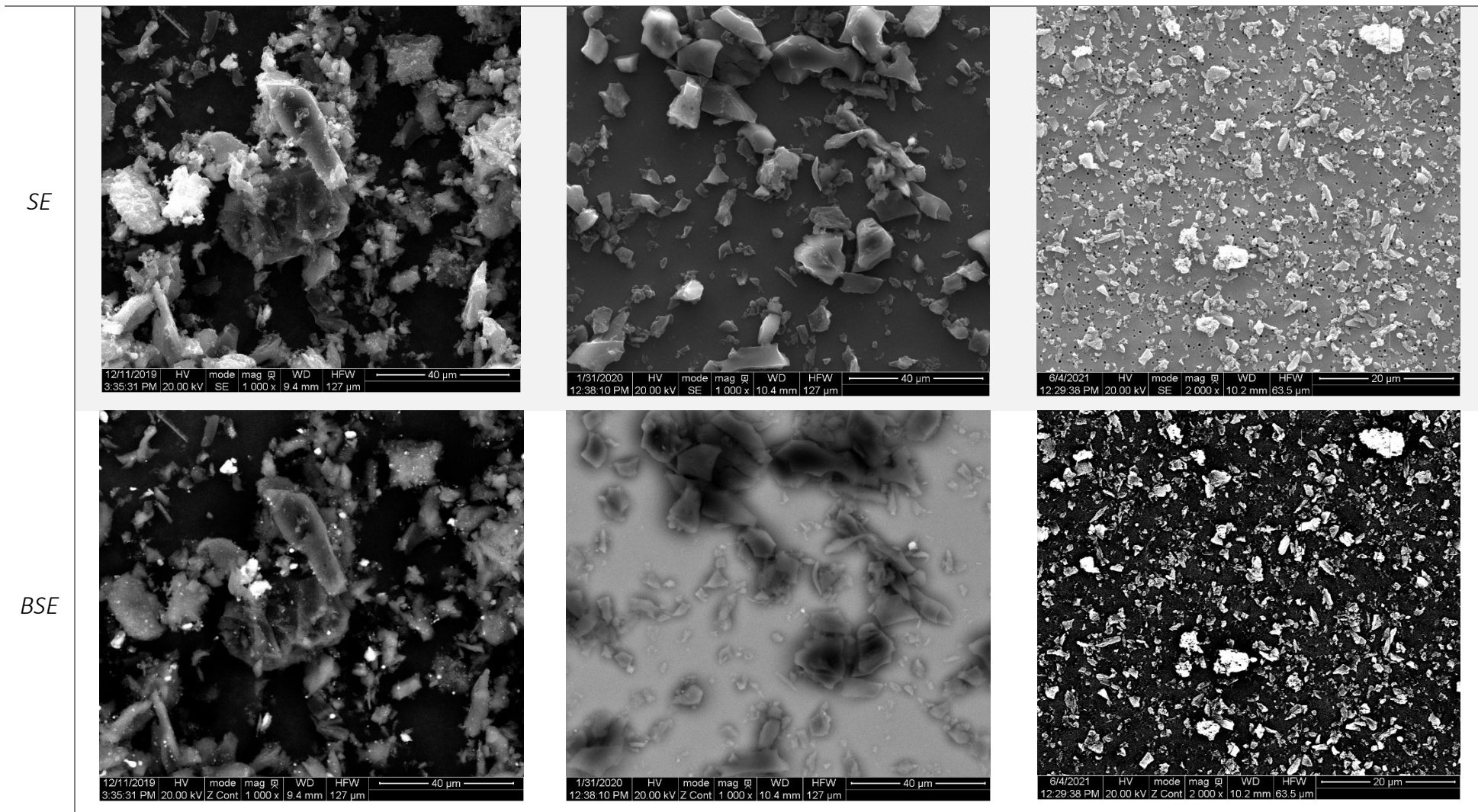
Figure 3.7 Comparison of different sample preparation methods for SEM imaging: both secondary electron (SE) and backscattered electron (BSE) images are presented.

41

3.4.1.2 Magnification and static image analysis method

After establishing the suitable sample preparation method, samples on SEM stubs were virtually divided into multiple zones and images were taken for each zone to be analysed via SIA. However, determination of an appropriate magnification proved to be challenging for a material such as PAC and SPAC due to their broad particle size range. At the time of writing no specific method for determination of PSD of SPAC or PAC via SIA and SEM imaging was available. Therefore, there are no specific guidelines available for adjusting the magnification for materials with such wide distribution and literature have mainly covered the analysis of synthetic nanomaterial with uniform shapes and size distributions. At lower magnifications large particles in the sample are counted and measured with ease, though, very small particles in the sample were difficult to detect and measure due to the low resolution of the image. On the other hand, at higher magnifications more of the smaller particles can be included in the total population. However, imaging entire large particles will become more difficult. ISO 13322-1 also requires particles that are cut off at the edge of the image (incomplete particle projection) to be omitted from the analysis. To summarize, lower magnification images will result in a size distribution biased towards larger sizes and higher magnification images will result in a size distribution biased towards lower particle sizes. Preliminary work using images at 2 different magnifications produced multimodal distributions, which based on current literature were unlikely and this approach was not further pursued. To address this issue a set of criteria was developed to determine a specific magnification based on the size distribution of each sample, which is explained in detail in Section 3.3.2.4.1. The developed criteria ensures that large particles can be imaged entirely by setting magnification properly. The set magnification should also cover the smallest particles as well, this was achieved by setting the lower threshold size of the analysed particles to 6 pixels, the filtration of the samples through 0.45 micron Isopore^{TM} membrane also helps with adjusting the lower boundary of size of the analyzed particles by removing very fine particles in the sample. Based on the preliminary images and the developed criteria in Section 3.3.2.4.1, the magnification of 2000x was chosen for analysis of all prepared SPAC samples. This magnification provided a field of view which would cover all the large particles since it provides a field of view 6 times wider than the diameter of the largest particle in the sample. At the 2000x magnification, the smallest visible particles had the minimum projected area of 6 pixels or 0.02 μm^2 ensuring that the small particles are included in the measured population and noise (detected objects with projected area less than 6 pixels) is removed.

As stated earlier, SIA is general method for analysis of objects in static images. Therefore, since SIA is not applied to SPAC PSD analysis before, the SIA method must have been finetuned to characteristics of the

samples in this study. The ImageJ (Rueden et al., 2017) automatic thresholding method was applied to the high contrast BSE images to achieve segmentation of foreground particles and the membrane. The threshold adjusted images were next fed to the "analyze particles" function of the ImageJ software, which gave satisfactory results in terms of Feret diameter measurements of particles in each image. The details of the analysis is thoroughly discussed in Section 3.3.2.3. The number of images that should be analyzed is directly dependent on the number of measurements required for the determination of size distribution with a specific confidence interval, which is explained in Section 3.3.2.4.2. The criterion takes the standard deviation of the particle diameter population and the target confidence level for the log normal particle size distribution as input and provides the number of samples (particles to be measured) to achieve such distribution. This criterion determines the total number of particles that need to be measured and therefore the number of images/sample stubs to be analysed. The method above was developed based on the general guidelines provided by ISO 13322-1 on general use of SIA.

The accuracy of the developed method was verified using reference material namely NIST traceable glass microsphere polydisperse particle standards with size distributions in the range of 0.1-1µm. The certificate of analysis for the polydisperse particle standard is provided in Appendix A.1. The analysis results with the developed method was well within the range of distributions provided by the standard material's certificate. Figure 3.8 compares the PSD determined by the SEM imaging and SIA method developed in this study with the PSDs determined by a variety of methods provided in the certificate. The detailed statistical report for the analysis of the polydisperse particle standard is also provided in Appendix A.2. The results from the analysis of the standard material indicates that the developed method for determination of particle sizes in the range of 0.1 to 1.2 µm fits well within the range of the PSDs obtained by other methods and is close to the reference SEM results.
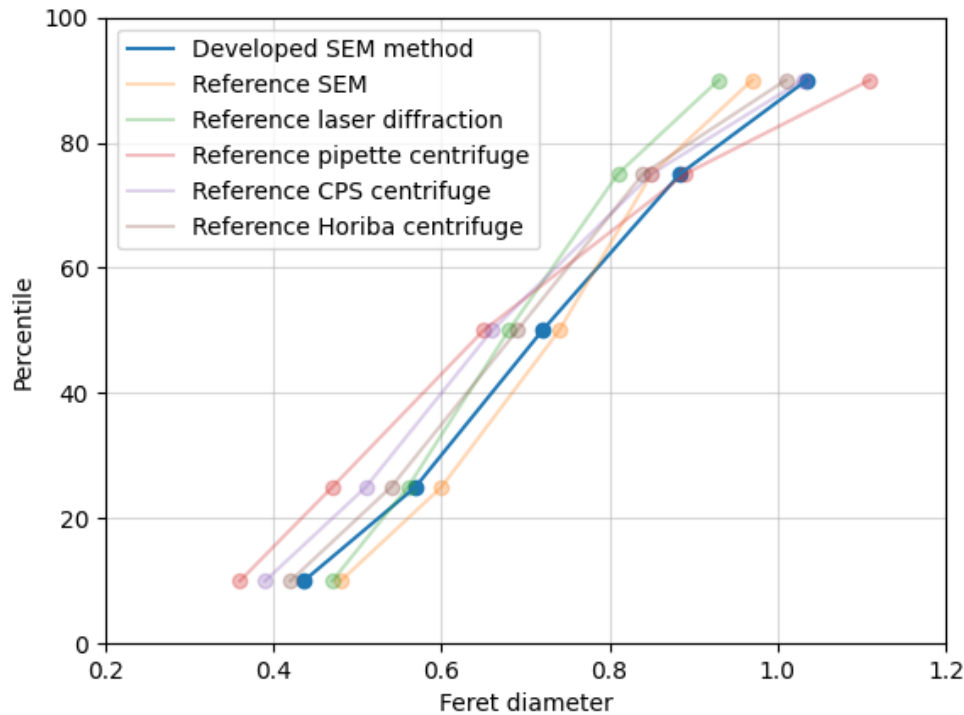
Figure 3.8 PSD of polydisperse particle standard using the developed SEM and SIA method compared to PSDs provided by the material's certificate of analysis

3.4.2 Carbon Properties

3.4.2.1 Size distribution of produced SPAC via SEM imaging

The developed PSD determination method via SEM imaging was used to determine the size distribution of the produced SPACs. The preliminary results showed that pulverization of PACs via the micronizing mill, even at the shorter times of 10 minutes, could reduce particle sizes substantially from median sizes in range of 19-27 µm to 2.5-4.3 µm. With longer pulverization times of 20, 30, and 60 minutes it could be seen that the median particle sizes are decreasing (i.e. determined median sizes for WPC (coconut-based) SPAC at 20, 30, and 60 min of pulverization was 2.4, 1.29, and 1.27 µm, respectively). However, these result show that there is a minimal difference in median particle sizes of samples pulverized for 30 minutes and 60 minutes, indicating that 30 minutes of pulverization could be the point of diminishing returns in terms of reducing the particles size of the PAC. The 60 minutes pulverization time was chosen to pulverize all PACs to ensure a narrower particle size distribution (this was based on visual observation) and was used to prepare all SPACs for subsequent adsorption and coagulation experiments.

Table 3.3 summarizes the PSD distribution and statistics of the three prepared SPACs which were used for the subsequent experiments in this study. For PSD determination of the coconut-based SPAC (WPC), 16885

particles were measured in 59 individual images over two samples prepared. The number of particles measured reached and surpassed the calculated minimum number of particles to achieve an accurate distribution with 95% based on Equations 3.4 of 9886. In terms of the wood-based SPAC (BG-HHM), 24968 particles were measure in 58 individual images over two samples, which also surpassed the calculated threshold number of particles of 21770. For the coal-based SPAC (COL-PL60-800), 13242 particles were measured in 55 individual images in two samples, again surpassing the calculated threshold number of particles of 13242.

Based on the number of measured particles, the cumulative distribution of each SPAC is established and presented in Figure 3.6. The median particles size (d50) of coconut-based (WPC), wood-based (BG-HHM), and coal-based (COL-PL60-800) were determined to be 1.27 μm, 1.33 μm, and 1.20 μm, respectively. The median sizes are very similar among the three types of SPAC produced, which is probably due to the identical milling process and the characteristics of the grinding material. The sample preparation and processing also affect the size distribution by affecting the lower limit of each population. The 0.45 μm Isopore[TM] membrane removes some of the ash and very small particles of the SPAC. However, this would not result in removal of all particles with sizes below 0.45 µm since not all particles in that size range would be able to pass through the pores freely.

The determined median size for prepared SPACs in this study is in the higher range of the targeted 0.6-1.2 µm median size range. These values are slightly higher than the ones reported in the literature for bench scaled prepared SPACs as d50 values are typically within the range of 0.4-1.2 µm (Ando et al., 2010; Bonvin et al., 2016; Matsui, Aizawa, Kanda, et al., 2007; Matsui, Hasegawa, et al., 2009; Murray et al., 2018)

Table 3.3 Particle Size Distribution and statistics of the produced SPACs via SEM imaging method

SPAC	Particle size distribution via SEM imaging (μm)					Number of images processed[1]	Number of particles measured	Number of particles required for 95% confidence based on the distribution of sample[2]
	Min.	25% (d25)	50% (d50)	75% (d75)	Max.			
WPC (coconut)	0.59	1.02	1.27	1.65	21.46	59 (2 samples)	16887	9886
BG-HHM (wood)	0.61	1.03	1.33	1.88	14.43	58 (2 samples)	24968	21770
COL-PL60-800 (coal)	0.59	0.96	1.20	1.60	16.68	55 (2 samples)	21181	13242

[1] **All images were acquired at a magnification of 2000x and analyzed by ImageJ software as per 3.3.2.3;**

[2] **Calculated as per 3.3.2.4.2**

3.4.2.2 Size distribution of parent PACs via laser diffraction

The PSD of PACs was determined by two runs each including 20 measurements, the summary of the results and statistics of the analysis are included in Appendix A.4. The median particle size (d50) of the as-received PACs for coconut-based (WPC), wood-based (BG-HHM), and coal-based (COL-PL60-800) are 27.75 μm, 19.50 μm, and 21.45 μm, respectively. Table 3.4 compares the median size of parent PACs and prepared SPACs and the batch of parent PACs used by Liu (2017).

Table 3.4 Median particle sizes of PAC and SPAC

Carbon	PAC from Liu (2017) original size d50 (average) [μm]	PAC original size[1] (Laser diffraction) d50 (average) [μm]	SPAC size[2] (SEM method) d50 (whole population) [μm]
WPC (coconut)	22.1	27.75	1.27
BG-HHM (wood)	31.9	19.50	1.33
COL-PL60-800 (coal)	45.1	21.45	1.19

[1] Determined experimentally at an external lab (Civil, Geological, and Mining Engineering at Polytechnique Montreal University); [2] Experimentally determined at University of Waterloo labs

3.4.3 Porosity and internal surface area

The BET surface area, DFT total pore volume, and pore size distribution of parent PACs and pulverized SPACs are summarized in Table 3.5. The nitrogen hysteresis plots at 77°K for PACs and SPACs used to calculate BET surface area and DFT pore size distribution are available in the Appendix A.5. The pore volume distribution and cumulative pore volume of PACs and SPACs can also be found in Appendix A.7.

The coconut-based PAC (WPC) had a BET surface area of 1060.34 m^2/g which remained mainly unchanged after pulverization and reduced only by 2.48 m^2/g or by 0.28% to 1057.86 m^2/g. The DFT total pore volume for the as-received PAC was 1.62 cm^3/g. It is worthy of mentioning that an abnormality was detected in the nitrogen hysteresis for coconut-based (WPC) SPAC consisting of a temporal reduction in loading, while relative pressure is increasing (Figure A.3). The abnormality might have been caused by flexibility in the structure of the porous material. The abnormality in hysteresis data of coconut-based PAC caused an incompatibility with the DFT kernel used for calculation of pore size distribution, therefore, the DFT pore volume distribution is not available for this SPAC.

In terms of the wood-based (BG-HHM) activated carbon, the parent PAC had a BET surface area of 1138.16 m^2/g, which was the greatest among the three PACs, however, the surface area was reduced by 15% to 962.3 m^2/g after pulverization to SPAC size. The DFT total pore volume of the wood-based was also the largest with the value of 3.71 cm^3/g which was also reduced by 21% to 2.93 cm^3/g after pulverization. From the pore size distribution, it is evident that most of the pore volume loss was in the mesoporous range.

The coal-based (COL-PL60-800) activated carbon had the lowest BET surface area of 697.59 m^2/g in PAC form, which was reduced by 26% to 513.6 m^2/g after pulverization. The DFT total pore volume for the as-received PAC was 1.29 cm^3/g, which reduced slightly after pulverization to SPAC size (to ?). The pore size distribution of the coal-based PAC and SPAC were similar, with slight differences in pore sizes in the secondary micropore range.

Liu (2017) calculated the molecular dimensions of MC-LR via MarvinSketch chemical editor (ChemAxon, Budapest, Hungary), yielding a molecular size of $2.032 \times 1.259\ nm$, which would indicate that MC-LR would be able to access mesopores but not micropores. Hence, the wood-based (BG-HHM) and coal-based (COL-PL60-800) with higher percentage of mesopore volumes (around 33%) in both PAC and SPAC sizes, would favour the adsorption of MC-LR, that is if there is enough contact time to access the surfaces that are within these pores.

Table 3.5 PAC and SPAC Properties

Carbon	Based material	Type	Bet surface area[1] (m^2/g)	DFT pore volume[2] (cm^3/g)	DFT PORE SIZE DISTRIBUTION[2]			% of pore volume in micropores[2,3]
					Primary Micropores < 0.8 nm (cm^3/g)	Secondary Micropores 0.8-2 nm (cm^3/g)	Mesopores 2-24 nm (cm^3/g)	
WPC	Coconut shell	PAC	1060	1.62	$4.26E^{-5}$	1.6	0.03	98.1
BG-HHM	Wood	PAC	1138	3.71	$1.16E^{-14}$	2.25	1.46	60.6
COL-PL60-800	Coal	PAC	698	1.29	0	0.87	0.42	67.7
WPC	Coconut shell	SPAC	1058	-[4]	-[4]	-[4]	—[4]	-[4]
BG-HHM	Wood	SPAC	962	2.93	$2.71E^{-14}$	1.95	0.98	66.7
COL-PL60-800	Coal	SPAC	514	1.19	$3.47E^{-13}$	0.80	0.39	66.9

[1]The PAC BET surface area was determined experimentally in the department of civil, geological, and mining engineering at Polytechnique Montreal University and the SPAC BET surface area was experimentally determined by nanotechnology lab at the University of Waterloo

[2] The DFT kernel fitting and calculation was applied to N_2 hysteresis data reported by the bet analysis of corresponding samples

[3] Micropores defined as $< 2nm$ in pore width (Rouquerol et al., 1994)

[4] The DFT pore size distribution could not be derived due the abnormal N_2 hysteresis for WPC (coconut-based) SPAC

3.4.3.1 pH point of zero charge

The point of zero charges (pH_{pzc}) of an older batch of three PACs was determined by Liu (2017) via the mass titration method based on Summers (1986). Analysis of the newer batch of PACs with a similar mass titration method Fiol & Villaescusa (2009) showed very close values for the points of zero charge. The values are summarized in Table 3.6.

The pH_{pzc} of the SPACs could not be measured due to limited amount of material available. However, Partlan et al. (2016) studied the effect of bead milling on the pH_{pzc} of 7 different commercial PACs made from a variety of base materials, including bituminous coal, lignite coal, wood, and coconut shell. The study observed a reduction in the pH_{pzc} of all PACs after bead milling with no exceptions. The study measured the pH_{pzc} as a function of milling time. Therefore, PACs from Partlan et al. (2016) with the closest initial pH_{pzc} value to the corresponding PAC in this study were chosen, and the reduction of pH_{pzc} after 1 hour of milling was calculated. The calculated reductions of pH_{pzc} values based on Partlan et al. (2016) were then used to estimate the reduction of point of zero charges for PACs in this study after 1 hour of bead milling. The estimated pH_{pzc} values are also reported in Table 3.6 and the data from Partlan et al. (2016) are included in Appendix A.8.

Table 3.6 Measured points of zero charge for parent PACs and estimated values for the prepared SPACs based on values from Partlan et al. (2016)

Activated carbon	pH_{pzc} of parent PACs Liu (2017)	pH_{pzc} of as received PACs	Estimated pH_{pzc} for 1 hour milled SPACs based on (Partlan et al., 2016)
WPC (coconut-based)	10.1	11.12	10.23
BG-HHM (wood-based)	3.5	4.10	3.01
COL-PL60-800 (coal-based)	10.8	11.30	9.00

The coconut-based and coal-based PACs have pH_{pzc} values above 9, before pulverization while wood-based PAC had a pH_{pzc} below 5. This would indicate that in the typical pH range of 6 to 8 in drinking water treatment scenarios the coconut-based and coal-based PACs would retain a positive surface charge and the wood-based would be negatively charged. The estimated values for pH_{pzc} after pulverization based on Partlan et al. (2016) would suggest that the surface charges would not switch polarity in the typical pH range for drinking water.

3.5 Conclusions

In this study, SPAC was produced from commercially available PACs by bead milling. The effect of pulverization via bead milling on median particle diameter, BET surface area, DFT pore volume, and pore size distribution of three different PACs - coconut-based (WPC), wood-based (BG-HHM), and coal-based (COL-PL60-800) - was assessed. A method for PSD determination via SEM imaging and SIA was developed and evaluated using reference standards and used for PSD determination of the prepared SPACs. The main findings from this chapter are summarized as below:

- The developed SEM imaging method can be an effective method for PSD determination of prepared SPACs, with relatively narrow particle size distribution in the range of 0.4 to 15 microns. Compared to typical DLS methods available with an effective range of 10 to 1000 nanometers, the SEM imaging method can provide better accuracy with samples with broad size distribution while giving valuable information about sample morphology and composition depending on the SEM instrument used. This method provide few recommendations for more accurate PSD determination of SPAC/PAC via SEM imaging other material in similar size ranges.

- The results showed that pulverization via a bench-scale bead mill (McCrone micronizing mill) for a relatively short time of 1 hour could effectively reduce the median particle size of the coal-based, coconut-based, and wood-based PACs to 1.19, 1.27 and 1.33 μm, respectively. Which would classify the prepared activated carbons as SPAC.

- As for the BET surface area, the internal surface area of produced coconut-based PAC remained mainly unchanged after pulverization; however, the wood-based and coal-based PACs experienced reductions in surface area by 15% and 26%, respectively. In terms of DFT total pore volume, wood-based and coal-based PACs again experienced a reduction in pore volume by approximately 21% and 7%. However, the wood-based PAC kept its place as the activated carbon with the highest pore volume after pulverization with a total DFT pore volume of 2.93 cm^3/g. The pore size distribution of wood-based and coal-based SPACs remained mainly unchanged after pulverization. The DFT pore volume distribution could not be determined for the WPC (coconut-based) SPAC due to an abnormality in its nitrogen hysteresis.

- In terms of point of zero charges (pH$_{pzc}$) of PACs, coconut-based and coal-based PACs had zero points of charge values above 9, indicating they would be charged positively, and wood-based PAC had zero point of charge value below 5, indicating that it would be retaining a negative charge in the typical pH range of 6 to 8 in drinking water treatment scenarios.

Overall, the findings in this study showed that bead milling could effectively reduce the median particle size of as received PACs to around 1 μm and affecting the pore size distribution and BET internal surface area of carbons. The developed SEM imaging and SIA method successfully determined the PSD of prepared SPACs.

Chapter 4
MC-LR adsorption by SPACs in ultrapure water

4.1 Introduction

Cyanobacteria, formerly known as blue-green algae, are prokaryote photosynthetic freshwater bacteria capable of producing hepatotoxic cyanotoxins such as microcystin-LR (MC-LR) as secondary metabolites. WHO guidelines have also issued a guideline on MC-LR requiring the maximum concentration of 1 µg/L since 2003 (World Health Organization, 2020), which was widely adapted by several governments worldwide. MC-LR along with other commonly detected cyanotoxins are included in the latest iteration of the USEPA contaminant candidate list (CCL 5). USEPA's health advisory requires MC-LR concentration in drinking water to be below 0.3 µg/L for children under six years old and a maximum concentration of 1.6 µg/L for all other age groups. In Canada, a maximum acceptable concentration (MAC) of 1.5 µg/L was set for MC-LR by the issued health advisory of Health Canada (Health Canada, 2017); this MAC was later applied to total microcystins in the latest iteration of health advisory (Health Canada, 2018).

Cyanobacteria and cyanotoxins are common in fresh surface waters during warm seasons, such as the Great Lakes in North America (Merel et al., 2010). In the US, microcystins were detected commonly in surface waters in the states of New York, Nebraska, New Hampshire, and Florida (Fristachi et al., 2008). Microcystins are also common in Canadian freshwaters as well; in British Columbia, concentrations of MC-LR ranging from 31 to 1363 µg/L were reported in lake waters during the summer of 1995 (Kotak & Zurawell, 2007). Samples from 22 lakes during the summer of 2001 in Quebec also revealed a concentration of microcystins (Giani et al., 2005). Lake Ontario also experienced microcystin concentrations as high as 400 µg/L during the peak of bloom seasons at Hamilton Harbour (Murphy et al., 2003).

Powdered activated carbon (PAC) is proven to be an effective treatment against seasonal taste and odor compounds (2-MIB and geosmin) caused by cyanobacteria and algae blooms due to its flexibility in application. PAC was also evaluated by several studies for the removal of MC-LR from drinking water (summarized in Table 2.2). These studies found that PAC can be an efficient treatment method for the removal of MC-LR. PACs with a higher volume of mesopores (pore diameters ranging from 2-50 nm) were proven to be most effective for removal of high concentrations of MC-LR (Donati et al., 1994; Park et al., 2017). Several studies reported that wood-based PACs have higher adsorption capacity for MC-LR due to their mesoporosity (Donati et al., 1994; Westrick et al., 2010; Zhu et al., 2016). Recent studies, including Liu (2017) and Mashile et al. (2018), have also found wood-based PACs to be superior for removal of MC-LR when comparing PACs with different base materials. However, wood-based PACs are typically more costly than PACs sourced from coal and coconut shells.

Although PAC is known as an effective treatment for seasonal taste and odor issues and cyanotoxins such as MC-LR, the performance of PAC is dependent on certain parameters of the treatment train; typical PAC-water contact time in drinking water treatment plants (WTPs) is under 2 hours which is substantially lower than the contact time required by PACs to reach equilibrium (Matsui et al., 2004). In the past decade a new form of PAC known as super-fine PAC (SPAC) has received substantial attention for its more robust performance in the removal of various contaminants from water compared to conventional PACs (Ando et al., 2010; Bonvin et al., 2016; Matsui et al., 2004, 2006).

SPAC is produced by pulverization of conventional PACs to low micron particle sizes, typically in the range of 0.6 to 1.1 μm. The reduction in particle size of activated carbon has an indirect relation with its adsorption kinetics, since it increases the available outer surface area of the particles (Najm et al., 1990). Since the early 2000s, multiple studies have evaluated the adsorption performance of SPACs for a variety of micropollutants, synthetic organic matter (SOC), natural organic matter (NOM), taste and odor compounds, and even selected viruses (Bonvin et al., 2016; Matsui, Aizawa, Kanda, et al., 2007; Matsui et al., 2004; Matsushita et al., 2013; Partlan et al., 2020). These studies are summarized in Table 2.3. Almost all these studies reported significant improvement in adsorption kinetics by pulverization of conventional PACs and reducing the particle sizes to around 1 micron. Furthermore, a few studies have reported that produced SPACs have higher adsorption capacity compared to normal sized PACs for high molecular weight (MW) NOM (Matsui et al., 2004; Partlan et al., 2020). This increase in adsorption capacity of SPAC for high MW NOM was first justified by an increase of mesoporous volume due to fracture of ink bottle like pore structure during pulverization (Matsui et al., 2004), although, later Ando et al. (2011) studied the adsorption of natural organic matter and polystyrene sulfonate (PSS) thoroughly through observation of solid-phase adsorbate concentration. The study revealed that the high MW fractions of NOM tend to adsorb on the surface of activated carbon instead of diffusing into the pore structure of particles; therefore, the higher adsorption capacity of SPAC is mainly due to its higher available surface area compared to the parent PAC.

At the time of writing, there is no study available on adsorption of cyanotoxins including MC-LR onto this relatively new form of activated carbon.

The Freundlich isotherm equation is conventionally only applied to equilibrium concentrations; however, recently the Freundlich model was also applied to non-equilibrium concentrations, mainly to assist with the application of ideal adsorbed solution theory – equivalent background compound (IAST-EBC) models to investigate the adsorption of geosmin and 2-MIB in the presence of organic compounds such as dissolved organic matter (DOM). Examples of this approach can be found in studies of Shimabuku et al. (2014) and Zoschke et al. (2011). In these studies, the Freundlich model was applied to non-equilibrium data of 2-MIB adsorption onto PAC in waters containing a background compound at a higher concentration, and the results

were next used as an input to the EBC model to investigate the competitive adsorption between 2-MIB and the background compound (i.e., DOM). Zietzschmann et al. (2016) also applied the Freundlich model to non-equilibrium adsorption data in a similar manner to investigate the competition of NOM with various micropollutants, such as benzotriazole, for adsorption onto PAC. Therefore, in this study, the Freundlich equation was applied to non-equilibrium adsorption time to evaluate the adsorption capacity of SPACs at the short contact times, which are more typical in drinking water treatment scenarios.

The main objective of this study was to evaluate the adsorption rate of MC-LR onto SPACs in ultrapure water in order to obtain baseline performance data. SPAC performance can then be compared with studies done with the parent PACs. The baseline data generated by the ultrapure water experiments can also be used as a reference for adsorption behavior and compared to the results from adsorption of MC-LR onto SPACs in the presence of background organics such as NOM. The detailed objectives of this study are first to evaluate the rate of adsorption of MC-LR onto SPACs produced from 3 commercially available PACs made from different base materials, and secondly to determine and compare the adsorption capacities of each SPAC for MC-LR under both equilibrium and non-equilibrium conditions. The short SPAC-water contact times of 0.5 and 1 h are representative of contact times employed in the industry, which are adapted from Liu (2017), this also make the results of this study comparable to the results for the parent PACs.

4.2 Materials and methods

4.2.1 Materials

Coal-based, wood-based, and coconut-based SPACs were produced as described in Section 3.2.1. Prepared slurries were dried in an oven at 110°C for a 48 hours period. After the first 48-hour period, the dried sample was weighed using an analytical scale and returned to the oven for another 2 hours and weighed again to confirm that that SPAC samples are moisture-free. The SPAC samples were stored in desiccators prior to dry weight measurement.

Microcystin-LR was obtained from Cayman Chemicals (MI, USA), cyclo (ArgAla-Asp-D-Phe-Val) (c(RADfV)) was obtained from Peptides International (KY, USA). Liquid chromatography-mass spectrometry (LC-MS) grade acetonitrile was obtained from Sigma-Aldrich (WI, USA). LC-MS grade formic acid was obtained from Fisher Chemical (MA, USA). Ultrapure water was produced by a Millipore Milli-Q UV PLUS water system (MA, USA). Luer lock syringes and 4 mm diameter 0.45 μm nylon syringe filters and 0.5-liter bottles were obtained from VWR International (PAS, USA).

4.2.2 Bottle-point method

Liu (2017) employed the bottle point method (Droste, 1997) to assess the adsorption of the original PACs in ultra-pure water at bench scale. The same method was used in this study in order for the results to be

comparable with Liu (2017) findings. 9 bottles were used for each SPAC, comprising 8 bottles with SPAC concentrations from 2 to 20 mg/L and 1 bottle as a positive control (MC-LR only). For each set of experiments, 5.5 litres of 100 µg/L of MC-LR were prepared in buffered Milli-Q water at pH 7.2, which was distributed to 9 glass bottles adapted from Liu (2017). The bottles for 2 mg/L and 4 mg/L points contained 1 liter of MC-LR spiked ultrapure water to facilitate the weighing process of dried SPAC, while the other points were prepared by addition of only 0.5 liter of the water in 0.5-liter bottles The SPACs were weighted via an analytical scale and added to the bottles at the start time of experiments. An extra bottle with SPAC concentration of 20 mg/L in Milli-Q water was also included as a negative control to account for compounds that possibly could be misidentified as MC-LR. The bottles dosed with 11 mg/L of SPACs were dedicated for adsorption rate determination and were sampled more frequently than the others.

4.2.3 Equilibrium vial-point method

Due to the rapid adsorption rate and high capacity of SPAC, the equilibrium point could not be determined under the bottle point experiment conditions. Therefore, an experiment with a higher concentration of MC-LR, 300 µg/L in 30 mL of buffered ultrapure water stored in 40 ml vials, was designed, and lower doses of SPACs of 1-10 mg/L were used to ensure that the residual concentration of MC-LR was above the minimum reporting level after reaching equilibrium. A vortexed slurry suspension (2 g/L) prepared by suspending dried SPAC in MilliQ water, was chosen for dosing the vials as weighing masses of dried SPAC below 2 mg was not possible due to the error (0.1 mg) of the available analytical scales.

4.2.4 Simple SPAC dispersibility test

To visually inspect the dispersibility of suspended SPACs in slurry form, a simple experiment was designed consisting of three vials each filled with 1 g/L suspension of each of the coconut-based, wood-based, and coal-based SPACs. Next the vials were shaken momentarily and placed upright so the settling time of SPACs can be monitored. The vials were photographed daily to monitor the state of suspension in the vial.

4.2.5 MC-LR analysis by LC-MS/MS

A Shimadzu 8030 LC-MS/MS system was used for the measurement of MC-LR concentrations. The LC-MS/MS consists of a tandem quadrupole mass spectrometer capable of analyzing various analytes via a multiple reaction monitoring (MRM) technique in which the specific precursor ion and corresponding product ion(s) of each analyte are monitored. A 50 mm × 2.1 mm Poroshell C18 analytical column with 2.7µm packing was used as the stationary phase and kept at 30°C. Cyclo(ArgAla-Asp-D-Phe-Val) (c(RADfV)) was used as the internal standard for analysis with a concentration of 100 µg/L adapted from Liu (2017). Eluents were filtered Milli-Q water and HPLC grade acetonitrile, both acidified with 0.1%

formic acid. A gradient was run at a flow rate of 0.3 ml/min. The details of the gradient used are described in Appendix B.1. The injection volume was set to 30 μL and MRM monitored 589.05>120.0 transition for c(RADfV) (internal standard, and 498.30>135.05 and 995.20>134.95 transitions for MC-LR.

A 12 point linear internal standard weighted calibration curve in range of 0.2 to 100 μg/L was established for the bottle point test. The calibration curve range was later extended to 0.2 to 300 μg/L for the vial point tests. The method detection limit (MDL) for MC-LR was determined based on Standard Methods (2012). The ultrapure water MDL for MC-LR was found to be 0.06 μg/L, the minimum reporting level (MRL) of the method was set to 0.2 μg/L roughly three times the MDL value. The set MRL was also the same concentration as the lowest point of the calibration curve. The collected samples were kept frozen at -20°C and were thawed before analysis within 3 days of sampling. During the analysis, one quality control standard was injected after every ten sample to monitor the measurement stability. A calibration curve was measured before every batch of samples to account for changes in instrument sensitivity between analysis of batches.

4.2.6 Data Analysis

4.2.6.1 Freundlich isotherm model

The empirical Freundlich isotherm model is widely known as the best fit for activated carbon adsorption modeling in the water treatment field (Worch, 2012). The Freundlich isotherm model is used by several studies to describe the adsorption of micropollutants onto PAC (Park et al., 2017) and recently onto SPAC (Matsui et al., 2013).

$$q_e = K_F C_e^{\frac{1}{n}}$$
(Equation 4. 1)

Where q_e represents the solid phase concentration of an adsorbate micropollutant pollutant such as MC-LR in μg adsorbed on mg of the adsorbate, which in this case is activated carbon. C_e represents MC-LR concentration at equilibrium in $\mu g/L$ and K_F and n are Freundlich parameters describing adsorption strength and energetic heterogeneity of the adsorbent -active- surface, respectively (Worch, 2012).

The Freundlich model is fitted to the experimental data via non-linear fitting, and the joint confidence regions (JCRs) are calculated via the covariances of the parameters via the modules in the python programming language. The code used and calculation procedures are provided in Appendix B.9.

4.2.6.2 Adsorption rate

As a means to compare the adsorption rates of SPACs, pseudo-first and second-order rate laws were applied to the adsorption data to assess the rates of adsorption in ultrapure water.

4.2.6.3 Pseudo-first-order model

The Pseudo-first order model proposed by Lagergren has been proven to be an effective model for describing the adsorption rate of a range of compounds onto various sorbents, including activated carbons, as summarized by (Ho & McKay, 1999).

The model for the adsorption kinetics can be described as below:

$$\frac{dq_t}{dt} = k_1(q_e - q_t) \qquad \text{(Equation 4.2)}$$

While t is the time elapsed in minutes, $q_t (\mu g/mg)$ represents the amount of sorbate adsorbed onto the sorbate at time t, q_e is the amount of sorbate adsorbed at equilibrium, and k_1 represents the pseudo-first-order adsorption rate constant.

Integrating the above equation over time, t, yields: 4.

$$\log(q_e - q_t) = \log q_e - \frac{k_1}{2.303}t \qquad \text{(Equation 4.3)}$$

4.2.6.4 Pseudo-second-order model

The empirical pseudo-second-order model has also been deemed to be a good fit for describing the adsorption rate of sorbates to activated carbons (Ho & McKay, 1999). Several studies have also used the pseudo-second-order model successfully to describe the adsorption rate of microcystins onto a variety of activated carbons (Liu, 2017; Mashile et al., 2018; Zhu et al., 2016).

The pseudo-second-order model can be expressed as below:

$$\frac{dq_t}{dt} = k_2(q_e - q_t)^2 \qquad \text{(Equation 4.4)}$$

Where t, q_t, and q_e are defined as per Equation 4.2 and k_2 is the pseudo-second-order adsorption rate constant.

Integrating Equation 4.4 over time yields:

$$q_t = \frac{q_e^2 k_2 t}{(1 + q_e k_2 t)} \qquad \text{(Equation 4.5)}$$

For ease in the determination of parameters, the above equation can be linearized as follows:

$$\frac{t}{q_t} = \frac{1}{k_2 q_e^2} + \frac{1}{q_e}t \qquad \text{(Equation 4.6)}$$

The adsorption data was then post processed to take the linear form and then fitted to Equation 4.6 via linear regression.

4.3 Results and discussion

4.3.1 Rate of adsorption in ultrapure water

The percent removal of MC-LR in ultrapure water using the three produced SPACs as a function of time is presented in Figure 4.1. By inspecting the removal rates of the three SPACs in buffered ultrapure water, at 11 mg/L the SPAC derived from BG-HHM (wood-based) had the fastest removal rate of MC-LR, reducing the concentration below MRL in less than 20 minutes of contact time. Next in line, WPC (coconut-based) SPAC was able to remove close to 100 percent of the toxin in less than 1.5 hours, and COL-PL60-800 (coal-based) needed at least 2 hours to remove the initial 100 μg/L MC-LR concentration.
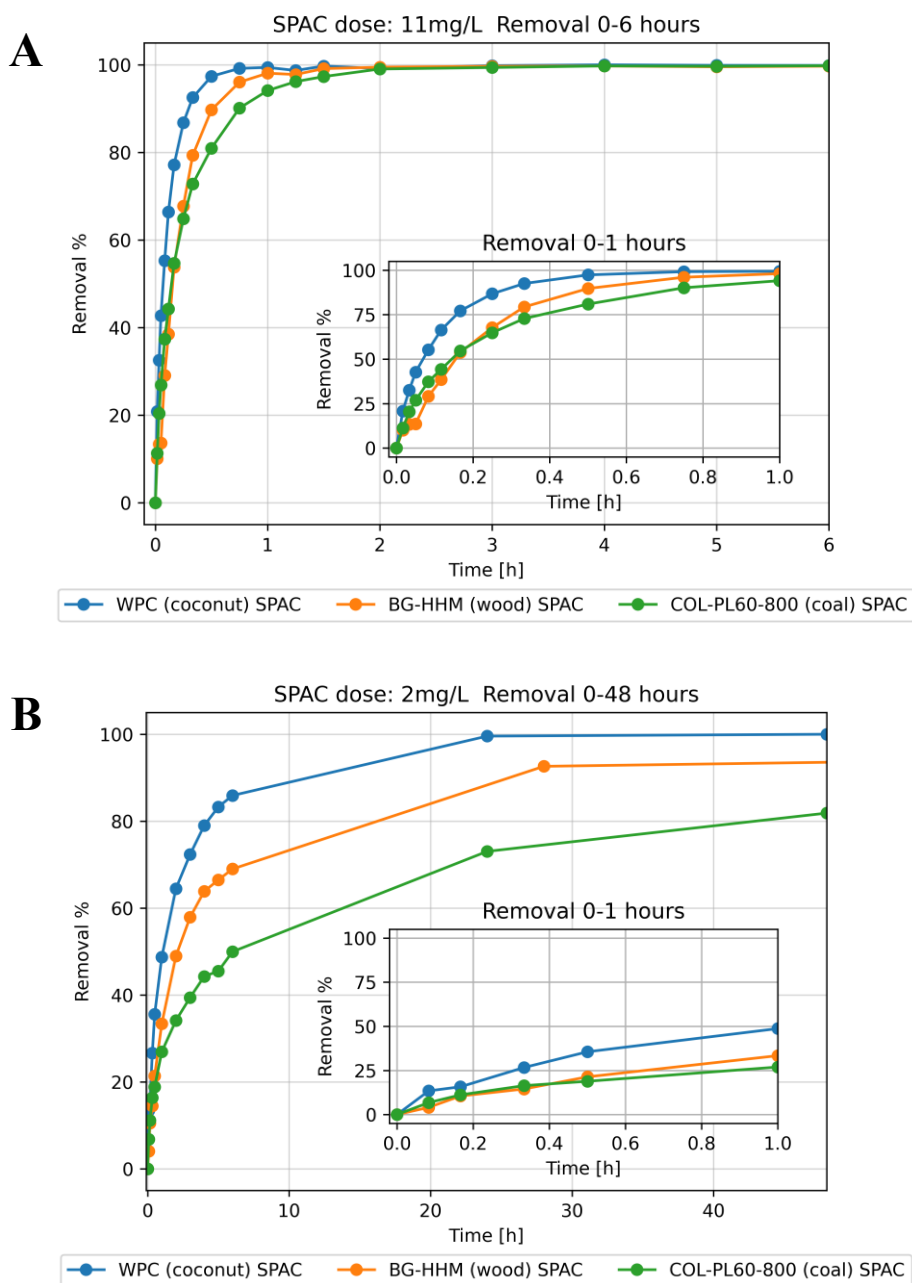
Figure 4.1 Percent removal of microcystin-LR in buffered ultrapure water (pH 7.2). (A) SPAC dose 11mg/L (used for adsorption rate experiments), (B) SPAC dose (2mg/L)

The concentration of microcystin-LR quickly drops below the MRL ($0.2\,\mu g/L$ − equivalent to 99.8 percent removal−) of the method from the initial $100\,\mu g/L$, since the SPACs presented much faster kinetics than their parent PACs even at low doses such as 2-20 mg/L. Therefore, making the determination of the equilibrium point is practically impossible even at the lowest SPAC dose

of 2mg/L, this could be suggesting that the SPACs have higher capacities for MC-LR compared to their parent PACs, since these experimental conditions with higher doses of parent PACs resulted in higher residual concentrations of MC-LR (above method's MRL). Although the concentration profiles of $2 \, mg/L$ suggest that the SPACs are close to equilibrium, hence, the partially flattened curve, the MC-LR concentrations keep dropping slightly in small amounts suggesting slow but progressing removal of MC-LR, the concentrations of MC-LR are presented in Appendix B.3. This was partially suspected to be the result of steady SPAC deposition on the rim of bottles while they shake for longer periods of time, images included in Appendix B4. This behavior was not problematic for the first 6 hours of the bottle point test since the bottles were sampled frequently, redistributing the SPAC in the solution. This behavior was not observed for the larger-sized parent PACs in preliminary tests and the tests done by Liu (2017).

It is important to note that the SPACs behaved differently after the pulverization and drying process. Coal-based and wood-based SPACs agglomerated during the drying process, with coal-based SPAC showing more agglomeration. The agglomerated particles certainly had an adverse effect on the adsorption rate of SPACs onto wood-based and coal-based SPACs as it is evident by the removal rates in Figure 4.1. Therefore, later experiments including the vial point equilibrium tests in this chapter and bottle point tests in the next chapter were done by dosing the SPACs in form of a prewetted slurry instead of as dry powder. On the other hand, the WPC (coconut-based) SPAC showed improved dispersibility after pulverization, quickly dispersing into a fine slurry after addition to the water in dry powder form. Images of a simple dispersion/settling test are included in Appendix B.5.

The empirical pseudo-first-order and -second-order adsorption models were applied to adsorption data from the bottle point tests. The two empirical models are used to compare the performance of the produced SPACs in ultrapure water. The parameters of the models are included in Appendix B.6, including the experimental equilibrium concentration on the SPAC, predicted equilibrium concentration on the SPAC, rate constant of the kinetic model, and R^2 value of the fitted models. The results of the pseudo-first-order fitting predicted lower adsorption rates compared to the pseudo-second-order model and the predicted equilibrium concentration of MC-LR were not comparable with the experimental values as presented in Appendix B.6 along with the residual plots of the fittings. The residual plots also revealed a trend of systematic error in the fittings, which was also observed by Liu (2017) while applying this model to MC-LR adsorption data onto parent PACs. Therefore, the pseudo-second-order rate model was applied to adsorption data in hopes of better describing the performance of SPACs in this study.

The pseudo-second-order rate model fits the adsorption rates better, with k_2 values ranging between $0.79 - 1.87 \, mg/\mu g/min$. The lower value is for the BG-HHM (wood-based) and the higher value is for WPC (coconut-based). The removal plot (Figure 4.1A) indicates that WPC, the coconut-based SPAC, is the fastest among the three and overall agrees with the order of the k_2 values provided by the pseudo-second-

order model, which would suggest that this rate model described the adsorption rate of MC-LR onto SPACs somewhat accurately. However, after investigating the residual plots for the pseudo-second-order model, included in Appendix B.7, a systematic error was observed in the residual values similar to one observed in pseudo-first-order plots. An explanation for the presence of the systematic error in both the pseudo-first and -second-order rate model results would be the lack of an actual equilibrium concentration since the MC-LR concentration quickly drops below the MRL. Furthermore, past studies have also shown that simple kinetics models such as pseudo-first and -second order rate models might not be suitable for characterizing the adsorption rate of micropollutants such as cyanotoxins onto PAC, as suggested by Liu (2017). Later studies on the performance of SPACs have also shown that finer adsorbent particles with complex pore structures are more adequately modeled using sophisticated kinetic models such as the homogenous surface diffusion model (HSDM) and branched pore kinetic model (BPKM) (Matsui et al., 2011).

The removal rates of MC-LR by the SPACs in ultrapure water are compared to the adsorption rate of MC-LR by parent PACs in Figure 4.2. It should be noted that the parent PACs were dosed at 50 mg/L (dashed lines), almost 5 times higher than the approximate 11mg/L SPAC dose used in this study (solid lines). As is evident from Figure 4.2 the coconut-based and coal-based SPACs outperformed their corresponding parent PACs despite the lower applied dose. The wood-based SPAC on the other hand failed to keep up with its parent PAC, though it should be noted that wood-based and coal-based SPACs suffered from agglomeration and parent PACs were dosed at a much higher concentration of 50 mg/L. The order of the adsorption rates was different from the ones found by Liu (2017) since in that study, the wood-based PAC was the fastest; the reason for this is primarily due to the dispersion issues from which wood-based and coal-based SPACs suffered.
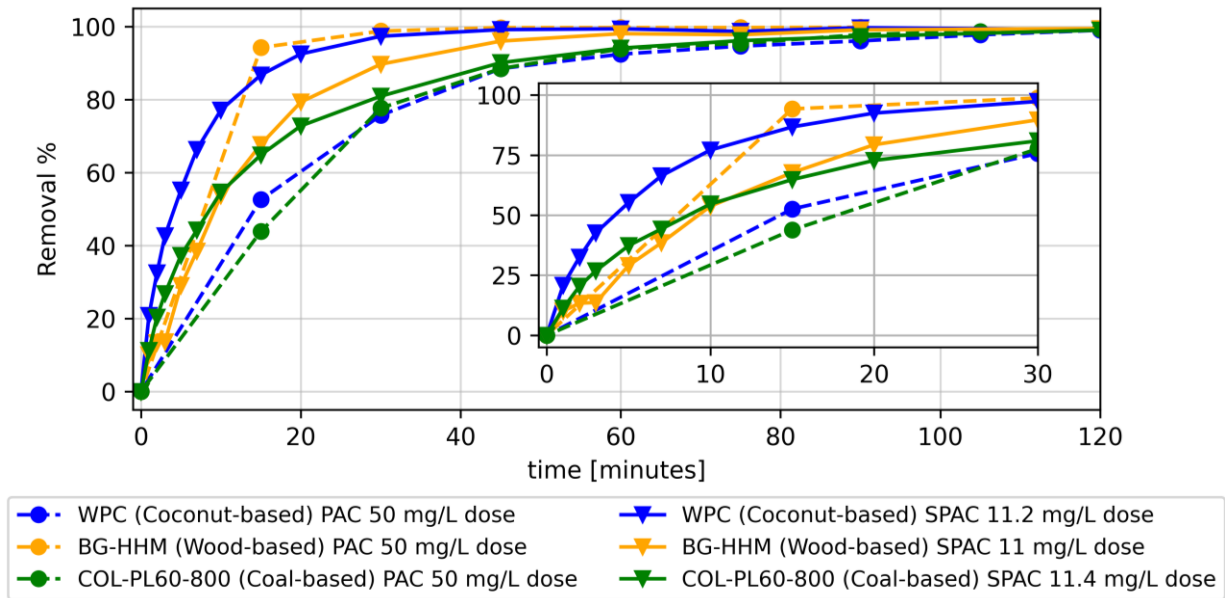
Figure 4.2 Removal of MC-LR in buffered ultrapure water via SPACs at dose of 11 mg/L (solid lines) compared to parent PACs at dose of 50 mg/L (dashed lines) (Liu, 2017)

The pseudo-second-order rate model parameters for parent PACs derived by Liu (2017) are provided in Appendix B.8 and the k_2 values are presented along with the values found for SPACs in Figure 4.3. Comparing the k_2 values provided by the pseudo-second-order rate model for the parent PACs and SPACs in ultrapure water also agrees with results found by visual inspection of Figure 4.2.
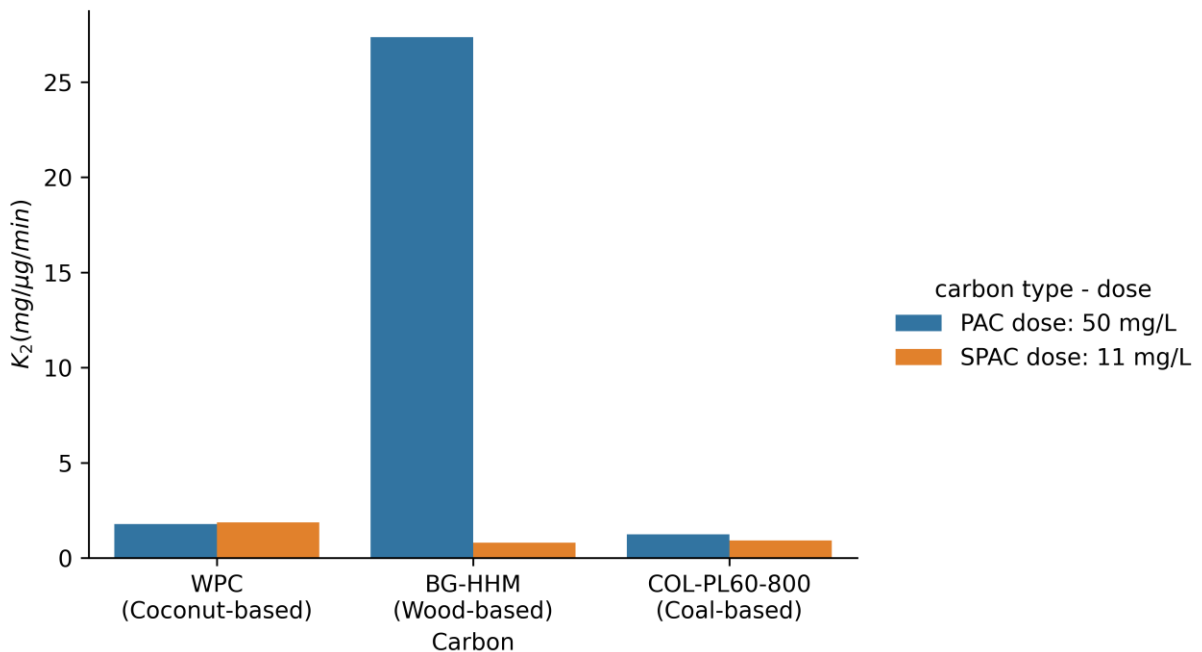
Figure 4.3 Comparison of k2 values for parent PAC at 50 mg/L dose and SPAC at 11 mg/L dose

4.3.2 Isotherms in ultrapure water

As mentioned in Section 4.3.1, it could not be confirmed that equilibrium was reached in the bottle point tests since MC-LR concentrations fell quickly below the MRL. Therefore, to determine the capacity of SPACs for MC-LR at equilibrium, a set of tests was done at a higher concentration ($300 \mu g/L$) MC-LR solution with SPAC doses of $1 - 10\ mg/L$. The dosing was done by the addition of corresponding volumes of a vortexed SPAC slurry per Section 4.2.3, which alleviated the problem of formation of carbon rings in bottle point tests as well.

4.3.2.1 Joint confidence regions

The Freundlich isotherm model is extensively used to describe the sorption processes at equilibrium (Ho & Newcombe, 2007; McDonough et al., 2008; Zhu et al., 2016). As is evident from the mathematic equation of the Freundlich model (Equation 4.1), the two parameters n and K_f are strongly correlated (Liu, 2017). However, uncertainty in the form of standard deviation and confidence intervals (CIs) of these two parameters are usually calculated independently, which could result in an overestimation of the uncertainty of parameters, primarily when the non-linear least squares method is used for fitting the model (Fairey & Wahman, 2013). Therefore, in this study, the concept of joint confidence region (JCR) was used to evaluate the confidence level of the calculated Freundlich parameters. The 95% JCR contours represent the region that combinations of Freundlich parameters that are probable with 95% confidence, though the optimum point in the middle is still the most plausible estimate of the parameters (Constales et al., 2017). The JCRs were calculated and are plotted for the three SPACs at 48h and 96h (equilibrium) in Figure 4.4. The JCRs presented in figures slightly deviate from a symmetric ellipsoidal shape, indicating a correlation between the Freundlich model parameters. The similarities between JCRs at 2 days and 4 days of contact time indicate that the SPACs have indeed reached equilibrium. Since the JCRs for adsorption of MC-LR onto three different SPACs have limited to no overlap, it can be concluded that the isotherm parameters of three different SPACs are statistically distinguishable.
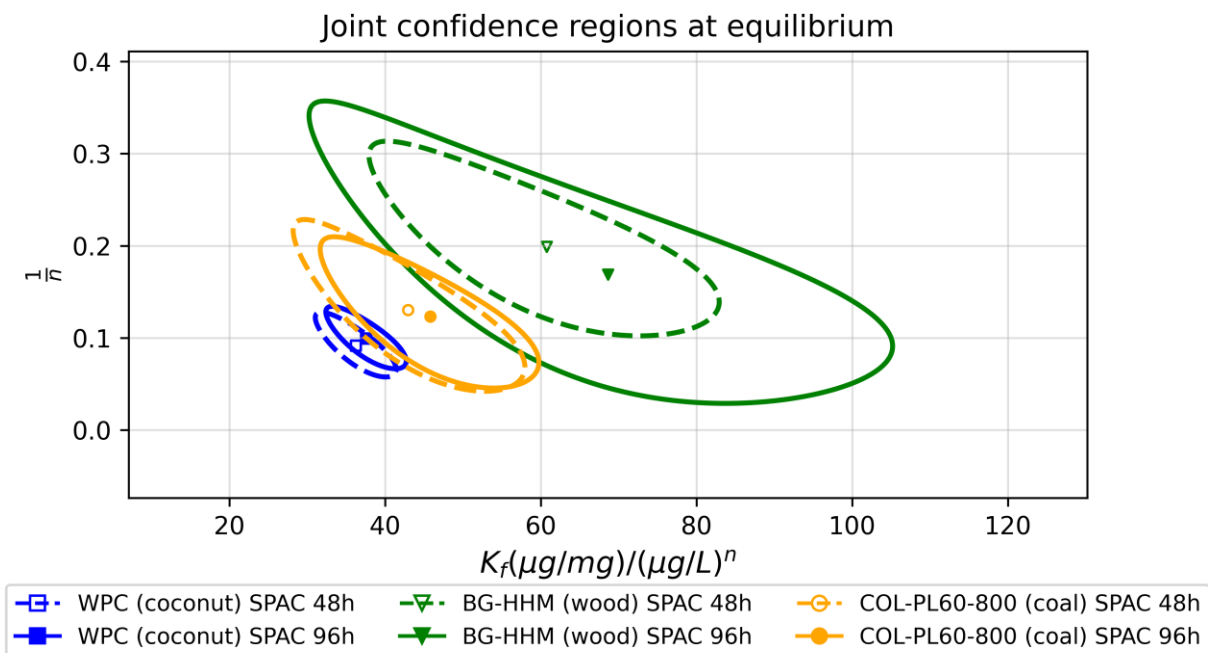
Figure 4.4 95% Joint confidence regions and point estimates of the Freundlich isotherm parameters for the adsorption of MC-LR onto produced SPACs at 48h and 96h

4.3.2.2 Freundlich Isotherms

The Freundlich isotherm model (Equation 4.1) was applied to the equilibrium data collected from the vial-point tests for adsorption of MC-LR onto the SPACs. The results of the fittings are visualized in Figure 4.5. As per Section 4.3.2.1, the JCRs of Freundlich parameters for adsorption of MC-LR onto three wood-based, coconut-based, coal-based SPACs showed that the adsorption performances of the three SPACs are statistically distinguishable. The BG-HHM (wood-based) SPAC showed the highest capacity for MC-LR, while COL-PL60-800 (coal-based) had a lower capacity than BG-HHM and WPC (coconut-based) have the lowest capacity among the three SPACs (Figure 4.5). The Freundlich isotherm fitting lines for adsorption of MC-LR onto three SPACs were diverging with growing equilibrium concentrations; this behavior was similar to what Liu (2017) observed for PACs.
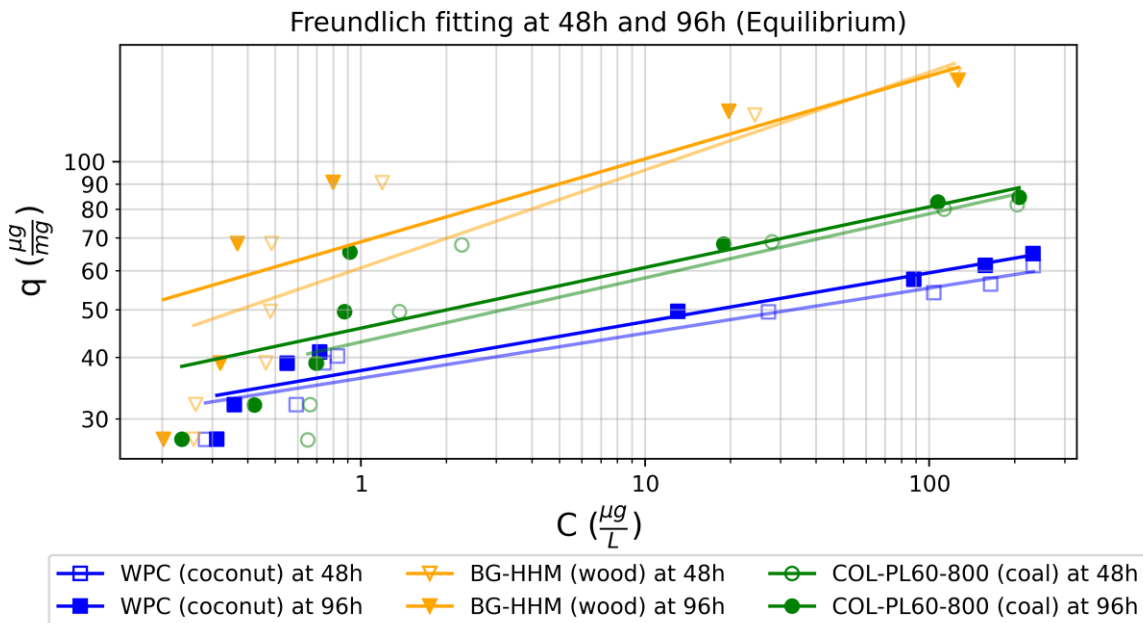
Figure 4.5 Freundlich isotherms for MC-LR adsorption onto the wood-, coconut- , coal-based SPACs in ultrapure water. (Markers represent data points and straight lines represent the fitted Freundlich model)

The Freundlich isotherm model parameters were determined using a non-linear least square model via the Levenberg–Marquardt error minimization algorithm and are summarized in Table 4.1. The residual plots for isotherms are provided in Appendix B.8, a trend of higher deviation at lower equilibrium concentrations was detected in the residual plots, which can also be observed in the isotherm fittings (Figure 4.5). However, the non-linear least squares method has unfavored the values in this range, since the error levels (residuals) are much less prominent compared to the errors at the higher end of the line.

Based on Table 4-1, BG-HHM has the highest K_f values of 60.7 and 68.6 $(\mu g/mg)/(\mu g/L)^n$ for 48h and 96h equilibrium times, respectively. COL-PL60-800 (coal-based) with K_f values of 42.9 and 45.9 $(\mu g/mg)/(\mu g/L)^n$ stands in the middle and WPC (coconut-based) with has the least K_f values 36.2 and 37.5 $(\mu g/mg)/(\mu g/L)^n$. In terms of $1/n$ values, the COL-PL60-800 and WPC SPACs had close $1/n$ values (0.9-0.13) and BG-HHM SPAC had higher $1/n$ values of (0.17-0.2).

Based on the Freundlich equation (Equation 4-1), if the $1/n$ are similar, a higher K_f value indicates higher SPAC adsorption capacity for MC-LR. Given that the $1/n$ are relatively similar in table 4-1, solely based on K_f values, BG-HHM (wood-based) SPAC had the highest capacity for MC-LR, followed by COL-PL60-800 (coal-based) SPAC. The WPC (coconut-based) SPAC had the lowest capacity for MC-LR compared to the other two produced SPACs. The aforementioned order of K_f values agree with the capacities found by visual inspection in Figure 4.5.

Table 4.1 Freundlich isotherm parameters for SPAC adsorption in ultrapure water at equilibrium times

SPAC	Contact time (h)	Number of data points	K_f $\left(\dfrac{\mu g}{mg}\right)/\left(\dfrac{\mu g}{L}\right)^n$	K_f 95% CI*	$1/n$	$1/n$ 95% CI*
BG-HHM	48	8	60.78	(46.79,74.76)	0.20	(0.14,0.26)
(wood)	96	6	68.64	(48.53,88.75)	0.17	(0.09,0.25)
WPC	48	8	36.26	(33.08,39.44)	0.09	(0.07,0.11)
(coconut)	96	8	37.59	(34.42,40.75)	0.10	(0.08,0.12)
COL-PL60-	48	8	42.97	(33.7,52.24)	0.13	(0.07,0.19)
800 (coal)	96	8	45.83	(37.15,54.52)	0.12	(0.07,0.17)
*(95% confidence interval calculated individually for K_f and $1/n$)						

The adsorption process of adsorbate onto adsorbents such as PAC/SPAC is complex and depends on multiple parameters rather than just one determining factor. The common parameters that can affect the adsorption process are the transport and binding mechanisms of adsorbate molecules to the adsorption sites; the transport of the adsorbate molecules could depend on the particle size, active surface area, and pore size distribution of adsorbents, while binding and attachment mechanisms are based on hydrophobic and electrostatic mechanism, which can be affected by the surface charge of the particles (Ando et al., 2011; Delgado et al., 2012; Liu, 2017; Matsui, Ando, et al., 2009; Pan et al., 2017). Considering these complexities in the adsorption process, relationships between adsorption performance of the three produced SPACs in this study with their characteristics are investigated. For the BET surface areas (Table 3.5), no relations between the internal surface area and adsorption capacities of SPACs for MC-LR were found.

In terms of DFT pore size distribution, as discussed in Section 3.4.2.2 and Table 3.5, WPC (coconut-based) SPAC is mainly microporous with 99.9% of its total pore volume in micropores, while the BG-HHM (wood-based) and COL-PL60-800 (coal-based) SPACs had substantially higher mesopore volumes with 0.98 and 0.39 cm^3/g, respectively. As mentioned earlier, MC-LR has a relatively large molecular size with estimated dimensions of $2.039 \times 1.259\ nm$ and therefore could fit into the mesopores (2-24 nm). The adsorption capacity of three SPACs seems to agree with this consideration since BG-HHM (wood-based) SPAC with the largest total pore volume and largest mesopore volume showed the highest adsorption capacity for MC-LR at equilibrium, followed by COL-PL60-800, which had the second-largest mesopore volume among the three SPACs. Furthermore, the BG-HHM (wood-based) is the only activated carbon product with the pH$_{pzc}$ of 4.1, below the typical surface water pH range of 6-8, which would make it

positively charged in that pH range; as discussed earlier in Section 2.1.1, MC-LR maintains a negatively charged functional group in the natural pH range, which might indicate that MC-LR molecules might have a greater affinity to adsorb onto the positively charged wood-based PAC/SPAC particles compared to the other two coal-based and coconut-based activated carbons. Park et al. (2017) also found that mesoporous PACs have a higher capacity for MC-LR in a variety of source waters. However, one must not conclude that the adsorption capacity of SPACs for large molecules such as MC-LR is solely dependent on the volume of the mesopores and/or surface charge of the activated carbon. Studies investigating the source of higher capacity of SPACs for certain large molecule adsorbents have found that compounds such as fractions of NOM and polystyrene sulfonates (PSSs) would preferentially adsorb on the outer surface of activated carbon rather than penetrating the pores (Ando et al., 2010, 2011; Pan et al., 2017). This could indicate that the adsorption capacity of SPACs for MC-LR is not only a function of SPACs mesopore volume, and external surface area and particle charges could also affect the adsorption capacity of SPACs as well.

4.3.3 Short-contact time (non-equilibrium) capacities

In a typical drinking water treatment plant, the PAC/SPAC contact time would be much shorter than the contact time required for activated carbons to reach their equilibrium capacity. Therefore, estimating adsorption capacities at short contact times would be useful. The Freundlich equation was applied to non-equilibrium experimental data collected during bottle point tests for adsorption of MC-LR onto the three produced SPACs. It is necessary to note that the bottle point tests were performed under different conditions than the equilibrium vial point test as described in Section 4.2.2. The equation was used to assist in interpretation of the data, as has been done by other researchers (i.e., Zoschke et al., 2011). The non-equilibrium data was collected at 5minutes, 10 minutes, 20 minutes, 30 minutes, 1 hours, 2 hours, and 3 hours of contact. The collected data and residual plots for the short contact times are included in Appendix B.12. In this study, 'capacity' is defined as the mass of MC-LR adsorbed onto SPACs at time 't' under controlled experimental conditions based on Liu (2017).

The JCRs are presented for the three different short contact times in the range of 5 to 180 minutes at the 95% confidence level in Figure 4.7. At 30 minutes of contact time, there is no overlapping in JCRs for the Freundlich parameters of the three SPACs, indicating that their performance in adsorption of MC-LR is statistically distinguishable. However, with the increase of contact time, the WPC (coconut-based) SPAC JCR started to grow and overlap with the wood-based SPAC at 60 minutes and 120 minutes. The growth in WPC (coconut) SPAC JCR with the increase of contact time can be explained mathematically. The concentrations for points with a higher dose of SPAC decrease to below the MRL with increasing contact time, and hence, the number of data points available for the fitting decreases from 8 points to 7 points for

60 minutes and to 5 points for 120 minutes of contact time. This contributes to increasing the uncertainty of the fit, therefore resulting in the growth of the JCR and the confidence interval of the model parameters. Comparing the JCRs of SPACs at different contact times (Figure 4.7), the JCRs of BG-HHM (wood-based) SPAC and COL-PL60-800 (coal-based) SPAC have no overlap at contact times of 30 minutes, 60 minutes, and 120 minutes, indicating a statistically significant difference in the adsorption performance of each of the SPACs with respect to different contact times. As for the WPC (coconut-based) SPAC, the JCRs at 30 minutes and 60 minutes have no overlap, indicating statistically significant changes to the model parameters between those two times, though, at 120 minutes and later, the larger JCR overlaps with the 60 minutes JCR, making these two times non-distinguishable statistically at 95% confidence.
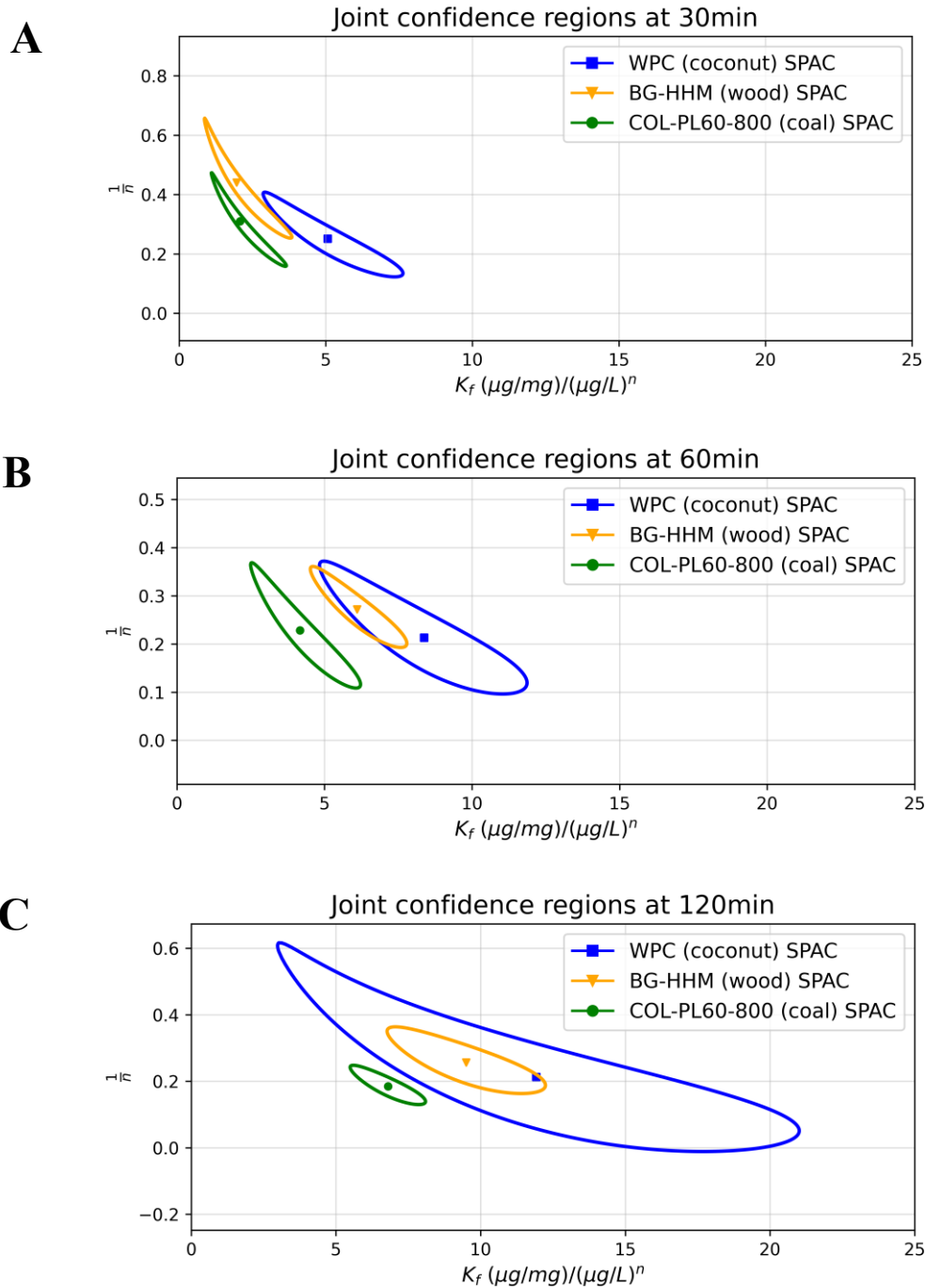
Figure 4.6 Comparing JCRs at short contact times of (A) 30 minutes, (B) 60 minutes, and (C) 120 minutes as an example in ultrapure water
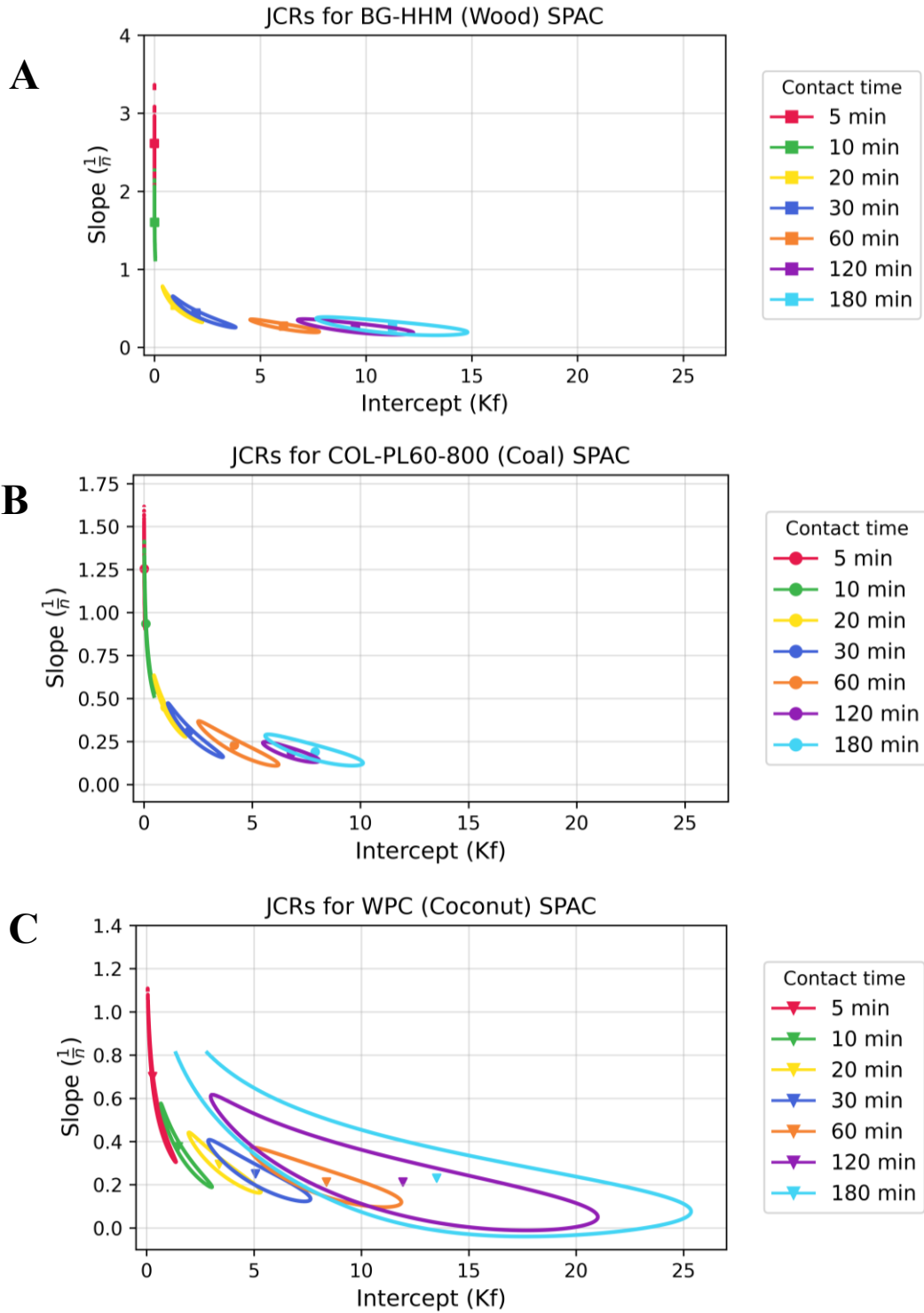
Figure 4.7 JCRs at short contact times for (A) BG-HHM (wood) SPAC, (B) COL-PL60-800 (coal) SPAC, and (C) WPC (coconut) SPAC for removal of MC-LR in ultrapure water

The Freundlich equation was fit to the non-equilibrium time data for the adsorption of MC-LR onto the three produced SPACs in this study at contact times of 5-180 minutes. However, It should be noted that the application of PAC/SPAC in a drinking water treatment plant can normally be approximated as a CFSTR process, whereas the experiments in this study were done in a batch system under controlled conditions. (It should be noted that time in a batch reactor can be equated to distance (and therefore time) in a plug flow reactor, however there is no direct equivalence between time in a batch reactor and the mean retention time of a CFSTR) Therefore, as also pointed out by Liu (2017) the non-equilibrium capacity evaluation results obtained through batch experiments do not necessarily hold valid in a full-scale scenario such as a DWTP. The fitting plots and Freundlich parameter values are available in Figure 4.9 and Table 4.2. However, for the sake of conciseness only the 30 minute, 60 minute, and 120 minute curves are compared to each other in Figure 4.8. As presented in Figure 4.9 the slope of the Freundlich curves decreased and intercepts increased with an increase in contact time. However, the trend of decreasing slope for the WPC (coconut) SPAC is not as distinct as it is for BG-HHM (wood) SPAC and COL-PL60-800 (coal) SPAC.

The non-equilibrium Freundlich parameters for the three SPACs with the confidence interval of 95% are summarized in Table 4.2. At contact times of 30, 60, and 120 minutes, the WPC (coconut-based) SPAC had the highest K_f values of $5.09 - 11.92 \ (\mu g/mg)/(\mu g/L)^n$ among the three SPACs, followed by the BG-HHM (wood-based) SPAC $1.96 - 9.50 \ ((\mu g/mg)/(\mu g/L)^n)$, while COL-PL60-800 (coal-based) SPAC had the lowest K_f values $(2.08 - 6.80 \ (\mu g/mg)/(\mu g/L)^n)$ at these three contact times. As the JCRs in Figure 4.6 suggest, the fitted Freundlich parameters for all three SPACs at 30 minutes of contact times are statistically distinguishable. However, this does not hold true for the 60 minutes and 120 minutes contact times in which the JCRs of WPC (coconut-based) and BG-HHM (wood-based) overlap and, therefore, make the given result statistically non-distinguishable. The 1/n values are relatively similar in the range of 0.18 to 0.27 with the exception of BG-HHM (wood-based) SPAC at 30-minute contact time with a 1/n value of 0.44. With exception of the latter, 1/n values are relatively similar, and it can be concluded that WPC (coconut-based) SPAC with the highest K_f values has the highest capacity for MC-LR at the three short contact times over the concentration range studied.
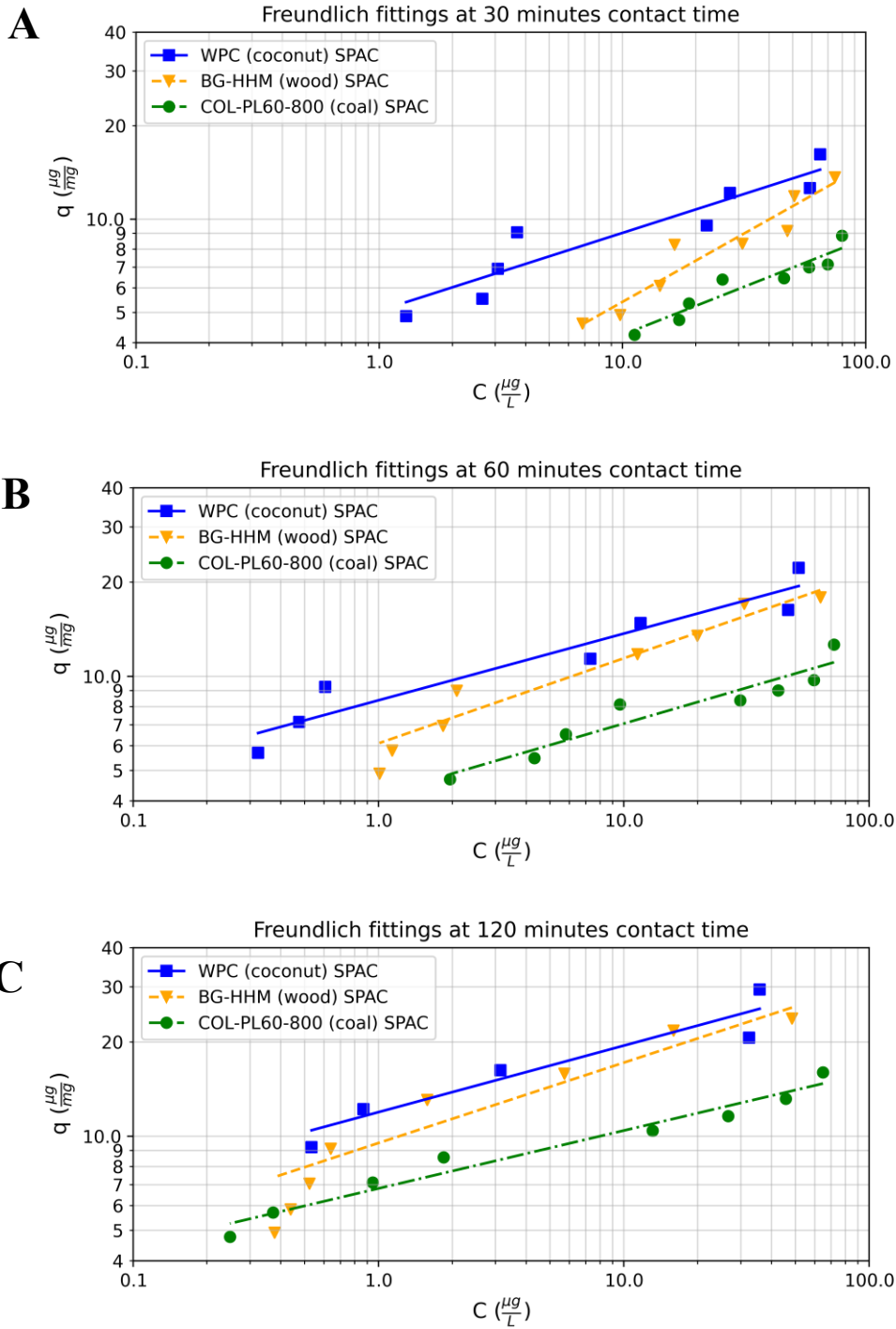
Figure 4.8 Freundlich fittings of WPC (coconut-based) SPAC, BG-HHM (wood-based) SPAC, and COL-PL60-800 (coal-based) SPAC at (A) 30 minutes, (B) 60 minutes, and (C) 120 minutes of contact time for removal of MC-LR in ultrapure water
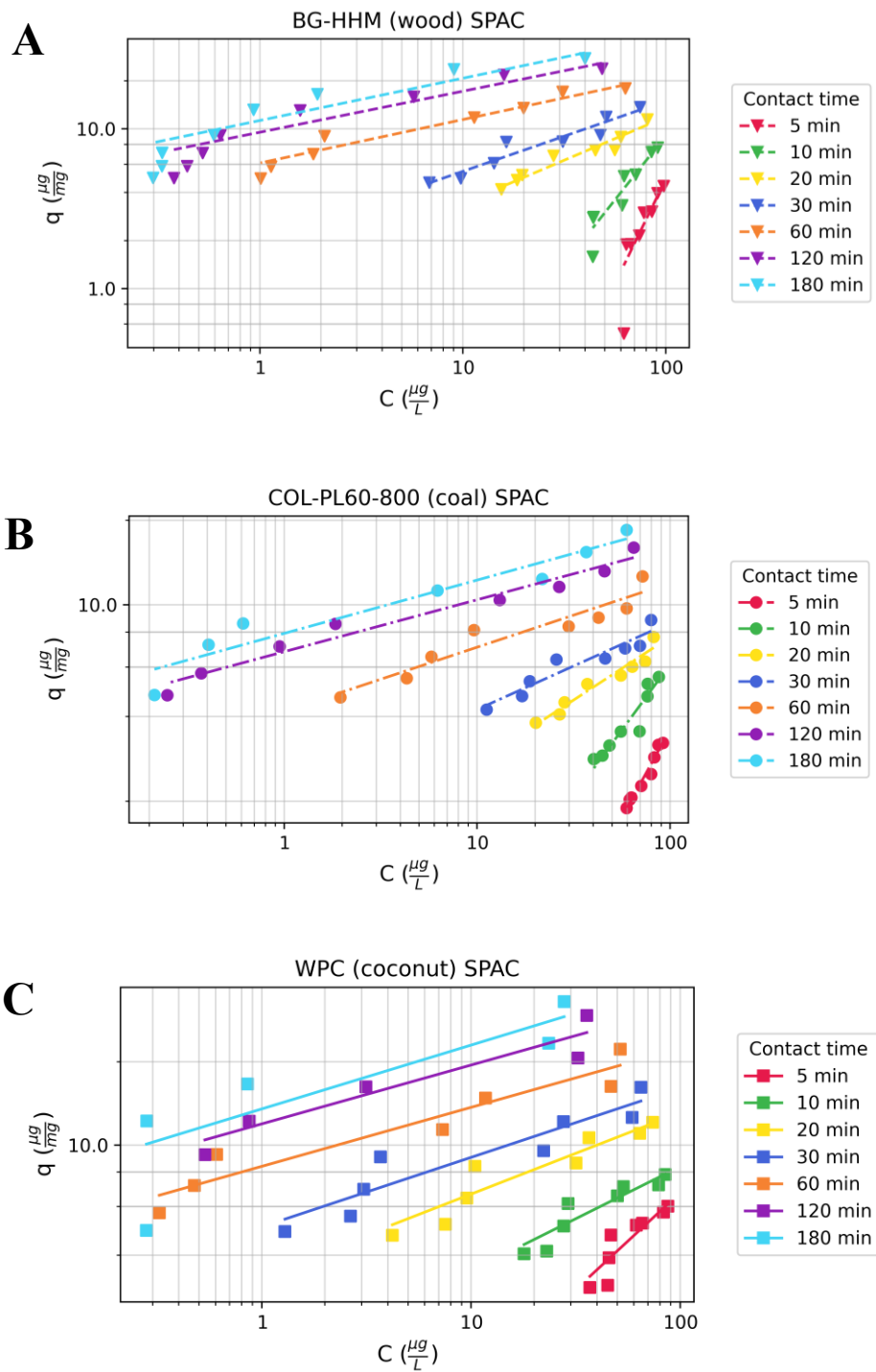
Figure 4.9 Best-fit Freundlich model curves at contact times in range of 5 to 180 minutes for (A) BG-HHM (wood-based) SPAC, (B) COL-PL60-800 (coal-based) SPAC, and (C) WPC (coconut-based) SPAC for removal of MC-LR in ultrapure water

74

By comparing the K_f values in Table 4.2 for short contact times with the values in Table 4.1 for equilibrium data, it is evident that the capacities at equilibrium are much higher than the ones at short contact times, as would be expected. It should be noted that the experiments for the determination of equilibrium capacities were done under different conditions than the ones done for kinetics and short contact times, as described in Sections 4.2.2 and 4.2.3.

As is evident from the Freundlich curves in Figure 4.9 for short contact times and Figure 4.5 for equilibrium times, the order of the K_f values of the short contact times are different than the ones fitted for equilibrium. The results from the equilibrium experiments showed that the wood-based SPAC have the highest capacity for MC-LR followed by the coal-based and coconut-based SPACs (Figure 4.5), whereas in the short contact time experiments the coconut-based SPAC had the highest capacity followed by the wood-based and coal-based SPACs at contact times of 30, 60 and 120 minutes (Figure 4.8). This is suspected to be the result of different experimental conditions, primarily the dosing method. The BG-HHM (wood-based) and COL-PL60-800 (coal-based) SPACs added to the bottles in the form of dry powder formed agglomerates upon contact with the solution. The WPC (coconut-based) SPAC shown better dispersibility characteristics and quickly dispersed in the bottles. However, the WPC (coconut-based) SPAC's short contact time capacity was less impacted by the dry powder dosing method; the better dispersibility of WPC (coconut-based) SPAC could explain its higher capacity at short contact times compared to the other two SPACs.

Table 4.2 Freundlich isotherm parameters for SPAC adsorption in ultrapure water at short contact times in the range of 5 to 180 minutes

SPAC	Contact time	number of data points	K_f $\left(\frac{\mu g}{mg}\right)$ $/\left(\frac{\mu g}{L}\right)^n$	K_f 95% CI*	1/n	1/n 95% CI*
BG-HHM (wood)	5 min	8	0	(0.00, 0,00)	2.61	(1.78, 3.44)
BG-HHM (wood)	10 min	8	0.01	(0.00, 0.02)	1.6	(1.21, 1.99)
BG-HHM (wood)	20 min	8	0.98	(0.45, 1.51)	0.54	(0.40, 0.68)
BG-HHM (wood)	30 min	8	1.96	(1.08, 2.84)	0.44	(0.32, 0.56)
BG-HHM (wood)	60 min	8	6.1	(5.08, 7.12)	0.27	(0.22, 0.32)
BG-HHM (wood)	120 min	8	9.5	(7.78, 11.23)	0.26	(0.19, 0.32)
BG-HHM (wood)	180 min	8	11.25	(9.00, 13.51)	0.26	(0.19, 0.34)
WPC (coconut)	5 min	8	0.27	(0.01, 0.54)	0.7	(0.45, 0.95)
WPC (coconut)	10 min	8	1.47	(0.78, 2.16)	0.38	(0.26, 0.50)
WPC (coconut)	20 min	8	3.37	(2.34, 4.41)	0.29	(0.21, 0.38)
WPC (coconut)	30 min	8	5.06	(3.60, 6.52)	0.25	(0.17, 0.33)
WPC (coconut)	60 min	7	8.37	(6.35, 10.40)	0.21	(0.14, 0.29)
WPC (coconut)	120 min	5	11.92	(7.82, 16.03)	0.21	(0.1, 0.33)
WPC (coconut)	180 min	5	13.51	(7.76, 19.25)	0.23	(0.09, 0.37)
COL-PL60-800 (coal)	5 min	8	0.01	(0.00, 0.02)	1.25	(1.04, 1.47)
COL-PL60-800 (coal)	10 min	8	0.08	(-0.02, 0.18)	0.94	(0.65, 1.22)
COL-PL60-800 (coal)	20 min	8	0.97	(0.55, 1.39)	0.45	(0.34, 0.56)
COL-PL60-800 (coal)	30 min	8	2.08	(1.32, 2.83)	0.31	(0.21, 0.41)
COL-PL60-800 (coal)	60 min	8	4.17	(3.04, 5.30)	0.23	(0.15, 0.31)
COL-PL60-800 (coal)	120 min	8	6.8	(6.01, 7.59)	0.18	(0.15, 0.22)
COL-PL60-800 (coal)	180 min	7	7.9	(6.61, 9.20)	0.19	(0.14, 0.24)

*(95% confidence interval calculated individually for K_f and $1/n$)

An experiment was designed and performed to investigate the dispersibility of the three SPACs involving the addition of a specific amount of SPAC to 30 mL of ultrapure water in vials and monitoring the vials as described in Section 4.2.4. The result showed that under the same conditions – i.e. in the absence of mixing and movement – the BG-HHM (wood-based) SPAC settled the fastest in only 1 day, and the COL-PL60-800 (coal-based) SPAC settled in 3 days. The WPC (coconut-based) SPAC did not settle and remained as a homogeneous suspension for the whole length of the experiment (6 days). The images from this simple experiment as a function of time passed are included in Appendix B.5. The better dispersibility of WPC SPAC is suspected to result from its surface charge properties, and this needs to be investigated more thoroughly in future studies (i.e. determination of zeta potential). Based on the performance difference between slurry-dosed and dry-powdered-dosed SPAC observed later in Chapter 5 and considering that the experimental commercial SPAC products such as PlumeStop liquid activated carbon (REGENESIS, San Clemente, CA) are delivered in the form of a suspended liquid, it is recommended that the SPAC be dosed as a properly wetted slurry.

4.3.4 Comparison with previously-determined values for the corresponding PACs

The equilibrium fittings from this study were compared to those from Liu (2017) Although the experimental conditions were different (i.e. higher MC-LR concentration and different dosing method), the K_f values of the equilibrium time fittings suggest that produced SPACs have much higher capacities compared to PACs. The JCRs of Freundlich parameters for adsorption of MC-LR onto both SPACs from this study and parent PACs from Liu (2017) at equilibrium are presented in Appendix B.13. The JCRs of the parent PACs do not overlap with ones for SPACs, therefore, it can be concluded that the difference in performance of SPACs and parent PACs is statistically significant. Figure 4.10 compares the best-fit Freundlich curves for SPACs and parent PACs at equilibrium. As it is evident from the Freundlich curves in Figure 4.10, the SPACs have significantly higher capacities for MC-LR compared to parent PACs in ultrapure water at equilibrium. The wood-based BG-HHM in the form of SPAC had the highest capacity for MC-LR compared to the other two coal-based and coconut-based SPACs, however, BG-HHM had the least capacity for MC-LR as PAC. The difference in range of MC-LR aqueous phase concentration (x axis) of PAC and SPAC adsorption data can be explained by the difference in experimental conditions, although the ranges overlap considerably; the equilibrium adsorption data for parent PACs were derived using bottle point tests with nominal initial MC-LR concentration of 100 μg/L (Liu, 2017) whereas the equilibrium adsorption data for SPACs in this study was derived using vial point tests with nominal initial MC-LR concentration of 300 μg/L as described in Section 4.2.3.
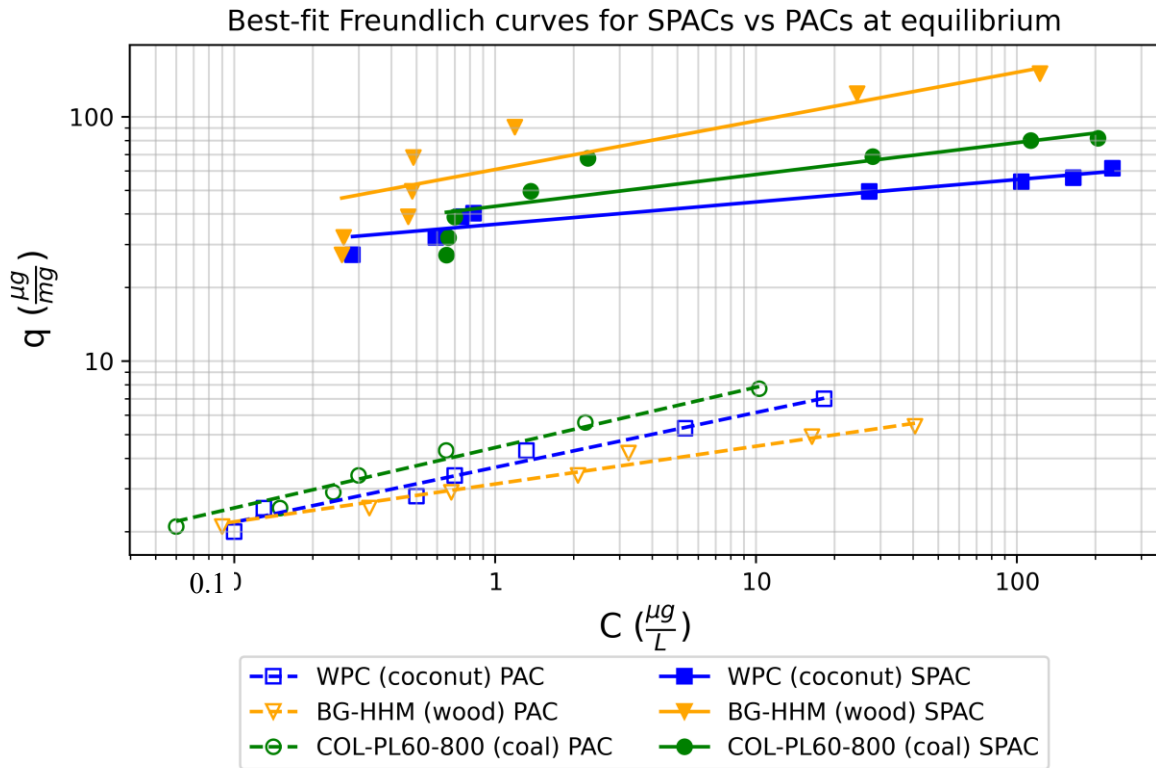
Figure 4.10 Comparison of best-fit Freundlich curves of SPACs for adsorption of MC-LR from this study and parent PACs from Liu (2017) at equilibrium in ultrapure water

The short contact time capacities (Freundlich fittings) for adsorption of MC-LR onto the three produced SPACs can be compared to values for MC-LR adsorption onto the three PACs determined by Liu (2017). The PACs used by Liu (2017) were the same wood-based BG-HHM, coal-based COL-PL60-800, and coconut-based WPC PACs, used in this study as the base material for the production of SPACs, and the bottle point test conditions were similar. Therefore, it is valid to directly compare the short contact time SPAC parameters determined in this study (30 and 60 minutes) with the PAC results reported by Liu (2017). The 95% JCRs for the Freundlich parameters of adsorption of MC-LR onto three parent PACs from Liu (2017) are presented Appendix B.14 along with the JCRs of the corresponding SPACs from this study at short contact times of 30 and 60 minutes. As is evident from the 95% JCRs, none of the PAC regions overlap with the SPAC regions, indicating that the performance of PACs and SPACs can be deemed statistically distinguishable. By visual inspection of the best-fit Freundlich curves in Figure 4.11, it can be concluded that the adsorption capacity of SPACs for MC-LR at short contact times of 30 minutes and 60 minutes substantially surpasses the capacity of corresponding PACs at these times. The superior performance of SPACs was despite the fact that the wood-based and coal-based SPACs experienced

agglomeration while dosed in form of dry powder. It is important to mention that the later experiments performed by dosing the SPACs in the form of a prewetted slurry in Lake Erie water (discussed in Chapter 5) showed that SPACs could perform with substantially faster adsorption rates when dosed in slurry form, resulting in having even higher capacities at short contact times when compared to parent PACs.
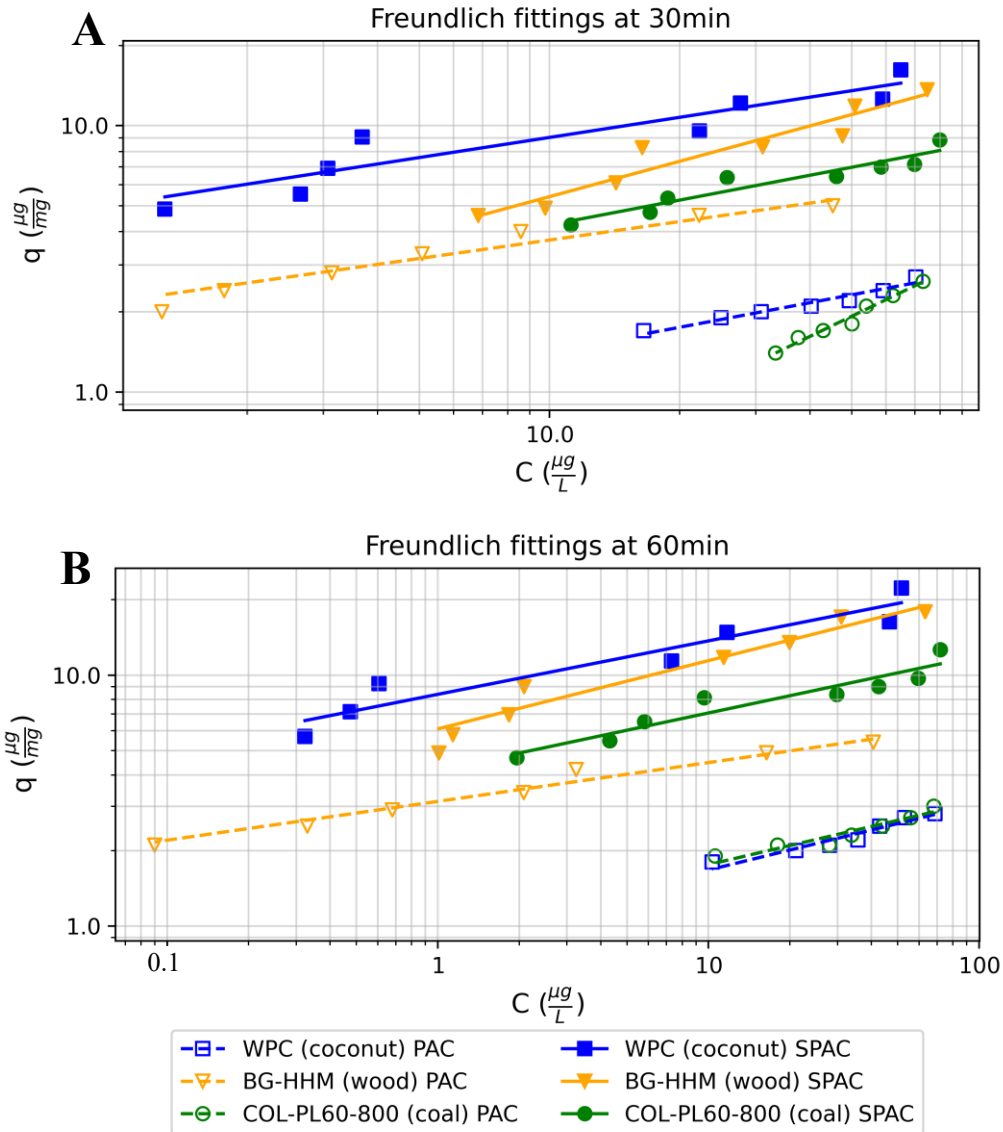
Figure 4.11 Best-fit Freundlich curves for adsorption of MC-LR onto the three PACs (dashed regions) and SPACs (solid regions) at three different contact times of (A) 30 minutes and (B) 60 minutes in ultrapure water

This increase in the adsorption capacity of the SPACs compared to the PACs can be explained by SPACs' significantly smaller particle size and high external surface area. Ando et al. (2010) hypothesized large

molecule compounds such as high-SUVA NOM and polystyrene sulfonates (PSSs) could not penetrate deep into activated carbon particles and would mainly get adsorbed onto the outer surface of particles. Matsui et al. (2011) have confirmed this hypothesis by investigating the adsorption of a variety of PSSs with MW ranging between 1100 to 1430 Da onto as received PACs and bench-scale produced SPACs. That study proposed a shell adsorption mechanism, which suggests that PSS molecules are principally adsorbed close to the external surface (shell) of carbon particles. Since the MW of MC-LR with a value of 995 Da is close to the MWs of PSSs (1100-1430 Da) used in the Matsui et al. (2011) study, it can be suggested that MC-LR is adsorbed onto SPAC particles in the same manner. The higher external surface area of SPACs have resulted in higher adsorption capacity for MC-LR. The higher capacities at short contact times are likely to be the result of the faster adsorption rates of SPAC compared to PAC.

4.4 Conclusions

This study investigated the adsorption in ultrapure water (pH 7.2) of MC-LR onto the three wood-based, coal-based, and coconut-based SPACs produced from commercially available PACs at bench-scale. The highlights and key conclusions drawn from the results in this chapter are summarized below:

- All three SPACs had relatively fast adsorption rates and reduced the MC-LR concentration to below MRL in less than two hours when using the same experimental conditions as for the parent PAC, which still had residual MC-LR concentration in solution at 2 hours. The BG-HHM (wood-based) SPAC presented the fastest adsorption rate for MC-LR, while COL-PL60-800 (coal-based) had the slowest;

- The pseudo-second-order rate constant model fitted the experimental results better than the pseudo-first-order model. However, a trend of systematic error was observed in residual values of both model fittings.

- At equilibrium, the SPACs had much higher capacity for MC-LR compared to the parent PACs (i.e. approximately 10 to 28 times higher depending on the base material of the SPAC). The BG-HHM (wood-based) SPAC had the highest capacity for MC-LR, while the WPC (coconut-based) SPAC had the lowest capacity for MC-LR.

- At short contact times, the SPACs presented different behavior in terms of capacity for MC-LR compared to equilibrium. The WPC (coconut-based) SPAC had the highest capacity for MC-LR, while the COL-PL60-800 (coal-based) SPAC had the least capacity. The difference between the order of capacities at non-equilibrium and equilibrium conditions can be largely explained by dispersibility issues of two of the SPACs when dosed as a dry powder.

- The WPC (coconut-based) SPAC showed excellent dispersibility while added as dry powder, while the wood-based and coal-based SPACs formed agglomerates upon contact with water, which took

at least an hour to be wetted and dispersed in the aqueous solution. Dosing the SPACs as a prewetted slurry alleviated these issues, therefore, SPACs were dosed as a prewetted slurry to an aqueous solution with a higher concentration of MC-LR to determine the capacities at equilibrium. To summarize, the produced SPACs presented a significantly better performance in adsorption of MC-LR compared to as-received PACs. The SPACs can perform much better when dosed as a prewetted slurry. However, the results showed that SPACs could outperform larger-sized PACs while dosed in either form of slurry or dry powder. The results from this chapter suggest that SPACs with small median sizes around 1 μm could be a reliable alternative to the current commercially available PACs with larger median sizes for the removal of MC-LR. However, it is necessary to investigate the effect of competing organic compounds such as NOM on the adsorption rates and capacities of SPACs.

Chapter 5

Adsorption of MC-LR in Lake Erie water

5.1 Introduction

The earlier results demonstrated that the SPACs could perform degrees of magnitude better than their PAC counterparts in terms of adsorption rate and capacity, mainly believed to be the result of their smaller particle size. PAC treatment, in general, can be an effective method for removal of cyanotoxins, including microcystins, from drinking water; however, it is known that the presence of competing background compounds such as NOM could hinder the adsorption performance of PAC for a variety of micropollutants (i.e., taste and odor compounds (2-MIB and geosmin), SOCs, microcystin-LR) (Bajracharya et al., 2018; Matsui et al., 2003; Newcombe et al., 2002). The NOM concentration in surface water -as a drinking water source- is typically much higher than the concentration of bloom-related compounds of concern such as 2-MIB, geosmin, and cyanotoxins, with DOC concentrations of 2 to 10 mg/L (Zoschke et al., 2011). The reduction in the capacity of PACs for cyanotoxins in the presence of NOM is attributed to the direct competition of NOM molecules with cyanotoxins for adsorption sites (Newcombe et al., 2002).

In terms of the adsorption of MC-LR in the presence of NOM onto PAC, it has been shown that the base material of the PAC could be a determining factor in terms of the reduction of the PAC adsorption capacity for MC-LR. Liu (2017) investigated the effect of NOM on adsorption of MC-LR onto wood-based, coal-based, and coconut-based PACs. The study revealed that the wood-based PAC adsorption capacity was impacted the least by the presence of NOM, while coal-based and coconut-based PACs adsorption capacities were substantially reduced by competition of NOM at a short contact time of 30 minutes. Bajracharya et al. (2018) performed a similar study using a wood-based PAC and a blend coal PAC, and also found that the wood-based PAC was impacted less by the presence of NOM at short contact times of 30 minutes and 60 minutes.

In terms of competition of NOM with target adsorbents/micropollutants in drinking water and wastewater treatment, SPAC is not immune to it either (Matsui et al., 2012). However, it is proven that SPACs have a higher adsorption capacity for the macromolecular fraction of NOM; these molecules tend to adsorb onto sites near the external surface of carbon particles (Ando et al., 2010; Matsui et al., 2010). Therefore, the adsorption capacity would increase with the increase of the external surface area of particles, which has an inverse relation with particle size (Ando et al., 2010).

The competitive effect of NOM on the adsorption capacity of SPACs for MC-LR has not yet been reported. It has been documented that NOM molecules with molecular weights in the range of 1100 to 2400 Da can compete with MC-LR for adsorption sites (Campinas et al., 2013).

As discussed in Section 2.2.3, several models were developed and applied to equilibrium adsorption data of micropollutants onto activated carbons in the presence of NOM to assess the competitive effect of organic matter as background compound on the performance of activated carbons in removal of micropollutants, such as the EBC model and SEBCM (Worch, 2012). Although these models are developed using equilibrium data as input, they have also been applied to non-equilibrium conditions for adsorption of taste and odor compounds (Shimabuku et al., 2014; Zoschke et al., 2011), and organic micropollutants (Zietzschmann et al., 2016). Matsui et al. (2012) also applied the EBC model to equilibrium data for MIB adsorption onto SPACs and acknowledged that the model could hold valid under non-equilibrium conditions. In this study, the SEBCM model was also selected to assess the competitive adsorption of MC-LR and NOM onto the prepared SPACs.

The main aim of this chapter is to assess the adsorption capacity of MC-LR onto SPACs in the presence of NOM at both equilibrium and short contact times; for this purpose, the experiments in this chapter were done using a sample of Lake Erie water collected at the intake of a water treatment plant. Lake Erie is affected by seasonal cyanobacteria blooms and typically contains DOC values in the range of 2 to 3 mg/L, making it suitable for this study.

The primary objectives of this study were to:

1. Evaluate the adsorption performance of the three prepared SPACs for adsorption of MC-LR in Lake Erie water at both equilibrium and short contact times

2. Apply SEBCM to adsorption data of SPACs under equilibrium and non-equilibrium conditions

3. Predict SPAC dose required to remove MC-LR from Lake Erie water at short contact times based on the SEBCM

5.2 Materials and methods

5.2.1 Materials

Three WPC (coconut-based), BG-HHM (wood-based), and COL-PL60-800 (coal-based) SPACs were used for the experiments in this chapter; the SPACs were prepared as explained in Section 3.3.1. The HPLC grade material, pure MC-LR, and c(RADfV) (internal standard) were obtained as per Section 4.2.1 for LC-MS/MS analysis. For sample preparation, Luer lock syringes and 25mm diameter 0.2 μm nylon syringe filters were obtained from Fisher Scientific (MA, USA).

The Lake Erie water was sampled at a water treatment plant located in southern Ontario. The water was sampled after the pH adjustment step (target pH 7.1-7.2) prior to the flash mixing tank on April 6, 2021. Water for selected raw water quality characteristics was transported in glass vials inside temperature-

controlled coolers and stored at 4°C before use. The normal pre-chlorination of the water was suspended for the purpose of sampling. The pH, turbidity, TOC, DOC, and UV_{254} of Lake Erie water were measured for characterization of the sampled water. The SUVA value was also calculated by dividing the UV_{254} absorbance (1/m) by DOC (mg C/L).

5.2.2 Bottle point method

The bottle point test method was again used for the determination kinetics and adsorption capacities of SPACs at short contact times in Lake Erie water. A 4.5 liter batch of Lake Erie water was spiked with MC-LR to achieve a nominal concentration of 100 µg/L, the actual starting concentration of the batch of spiked water was later measured via LC-MS/MS method; the batch was next distributed into 9 0.5-liter bottles. Eight of the bottles were dosed with SPAC doses in the range of 2-20 mg/L, while one bottle was reserved as a positive control (i.e. no SPAC added) during the experiments. Because of the problems with dried SPAC addition in the ultrapure water experiments, a prepared vortexed slurry with a concentration of 2 g/L was used for dosing the bottles in surface water experiments. However, 1 bottle for each SPAC with a concentration of 11 mg/L was dosed with a dry powder to compare the adsorption rate of MC-LR to the same water dosed with vortexed SPAC slurry. For all experiments, a bottle containing the maximum SPAC dose of 20 mg/L in non-spiked Lake Erie water was also prepared as a negative control.

5.2.3 MC-LR analysis by LC-MS/MS

The LC-MS/MS method for the measurement of MC-LR concentration is described in Section 4.2.3. The MDL of the method in Lake Erie water was determined to be 0.054 µg/L, and the MRL was set to 0.2 µg/L, which was also the lowest concentration of the calibration curve. The measured MC-LR concentrations above MRL were used to calculate adsorption curves and isotherms.

5.2.4 Modeling of competitive adsorption of NOM and microcystin-LR

The SEBCM model was chosen to describe the competitive adsorption of NOM with MC-LR onto SPACs in this study. The mathematical expression of the SEBCM model is a two-parameter equation. The model was fitted to the experimental adsorption data under equilibrium and non-equilibrium conditions to determine the model parameters (Equation 5.1), (Worch, 2012)).

$$ln\left(\frac{C_{1,0}}{C_1} - 1\right) = n_1 \ln\left(\frac{m}{V}\right) - ln(A) \qquad \text{(Equation 5.1)}$$

While $C_{1,0}$ is the initial concentration of the target micropollutant, C_1 is the concentration of the target micropollutant, n_1 is the Freundlich exponent for the target micropollutant, m is the adsorbent mass, V is

the volume of the solution, and A is the model parameter that incorporates the initial concentration and Freundlich exponent of the equivalent background compound (EBC).

The parameters $C_{1,0}$, C_1, m and V were obtained from the bottle point and vial point tests, while A and n_1 were determined by fitting the model to the adsorption data. The required dose for removal of target contaminant can be predicted via Equation 5.2.

$$\frac{m}{V} = A^{1/n_1} \left(\frac{C_{1,0}}{C_1} - 1\right)^{\frac{1}{n_1}}$$
(Equation 5.2)

The SEBCM was applied to both equilibrium and non-equilibrium (30 and 60 minutes of contact time) adsorption data for MC-LR onto the SPACs.

5.3 Results and discussion

5.3.1 Lake Erie water characterization

The properties of the sampled Lake Erie water in April, 2021 are summarized in Table 5.1. The collected raw water was not pre-chlorinated prior to sampling. The samples were taken following the pH adjustment in the plant, targeting a pH range between 7.1 to 7.2; however, the measured pH of the water at the time of receiving the samples was 7.5. The turbidity of the received water was 17.6 upon receiving the sample. The TOC of the water was measured to be 2.33 mg/L, slightly higher than its DOC of 2.28 mg/L. The SUVA, the ratio of UV_{254} absorbance to DOC concentration, was measured to be 1.99 $L/(m * mg)$. The received water sample was not filtered prior to the adsorption experiments.

Table 5.1 Lake Erie water properties at time of sample collection

Properties	Lake Erie water
pH	7.5
Turbidity (NTU)	17.6
TOC (mg/L)	2.331
DOC (mg/L)	2.285
UV_{254} (1/m)	0.13
SUVA ($L/m * mg$)	1.99

5.3.2 Rate of adsorption in Lake Erie water and effect of the dosing method

The MC-LR concentration with respect to time for dosing of 11 mg/L of each SPAC with different combinations of waters and dosing methods is presented in Figure 5.1. By visual inspection of Figure 5.1, it can be found that the performance of the SPAC when dosed as a powder to Lake Erie was lower compared to the ultrapure water experiments, which is expected to be the result of competitive adsorption of NOM in Lake Erie water. However, when the SPAC was dosed as a prewetted slurry the adsorption rate increased substantially, surpassing the performance of powdered dosed SPACs in both ultrapure and Lake Erie water. The faster adsorption rate of MC-LR via the slurry dosing method is evident from the concentration curves of MC-LR, and it is postulated that this faster adsorption rate is primarily the result of better dispersion of SPACs in the form of prewetted slurry. Due to the substantially faster performance of SPACs in the form of prewetted slurry, all the experiments from this point forward were done via the slurry dosing method. Slurry dosing is also deemed a viable method for the use of SPAC in water treatment practice; the SPAC is produced via wet milling, which makes the form of the final product a concentrated slurry. Considering that drying the slurry is time and energy consuming and SPAC performs better in the form of a prewetted slurry, it is recommended that SPAC would be dosed in slurry form. It is also expected that the adsorption rate of SPACs could further improve with the sonification of the slurry and addition of emulsifiers. However, investigating the effect of sonification and emulsifiers is out of this study's scope since sonification could not be performed at larger scales in typical drinking water treatment scenarios, and the addition of emulsifiers could hinder the adsorption capacity SPAC.
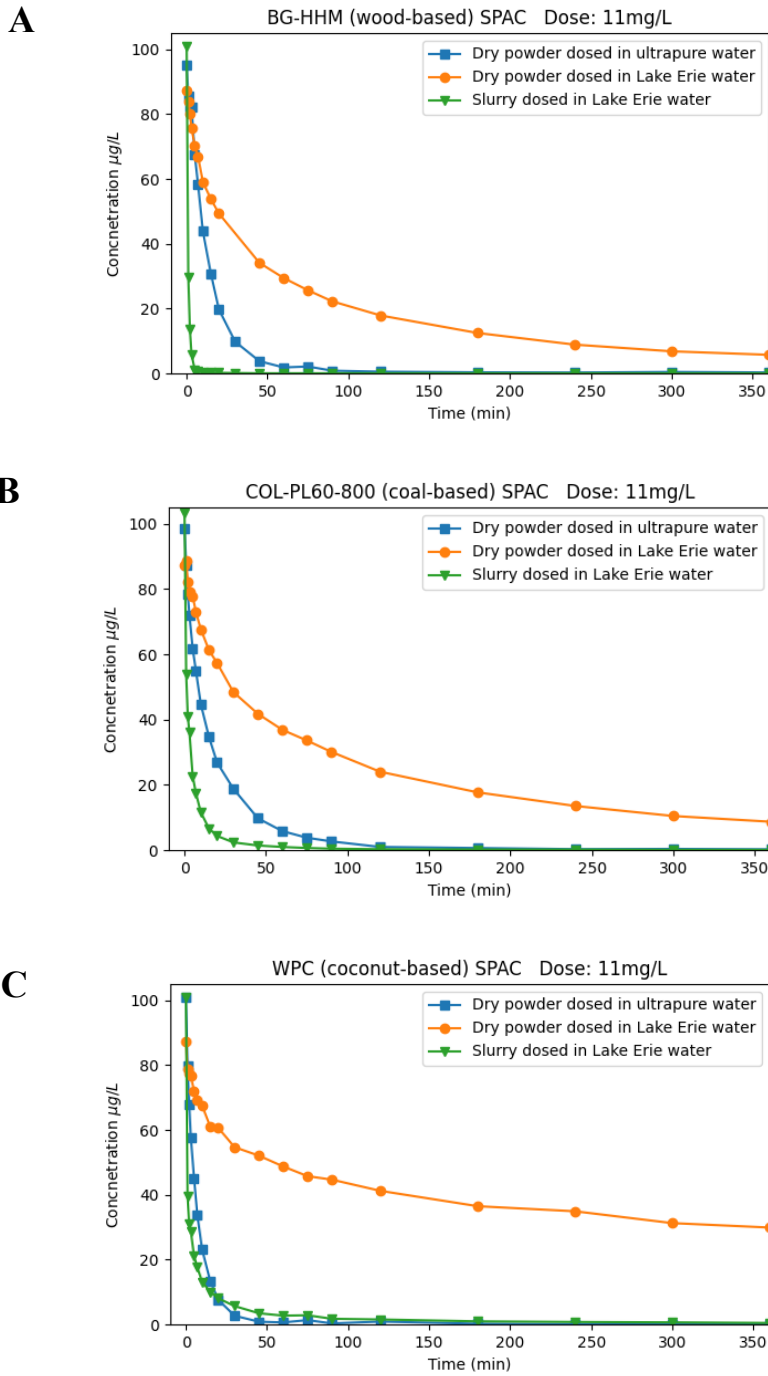
Figure 5.1 Comparison of the adsorption rate of MC-LR onto the three (A) wood-based, (B) coal-based, and (C) coconut-based SPACs at a dose of 11 mg/L using different dosing methods and water types: dry powder in ultrapure water, dry powder in Lake Erie water, and slurry in Lake Erie water

The pseudo-first and -second-order rate models were applied to adsorption rates of MC-LR onto the three SPACs. Similar to ultrapure water results, the coefficient of determination (R^2) values of the pseudo-first-order model was lower than the values for the pseudo-second-order model, and the predicted equilibrium concentrations deviated substantially from the experimental ones. Therefore, only the pseudo-second-order rate model was used to describe the adsorption rate of MC-LR onto the SPACs; the fittings are presented in Figure 5.2 and the residual plots are included in Appendix C.4 . The parameters of the pseudo-second-order rate model fitted to the MC-LR adsorption data onto the three SPACs are presented in Table 5.2. When comparing K_2 values for ultrapure water with those for Lake Erie water both dosed with dry powder, it can be concluded that the adsorption rate of MC-LR onto the three SPACs was highly impacted by the NOM in the Lake Erie water, with WPC (coconut-based) SPAC the most impacted. However, when the three SPACs were dosed in the form of prewetted slurry in the Lake Erie water, the adsorption rates increased substantially, with K_2 values as high as $16.49\ mg/\mu g/min$ surpassing the values determined for ultrapure water (Table 5.2 and Figure 5.3). This substantial increase in adsorption rate is primarily due to the very fast dispersion of the carbon particles and the absence of agglomerates in the mixture.
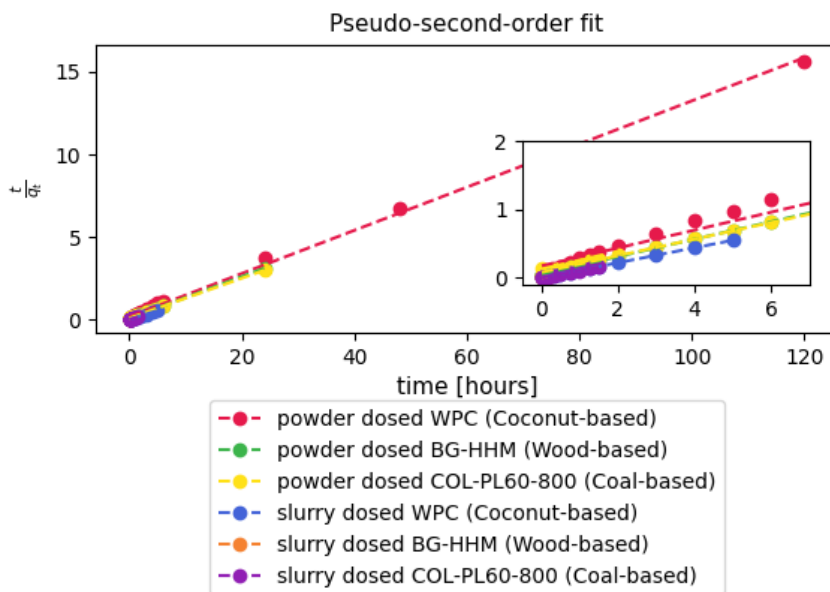
Figure 5.2 Pseudo-second-order fits for SPACs comparing dry powder and slurry dosing methods

Table 5.2 Pseudo-second-order rate model parameters for different water and dosing method combinations (Ultrapure water results are from Chapter 4)

Water and dosing method	Carbon	q_e experimental $(\mu g/mg)$	q_e predicted $(\mu g/mg)$	$K_2(mg/\mu g/min)$	R^2
Ultrapure powder dosed 11 mg/L	WPC (Coconut-based)	8.97	9.32	1.88	0.9994
	BG-HHM (Wood-based)	8.62	8.91	0.80	0.9984
	COL-PL60-800 (Coal-based)	8.62	8.85	0.92	0.9998
Lake Erie powder dosed 11mg/L	WPC (Coconut-based)	7.89	7.65	0.10	0.9980
	BG-HHM (Wood-based)	7.76	7.86	0.29	0.9998
	COL-PL60-800 (Coal-based)	8.16	8.26	0.18	0.9991
Lake Erie slurry dosed 11mg/L	WPC (Coconut-based)	9.13	9.15	4.70	1.0000
	BG-HHM (Wood-based)	9.14	9.54	16.49	0.9994
	COL-PL60-800 (Coal-based)	9.38	9.52	4.73	1.0000
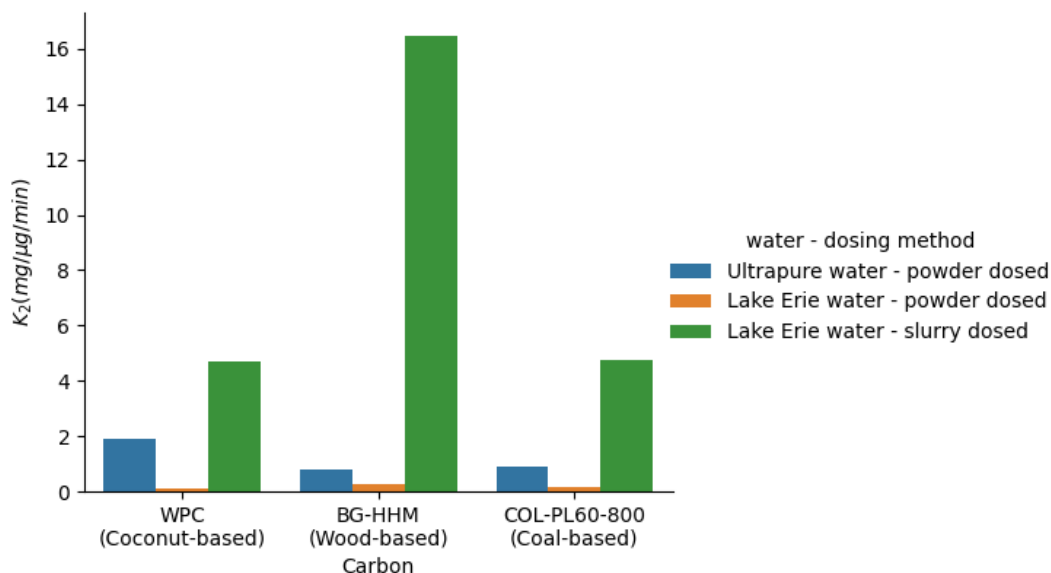
Figure 5.3 Comparison of K_2 values for different waters and dosing methods in this study

Figure 5.4 summarizes the removal rate of MC-LR via the three prepared SPACs as a function of time in Lake Erie water; it should be noted that these results were acquired by dosing the SPACs in the form of a prewetted vortexed slurry. The BG-HHM (wood-based) SPAC adsorbed the MC-LR the fastest among the three different SPACs, followed by the COL-PL60-800 (coal-based) SPAC, while the WPC (coconut-based) SPAC was the slowest. However, the adsorption of MC-LR by the three SPACs was fast, removing > 90% of MC-LR in less than 1 hour of contact time (Figure 5-1A).The concentration of MC-LR in the kinetics experiments when 11mg/L of SPACs added quickly dropped from the initial ~100 µg/L to below MRL, which would indicate that the SPACs have high capacities for MC-LR. Therefore, the determination of equilibrium time was not possible at the SPAC dose of 11 mg/L. At the dose of 2 mg/L – the lowest dose of applied SPACs – the equilibrium time could be determined; since the dose of SPAC was very low and a residual MC-LR concentration above MRL could be measured. As evident in Figure 5.4B, the three SPACs reached equilibrium in under 20 minutes. At the dose of 2 mg/L, the WPC (coconut-based) and COL-PL60-800 (coal-based) SPACs presented an abnormal trend in adsorption of MC-LR; the concentration of MC-LR quickly dropped in the first 20 minutes of experiments, and then increased slightly before reaching a steady concentration. This trend could be indicating that a certain fraction of NOM might be displacing the adsorbed MC-LR on the SPACs. However, a certain conclusion cannot be derived by only two observations, and this hypothesis should be more thoroughly investigated in future studies.
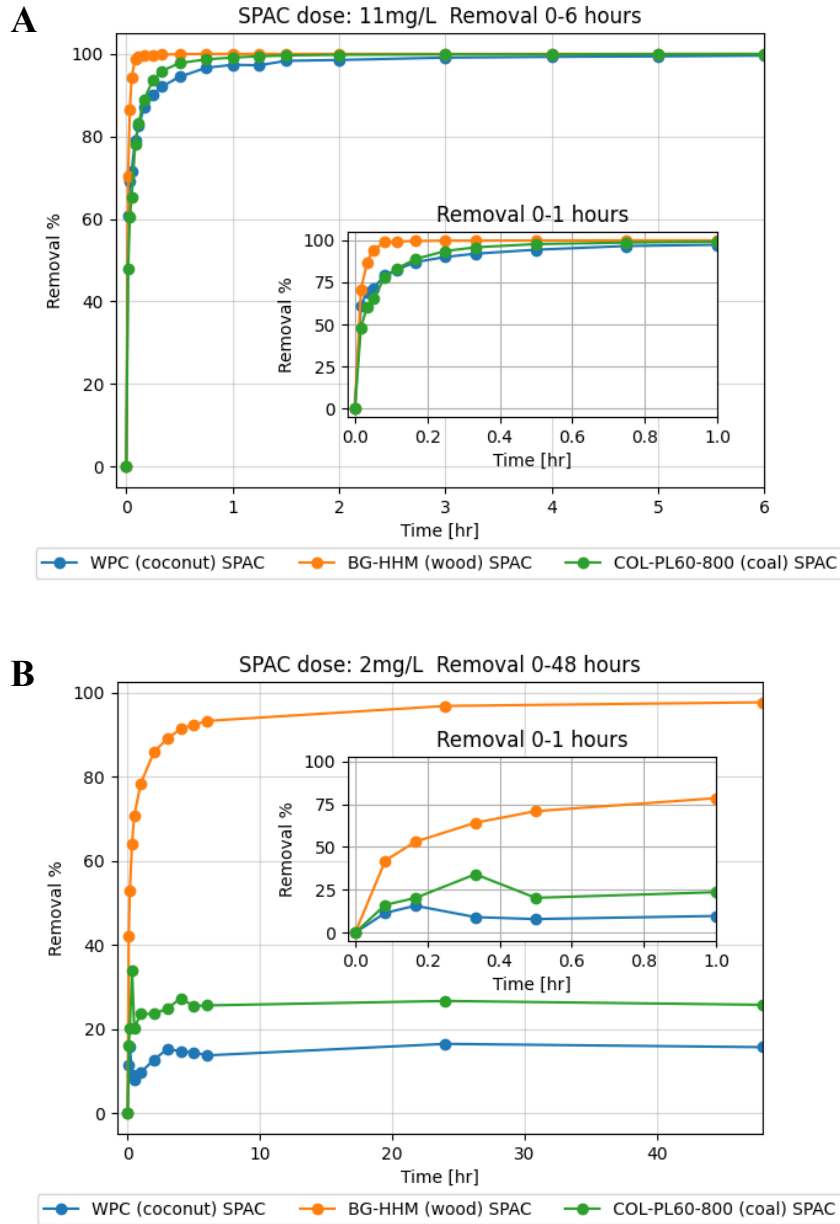
Figure 5.4 MC-LR removal rate in Lake Erie water via slurry dosed SPACs at a dose of (A) 11 mg/L and (B) 2 mg/L

The adsorption rate of MC-LR onto SPACs is compared to parent PACs studied by Liu (2017). The k_2 values for the pseudo-second-order rate model for SPAC and parent PACs are compared in Figure 5.5. It should be noted that the parent PACs were dosed as dry powder at 50 mg/L, approximately 5 times higher than the 11 mg/L dose used for SPACs. As is evident from Figure 5.4 the SPACs dosed as prewetted slurry outperformed the parent PACs, However, the SPACs dosed as dry powder failed to outperform the parent PACs, primarily due to the lower applied dose.
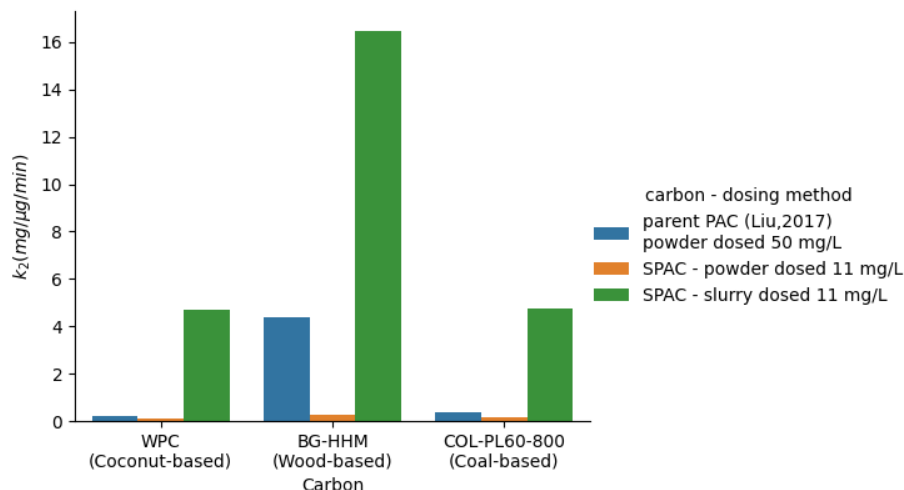
Figure 5.5 Pseudo-second-order rate constants of SPACs compared to parent PACs from Liu (2017) in Lake Erie water

5.3.3 Isotherms in Lake Erie water

5.3.3.1 Joint confidence regions of Freundlich parameters (Equilibrium condition)

The JCRs for the adsorption of the MC-LR onto the three SPACs at equilibrium times (vial point tests) are determined and presented in Appendix C.5.

As is evident, the JCRs at contact times of 48h and 96h are very similar and overlap, indicating that SPACs have essentially reached equilibrium at these times, since the performance of the SPACs at these two times are not statistically distinguishable. The JCRs for all three SPACs are completely distinguishable from each other; therefore, it can be concluded that the performance of the three SPACs for adsorption of MC-LR in Lake Erie at equilibrium is statistically distinguishable (Figure 5.6). The larger size of BG-HHM (wood-based) SPAC JCRs is mathematically explainable since the available data points for the fitting were only 5 because three data points were below the MRL and could not be used for the fitting.
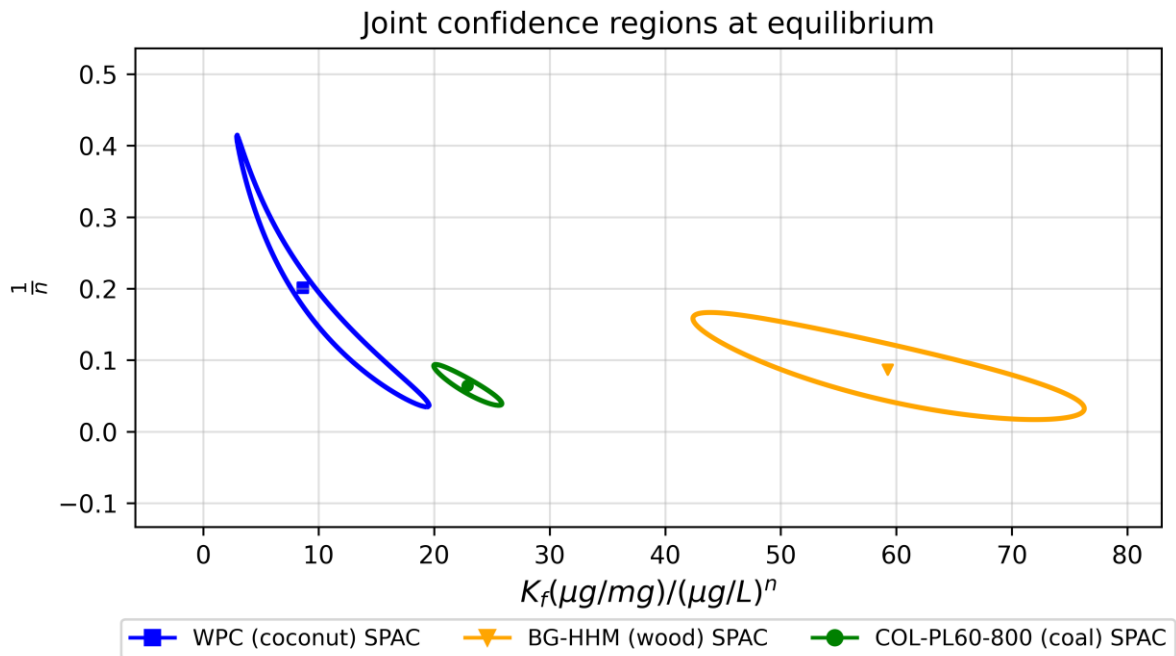
Figure 5.6 JCRs for adsorption of MC-LR on to the three prepared SPACs in Lake Erie water at equilibrium time of 48h

5.3.3.2 Freundlich parameters determination (equilibrium conditions)

The Freundlich isotherm model was applied to the adsorption data of MC-LR onto the BG-HHM (wood-based), WPC (coconut-based), and COL-PL60-800 (coal-based) SPACs at both 48h and 96h equilibrium times. The determined model parameters, along with the confidence intervals, are summarized in table 5.3. The Freundlich fitting curves are also presented in Figure 5.7.

Based on visual observation in Figure 5.7, the BG-HHM (wood-based) SPAC showed the highest capacity equilibrium capacity for MC-LR, with mass loadings in the range of 45 to 90 µg/mg of wood-based SPAC. The COL-PL60-800 (coal-based) SPAC had MC-LR capacities in the range of 20 to 38 µg/mg, which was in between the other two SPACs. The WPC (coconut-based) SPAC had the lowest capacity for MC-LR in Lake Erie water under equilibrium conditions with mass loading rates ranging from 12 to 31 µg/mg. The COL-PL60-800 (coal-based) and WPC (coconut-based) SPACs' Freundlich curves converge as the liquid phase concentration of MC-LR increases, and this indicates that the coal-based and coconut-based SPACs could have a more similar performance at higher MC-LR concentrations.
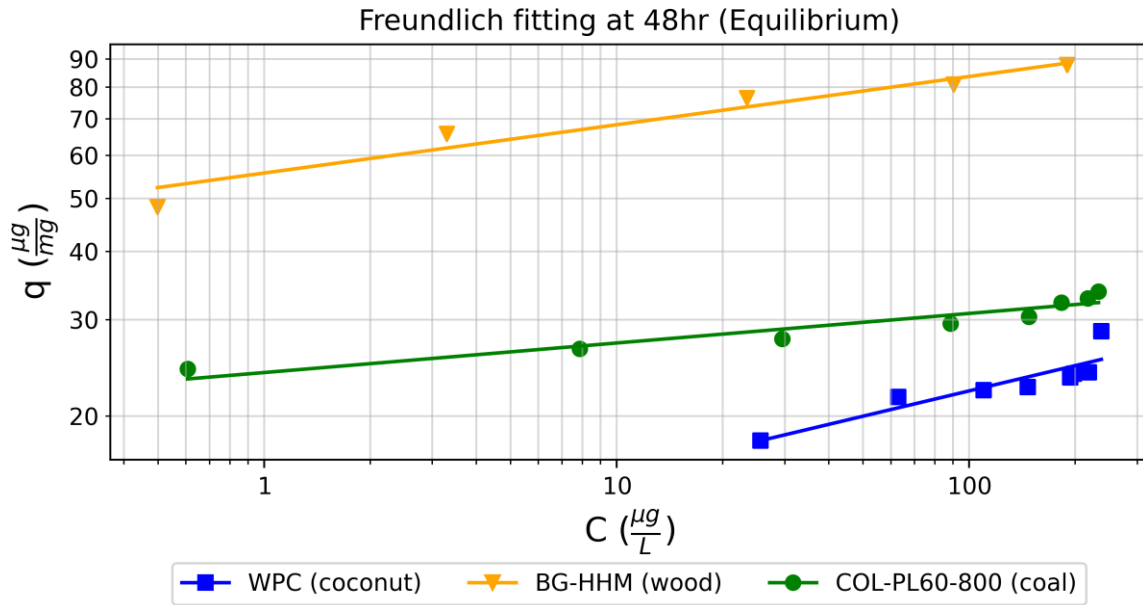
Figure 5.7 Freundlich fitting curves for adsorption of MC-LR onto the three SPACs at equilibrium times of 48hr

From the Freundlich parameters in Table 5.3, the order of K_f values for the three SPACs agrees with the order of capacities found by visual inspection of the curves in Figure 5.7. By inspecting the values in Table 5.3, it is evident that both the K_f and 1/n values are very similar for the 48hr and 96hr contact times. The residual plots for the Freundlich curves are presented in Appendix C.10; no trend of systematic error was found in the residuals of BG-HHM (wood-based) and COL-PL60-800 (coal-based) SPACs fittings. However, a trend could be observed for the residuals of WPC (coconut-based) SPAC, which could explain the larger confidence intervals for both K_F and 1/n parameters of this SPAC. Disregarding the effect of 1/n values, the K_F values would suggest that the wood-based BG-HHM SPAC has the highest capacity for MC-LR in Lake Erie water at equilibrium, followed by the coal-based COL-PL60-800 SPAC. The coconut-based WPC SPAC had the lowest capacity for MC-LR in Lake Erie water. However, this interpretation is qualitative because of the correlation between K_F and 1/n.

Table 5.3 Best-fit Freundlich parameters for adsorption of MC-LR onto the three SPACs at equilibrium times of 48h and 96h

SPAC	Contact time	Number of data points	K_f $\left(\frac{\mu g}{mg}\right)/\left(\frac{\mu g}{L}\right)^n$	K_f 95% CI	$1/n$	$1/n$ 95% CI
BG-HHM (wood)	48h	5	55.65	(50.47, 60.82)	0.09	(0.06, 0.11)
	96h	5	59.24	(51.48, 66.99)	0.09	(0.05, 0.12)
WPC (coconut)	48h	8	10.94	(6.81, 15.08)	0.15	(0.08, 0.23)
	96h	8	8.63	(3.89, 13.37)	0.2	(0.09, 0.31)
COL-PL60-800 (coal)	48h	8	24.01	(22.32, 25.7)	0.05	(0.04, 0.07)
	96h	8	22.89	(21.09, 24.69)	0.06	(0.05, 0.08)

The results from equilibrium experiments in this chapter were compared to the equilibrium results for the parent PACs from Liu (2017), since the PAC products used by Liu (2017) were the same as the products used in this study for preparation of SPACs. The DOC in the batch of Lake Erie water used by Liu (2017) for determination adsorption MC-LR onto the three PACs was 2.3 mg/L, which is very close to the value measured for Lake Erie water in this study (2.28 mg/L). The similar DOC values suggest that the results from this study and the ones collected by Liu (2017) can be compared to each other. The 95% confidence level JCRs for Freundlich parameters for adsorption of MC-LR onto SPACs and parent PACs are presented in Appendix C.8. Since the JCRs of SPACs do not overlap with the ones for parent PACs, it can be concluded that the performance of SPACs and parent PACs are statistically distinguishable. The best-fit curves for the parent PACs and SPACs are presented Figure 5.8. By visual investigation of the curves, it can be concluded that the capacity of SPACs is significantly higher than that of the parent PACs. However, it should be noted that the initial MC-LR concentration and dose of SPACs are different than the ones used in experiments by Liu (2017) hence the difference in the range of the curves in terms of equilibrium MC-LR concentration (x axis). It is also interesting to observe that the order of the capacities for different base material (i.e. coconut, wood, coal) is the same for both SPACs and PACs.
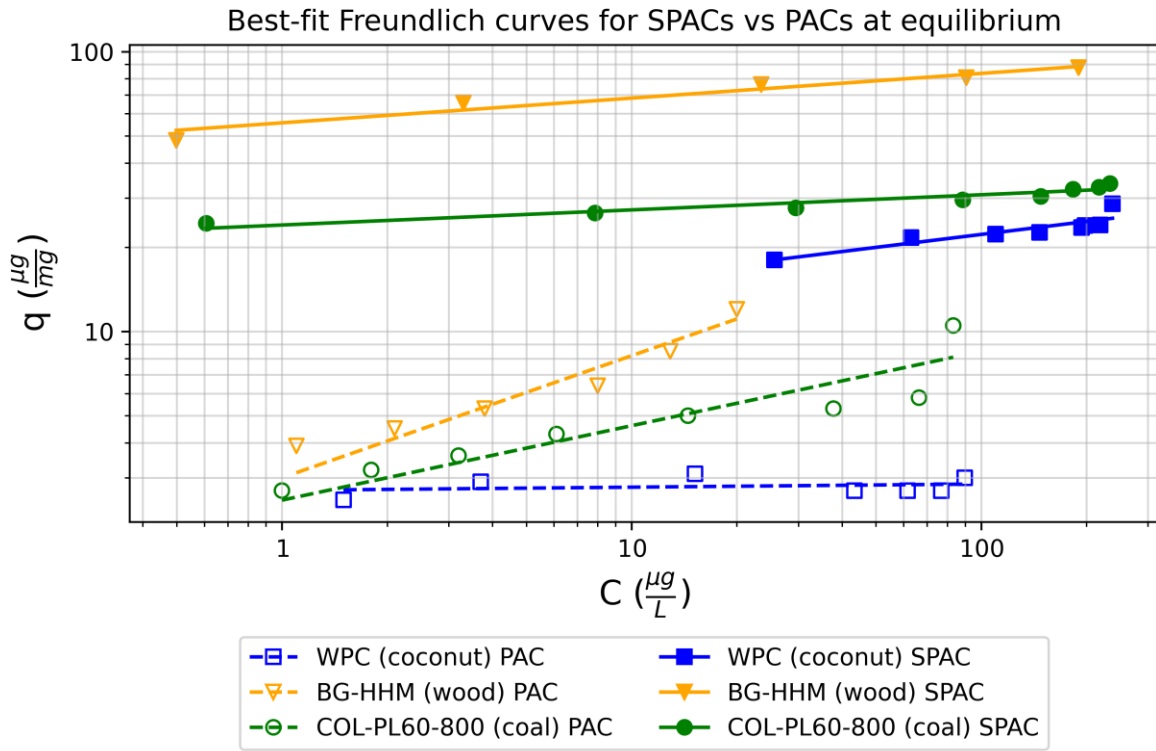
Figure 5.8 Best-fit Freundlich curves for SPACs vs PACs at equilibrium for removal of MC-LR in Lake Erie water
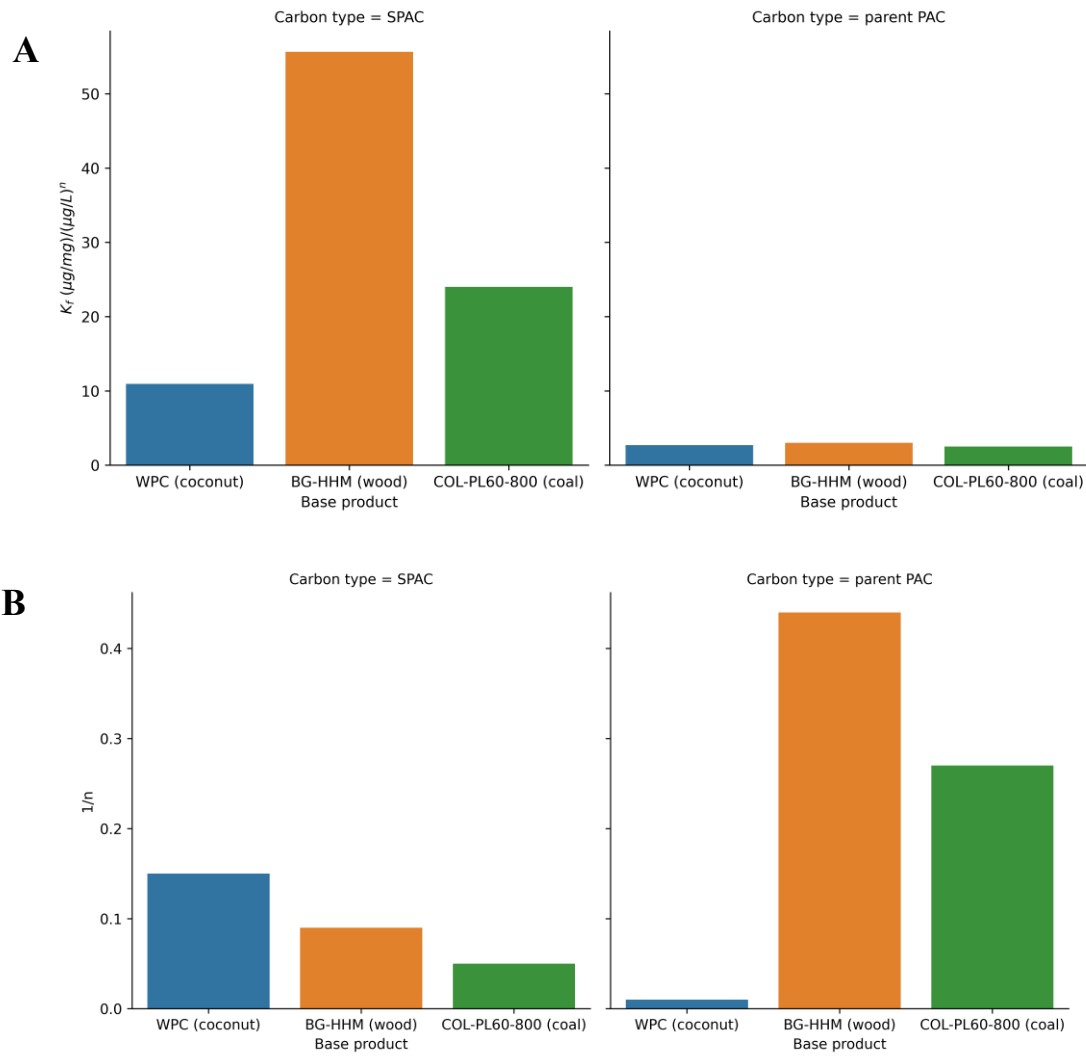
Figure 5.9 Comparison of Freundlich parameters for SPACs vs PACs including (A) K_f and (B) $1/n$

The Freundlich parameter values for the SPACs and parent PACs are also compared in Figure 5.9. The differences in K_f values between SPACs and PACs (Figure 5.9A) agrees with the results found by visual inspection in Figure 5.8. Interestingly, when comparing the 1/n values between the SPACs and parent PACs it can be seen that the change of 1/n for SPACs is not as drastic as for the PACs and generally lower, which would be an indication that the change in capacity of SPACs at different applied doses is less pronounced than that for the parent PACs.

The capacities of SPACs for MC-LR in this study are also compared to the capacities found by Bajracharya et al. (2018) for wood-based, coal-based and coconut-based PACs by dosing the PACs in the form of prewetted slurry in water containing 5 mg/L of Suwannee river fulvic acid (with a resulting DOC of 2.56

mg/L). By comparing the equilibrium capacities from Bajracharya et al. (2018) with capacities of parent PACs and SPACs, it was found that SPACs outperformed the PACs used in that study, since the capacities for prewetted PACs used by Bajracharya et al. (2018) were close to what Liu, (2017) found for the dry dosed parent PACs.

The adsorption of MC-LR via SPACs is not covered by the literature at the time of writing, However, the adsorption capacity of SPACs prepared from different base materials for different micropollutants such as 2MIB, geosmin, a variety of pharmaceuticals, NOM and polystyrene sulfonates (PSSs), and per- and polyfluoroalkyl substances (PFAS) are established by the literature (Bonvin et al., 2016; Matsui et al., 2004, 2011, 2013; Murray et al., 2018). All of the aforementioned studies have found that the SPACs have similar or superior capacity for the mentioned micropollutants at equilibrium, although the gain in equilibrium adsorption capacity is highly correlated with the micropollutant characteristics (i.e. MW and charge) and the type of activated carbon base material (e.g. wood-based, coal-based, and coconut-based).

5.3.4 Influence of NOM on the adsorption of microcystin-LR

The characteristics of the batch of Lake Erie water used for experiments to evaluate the adsorption capacity of MC-LR onto the three SPACs are summarized in Table 4.1. The turbidity of the raw water received was measured to be 17.6 NTU, the pH measured was 7.5, and the TOC and DOC values were 2.33 and 2.29 mg C/L. The UV_{254} and SUVA values were also measured with values of 0.13 $1/m$ and 1.99 $L/m*m$g.

The removal percentages of DOC by the three SPACs at the highest dose of 20 mg/L are reported in Appendix C.8. The WPC (coconut-based) and COL-PL60-800 (coal-based) SPACs removed the DOC in Lake Erie water similarly, with removals of 49.8% and 50.3%, respectively. The mesoporous BG-HHM (wood-based) SPAC surprisingly removed only 40.5% of the DOC though it had the highest capacity for MC-LR in ultrapure water and Lake Erie water. This suggests that the wood-based SPAC had a selective behavior when it comes to the removal of MC-LR in the presence of NOM. This could be attributed to the positive surface charge of the wood-based SPAC in the natural water pH range of 6 to 8 due its pH_{pzc} of 4.1. The positively charged wood-based PAC/SPAC could show a greater affinity to negatively charged MC-LR molecules.

By comparing the JCRs for adsorption of MC-LR via the SPACs at equilibrium times of 48 hours and 96 hours in ultrapure water versus Lake Erie water, it can be concluded that the performance difference of each SPAC in ultrapure water and Lake Erie water is statistically significant (Figure 5.10 for 48h and Appendix C.7 for 96h). However, at 96h of contact, the performance of the BG-HHM (wood-based) SPAC in ultrapure water and Lake Erie water becomes less statistically distinguishable, because of the overlap between its JCRs for the different waters.

Figure 5.11 compares the Freundlich plots for adsorption of MC-LR by the three SPACs in both ultrapure water and Lake Erie water at equilibrium times of 48 h. The plots for the WPC (coconut-based) and COL-PL60-800 (coal-based) SPACs show that the performance of these SPACs was substantially hindered by the presence of NOM at equilibrium. If the effect of 1/n is disregarded, by qualitatively comparing the K_f values in Table 5.3 with values for the ultrapure water at equilibrium in Table 4.1, it can be inferred that the BG-HHM (wood-based) SPAC capacity was reduced by approximately 8-13% in Lake Erie water, while COL-PL60-800 (coal-based) capacity was reduced by 44-50% and WPC (coconut-based) SPAC experienced 69-77% reduction in capacity. This might indicate that the performance of microporous WPC (coconut-based) SPAC in adsorption of MC-LR is the most vulnerable to competitive effects of NOM while mesoporous BG-HHM (wood-based) SPAC was affected the least. Interestingly, the order in the reduction in capacity of SPACs for MC-LR in Lake Erie water is very similar to what Liu (2017) observed for the parent PACs.
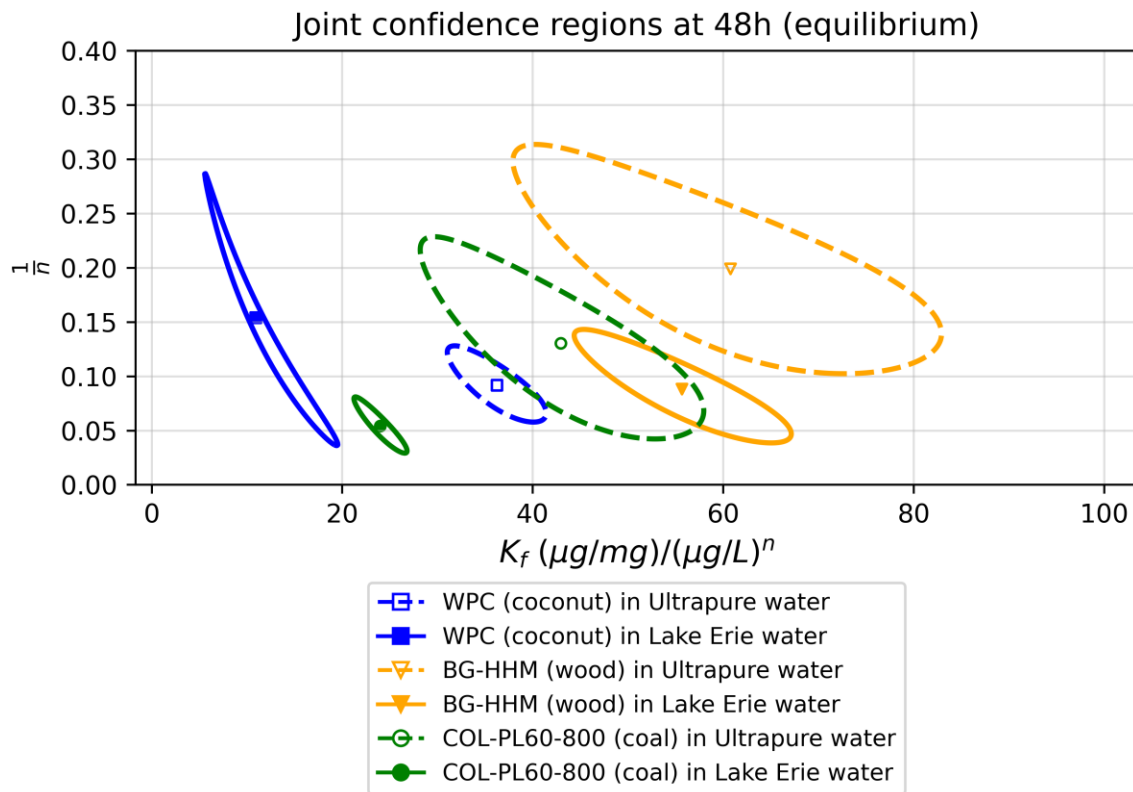
Figure 5.10 The 95% JCRs for Freundlich parameters of adsorption of MC-LR onto SPACs in ultrapure water (dashed lines) and surface water (solid lines) at equilibrium (48 h)
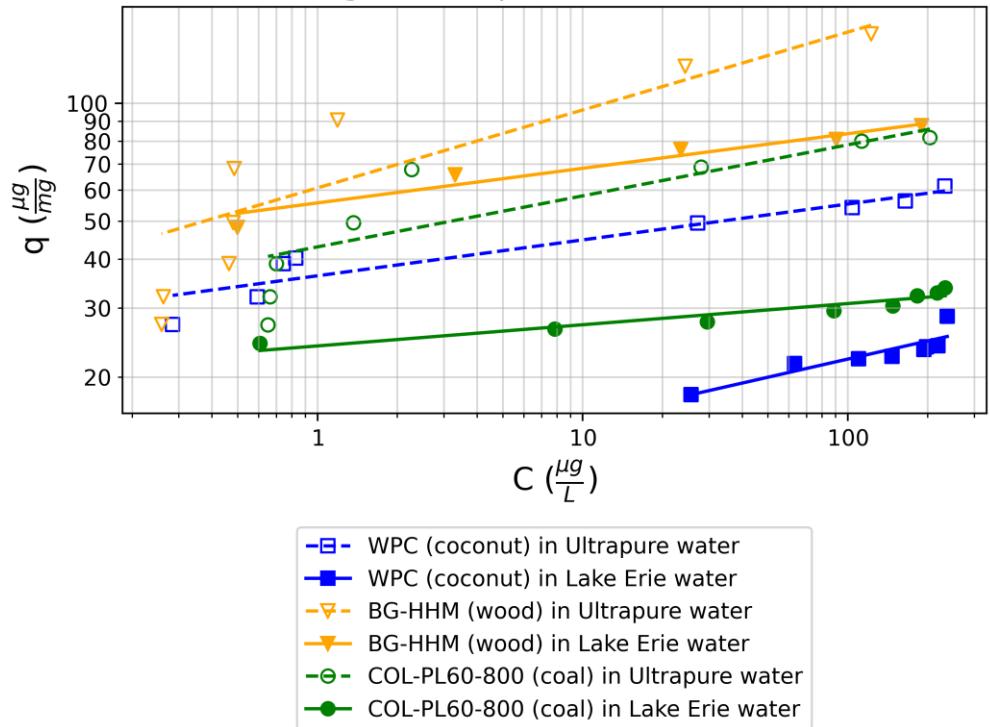
Figure 5.11 Best-fit Freundlich fitting curves of SPACs at equilibrium time of 48hr in both Lake Erie water and ultrapure water

5.3.5 Short-contact time (non-equilibrium, bottle point tests) Freundlich parameters

As mentioned earlier, the typical PAC/SPAC water contact times at DWTPs are less than 1 hour, therefore, it is essential to evaluate the capacity of SPACs at short contact times in Lake Erie water to investigate the competitive effect of NOM on the adsorption of MC-LR.

To establish the capacities of SPACs at short contact times, the bottles from the bottle point tests were sampled at contact times ranging from 5-180 minutes. The JCRs for these contact times are presented in Appendix C.11, the JCRs for WPC (coconut-based) SPAC with respect to time are also presented in Figure 5.13 as an example. The JCRs of the Freundlich model parameters for adsorption of MC-LR onto the three SPACs at a time of 30 minutes are presented in Figure 5.12 as an example and the 60 and 120 minutes JCRs can also be found in Appendix C.12. For all contact times in the range of 5 to 180 minutes, the JCRs of the three SPACs in Lake Erie water did not overlap at all, indicating that the performance difference of three SPACs in adsorption of MC-LR is statistically significant. However, for BG-HHM (wood-based) SPAC, the JCRs could not be established due to the limited number of data points above MRL; to be more specific fewer than 3 data points were available for contact times in the range of 60 to 180 minutes, though the large

difference in the fitted K_f values would suggest that the results could be statistically distinguishable. The low number of data points is associated with the very fast adsorption of MC-LR by the BG-HHM (wood-based) SPAC when dosed in the form of a prewetted slurry; the concentration of MC-LR in the aqueous phase quickly dropped below MRL when doses in the range of 8 to 20 mg/L of SPAC were used.
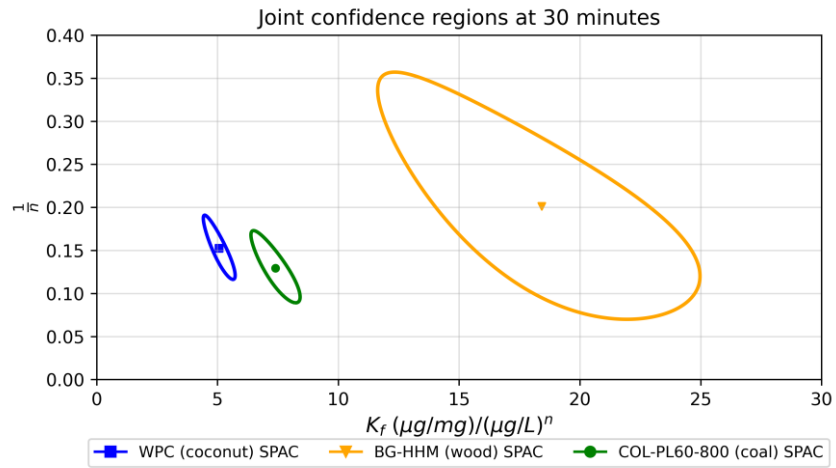
Figure 5.12 JCRs for adsorption of MC-LR onto SPACs at short contact time of 30 minutes
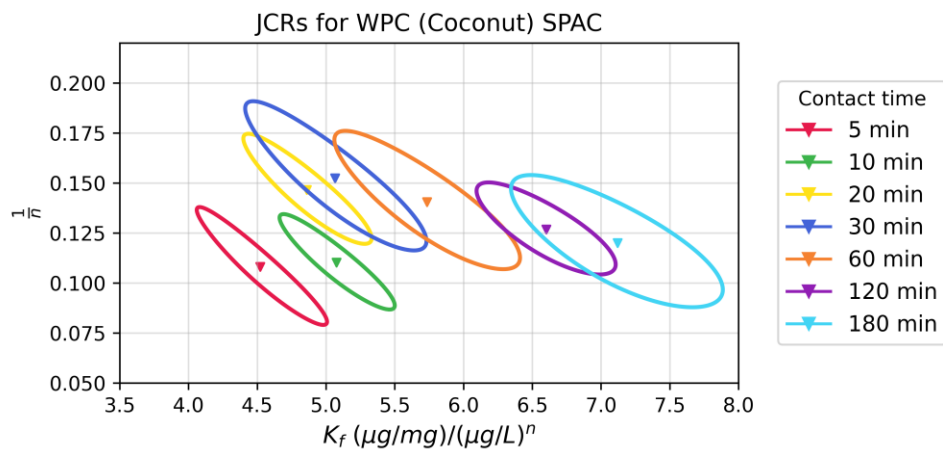
Figure 5.13 JCRs of the Freundlich parameters for the WPC (coconut-based) SPAC with respect to time
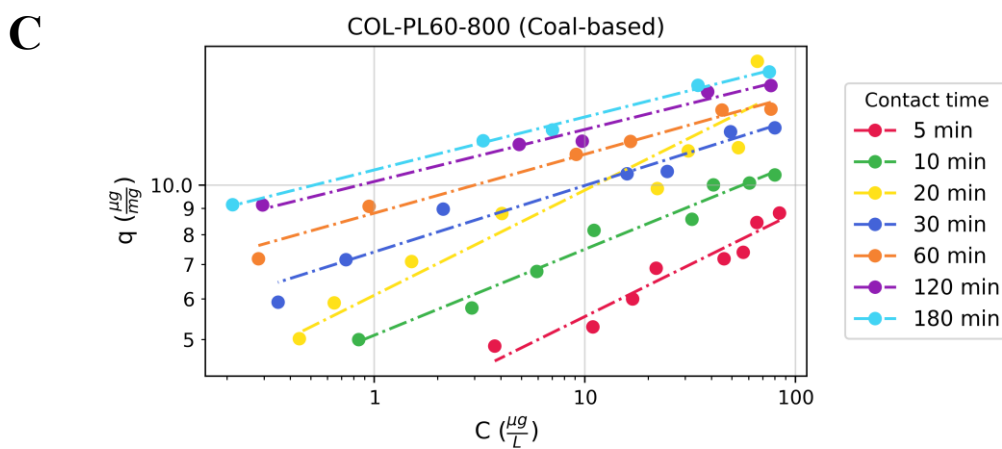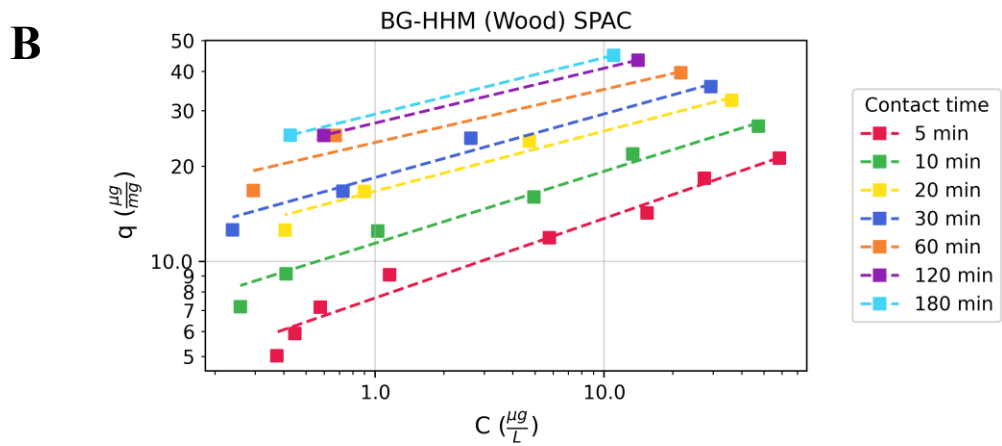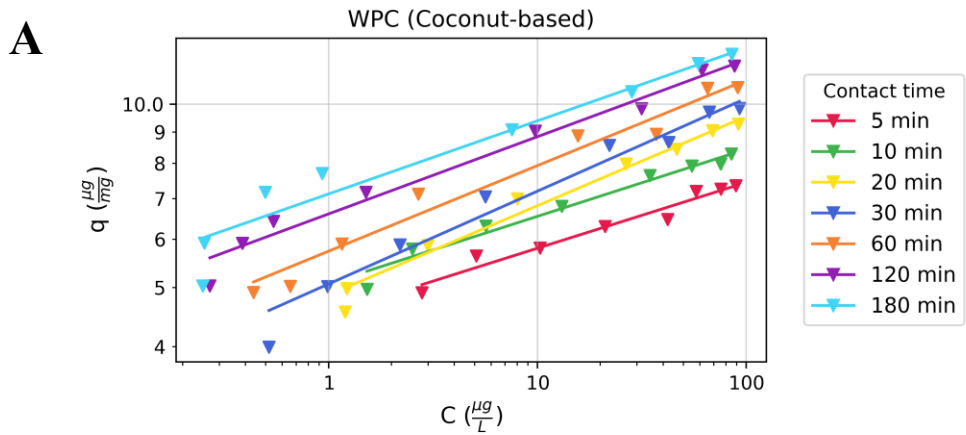
Figure 5.14 Freundlich fitting relationships in respect to time for the three (A) WPC (coconut-based), (B) BG-HHM (wood-based), and (C) COL-PL60-800 (coal-based) SPACs

The best-fit Freundlich parameters for adsorption of MC-LR onto the three WPC (coconut-based), BG-HHM (wood-based), and COL-PL60-800 (coal-based) SPACs at all contact times of 5 to 180 minutes are summarized in Table 5.4; the Freundlich fitting plots are also presented in Figure 5.14 for these contact times. Although deriving the Freundlich parameters by fitting the model to only 2-3 data points is mathematically inaccurate, the trend in Freundlich fitting plots of the BG-HHM (wood-based) SPAC at different contact times (Figure 5.14B) would suggest that the fittings with a lower number of data points could at least provide a relatively good estimate of Freundlich parameters. With respect to the WPC (coconut-based) SPAC, the K_f values were the least among the three prepared SPACs, ranging from 4.52 to 7.12 $(\mu g/mg)/(\mu g/L)^n$. The COL-PL60-800 (coal-based) SPAC had K_f values in a range of 3.48 to 10.69 $(\mu g/mg)/(\mu g/L)^n$ at short contact times, standing in the middle of the queue, while the BG-HHM (wood-based) SPAC had the highest K_f values in a range of 7.65 to 29.24 $(\mu g/mg)/(\mu g/L)^n$. The order of the K_f values at short contact times agree with the order of K_f values at equilibrium from the equilibrium vial point test with the exception of 5 minute of contact time, in which the coal-based SPAC had the worst performance compared to the other SPACs instead of coconut-based SPAC. The $1/n$ values at short contact times were similar, ranging from 0.1 to 0.25 for all three SPACs. Disregarding the effect of $1/n$, the K_f values could represent the capacity of each SPAC for MC-LR at short contact times. By visual inspection of Figure 5.14A-C it can be seen that the capacities of SPACs are distinguishable at short contact times in the range of 5 to 20 minutes, though after that time the gains in capacities start to diminish and the curves become less distinguishable, which is primarily the result of the fast kinetics of the SPACs. The best-fit Freundlich plots of the three SPACs are also compared to each other at different contact times and can be found in Appendix C.13. The visual inspection of Freundlich plots at 30 minute of contact time in Figure 5.15 would also confirm the order of capacities derived from the Freundlich parameters (K_f). This also holds true for other contact times (Appendix C.13) with the exception of 5 minutes, at which time the curves of coal-based and coconut-based SPACs collide.
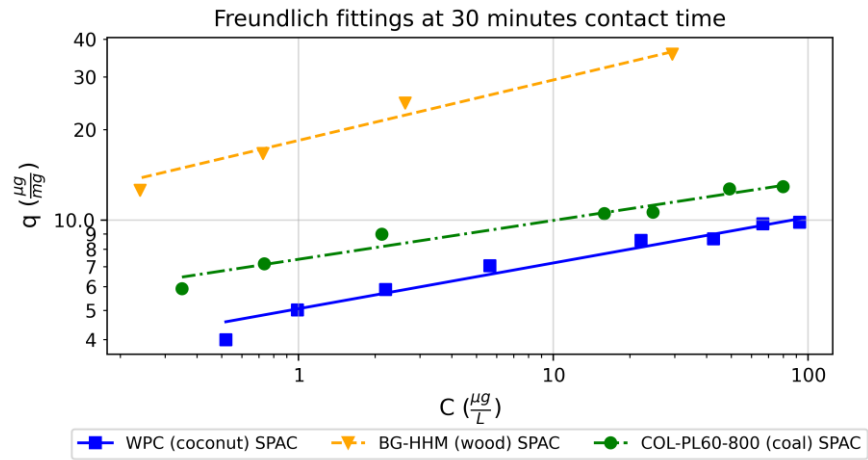
Figure 5.15 Best-fit Freundlich curves for adsorption of MC-LR onto the SPACs at contact times of 30 minutes

Table 5.4 Best-fit Freundlich parameters and 95% confidence intervals at short contact times

SPAC	Contact time	number of data points	K_f	K_f 95% CI	1/n	1/n 95% CI
BG-HHM (wood) SPAC	5 min	8	7.65	(6.93, 8.38)	0.25	(0.22, 0.28)
	10 min	6	11.41	(10.34, 12.48)	0.23	(0.20, 0.26)
	20 min	4	16.68	(14.72, 18.63)	0.19	(0.15, 0.23)
	30 min	4	18.42	(16.28, 20.56)	0.20	(0.16, 0.25)
	60 min	3	23.79	(18.85, 28.72)	0.17	(0.09, 0.25)
	120 min	2	27.41	(-inf, inf)*	0.17	(-inf, inf)*
	180 min	2	29.24	(-inf, inf)*	0.18	(-inf, inf)*
WPC (coconut) SPAC	5 min	8	4.52	(4.23, 4.81)	0.11	(0.09, 0.13)
	10 min	8	5.08	(4.82, 5.33)	0.11	(0.10, 0.12)
	20 min	8	4.86	(4.57, 5.15)	0.15	(0.13, 0.16)
	30 min	8	5.07	(4.66, 5.47)	0.15	(0.13, 0.18)
	60 min	8	5.73	(5.32, 6.15)	0.14	(0.12, 0.16)
	120 min	8	6.60	(6.29, 6.91)	0.13	(0.11, 0.14)
	180 min	8	7.12	(6.65, 7.59)	0.12	(0.10, 0.14)
COL-PL60-800 (coal) SPAC	5 min	8	3.48	(2.87, 4.08)	0.20	(0.16, 0.25)
	10 min	8	5.09	(4.61, 5.58)	0.17	(0.14, 0.19)
	20 min	8	6.10	(4.44, 7.75)	0.20	(0.12, 0.28)
	30 min	7	7.40	(6.81, 7.99)	0.13	(0.11, 0.15)
	60 min	6	8.81	(8.34, 9.28)	0.11	(0.10, 0.13)
	120 min	5	10.15	(9.52, 10.79)	0.10	(0.08, 0.12)
	180 min	5	10.69	(10.41, 10.98)	0.10	(0.09, 0.11)

*Not enough data points available for determination of confidence intervals

The capacities obtained at shorter contact times are not directly comparable with ones derived for ultrapure water experiments, since the bottle point tests for ultrapure water used the dry powder dosing method whereas the prewetted slurry dosing method was used for bottle point tests performed with Lake Erie water. As mentioned previously, the dry powder dosing method used for ultrapure water experiments led to formation of agglomerates, therefore slowing down the adsorption rates and decrease the adsorption capacity at short contact times.

The short contact time capacities of SPACs for MC-LR are compared with the results from Liu (2017) in which the capacities of the BG-HHM (wood-based), COL-PL60-800 (coal-based), and WPC (coconut-based) parent PACs in lake Erie water were determined. The 95% joint confidence regions of Freundlich parameters for adsorption of MC-LR onto both PACs from Liu (2017) and the SPACs from this study are demonstrated in Appendix C.15. As is evident from the figures in Appendix C.15, the JCRs of the PACs do not overlap the JCRs of the SPAC at either the 30 or 60 minutes contact time, which would indicate the performance of PACs and SPACs are significantly different. The JCR for the BG-HHM (wood-based) SPAC at 60 minutes contact time could not be derived, hence the limited number of data points/concentrations available above MRL.

The best-fit Freundlich lines for adsorption of MC-LR in Lake Erie water for PACs at both short contact times and equilibrium were compared with the lines for SPACs at short contact times in Figure 5.16. It should be noted that the SPAC experiments in Lake Erie water were performed using the slurry dosing method. By visual inspection of the curves for PACs and SPACs in Figure 5.16, it can be found that SPACs have out-performed the PACs in Lake Erie water. The similar DOC values of batch waters used in this study and the one used by Liu (2017) could suggest that the results from this study and the ones collected by Liu (2017) are relatively comparable if the effect of the different dosing methods is disregarded. The typically shorter contact times in drinking water treatment scenarios could be resulting in the waste of PACs' full capacity and potential to remove micropollutants such as MC-LR. The removal rate of MC-LR by the prepared SPACs is substantially faster than the as-received PACs, which could translate to higher adsorption capacity in shorter contact times. This means lower doses of SPAC can perform similarly to higher doses of regular sized PACs. Hence, SPACs could be a good candidate as an alternative to PAC in the removal of MC-LR in DWTPs.
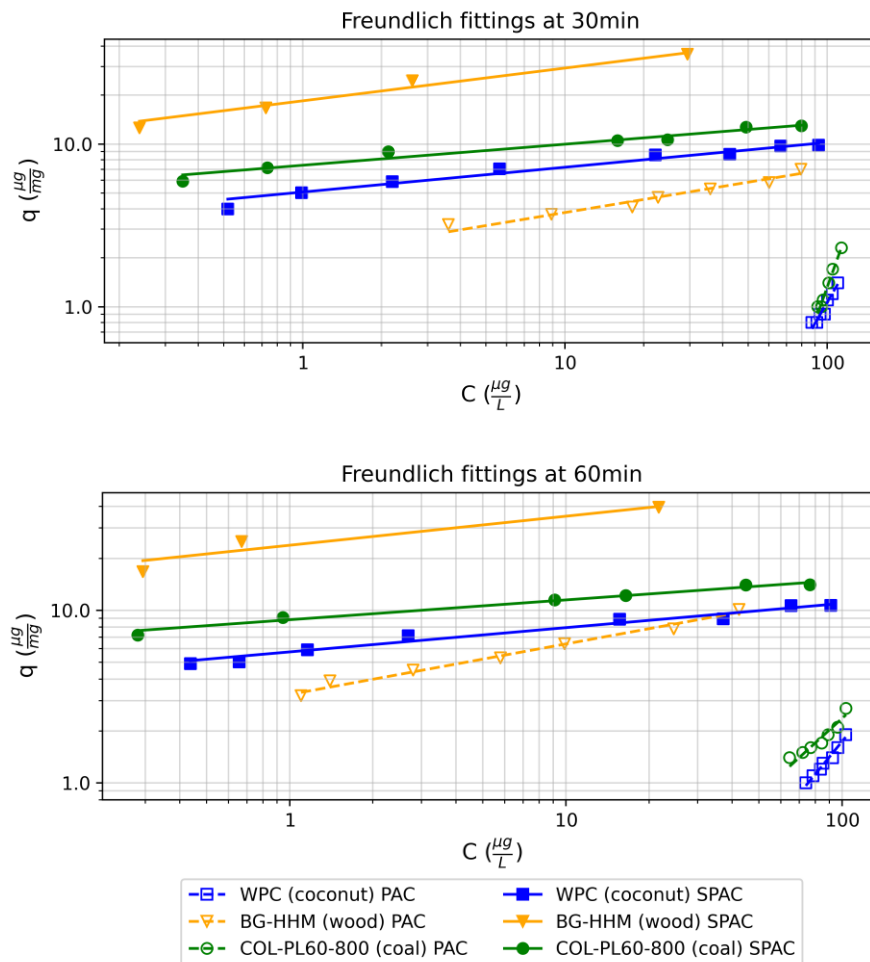
Figure 5.16 Best-fit Freundlich curves of SPACs compared to PACs (data from Liu (2017)) in Lake Erie water at contact times of 30 and 60 minutes

5.3.6 Simplified Equivalent Background Compound Model (SEBCM)

The SEBCM model was used to predict the dose required for removal of MC-LR to a preset target concentration in Lake Erie water by accounting for competitive adsorption of NOM, since MC-LR is typically present during cyanobacterial blooms in Great Lakes waters which contain NOM in range of 2-8 mg DOC/L. The adsorption data of MC-LR at short contact times (5, 10, 20, 30 minutes) in Lake Erie water with DOC of 2.3 mg/L was used for the SEBCM modeling since these contact times are closer to contact times typical in conventional drinking water treatment scenarios. The SEBCM model is also applied to the 60, 120 minutes and equilibrium data for the adsorption of MC-LR, for which model parameters, fitting plots, and dose predictions for them can be found in Appendix C.9. The model parameters A and n_1 for the SEBCM model were determined by fitting the model (Equation 5.1) to the experimental data. The fitting

curves and residual plots are provided in Appendices C.17 and C.18. The resulting model parameters are summarized in Table 5.5. The R^2 values for all fits were ranging from 0.956 to 0.999, which could be an indication of the goodness of fit of the model to the data. Figure 5.17 demonstrates the fit of SEBCM estimated capacities to the experimental data; however, for WPC (coconut-based) and COL-PL60-800 (coal-based) SPACs, a deviation from the estimated capacities in SPAC doses in the range of 3 to 8 mg/L can be observed.

It should be noted that the SEBCM model was developed under certain assumptions, which are as follows; (1) the removal of the target contaminant is independent of the initial concentration as found by Qi et al. (2007), (2) The EBC is present at much higher concentrations compared to the target contaminant, and (3) the SEBCM is only applicable to studies done under batch conditions at equilibrium. However, Zoschke et al. (2011) have shown that the SEBCM can also be applied at non-equilibrium conditions as well - which could justify the application of this model at short contact times in this study –. The authors also stated that the SEBCM could be applied to mixed-flow systems under the condition that the adsorbent mass and volume of the batch are replaced by the corresponding fluxes of mass per time and volume per time, though this is not proven experimentally. As for the assumption that EBC is present at a higher concentration compared to the target adsorbate/contaminant, the assumption could hold true under typical drinking water treatment scenarios, it should be noted that cyanotoxins such as MC-LR could be present at much lower concentrations than the 100 µg/L that was used in this study. The surveys from the Ontario Ministry of Environment's Drinking Water Surveillance Program from years 2008-2018 reported concentrations of MC-LR in range of 0.1 to 7.85 µg/L in the raw water intakes of DWTPs across the province. The NOM concentration could also vary in the Great Lakes, therefore resulting in different EBC concentrations.

Table 5.5 The SEBCM model parameters for SPACs at contact times ranging from 5 minutes to 30 minutes

SPAC	Contact time	Number of data points	A	$1/n_1$	R^2
WPC (coconut-based) SPAC	5 minutes	8	75.7	2.47	0.979
	10 minutes	8	83.5	2.71	0.969
	20 minutes	8	146.01	3.14	0.988
	30 minutes	8	208.7	3.43	0.991
BG-HHM (wood-based) SPAC	5 minutes	8	15.4	2.83	0.984
	10 minutes	6	9.7	3.15	0.992
	20 minutes	4	6.9	3.62	0.999
	30 minutes	4	5.04	3.69	0.999
COL-PL60-800 (coal-based) SPAC	5 minutes	8	29.7	1.97	0.966
	10 minutes	8	44.6	2.55	0.964
	20 minutes	8	39.7	2.89	0.956
	30 minutes	7	78.7	3.36	0.973
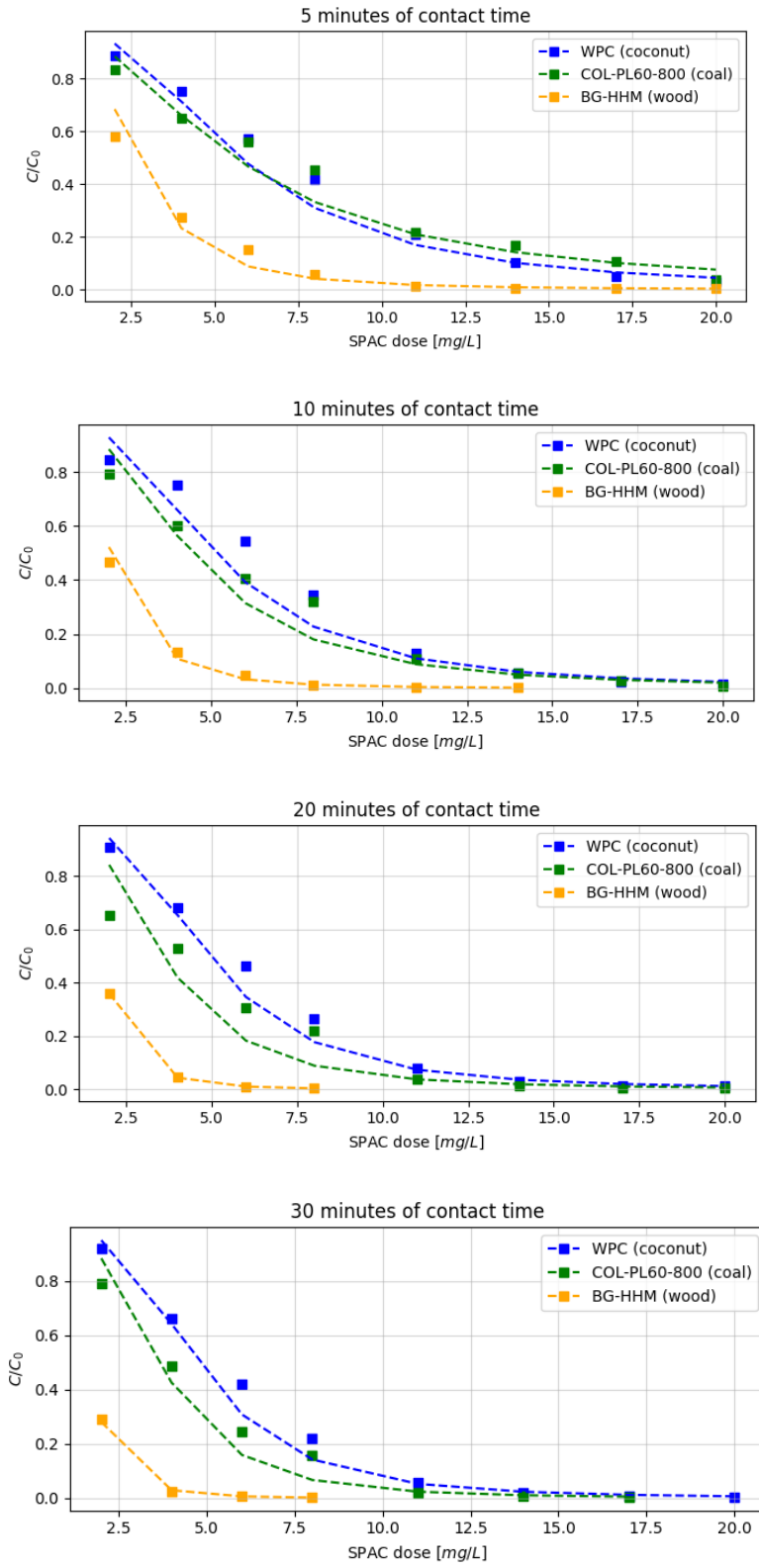
Figure 5.17 Capacity estimation of fitted SEBCM model to experimental data

The SEBCM parameters found from the fitting of the model to the experimental data can be used to estimate the dose required of each SPAC for proportional removal (C/C_0) of MC-LR based on Equation 5.2. This would enable the model to estimate the SPAC dose required to reduce the MC-LR concentration from the influent concentration to a given target effluent concentration. In this study, the target concentration was set to 0.4 µg/L following the latest Health Canada guideline setting this concentration as a threshold for the public to use an alternative drinking water source for bottle-fed infants (Health Canada 2018) however, the nominal MAC for MC-LR in drinking water for adults is currently 1.5 µg/L. Figure 5.18 demonstrates the estimated required dose of each SPAC for reducing the influent MC-LR concentration to 0.4 µg/L at the effluent for contact times of 5, 10, 20, and 30 minutes. At contact times ranging from 5 to 30 minutes, the BG-HHM (wood-based) SPAC outperforms the other two SPACs, requiring only a dose of 8 mg/L to reduce an influent concentration of 100 µg/L to 0.4 µg/L at 30 minutes of contact time while requiring about 20 mg/L at 5 minutes of contact time. In terms of the COL-PL60-800 (coal-based) SPAC, at 5 minutes of contact time, it presented the worst performance for removal of MC-LR compared to the other two SPACs, though its performance quickly increased, catching up with the WPC (coconut-based) SPAC at 10 minutes and surpassing the coconut-based SPAC at 20 minutes of contact time. The WPC (coconut-based) SPAC presented the least performance compared to the wood-based and coal-based SPACs, with the exception of 5 minutes of contact time when it showed better performance than coal-based SPAC. Overall, The SPACs performance in removal of MC-LR to a relatively low concentration of 0.4 µg/L in Lake Erie water is very promising at a short contact time of 30 minutes, with required doses of 8, 18, 24 mg/L for BG-HHM (wood-based), COL-PL60-800 (coal-based), and WPC (coconut-based) SPACs, respectively, to reduce influent concentrations in the range of 1 to 100 µg/L to 0.4 µg/L. Obviously, the required dose for MC-LR influent concentrations below 100 µg/L would be substantially lower, depending on the actual influent concentration of MC-LR. As an example, for reduction of an influent MC-LR concentration of 10 µg/L to target concentration of 0.4 µg/L, the predicted required dose at 30 minutes of contact time would be 12, 9.5, and 3.7 mg/L for the coconut-based, coal-based and wood-based SPACs, respectively. However, the DOC levels of the Lake Erie water and Great Lakes in general could be higher at times compared to the values measured for the batch of sampled water in this study. Therefore, the predicted SPAC doses could be different depending on the DOC level of the surface water.
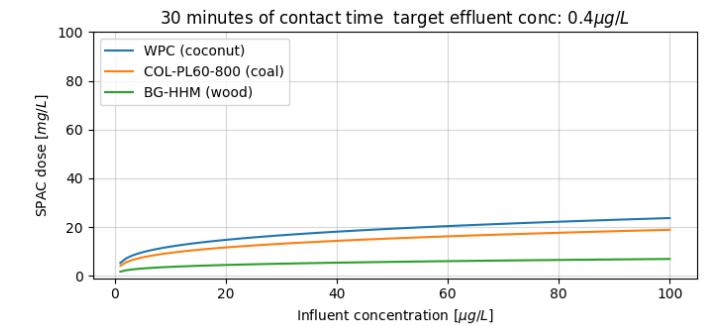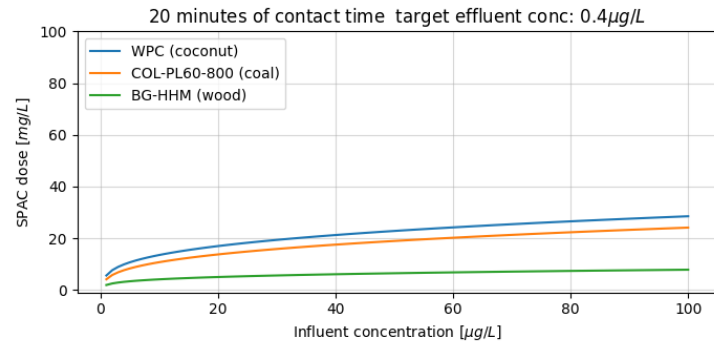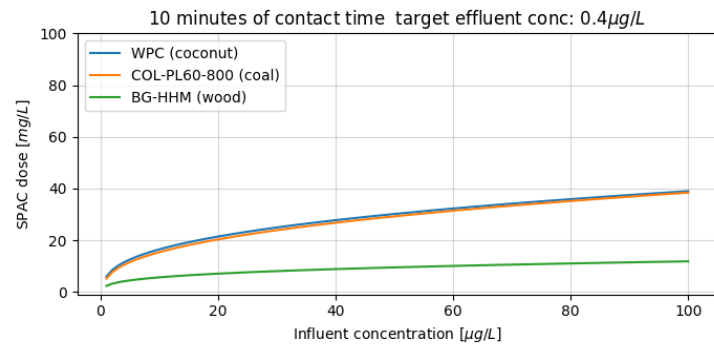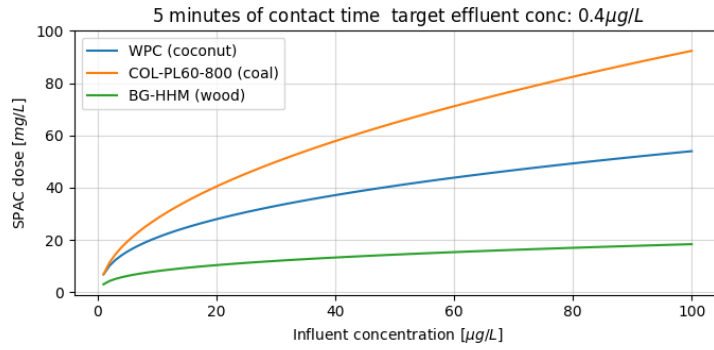
Figure 5.18 Dose prediction for reduction of influent MC-LR concentration to target effluent concentration of 0.4 µg/L at contact times of (A) 5 minutes, (B) 10 minutes, (C) 20 minutes, and (D) 30 minutes
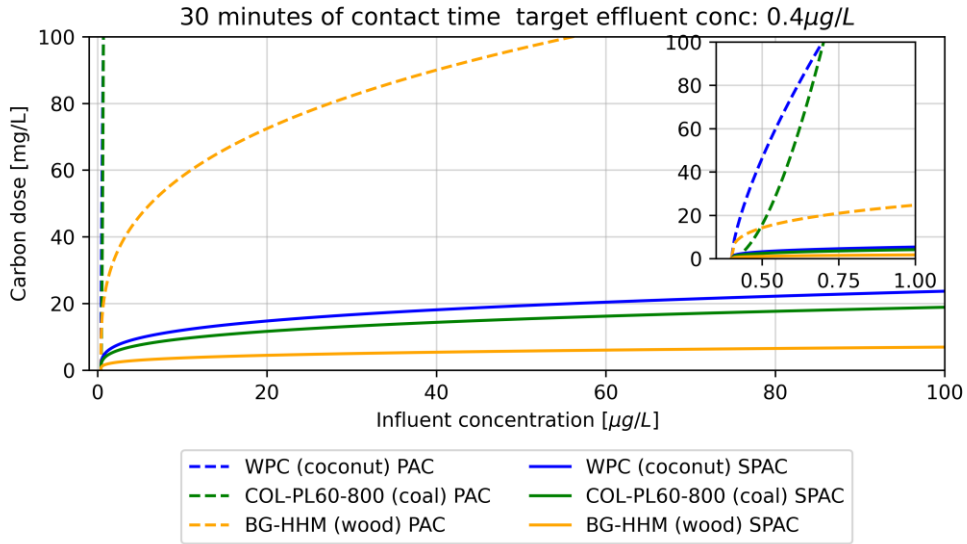
Figure 5.19 Comparison of predicted dose of SPACs vs PACs required for reduction of MC-LR to target concentration to target concentration of 0.4 µg/L

Liu (2017) also applied the SEBCM model to the adsorption data of MC-LR onto the parent PACs for 30 minutes of contact time. The predicted doses of each parent PAC for reduction of influent concentrations of MC-LR in range of 0.1-100 µg/L to target concentration of 0.4 µg/L are compared to predicted doses for corresponding SPACs in Figure 5.19. By visually inspecting the predicted doses for SPACs and parent PACs, it can be found that SPACs would require much lower doses compared to their corresponding parent PACs. The BG-HHM (wood-based) parent PAC is the only activated carbon that can be practically dosed for removal of MC-LR for the conditions modelled. The WPC (coconut-based) and COL-PL60-800 (coal-based) PACs predicted doses increase with a steep slope with increase of influent MC-LR concentration. Therefore, for the conditions modelled, the modelling suggests that these PACs would not be effective. Further modelling should investigate their effectiveness for a higher target concentration, and for longer contact times.

5.4 Conclusions

The Adsorption of MC-LR onto the BG-HHM (wood-based), COL-PL60-800 (coal-based), and WPC (coconut-based) SPACs in Lake Erie water was investigated at short contact times and at equilibrium using the bottle-point and vial-point tests, respectively.

The key findings of this chapter with respect to the investigated SPACs are as follows:

- SPACs outperformed parent PACs (PACs used as base material for preparation of SPACs in this study) in Lake Erie water in terms of kinetics and capacity under similar experiment conditions at

short contact times and equilibrium conditions. The faster kinetics of SPACs are primarily due to their higher external surface area compared to parent PACs, which exposes adsorption sites which were not immediately accessible to MC-LR before. The increased capacity at equilibrium is also postulated to be the result of improved accessibility of MC-LR molecules to the sites near the external surface of the smaller particles and shortened distance of these adsorption sites to the center of particles.

- Under equilibrium conditions, the BG-HHM (wood-based) SPAC presented the highest capacity for MC-LR and adsorbed the least amount of DOC, while COL-PL60-800 (coal-based) SPAC had a lower capacity and WPC (coconut-based) SPAC had the lowest capacity in Lake Erie water.

- At short contact times of 30, 60, 120 minutes, the order of the capacities of the SPACs was the same as it was at equilibrium conditions.

- The SEBCM was applied to experimental data of adsorption of MC-LR in Lake Erie water at short contact times of 5, 10, 20, and 30 minutes to predict the SPAC dose required for reduction of influent concentrations in the range of 1 to 100 µg/L to an effluent concentration of 0.4 µg/L. The predicted required doses for reducing an influent MC-LR concentration of 10 µg/L to 0.4 µg/L were 12, 9.5, and 3.7 mg/L for the coconut-based, coal-based and wood-based SPACs, respectively. The estimated required doses of SPACs were degrees of magnitude lower than predicted doses for parent PACs, especially for the coal-based and coconut-based carbons.

- The wood-based BG-HHM SPAC outperformed the other two SPACs in terms of kinetics, reducing the MC-LR concentration to below MRL (0.2 µg/L) in less than 15 minutes when dosed as prewetted slurry, followed by the COL-PL60-800 (coal-based) SPAC. The WPC (coconut-based SPAC had the slowest adsorption rate in Lake Erie water

- The dosing method of SPACs plays an important role in the adsorption rate of MC-LR onto SPACs and short contact time capacities. The prewetted slurry-dosed SPACs presented substantially faster adsorption rates compared to dry powder dosing of the same material due to better dispersion of the particles.

Overall, The SPACs performed substantially better than PACs in Lake Erie when dosed as a prewetted slurry. Dispersion of the SPACs can play an important role in capacities of SPACs at short contact times, and further investigation is required on the effects of the source water characteristics and constituents on the dispersion of SPACs when applied in DWTPs

Chapter 6

Coagulation/Flocculation/Settling for Removal of SPAC from Lake Erie Water

6.1 Introduction

PAC treatment is proven to be an effective method for the removal of cyanotoxins such as MC-LR and taste & odor compounds such as geosmin and 2MIB, as well as SOCs and pharmaceuticals from drinking water. However, it is necessary to separate PAC from water to remove the particulate matter (Huang et al., 2020) and also to prevent the release of micropollutants back into the treated water(Huang et al., 2020). PAC can be applied to a variety of treatment trains consisting of different treatment technologies. The treatment plants with microfiltration (MF) can take advantage of PAC as a pretreatment method, so that PAC could adsorb the low molecular weight humic acid portions of NOM and reduce the fouling rate of the MF membranes (Song et al., 2015). MF can be deemed an efficient barrier for the removal of PAC since it can retain the fine particles. PAC can also be used in conventional DWTPs which typically include coagulation, flocculation, sedimentation (CFS), rapid media filtration (CFS-F), and final disinfection. However, the activated carbon particles can escape to the filter effluent and increase the residual turbidity, exceeding the regulated limits. The current filter effluent regulated turbidity level in Ontario is 1 NTU which should not be exceeded at any time point. Schedule 16 of Ontario Regulation 170/03 provides a performance criterion for conventional filtration in drinking water treatment systems that requires the turbidity levels in all individual filter effluents to be equal or below 0.3 NTU for 95% of the time. The infiltration of the fine PAC particles into the distribution system could make the water visually more turbid, black, or grey, which can certainly provoke complaints from consumers (Nakazawa et al., 2018b). The leakage of the PAC particles into the distribution system is primarily due to inadequate coagulation/flocculation or application of high doses of PAC ((AWWA) & (ASCE), 2012). Huang et al. (2020) have studied the effect of PAC addition on coagulation/flocculation of two synthetic waters consisting of humic acids (HA) and HA-kaolin, respectively. The study showed that addition of PAC to the synthetic water containing HA enhanced the floc size and formation rate, though did not affect the HA-kaolin water floc properties. Addition of PAC increased the residual turbidity, however, the authors reported that addition of PAC to HA water resulted in formation of stronger and more compact flocs, though it seemed that the settling of the aforementioned flocs was inferior compared to flocs formed in the absence of PAC. Campinas et al. (2021) also studied the effects of PAC addition on the coagulation/flocculation of low turbidity (<3 NTU) surface water while removing micropollutants at pilot scale. The authors' findings indicated that residual turbidity of the treated water could be impacted by addition of high doses of PAC; addition of 20-24 mg/L of PAC to a CFS in this

study increased the residual turbidity of the treated water, resulting in turbidity levels ranging from 1.2-1.9 NTU and almost equivalent to the turbidity of the source water. However, doses in range of 2-9 mg/L of PAC did not increase the residual turbidity above 1 NTU and it was much lower than the source water turbidity. Although the turbidity level after CFS and before filtration is not regulated, DWTPs usually target a value around 1 NTU to maintain an adequate filter performance. The results of the study by Campinas et al. (2021) also indicated that the filtration step (rapid sand filtration which typically follows the CFS in conventional DWTPs) can play an important role in preventing PAC fines from infiltrating the finished water, reducing the residual turbidity below 0.3 NTU. These results indicate that PAC can be efficiently removed from the finished water via CFS-F when dosed at concentrations below 10 mg/L and this level of success in removal of PAC from the treated water provides a reference point for removal of SPAC from drinking water.

As is evident from previous chapters, SPAC consists of substantially smaller particles (median particle size of around 1 µm) compared to commercially available PACs (median particle size in range of 10 to 40 µm) typically used in drinking water treatment applications. Therefore, the risk of fine particles of SPAC escaping into finished water in treatment plants relying on CFS-F is suspected to be higher in theory compared to PAC (Nakazawa et al., 2018b). Matsui et al. (2009) studied the effect of SPAC addition concurrent with coagulation as a pretreatment for microfiltration and its implications for the trans-membrane pressure buildup. The study compared the sizes of flocs formed by both SPAC and PAC and found that SPAC formed larger flocs compared to PAC in water containing NOM, which resulted in a lower likelihood to cause premature membrane fouling. The results also indicated that SPAC floc size was not impacted by the presence of NOM, while the size of flocs formed by PAC decreased in the presence of NOM. Nakazawa et al. (2018a) studied the residual carbon particles after use of SPAC and PAC in a CFS-F setup. The results showed that the turbidity of sand filter effluent was very low (~0.05 NTU). However, after filtering the permeate through a 0.1 µm membrane and imaging the membranes under a microscope, it was revealed that fine particles of PAC and SPAC could be detected in sand filter effluents, though the number of particles was not enough to affect the turbidity of the effluent. When the same dose of PAC and SPAC was used (30 mg/L), the number of residual fine particles for SPAC was higher compared to PAC. However, since SPAC typically could achieve the same micropollutant removal rates at doses substantially lower than PAC (i.e. for removal of 2MIB, SPAC can achieve same results at doses 25% of PACs (Nakazawa et al., 2018a)), the log removals of fine PAC and SPAC particles through rapid media filtration were comparable when a lower dose of SPAC was used (7.5 mg/L as opposed to 30 mg/L). Overall, the study concluded that use of SPAC as an alternate to PAC for removal of micropollutants in CFS-F drinking water treatment setups would not substantially affect the number of fine activated carbon particles that may escape to the treated water. Furthermore, the same authors in another study investigated the effects of

coagulant properties and conditions on the number of residual SPAC particles in water treated by CFS-F. The results indicated that the G (velocity gradient) value in the flash mixing of coagulation process is the determining parameter for enhancing the removal of residual SPAC particles in sand filtrate. An increase in the G value translates directly into a larger amount of energy input into the mixture of coagulant/SPAC/water, therefore resulting in better dispersion of coagulant and adequate charge neutralization of SPAC particles (Nakazawa et al., 2018b). The authors also found that use of coagulants such as poly-aluminum chloride (PACl) with higher basicity could also enhance the charge neutralization of SPAC particles, however, the superiority of high-basicity PACl as coagulant was conditional on adequate flash mixing, hence the dominance of the G value as the governing parameter on performance of fine SPAC particle removal by CFS-F treatment. The latest study by Nakazawa et al. (2021) investigated the removal of residual SPAC particles in CFS-F treatment further with a focus on the configuration of mixing reactors for the coagulation/flocculation stage and the effects of ripening of rapid sand filters on the residual SPAC particles in the sand filtrate. As for the configuration of the mixing reactors, the results showed that the use of a multi-chambered rapid mixing tank for the coagulation process can substantially decrease the number of residual SPAC particles in sand filtrate for both high and medium-basicity PACls. The authors also found that the number of residual SPAC particles were reduced substantially during the ripening process of sand filtration (Nakazawa et al., 2021).

The results from the studies cited above clearly suggest that SPAC could be used as an alternative to PAC in conventional DWTPs which use CFS-F trains. In the present study, the main objective is to confirm that adequate removal of the produced SPAC, employed under conditions representative for MC-LR removal in Great Lakes water can be achieved by CFS. More specifically, subobjectives are (1) to evaluate the removal of SPACs in terms of residual turbidity at the maximum dose required for the removal of MC-LR from Lake Erie water, (2) to determine the optimum coagulant dose (liquid alum) for reducing the residual turbidity of the Lake Erie water below 1 NTU in the presence of 20 mg/L of each prepared SPAC, and (3) to investigate the effect of SPAC additions on the pH of the Lake Erie water before and after application of different coagulant doses.

6.2 Materials and methods

6.2.1 Materials

The BG-HHM (wood-based), COL-PL60-800 (coal-based), and WPC (coconut-based) SPACs were prepared by pulverization of as-received commercially available PACs as described in Section 3.3.1. Lake Erie water was sampled on June 14th, 2021 from the intake of a DWTP after the pH adjustment step (target pH of 7.1-7.2). The usual pre-chlorination of the water at the intake was suspended for the purpose of

sampling. Aluminum sulphate 48% in the form of liquid-alum ($Al_2(SO_4)_3$-$14H_2O$) with specific gravity of 1.3 kg/L was acquired from Anchem Sales (London, ON, Canada) and used as the only coagulant in this study. No coagulant or flocculant aid was used

6.2.2 Jar test procedure

The jar test procedure was adopted from ASTM D2035-13 (Committee, 2013) standard. A Phipps and Bird (Phipps and Bird inc., Richmond, VA) 6-paddle jar tester with B-KER square jars was used for the jar tests. For each set of experiments the jars were filled with 1 liter of Lake Erie water and dosed with 20 mg/L of the corresponding SPAC using a 2 g/L slurry. The 20 mg/L dose of SPAC was the highest dose used for adsorption of MC-LR in this study. For the experiments with SPAC the 20 mg/L of SPAC was dosed to the jar 30 minutes prior to the alum dosing. The first experiment was done without addition of SPAC to evaluate the coagulant demand of the sampled Lake Erie water. The jar tester was next set to 120 ± 2 RPM (approximately a G-value of 126 s^{-1}, based on the G curve of the B-KER included in Appendix D.1) for the flash mixing stage. The jars were then dosed with 10-45 mg/L of liquid alum. The jars were then flash mixed for 1 minute after the dosing of alum and then the paddle speed was reduced to 30 ± 1 RPM (approximate G-value of 23 s^{-1}) for 20 minutes to allow the formation of flocs. The floc size was monitored during the slow mixing by taking images at 5, 10, 15 min. After 20 minutes of slow mixing, the paddles were retracted, and the floc was allowed to settle for 15 min. A 10 mL sample was then taken from 1/3 of the depth of the jar for pH and turbidity measurements. Another sample was also taken at 30 min to evaluate the floc settlement at an extended settling time. All experiments were done at room temperature of 21°C, and the pH and turbidity of the waters were measured before addition of SPAC, after addition of SPAC, and after the coagulation process at the settling time of 15 min.

6.2.3 Turbidity, pH, and alkalinity

The turbidity of the samples was measured using a 2100Q Hach portable turbidity meter (Hach Water Analysis Solutions, London, Ontario, Canada). The pH was measured by a benchtop Orion 420A pH/mV meter (Thermo Scientific, MA, USA). The alkalinity of the Lake Erie water was measured based on Standard Methods for the Examination of Water and Wastewater, Method 2320 B (Standard Methods, 2017)

6.3 Results and discussion

6.3.1 Lake Erie water characteristics

The turbidity of the sampled Lake Erie water was 2.0 NTU at the time of receiving the sample, which would categorize the sampled water as low-turbidity surface water, as the turbidity level is below 3 NTU,

according to a description provided by Campinas et al. (2021). The low turbidity of the Lake Erie water used in this study is beneficial since it is reported that PAC addition could negatively impact the residual turbidity after treatment of low-turbidity source waters via CSF (Campinas et al., 2021; Huang et al., 2020). Therefore, it is implied that this study investigated the removal of SPAC from Lake Erie water at its most vulnerable turbidity. The pH of the as-received water was 7.56 and the alkalinity was 94 mg $CaCO_3$/L. The water did not contain any chlorine residual as the pre-chlorination was turned off during sampling.

6.3.2 Turbidity removal by CFS and its impact on pH

In this chapter the performance of CFS for removal of SPAC from the treated was evaluated in terms of turbidity removal. However, the performance of rapid media filtration for removal of residual turbidity after CFS was not evaluated in this study due to time constraints. There are currently no regulations available for the turbidity level after CFS, prior to rapid media filtration, though the current regulations require a max turbidity level of 0.3 NTU at the filter effluent and turbidity values of 1 NTU and above should be avoided at all costs and reported. Therefore, in this study the target turbidity limit after CFS/prior rapid filtration was set to 1 NTU and below.

6.3.2.1 Lake Erie water coagulation performance without addition of SPAC

The results of the coagulation experiments in terms of residual turbidity and changes in pH are summarized in Tables 6.1 and 6.2. For the Lake Erie water without addition of SPAC (Figure 6.1) the initial turbidity was 2.0 NTU before addition of alum. The residual turbidity levels of the raw water dropped below 1 NTU to values around 0.25 NTU after addition of alum doses in the range of 10 to 45 mg/L, after 15 min of settling time. The extended 30 min settling time did not improve the residual turbidity for alum doses in the range of 10-20 mg/L though it provided an improvement of approximately 30% for alum doses of 30 and 45 mg/L.

The images from the jars during floc formation are provided in Appendices D.2-5. The floc size for the Lake Erie water without SPAC addition was difficult to distinguish from the water due its transparent look caused by the low initial turbidity of the water and a lack of dark particles. The formed flocs were silver coloured and almost transparent. The floc formation at 10 and 15 mg/L of alum was slow and flocs were not visible until 20 min after slow mixing started. For 20 and 30 mg/L doses the floc formation was relatively fast, and distinct flocs were apparent at 10 minutes of slow mixing. At the highest dose of 45 mg/L the floc formed very quickly though the structure of the flocs was smaller and more interconnected, resulting in a cloudier solution. Table 6.3 summarizes the floc formation behavior of Lake Erie water without SPAC with three different alum doses as an example.

119

The initial pH of the water was 7.56 as reported in Section 6.3.1. The addition of 10 mg/L of alum did not affect the pH. However, starting at 15 mg/L of alum the pH decreased with an increase in applied alum dose, as would be expected. The pH of the water did not drop below 7.1 with addition of the highest alum dose of 45 mg/L, which is in the range of the pH targeted at the treatment plant (i.e. pH 7.1-7.2).

Table 6.1 Residual turbidity of Lake Erie water with and without SPACs after CFS with different alum doses
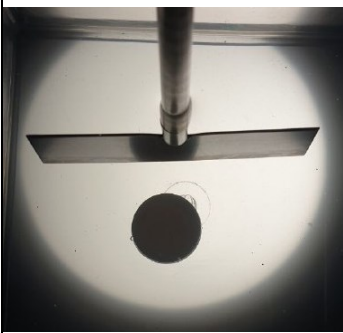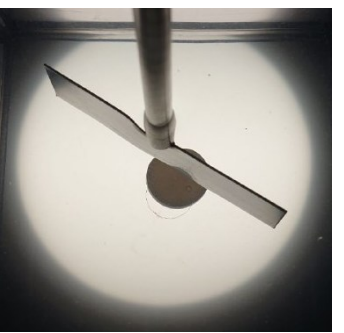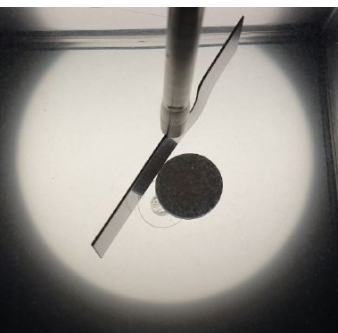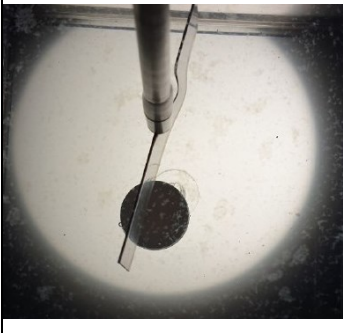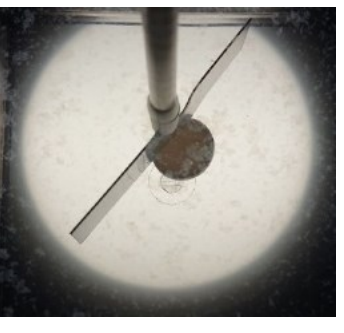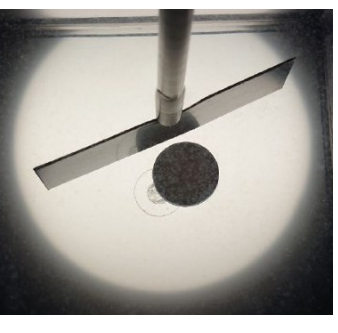
SPAC	Settling time	Alum dose (mg/L)						
		0	10	15	20	30	45	
			Residual turbidity (NTU)					
None	15 min	2	0.27	0.32	0.13	0.25	0.24	
	30 min		0.25	0.25	0.26	0.17	0.15	
WPC (Coconut-based)	15 min	104	4.8	1.86	1.08	0.27	0.63	
	30 min		4.51	1.95	0.93	0.26	0.13	
BG-HHM (Wood-based)	15 min	38.2	0.58	0.33	0.18	0.44	0.60	
	30 min		0.55	0.31	0.13	0.12	0.11	
COL-PL60-800 (Coal-based)	15 min	41.9	1.17	0.5	0.27	0.16	0.27	
	30 min		0.99	0.61	0.24	0.16	0.13	

Table 6.2 Changes in pH of Lake Erie water with and without SPACs after coagulation with different alum doses after 15 min settling time

SPAC	Alum dose (mg/L)					
	0	10	15	20	30	45
	pH					
None	7.56	7.55	7.48	7.41	7.25	7.12
WPC (Coconut-based)	8.10	7.76	7.75	7.58	7.50	7.32
BG-HHM (Wood-based)	7.84	7.82	7.75	7.58	7.47	7.44

COL-PL60-800 (Coal-based)	8.14	7.64	7.61	7.56	7.34	7.14

Table 6.3 Floc formation for Lake Erie water without SPAC with addition of different doses of alum

Time/Alum	10 mg/L	20 mg/L	45 mg/L
5 min			
15 min			
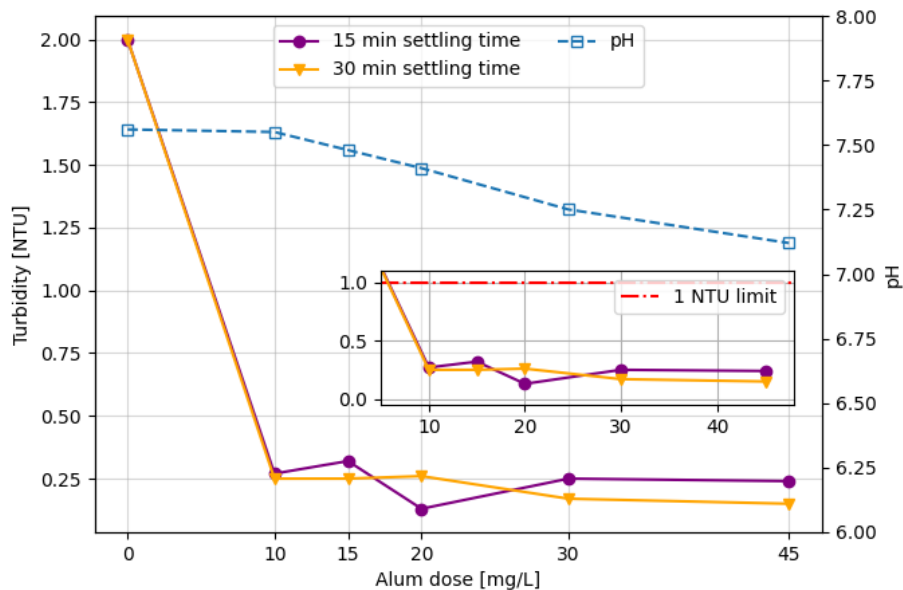
Figure 6.1 Lake Erie water residual turbidity and pH after CFS with different alum doses (the insert provides a closer view on the residual turbidities)

6.3.2.2 Coagulation performance of Lake Erie water containing SPACs
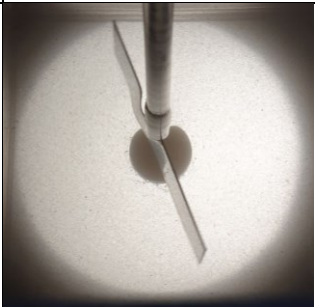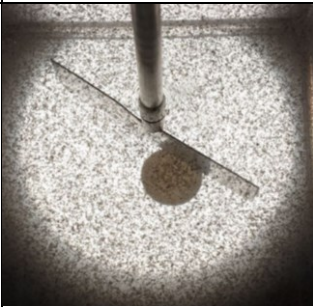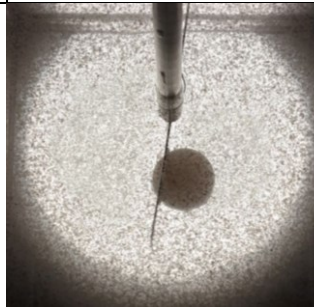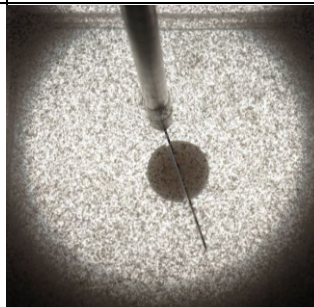
The addition of 20 mg/L of WPC (coconut-based) SPAC in form of prewetted slurry to Lake Erie water 30 minutes prior to addition of alum, increased the turbidity of Lake Erie water substantially from 2 NTU to 104 NTU. Subsequent coagulation with 10 and 15 mg/L of alum after 15 min settling time decreased the residual turbidity substantially to 4.8 NTU and 1.86 NTU, respectively. At an alum dose of 20 mg/L the residual was around 1 NTU, and higher doses of 30 and 45 mg/L of alum successfully reduced the residual turbidity to below 1 NTU. However, the goal of CFS alone is not to reduce the turbidity as much as possible, very low turbidity at rapid media filter influent can translate to very low particulate matter concentration and effect the filter performance especially during ripening stage after each backwash. As for the extended 30 min settling time, the extra 15 min of settling did not affect the residual turbidity substantially and it only provided a slight improvement of the residual turbidity for the alum dose of 45 mg/L (Figure 6.2).

The floc formation at alum doses of 10 and 15 mg/L was relatively slow and minimal 5 minutes into the slow mixing process. However, with time substantial amounts of flocs formed, providing adequate flocculation. The 20 and 30 mg/L doses of alum resulted in the formation of large and stable flocs. The floc sizes were the largest for 20 mg/L of alum compared to other applied doses, although, the exact reason for this is unknown. Interestingly, the highest alum dose of 45 mg/L formed dispersed small size flocs. Table

6.4 summarizes the floc formation of WPC (coconut-based) SPAC in three different alum dosages in Lake Erie water as an example.

Addition of WPC (coconut-based) SPAC increased the pH of the water from 7.56 to 8.10. This is primarily due to the high negative surface charges of the coconut-based SPAC as is evident from its high pH_{pzc} of 11.12. However, with the addition of alum the pH decreased, thereby off-setting the initial increase in pH due to the addition of WPC SPAC.

Table 6.4 Floc formation of WPC (coconut-based) SPAC in Lake Erie water with addition of different doses of alum

Time/Alum	10 mg/L	20 mg/L	45 mg/L
5 min			
15 min			
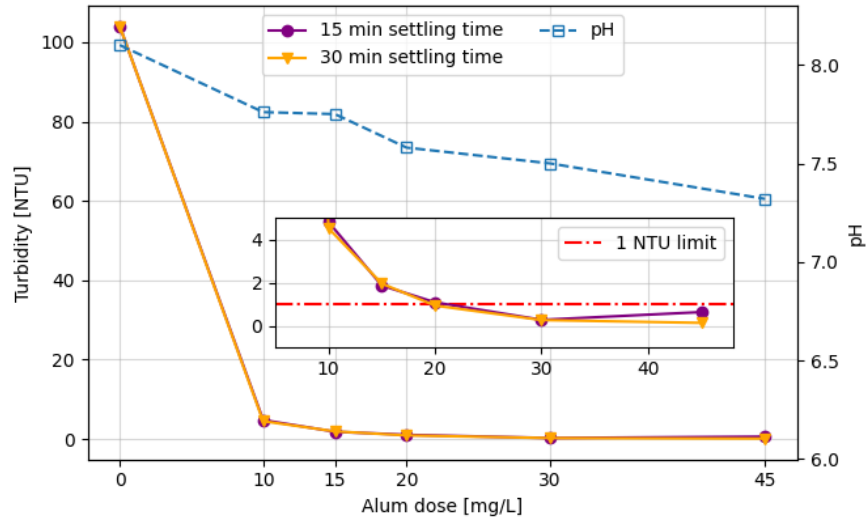
Figure 6.2 Coagulation results for Lake Erie water with 20 mg/L of WPC (coconut-based) SPAC: Residual turbidity and pH after addition of different alum doses (the insert provides a closer view on the residual turbidities)

In terms of COL-PL60-800, the coal-based SPAC increased the initial turbidity of the water to 41.9 NTU. Addition of the lowest alum dose of 10 mg/L decreased the residual turbidity to 1.17 NTU, and addition of alum doses of 15 mg/L or higher successfully reduced the residual turbidity to values below 1 NTU at 15 min of settling time. The 30 min extended settling time again only affected the residual turbidity for the highest dose of 45 mg/L of alum.

The floc formation of the COL-PL60-800 was similar to that for the coconut-based SPAC. The floc formation at a low dose of 10 mg/L was slow, although a substantial amount of floc was formed by the end of the slow mixing process. The largest and most stable flocs were formed at alum doses of 20 and 30 mg/L. Similar to what was observed for WPC (coconut-based) SPAC, the flocs formed at alum dose of 45 mg/L were more dense and smaller in size.

As for the pH, the addition of COL-PL60-800 (coal-based) SPAC increased the initial pH of the water from 7.56 to 8.14. This amount of increase in pH was very similar to what observed for addition of WPC (coconut-based) SPAC, since the COL-PL60-800 and WPC SPACs have very similar pH_{pzc} values of 11.30 and 11.12. The high pH_{pzc} of these SPACs indicate that they have negative surface charges and therefore, they have higher affinity for positive charges. This could explain the increase in pH of the raw water upon addition of these SPACs.

124
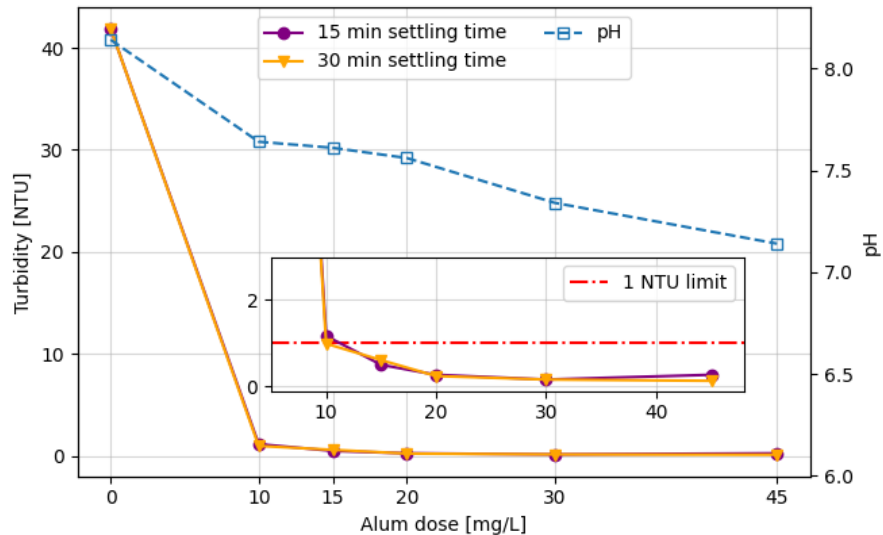
Figure 6.3 Coagulation results for Lake Erie water with 20 mg/L of COL-PL60-800 (coal-based) SPAC: Residual turbidity and pH after addition of different alum doses (the insert provides a closer view on the residual turbidities)

The addition of BG-HHM (wood-based) SPAC increased the turbidity of Lake Erie water the least to 38.2 NTU compared to the WPC (coconut-based) (104 NTU) and COL-PL60-800 (coal-based) (41.9 NTU) SPACs. As for removal of BG-HHM (wood-based) SPAC via CFS, all of the alum doses in the range of 10 to 45 mg/L used in this study successfully achieved a residual turbidity level below 1 NTU after 15 min settling time. The minimum residual turbidity at 15 minutes of settling was achieved with the addition of 20 mg/L of alum. The 30 min extended settling time again only improved the residual turbidities when higher doses of 30 and 45 mg/L of alum were used.

As for the floc formation, the rate of formation at the lowest alum dose of 10 mg/L was again slow, with distinct flocs forming 5 minutes into the slow mixing step. However, floc formation was quicker compared to the WPC (coconut-based) SPAC. The flocs formed after addition of 20 mg/L alum were the largest and most stable by visual inspection. The higher alum doses of 30 and 45 mg/L formed smaller flocs resulting in a cloudier solution similar to what was observed for the coconut-based and coal-based SPACs.

As for the change in pH, the BG-HHM (wood-based) SPAC increased the pH the least, increasing the raw water pH from 7.56 to 7.84 by only 0.28. The smaller increase of pH by the wood-based SPAC can be explained by its low pH_{pzc} of 4.1. The addition of alum reduced the pH as expected, though interestingly the reduction in pH after alum addition was less pronounced in the presence of BG-HHM (wood-based)

SPAC compared to the other 2 SPACs, which might suggest that the wood-based SPAC had a buffering effect.
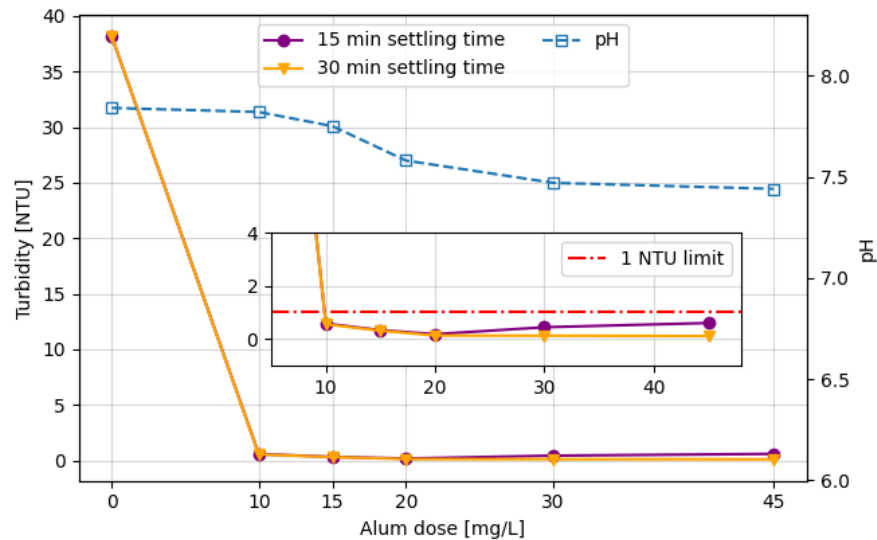
Figure 6.4 Coagulation results for Lake Erie water with 20 mg/L of BG-HHM (wood-based) SPAC: Residual turbidity and pH after addition of different alum doses (the insert provides a closer view on the residual turbidities)

Figure 6.5 compares CFS results, both residual turbidity and changes in pH, for the Lake Erie water with and without SPAC addition. As is evident from the zoomed-in plot, the Lake Erie water without SPAC along with the water with BG-HHM (wood-based) SPAC could easily be treated with alum doses as low as 10 mg/L to reach a residual turbidity below the 1 NTU, while COL-PL60-800 (coal-based) SPAC requires at least 15 mg/L of alum and WPC (coconut-based) SPAC requires at least 30 mg/L of alum to achieve the same results. The higher alum consumption of the Lake Erie water with WPC SPAC is mainly due to the fact that it increased the turbidity of the water the most by more than 100 NTU to 104 NTU which was more than two times the turbidity of water with the wood-based and coal-based SPACs and its high negative surface charge. It is necessary to mention that the residual turbidity values reported were measured after sedimentation, and it is very likely that rapid media filtration could reduce the residual turbidities even lower based on the findings of Nakazawa et al. (2018b, 2021). These results could indicate that SPACs can be efficiently removed from the treated Lake Erie water via CFS-F at doses required for adequate removal of MC-LR.
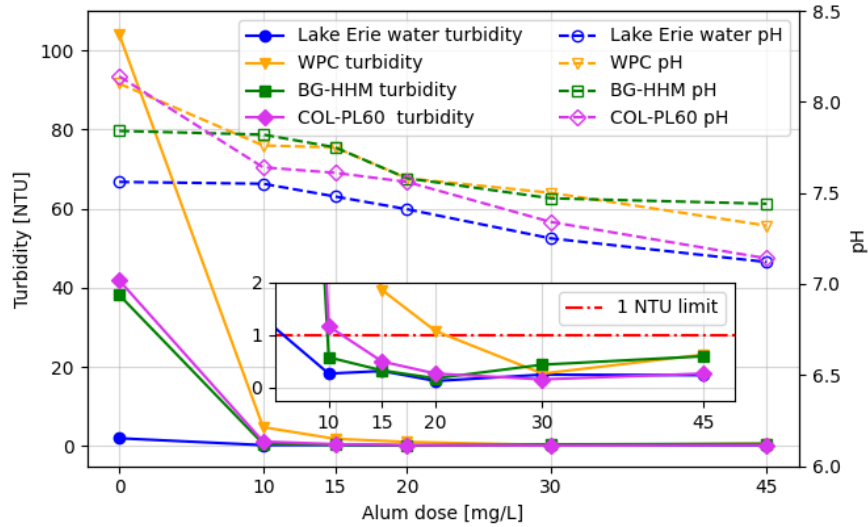
Figure 6.5 Comparison of coagulation results for Lake Erie water with and without SPAC: Residual turbidity and pH after addition of different doses of alum and a settling time of 15 min

6.4 Conclusions

The removal of the three SPACs, WPC (coconut-based), COL-PL60-800 (coal-based), and BG-HHM (wood-based) via CFS processes from low turbidity Lake Erie water was evaluated via a set of jar tests. The performance was measured in terms of residual turbidity and the optimum minimum doses for the reduction of the residual turbidity below 1 NTU, a value which is commonly targeted after sedimentation.

The main findings from this chapter are as follows:

- Addition of SPAC to the Lake Erie water increased the initial turbidity of the water substantially. The WPC (coconut-based) SPAC increased the initial turbidity the most from 2 to 104 NTU. The increase in initial turbidity by the BG-HHM (wood-based) and COL-PL60-800 (coal-based) SPACs was also drastic but not as pronounced as the coconut-based WPC.

- For the low-turbidity Lake Erie water, any dose of alum in the range of 10-45 mg/L was sufficient to achieve a residual turbidity below 1 NTU. The BG-HHM (wood-based) SPAC was also removed successfully to a residual turbidity below 1 NTU with any dose of alum, though the residual turbidity at low alum doses of 10 and 15 mg/L was slightly higher compared to the Lake Erie water without SPAC. The Lake Erie water with COL-PL60-800 (coal-based) SPAC required at least 15 mg/L of alum to achieve a residual turbidity below 1 NTU and WPC (coconut-based) SPAC required the substantial alum dose of 30 mg/L to achieve residual turbidity below 1 NTU.

127

- The pH of the Lake Erie water was impacted by the addition of SPACs, with all of the SPACs increasing the initial pH of the water. The BG-HHM (wood-based) SPAC increased the initial pH slightly while the initial pH increase by WPC (coconut-based) and COL-PL60-800 (coal-based) SPACs was more substantial. As expected, the addition of alum decreased the pH with increasing alum doses, which offset the increase in pH due to SPAC addition. The Lake Erie water with BG-HHM wood-based SPAC resisted the pH drop due to the addition of alum better compared to the Lake Erie water without SPAC or with other two SPACs.

- The flocs formed at alum doses of 20 and 30 mg/L were the largest and most stable and settled more quickly than the dense flocs formed at higher alum dose of 45 mg/L. Floc formation at low alum dose of 10 mg/L was substantially slower, though the formed flocs at the end of the slow mixing step (20 minutes of flocculation) were satisfactory in size and had good overall stability.

Overall, the prepared SPACs at the maximum applied dose of 20 mg/L were proven to be well removed to turbidities below 1 NTU at reasonable alum doses in the range of 10-30 mg/L depending on the type of SPAC used. The results from experiments in this chapter indicate that the prepared SPACs can be removed from surface water via conventional CFS-F similarly to SPACs used in other studies and PACs. These results are promising in terms of practicality and feasibility of SPAC use in conventional DWTPs. It is important to note that the residual turbidities reported in this study were measured after CFS, and rapid media filtration was not simulated in the bench-scale experiments due to time constraints. Based on the study by Nakazawa et al. (2021) which indicated that rapid sand filtration can reduce the residual turbidity and number of residual SPAC/PAC particles substantially, it is expected that rapid media filtration would further reduce the turbidity of Lake Erie water containing the produced SPACs, likely to below regulated turbidity levels. However, it is necessary to assess this in future studies. It would also be beneficial to evaluate removal of SPACs from surface waters by different coagulants and coagulant aids, and relate performance to coagulant and coagulant aid characteristics such as basicity.

Chapter 7

Conclusions and Recommendations

7.1 Summary and Conclusions

The overarching focus of this thesis was to evaluate the potential of SPAC which is a form of powdered activated carbon (PAC) pulverized to have a median particle size in the range of 0.6-1.2 microns, for removal of microcystin-LR (MC-LR). After a thorough literature review (Chapter 2), it was found that SPAC has untapped potential as an alternative to conventionally sized PAC for removal of a wide variety of micropollutants since, due to its smaller particles size, it provides faster adsorption rates for adsorbates. However, SPAC is a relatively new technology, and there are substantial knowledge gaps, including the fact that removal of cyanotoxins in surface water was not assessed by SPAC at the time of writing. Therefore, the main objective of this study was to prepare SPACs by pulverization of three commercially available PACs (WPC (coconut-based), COL-PL60-800 (coal-based), and BG-HHM (wood-based)) and to evaluate their performance for the removal of MC-LR in ultrapure water and surface water. The removal of the SPACs from surface water by conventional coagulation, flocculation, and sedimentation (CFS) was also evaluated.

Initially, a pulverization method was developed using a commercially available benchtop wet bead mill, and SPACs with median sizes close to 1 micron were prepared. A method for determination of the particle size distribution (PSD) of the prepared SPACs based on scanning electron microscope (SEM) imaging and static image analysis was also developed, successfully evaluated and used for characterization of SPACs. Other parameters such as BET internal surface area, DFT pore size distribution, and point of zero charge were also determined for the SPACs (chapter 3). As for the adsorption performance of SPACs for removal of MC-LR, the adsorption rates (removal rates) and capacities of SPACs for MC-LR were assessed in two water matrices: (1) ultrapure water, where MC-LR was present as a single solute, to determine the baseline adsorption performance (chapter 4) and (2) Lake Erie water where adsorption of MC-LR was evaluated in competition with dissolved NOM (chapter 5). The capacities of SPACs for MC-LR were evaluated at both equilibrium (isotherms) and at shorter contact times in the range of 5 to 180 minutes. A simplified equivalent compound model (SEBCM) was used to successfully describe the competitive adsorption of MC-LR and NOM onto the SPACs and to predict the required dose of each SPAC to reduce a range of MC-LR influent concentrations to a target effluent concentration below regulated levels at both short contact times of 30 and 60 minutes, and equilibrium. The SEBCM model was proven to be valid under both equilibrium and non-equilibrium conditions (Zietzschmann et al., 2016; Zoschke et al., 2011). The results for adsorption rates and capacities of the prepared SPAC for MC-LR in this study were then compared to

results for parent PACs which were derived by Liu (2017). Lastly, the removal of SPACs from Lake Erie water via conventional CFS was evaluated by a series of jar tests. Alum was used as the only coagulant in ranges typically used in drinking water treatment plants. The main findings and key conclusions in this study are summarized as below:

7.1.1 Preparation of SPACs via wet bead-milling and their characterization (Chapter 3)

- The developed SEM imaging and SIA method performed well for PSD determination of prepared SPACs. The method was also evaluated via a polydisperse particle size reference standard in the range of 0.1-1 μm.

- The wet bead-milling via the McCrone micronizing mill successfully reduced the median particle size of the parent PACs to 1.19-1.33 μm after 1 hour of milling, which characterizes the pulverized PACs as SPACs.

- The pulverization of PACs did not affect the BET internal surface area of the WPC coconut-based activated carbon. However, the internal surface area of the BG-HHM (wood-based) and COL-PL60-800 (coal-based) SPACs were reduced compared to their parent PACs. In terms of the DFT total pore volume, the pore volume of wood-based and coal-based SPACs was again reduced as the result of the pulverization. However, the DFT total pore volume and pore size distribution could not be determined for the coconut-based SPAC due its abnormal nitrogen hysteresis data.

- The point of zero charge (pH_{pzc}) of parent PACs was determined using the mass titration method. WPC (coconut-based) and COL-PL60-800 (coal-based) PACs had pH_{pzc} values of 11.12 and 11.30, respectively. These pH_{pzc} values imply that these SPACs retain a positive charge at typical surface water pH values of 6-8. The BG-HHM (wood-based) PAC had a pH_{pzc} value of 4.10 which would indicate that it would retain a negative charge in the typical surface water pH range. The pH_{pzc} could not be measured for the prepared SPACs, but are expected to be on average about 18% lower compared to their parent PACs based on work by Partlan et al. (2016).

7.1.2 Adsorption of MC-LR via prepared SPACs in buffered ultrapure water (Chapter 4)

- The prepared SPACs showed significantly higher MC-LR capacities than the parent PACs at equilibrium in ultrapure water. The wood-based BG-HHM SPAC had the highest capacity for MC-LR, whereas the coconut-based WPC SPAC had the lowest.

- At short contact times, the SPACs again outperformed the parent PACs with a statistically significant difference (i.e. 40 to 80 percent higher capacity at short contact times). However, due to the different dosing methods (dry powder dosing instead of slurry dosing), the order of capacities

was different, since WPC (coconut-based) SPAC outperformed the wood-based and coal-based SPACs due to its better dispersibility when dosed as a dry powder.

- The pseudo-second-order rate model described the adsorption rate of the SPACs in ultrapure water substantially better than the pseudo-first-order model. However, the residual plots of pseudo-second-order revealed a trend of systematic error as well, which could indicate that simple kinetic models are not highly accurate for describing the adsorption rate of MC-LR via SPACs. The adsorption rates of MC-LR by the SPACs were substantially higher than those for the parent PACs.

- Due to the high capacity of SPACs, the residual MC-LR concentrations in the rate experiments (kinetics) were quickly reduced below the method reporting level (MRL) of the quantification method. This would indicate that SPACs have very high capacity for MC-LR at low doses. Therefore, a different experimental condition was chosen to evaluate the equilibrium capacities of SPACs for MC-LR

- The experiments in this chapter showed that the dry powder dosing method for SPACs could be problematic since it would cause the SPACs to agglomerate upon dosing. Therefore, the slurry dosing method was chosen for the rest of the experiments in this study.

7.1.3 Adsorption of MC-LR via prepared SPACs in Lake Erie water (Chapter 5)

- Under similar experimental conditions SPACs outperformed parent PACs in Lake Erie water in terms of kinetics and capacities at short contact times and equilibrium conditions.

- Under equilibrium conditions, the BG-HHM (wood-based) SPAC had the highest capacity for MC-LR and adsorbed the least amount of DOC, whereas the COL-PL60-800 (coal-based) SPAC had a lower capacity and WPC (coconut-based) SPAC had the lowest capacity for MC-LR in Lake Erie water.

- At contact times of 30, 60, 120 minutes, the SPACs outperformed parent PACs, and the order of the capacities of the SPACs was the same as it was at equilibrium conditions.

- The SEBCM was applied to experimental data for adsorption of MC-LR in Lake Erie water at short contact times of 5, 10, 20, and 30 minutes to predict the SPAC dose required to reduce influent concentrations in the range of 1 to 100 µg/L to an effluent concentration of 0.4 µg/L, the chosen target concentration was based on USEPA's strictest guideline. The predicted required doses for reducing an influent MC-LR concentration of 10 µg/L to 0.4 µg/L were 12, 9.5, and 3.7 mg/L for the coconut-based, coal-based, and wood-based SPACs, respectively. The estimated doses required for reducing the MC-LR concentrations to below regulated levels can be

reasonably applied if SPACs were to be employed in practice since the predicted doses for SPACs were degrees in magnitude lower compared to parent PACs.

- The wood-based BG-HHM SPAC outperformed the other two SPACs in terms of kinetics, reducing the MC-LR concentration to below MRL (0.2 µg/L) in less than 15 minutes when dosed as prewetted slurry followed by the COL-PL60-800 (coal-based) SPAC. The WPC (coconut-based) SPAC had the slowest adsorption rate in Lake Erie water

- The dosing method of SPACs plays an essential role in the adsorption rate of MC-LR onto SPACs and short contact time capacities. The prewetted slurry-dosed SPACs presented substantially faster adsorption rates compared to dry powder dosing of the same material due to better dispersion of the particles.

7.1.4 Removal of SPACs from the Lake Erie via conventional coagulation, flocculation and sedimentation (CFS) (chapter 6)

- The addition of SPAC to the Lake Erie water increased the initial turbidity of the water substantially. The WPC (coconut-based) SPAC increased the initial turbidity the most, whereas the increase in initial turbidity by the BG-HHM (wood-based) and COL-PL60-800 (coal-based) SPACs, while drastic, was not as pronounced as for the coconut-based WPC.

- For the low turbidity Lake Erie water without any SPAC addition, any dose of alum in the range of 10-45 mg/L was sufficient to achieve a residual turbidity below 1 NTU. The BG-HHM (wood-based) SPAC was also removed successfully to a residual turbidity below 1 NTU with any alum dose. The Lake Erie water with COL-PL60-800 (coal-based) SPAC required at least 15 mg/L of alum to achieve the same result whereas WPC (coconut-based) SPAC required the substantial alum dose of 30 mg/L to achieve residual turbidity below 1 NTU.

- The pH of the Lake Erie water was impacted by the addition of SPACs, with all of the SPACs increasing the initial pH of the water. The BG-HHM (wood-based) SPAC increased the initial pH slightly by 0.28, while the initial pH increase by WPC (coconut-based) (by 0.54) and COL-PL60-800 (coal-based) (by 0.58) SPACs was more substantial. The addition of alum decreased the pH with increasing alum doses, which offset the increase in pH due to SPAC addition. The Lake Erie water with BG-HHM wood-based SPAC resisted the pH drop due to the addition of alum better compared to the Lake Erie water without SPAC or with the other two SPACs.

7.2 Relevance to industry

Based on the bench scale experimental results in this study, the application of SPAC proved to be an excellent alternative to PAC for the removal of microcystin-LR (MC-LR) in extracellular form from drinking water. The faster adsorption rate of SPACs for MC-LR compared to PACs translates to higher short contact time capacities, and lower required doses of SPACs for treating MC-LR-laden surface water compared to PACs. The contact times of PAC with water in conventional DWTPs is often short (i.e. 20 to 60 minutes) which would result in waste of PAC equilibrium capacity for MC-LR and increase in required PAC dose for treatment. Therefore, the fast adsorption rate of SPACs and their higher short contact time capacities are very important for conventional DWTPs. Furthermore, the simplified equivalent background compound model (SEBCM) was used to predict the SPAC doses required to remove MC-LR to below regulated levels in NOM-containing surface waters. The results of the fitting of this model to the experimental data showed that SEBCM could possibly assist with the choice of the SPACs and prediction of required doses as a decision-making support tool. The CFS experiment results also showed that SPACs can be removed effectively similar to PACs from surface water in conventional DWTPs, as measured by turbidity. However, it is necessary to assess the health impacts of SPAC particles breaking through into the distribution system.

As for further steps, pilot scale studies are recommended to evaluate the removal of MC-LR via SPAC in more realistic conditions. However, the cost of MC-LR would make a pilot study with spiked water infeasible, though pilot studies during a cyanobacteria bloom would be feasible and should provide valuable results.

7.3 Recommendations for future research

The time and effort required to prepare SPACs at bench scale and the cost and availability of laboratory-grade microcystin-LR caused limitations on the number of experiments that could be done in this study. Some study areas require more investigations that could not be further assessed due to time and resource limitations. Future studies should consider the following recommendations:

- The adsorption of MC-LR, the most commonly detected cyanotoxin in surface water, via SPAC was evaluated. However, it is necessary to evaluate the removal of other commonly detected microcystins such as microcystin-RR, microcystin-YR, and total microcystins. The removal of other cyanotoxins such as cylindrospermopsin and anatoxin-A by SPAC is also necessary to investigated.

- This study evaluated the competitive effect of dissolved natural organic matter (NOM) on the adsorption performance of SPACs for MC-LR. The MC-LR is typically present during

cyanobacterial blooms. Cyanobacteria cells also excrete algogenic organic matter (AOM). It is necessary to evaluate the performance of SPAC for the removal of MC-LR in the presence of AOM in surface water.

- The removal of SPACs from the Lake Erie water via CFS was evaluated in this study, and the results revealed that SPAC can be removed from surface water with conventional CFS. However, due to time constraints the removal of residual SPAC particles via rapid media filtration could not be assessed and further investigation is required to evaluate the health effects of SPAC particles breaking through to finished drinking water.

- The McCrone micronizing mill was used in this study for pulverization of parent PACs and the median particles in the range of 1.19 to 1.33 microns were achieved for SPACs. Although the achieved sizes were aligned with the recommended optimum size range from the literature, it would be beneficial to assess the adsorption of MC-LR via SPACs prepared via other milling methods (i.e. grinding material, apparatus, etc.) in different size ranges (smaller and larger).

- The point of zero charge (pH_{pzc}) of the SPACs could not be determined experimentally due to the limited amount of material available, and the values were estimated based on the data provided in the literature (Partlan et al., 2016). It is recommended that the pH_{pzc} values for prepared SPACs be measured via more accurate methods such as potentiometric mass titration (PMT) (Fiol & Villaescusa, 2009).

- The pore size distribution of SPACs in this study was determined via density function theory (DFT) based on nitrogen hysteresis data. However, this method failed to describe the pore size distribution of WPC (coconut-based) SPAC due to its abnormal nitrogen hysteresis. Furthermore, the DFT has not been deemed the most accurate method for determination of pore size distribution of porous material with complex pore networks, and use of more accurate methods such as mercury intrusion is recommended in future studies.

References

Alexander, J. A., Zaini, M. A. A., Surajudeen, A., Aliyu, E.-N. U., & Omeiza, A. U. (2018). Surface modification of low-cost bentonite adsorbents—A review. *Particulate Science and Technology*, *37*(5), 1–12. https://doi.org/10.1080/02726351.2018.1438548

Amaral, P., Partlan, E., Li, M., Lapolli, F., Mefford, O. T., Karanfil, T., & Ladner, D. A. (2016). Superfine powdered activated carbon (S-PAC) coatings on microfiltration membranes: Effects of milling time on contaminant removal and flux. *Water Research*, *100*(Water Res. 45 2011), 429–438. https://doi.org/10.1016/j.watres.2016.05.034

Ando, N., Matsui, Y., Kurotobi, R., Nakano, Y., Matsushita, T., & Ohno, K. (2010). Comparison of natural organic matter adsorption capacities of super-powdered activated carbon and powdered activated Carbon. *Water Research*, *44*(14), 4127–4136. https://doi.org/10.1016/j.watres.2010.05.029

Ando, N., Matsui, Y., Matsushita, T., & Ohno, K. (2011). Direct observation of solid-phase adsorbate concentration profile in powdered activated carbon particle to elucidate mechanism of high adsorption capacity on super-powdered activated carbon. *Water Research*, *45*(2), 761–767. https://doi.org/10.1016/j.watres.2010.08.050

Apeldoorn, M. E. van, Egmond, H. P. van, Speijers, G. J. A., & Bakker, G. J. I. (2007). Toxins of cyanobacteria. *Molecular Nutrition & Food Research*, *51*(1), 7–60. https://doi.org/10.1002/mnfr.200600185

Ateia, M., Erdem, C. U., Ersan, M. S., Ceccato, M., & Karanfil, T. (2019). Selective removal of bromide and iodide from natural waters using a novel AgCl-SPAC composite at environmentally relevant conditions. *Water Research*, *156*(Environ. Sci. Technol. 51 12 2017), 168–178. https://doi.org/10.1016/j.watres.2019.03.028

(AWWA), T. A. W. W. A., & (ASCE), T. A. S. of C. E. (2012). *Water Treatment Plant Design, Fifth Edition* (5th ed.). McGraw-Hill Education. https://www.accessengineeringlibrary.com/content/book/9780071745727

Bajracharya, A., Liu, Y.-L., & Lenhart, J. J. (2018). The influence of natural organic matter on the adsorption of microcystin-LR by powdered activated carbon. *Environmental Science: Water Research & Technology*, *5*(2), 256–267. https://doi.org/10.1039/c8ew00582f

Batista, T., Sousa, G. de, Suput, J. S., Rahmani, R., & Šuput, D. (2003). Microcystin-LR causes the collapse of actin filaments in primary human hepatocytes. *Aquatic Toxicology*, *65*(1), 85–91. https://doi.org/10.1016/s0166-445x(03)00108-5

Bonvin, F., Jost, L., Randin, L., Bonvin, E., & Kohn, T. (2016). Super-fine powdered activated carbon (SPAC) for efficient removal of micropollutants from wastewater treatment plant effluent. *Water Research*, *90*(Chem. Eng. J. 210 2012), 90–99. https://doi.org/10.1016/j.watres.2015.12.001

Campinas, M., & Rosa, M. J. (2012). Comparing PAC/UF and conventional clarification with PAC for removing microcystins from natural waters. *Desalination and Water Treatment*, *16*(1–3), 120–128. https://doi.org/10.5004/dwt.2010.1092

Campinas, M., Silva, C., Viegas, R. M. C., Coelho, R., Lucas, H., & Rosa, M. J. (2021). To what extent may pharmaceuticals and pesticides be removed by PAC conventional addition to low-turbidity surface waters and what are the potential bottlenecks? *Journal of Water Process Engineering*, *40*, 101833. https://doi.org/10.1016/j.jwpe.2020.101833

Campinas, M., Viegas, R. M. C., & Rosa, M. J. (2013). Modelling and understanding the competitive adsorption of microcystins and tannic acid. *Water Research*, *47*(15), 5690–5699. https://doi.org/10.1016/j.watres.2013.06.048

Carrière, A., Prévost, M., Zamyadi, A., Chevalier, P., & Barbeau, B. (2009). Vulnerability of Quebec drinking-water treatment plants to cyanotoxins in a climate change context. *Journal of Water and Health*, *8*(3), 455–465. https://doi.org/10.2166/wh.2009.207

Chorus, I., Falconer, I. R., Salas, H. J., & Bartram, J. (2000). HEALTH RISKS CAUSED BY FRESHWATER CYANOBACTERIA IN RECREATIONAL WATERS. *Journal of Toxicology and Environmental Health, Part B*, *3*(4), 323–347. https://doi.org/10.1080/109374000436364

Coe, J., Kupitz, C., Basu, S., Conrad, C. E., Roy-Chowdhury, S., Fromme, R., & Fromme, P. (2015). Methods in Enzymology. *Methods in Enzymology*, *557*, 459–482. https://doi.org/10.1016/bs.mie.2015.01.011

Committee, D. (2013). *Practice for Coagulation-Flocculation Jar Test of Water* (Standard ASTM D2035-13). ASTM International. http://www.astm.org/cgi-bin/resolver.cgi?D2035

Constales, D., Yablonsky, G. S., D'hooge, D. R., Thybaut, J. W., & Marin, G. B. (2017). *Advanced Data Analysis and Modelling in Chemical Engineering*. 285–306. https://doi.org/10.1016/b978-0-444-59485-3.00009-6

Cook, D., & Newcombe, G. (2002). Removal of microcystin variants with powdered activated carbon. *Water Supply*, *2*(5–6), 201–207. https://doi.org/10.2166/ws.2002.0170

Cook, D., & Newcombe, G. (2008). COMPARISON AND MODELING OF THE ADSORPTION OF TWO MICROCYSTIN ANALOGUES ONTO POWDERED ACTIVATED CARBON. *Environmental Technology*, *29*(5), 525–534. https://doi.org/10.1080/09593330801984415

Davis, T. W., Berry, D. L., Boyer, G. L., & Gobler, C. J. (2009). The effects of temperature and nutrients on the growth and dynamics of toxic and non-toxic strains of Microcystis during cyanobacteria blooms. *Harmful Algae*, *8*(5), 715–725. https://doi.org/10.1016/j.hal.2009.02.004

Delgado, L. F., Charles, P., Glucina, K., & Morlay, C. (2012). The removal of endocrine disrupting compounds, pharmaceutically activated compounds and cyanobacterial toxins during drinking water preparation using activated carbon—A review. *Science of The Total Environment*, *435*, 509–525. https://doi.org/10.1016/j.scitotenv.2012.07.046

Donati, C., Drikas, M., Hayes, R., & Newcombe, G. (1994). Microcystin-LR adsorption by powdered activated carbon. *Water Research*, *28*(8), 1735–1742. https://doi.org/10.1016/0043-1354(94)90245-3

Drogui, P., Daghrir, R., Simard, M.-C., Sauvageau, C., & Blais, J. F. (2012). Removal of microcystin-LR from spiked water using either activated carbon or anthracite as filter material. *Environmental Technology*, *33*(4), 381–391. https://doi.org/10.1080/09593330.2011.575186

Du, X., Liu, H., Yuan, L., Wang, Y., Ma, Y., Wang, R., Chen, X., Losiewicz, M. D., Guo, H., & Zhang, H. (2019). The Diversity of Cyanobacterial Toxins on Structural Characterization, Distribution and Identification: A Systematic Review. *Toxins*, *11*(9), 530. https://doi.org/10.3390/toxins11090530

Duy, T. N., Lam, P. K. S., Shaw, G. R., & Connell, D. W. (2000). Reviews of Environmental Contamination and Toxicology, Continuation of Residue Reviews. *Reviews of Environmental Contamination and Toxicology*, *163*, 113–185. https://doi.org/10.1007/978-1-4757-6429-1_3

E.W., R., L., B., Association, A. P. H., Association, A. W. W., & Federation, W. E. (2017). *Standard Methods for the Examination of Water and Wastewater* (22nd ed.). American Public Health Association. https://www.wef.org/resources/publications/books/StandardMethods/

Fairey, J. L., & Wahman, D. G. (2013). Bayesian and Frequentist Methods for Estimating Joint Uncertainty of Freundlich Adsorption Isotherm Fitting Parameters. *Journal of Environmental Engineering*, *139*(2), 307–311. https://doi.org/10.1061/(asce)ee.1943-7870.0000634

Falconer, I. R. (1993). *Algal Toxins in Seafood and Drinking Water*. 177–186. https://doi.org/10.1016/b978-0-08-091811-2.50016-2

Fiol, N., & Villaescusa, I. (2009). Determination of sorbent point zero charge: usefulness in sorption studies. *Environmental Chemistry Letters*, *7*(1), 79–84. https://doi.org/10.1007/s10311-008-0139-0

Fristachi, A., Sinclair, J. L., Hall, S., Berkman, J. A. H., Boyer, G., Burkholder, J., Burns, J., Carmichael, W., DuFour, A., Frazier, W., Morton, S. L., O'Brien, E., & Walker, S. (2008). Cyanobacterial Harmful Algal Blooms: State of the Science and Research Needs. *Advances in Experimental Medicine and Biology*, *619*, 45–103. https://doi.org/10.1007/978-0-387-75865-7_3

Giani, A., Bird, D. F., Prairie, Y. T., & Lawrence, J. F. (2005). Empirical study of cyanobacterial toxicity along a trophic gradient of lakes. *Canadian Journal of Fisheries and Aquatic Sciences*, *62*(9), 2100–2109. https://doi.org/10.1139/f05-124

Graham, M., Summers, R., Simpson, M., & MacLeod, B. (2000). Modeling equilibrium adsorption of 2-methylisoborneol and geosmin in natural waters. *Water Research*, *34*(8), 2291–2300. https://doi.org/10.1016/s0043-1354(99)00390-5

Hallé, C., Huck, P. M., & Peldszus, S. (2015). Emerging Contaminant Removal by Biofiltration: Temperature, Concentration, and EBCT Impacts. *Journal - American Water Works Association*, *107*(7), E364–E379. https://doi.org/10.5942/jawwa.2015.107.0086

Harada, K., Tsuji, K., Watanabe, M. F., & Kondo, F. (1996). Stability of microcystins from cyanobacteria—III. Effect of pH and temperature. *Phycologia*, *35*(sup6), 83–88. https://doi.org/10.2216/i0031-8884-35-6s-83.1

Heijman, S., Hamad, J., Kennedy, M., Schippers, J., & Amy, G. (2012). Submicron powdered activated carbon used as a pre-coat in ceramic micro-filtration. *Desalination and Water Treatment*, *9*(1–3), 86–91. https://doi.org/10.5004/dwt.2009.755

Ho, L., Lambling, P., Bustamante, H., Duker, P., & Newcombe, G. (2011). Application of powdered activated carbon for the adsorption of cylindrospermopsin and microcystin toxins from drinking water supplies. *Water Research*, *45*(9), 2954–2964. https://doi.org/10.1016/j.watres.2011.03.014

Ho, L., & Newcombe, G. (2007). Evaluating the adsorption of microcystin toxins using granular activated carbon (GAC). *Journal of Water Supply: Research and Technology-Aqua*, *56*(5), 281–291. https://doi.org/10.2166/aqua.2007.080

Ho, Y. S., & McKay, G. (1999). Pseudo-second order model for sorption processes. *Process Biochemistry*, *34*(5), 451–465. https://doi.org/10.1016/s0032-9592(98)00112-5

Huang, X., Wan, Y., Shi, B., & Shi, J. (2020). Effects of powdered activated carbon on the coagulation-flocculation process in humic acid and humic acid-kaolin water treatment. *Chemosphere*, *238*, 124637. https://doi.org/10.1016/j.chemosphere.2019.124637

Huck, P., & Sozanski, M. (2011). *Chemical Basis for Water Technology*. Elsevier B.V.

Iacomi, P., & Llewellyn, P. L. (2019). *pyGAPS: A Python-Based Framework for Adsorption Isotherm Processing and Material Characterisation*. https://doi.org/10.26434/chemrxiv.7970402

Knappe, D., Snoeyink, V., Roche, P., Prados, M., & Bourbigot, M. (1999). Atrazine removal by preloaded GAC. *Journal - American Water Works Association*, *91*(10), 97–109. https://doi.org/10.1002/j.1551-8833.1999.tb08719.x

Kotak, B. G., & Zurawell, R. W. (2007). Cyanobacterial toxins in Canadian freshwaters: A review. *Lake and Reservoir Management*, *23*(2), 109–122. https://doi.org/10.1080/07438140709353915

Kumar, P., Hegde, K., Brar, S. K., Cledon, M., & pour, A. K. (2018). Physico-chemical treatment for the degradation of cyanotoxins with emphasis on drinking water treatment—How far have we come? *Journal of Environmental Chemical Engineering*, *6*. https://doi.org/10.1016/j.jece.2018.08.032

Lalezary-Craig, S., Pirbazari, M., Dale, M. S., Tanaka, T. S., & McGuire, M. J. (1988). Optimizing the Removal of Geosmin and 2-Methylisobomeol by Powdered Activated Carbon. *Journal - American Water Works Association*, *80*(3), 73–80. https://doi.org/10.1002/j.1551-8833.1988.tb03011.x

Liang, G., Xie, P., Chen, J., & Yu, T. (2011). Comparative Studies on the pH Dependence of D OW of Microcystin-RR and -LR Using LC-MS. *The Scientific World JOURNAL*, *11*, 20–26. https://doi.org/10.1100/tsw.2011.17

Liu, Y. (2017). *Treatment of the Cyanotoxins Cylindrospermopsin, Microcystin-LR, and Anatoxin-a by Activated Carbon in Drinking Water.pdf*.

Maagd, P. G.-J. de, Hendriks, A. J., Seinen, W., & Sijm, D. T. H. M. (1999). pH-Dependent hydrophobicity of the cyanobacteria toxin microcystin-LR. *Water Research*, *33*(3), 677–680. https://doi.org/10.1016/s0043-1354(98)00258-9

Mashile, P. P., Dimpe, M. K., & Nomngongo, P. N. (2019). Application of waste tyre-based powdered activated carbon for the adsorptive removal of cylindrospermopsin toxins from environmental matrices: Optimization using response surface methodology and desirability function. *Journal of Environmental Science and Health, Part A*, *54*(7), 679–685. https://doi.org/10.1080/10934529.2019.1579538

Mashile, P. P., Mpupa, A., & Nomngongo, P. N. (2018). Adsorptive removal of microcystin-LR from surface and wastewater using tyre-based powdered activated carbon: Kinetics and isotherms. *Toxicon*, *145*, 25–31. https://doi.org/10.1016/j.toxicon.2018.02.044

Massey, I. Y., Yang, F., Ding, Z., Yang, S., Guo, J., Tezi, C., Al-Osman, M., Kamegni, R. B., & Zeng, W. (2018). Exposure routes and health effects of microcystins on animals and humans: A mini-review. *Toxicon*, *151*, 156–162. https://doi.org/10.1016/j.toxicon.2018.07.010

Masuda, H., & Gotoh, K. (1999). Study on the sample size required for the estimation of mean particle diameter. *Advanced Powder Technology*, *10*(2), 159–173. https://doi.org/10.1016/s0921-8831(08)60447-1

Matsui, Y., Aizawa, T., Kanda, F., Nigorikawa, N., Mima, S., & Kawase, Y. (2007). Adsorptive removal of geosmin by ceramic membrane filtration with super-powdered activated carbon. *Journal of Water Supply: Research and Technology-Aqua*, *56*(6–7), 411–418. https://doi.org/10.2166/aqua.2007.017

Matsui, Y., Aizawa, T., Suzuki, M., & Kawase, Y. (2007). Removal of geosmin and algae by ceramic membrane filtration with super-powdered activated carbon adsorption pretreatment. *Water Science and Technology: Water Supply*, *7*(5–6), 43–51. https://doi.org/10.2166/ws.2007.080

Matsui, Y., Ando, N., Sasaki, H., Matsushita, T., & Ohno, K. (2009). Branched pore kinetic model analysis of geosmin adsorption on super-powdered activated carbon. *Water Research*, *43*(12), 3095–3103. https://doi.org/10.1016/j.watres.2009.04.014

Matsui, Y., Ando, N., Yoshida, T., Kurotobi, R., Matsushita, T., & Ohno, K. (2011). Modeling high adsorption capacity and kinetics of organic macromolecules on super-powdered activated carbon. *Water Research*, *45*(4), 1720–1728. https://doi.org/10.1016/j.watres.2010.11.020

Matsui, Y., Fukuda, Y., Inoue, T., & Matsushita, T. (2003). Effect of natural organic matter on powdered activated carbon adsorption of trace contaminants: characteristics and mechanism of competitive adsorption. *Water Research*, *37*(18), 4413–4424. https://doi.org/10.1016/s0043-1354(03)00423-8

Matsui, Y., Hasegawa, H., Ohno, K., Matsushita, T., Mima, S., Kawase, Y., & Aizawa, T. (2009). Effects of super-powdered activated carbon pretreatment on coagulation and trans-membrane pressure buildup during microfiltration. *Water Research*, *43*(20), 5160–5170. https://doi.org/10.1016/j.watres.2009.08.021

Matsui, Y., Murase, R., Sanogawa, T., Aoki, N., Mima, S., Inoue, T., & Matsushita, T. (2004). Micro-ground powdered activated carbon for effective removal of natural organic matter during water treatment. *Water Science and Technology: Water Supply*, *4*(4), 155–163. https://doi.org/10.2166/ws.2004.0073

Matsui, Y., Murase, R., Sanogawa, T., Aoki, N., Mima, S., Inoue, T., & Matsushita, T. (2005). Rapid adsorption pretreatment with submicrometre powdered activated carbon particles before microfiltration. *Water Science and Technology*, *51*(6–7), 249–256. https://doi.org/10.2166/wst.2005.0644

Matsui, Y., Nakano, Y., Hiroshi, H., Ando, N., Matsushita, T., & Ohno, K. (2010). Geosmin and 2-methylisoborneol adsorption on super-powdered activated carbon in the presence of natural organic matter. *Water Science and Technology : A Journal of the International Association on Water Pollution Research*, *62*(11), 2664–2668. https://doi.org/10.2166/wst.2010.415

Matsui, Y., Nakao, S., Taniguchi, T., & Matsushita, T. (2013). Geosmin and 2-methylisoborneol removal using superfine powdered activated carbon: Shell adsorption and branched-pore kinetic model analysis and optimal particle size. *Water Research*, *47*(8), 2873–2880. https://doi.org/10.1016/j.watres.2013.02.046

Matsui, Y., Sanogawa, T., Aoki, N., Mima, S., & Matsushita, T. (2006). Evaluating submicron-sized activated carbon adsorption for microfiltration pretreatment. *Water Science and Technology: Water Supply*, *6*(1), 149–155. https://doi.org/10.2166/ws.2006.017

Matsui, Y., Yoshida, T., Nakao, S., Knappe, D. R. U., & Matsushita, T. (2012). Characteristics of competitive adsorption between 2-methylisoborneol and natural organic matter on superfine and conventionally sized powdered activated carbons. *Water Research*, *46*(15), 4741–4749. https://doi.org/10.1016/j.watres.2012.06.002

Matsushita, T., Suzuki, H., Shirasaki, N., Matsui, Y., & Ohno, K. (2013). Adsorptive virus removal with super-powdered activated carbon. *Separation and Purification Technology*, *107*, 79–84. https://doi.org/10.1016/j.seppur.2013.01.017

Mazzoli, A., & Favoni, O. (2012). Particle size, size distribution and morphological evaluation of airborne dust particles of diverse woods by Scanning Electron Microscopy and image processing program. *Powder Technology*, *225*, 65–71. https://doi.org/10.1016/j.powtec.2012.03.033

McDonough, K. M., Fairey, J. L., & Lowry, G. V. (2008). Adsorption of polychlorinated biphenyls to activated carbon: Equilibrium isotherms and a preliminary assessment of the effect of dissolved organic matter and biofilm loadings. *Water Research*, *42*(3), 575–584. https://doi.org/10.1016/j.watres.2007.07.053

Merel, S., Clément, M., & Thomas, O. (2010). State of the art on cyanotoxins in water and their behaviour towards chlorine. *Toxicon*, *55*(4), 677–691. https://doi.org/10.1016/j.toxicon.2009.10.028

Merel, S., Walker, D., Chicana, R., Snyder, S., Baurès, E., & Thomas, O. (2013). State of knowledge and concerns on cyanobacterial blooms and cyanotoxins. *Environment International*, *59*, 303–327. https://doi.org/10.1016/j.envint.2013.06.013

Müller, K. M., Chhun, A., Guildford, S. J., Yakobowski, S. J., & Jonlija, M. (2017). Molecular and ecological characterization of toxic cyanobacteria from the Bay of Quinte (Lake Ontario) and Maumee Bay (Lake Erie). *Journal of Great Lakes Research*, *43*(6), 1067–1083. https://doi.org/10.1016/j.jglr.2017.03.021

Murphy, T., Irvine, K., Guo, J., Davies, J., Murkin, H., Charlton, M., & Watson, S. (2003). New Microcystin Concerns in the Lower Great Lakes. *Water Quality Research Journal*, *38*(1), 127–140. https://doi.org/10.2166/wqrj.2003.008

Murray, C. C., Vatankhah, H., McDonough, C. A., Nickerson, A., Hedtke, T. T., Cath, T. Y., Higgins, C. P., & Bellona, C. L. (2018). Removal of Per- and Polyfluoroalkyl Substances using Super-Fine Powder Activated Carbon and Ceramic Membrane Filtration. *Journal of Hazardous Materials*, *366*(Swedish University of Agricultural Sciences Faculty 2015), 160–168. https://doi.org/10.1016/j.jhazmat.2018.11.050

Najm, I. N., Snoeyink, V. L., Lykins, B. W., & Adams, J. Q. (1991). Using Powdered Activated Carbon: A Critical Review. *Journal - American Water Works Association*, *83*(1), 65–76. https://doi.org/10.1002/j.1551-8833.1991.tb07087.x

Najm, I. N., Snoeyink, V. L., & Richard, Y. (1991). Effect of Initial Concentration of a SOC in Natural Water on Its Adsorption by Activated Carbon. *Journal - American Water Works Association*, *83*(8), 57–63. https://doi.org/10.1002/j.1551-8833.1991.tb07200.x

Najm, I. N., Snoeyink, V. L., Suidan, M. T., Lee, C. H., & Richard, Y. (1990). Effect of Particle Size and Background Natural Organics on the Adsorption Efficiency of PAC. *Journal - American Water Works Association*, *82*(1), 65–72. https://doi.org/10.1002/j.1551-8833.1990.tb06907.x

Nakazawa, Y., Abe, T., Matsui, Y., Shirasaki, N., & Matsushita, T. (2021). Stray particles as the source of residuals in sand filtrate: Behavior of superfine powdered activated carbon particles in water treatment processes. *Water Research*, *190*, 116786. https://doi.org/10.1016/j.watres.2020.116786

Nakazawa, Y., Matsui, Y., Hanamura, Y., Shinno, K., Shirasaki, N., & Matsushita, T. (2018a). Identifying, counting, and characterizing superfine activated-carbon particles remaining after coagulation, sedimentation, and sand filtration. *Water Research*, *138*(Water Res. 37 9 2003), 160–168. https://doi.org/10.1016/j.watres.2018.03.046

Nakazawa, Y., Matsui, Y., Hanamura, Y., Shinno, K., Shirasaki, N., & Matsushita, T. (2018b). Minimizing residual black particles in sand filtrate when applying super-fine powdered activated carbon: Coagulants and coagulation conditions. *Water Research*, *147*(Water Res. 37 9 2003), 311–320. https://doi.org/10.1016/j.watres.2018.10.008

Newcombe, G. (2002). *Removal of algal toxins from drinking water using ozone and GAC*.

Newcombe, G., Morrison, J., Hepplewhite, C., & Knappe, D. R. U. (2002). Simultaneous adsorption of MIB and NOM onto activated carbon II. Competitive effects. *Carbon*, *40*(12), 2147–2156. https://doi.org/10.1016/s0008-6223(02)00098-2

Newcombe, G., & Nicholson, B. (2004). Water treatment options for dissolved cyanotoxins. *Journal of Water Supply: Research and Technology-Aqua*, *53*(4), 227–239. https://doi.org/10.2166/aqua.2004.0019

Organization, W. H. (2020). *Cyanobacterial toxins: microcystins*.

Paerl, H. W., & Huisman, J. (2009). Climate change: a catalyst for global expansion of harmful cyanobacterial blooms. *Environmental Microbiology Reports*, *1*(1), 27–37. https://doi.org/10.1111/j.1758-2229.2008.00004.x

Pan, L., Matsui, Y., Matsushita, T., & Shirasaki, N. (2016). Superiority of wet-milled over dry-milled superfine powdered activated carbon for adsorptive 2-methylisoborneol removal. *Water Research*, *102*, 516–523. https://doi.org/10.1016/j.watres.2016.06.062

Pan, L., Nishimura, Y., Takaesu, H., Matsui, Y., Matsushita, T., & Shirasaki, N. (2017). Effects of decreasing activated carbon particle diameter from 30 μm to 140 nm on equilibrium adsorption capacity. *Water Research*, *124*, 425–434. https://doi.org/10.1016/j.watres.2017.07.075

Pantelić, D., Svirčev, Z., Simeunović, J., Vidović, M., & Trajković, I. (2013). Cyanotoxins: Characteristics, production and degradation routes in drinking water treatment with reference to the situation in Serbia. *Chemosphere*, *91*(4), 421–441. https://doi.org/10.1016/j.chemosphere.2013.01.003

Park, J.-A., Jung, S.-M., Choi, J.-W., Kim, J.-H., Hong, S., & Lee, S.-H. (2017). Mesoporous carbon for efficient removal of microcystin-LR in drinking water sources, Nak-Dong River, South Korea: Application to a field-scale drinking water treatment plant. *Chemosphere*, *193*, 883–891. https://doi.org/10.1016/j.chemosphere.2017.11.092

Particle size analysis. Image analysis methods: Static image analysis methods (Standard BS ISO 13322-1:2014). (2014). BSI Standards Publication.

Partlan, E., Davis, K., Ren, Y., Apul, O. G., Mefford, O. T., Karanfil, T., & Ladner, D. A. (2016). Effect of bead milling on chemical and physical characteristics of activated carbons pulverized to superfine sizes. *Water Research*, *89*, 161–170. https://doi.org/10.1016/j.watres.2015.11.041

Partlan, E., Ren, Y., Apul, O. G., Ladner, D. A., & Karanfil, T. (2020). Adsorption kinetics of synthetic organic contaminants onto superfine powdered activated carbon. *Chemosphere*, *253*, 126628. https://doi.org/10.1016/j.chemosphere.2020.126628

Qi, S., Schideman, L., Mariñas, B. J., Snoeyink, V. L., & Campos, C. (2007). Simplification of the IAST for activated carbon adsorption of trace organic compounds from natural water. *Water Research*, *41*(2), 440–448. https://doi.org/10.1016/j.watres.2006.10.018

Richardson, J., Miller, C., Maberly, S. C., Taylor, P., Globevnik, L., Hunter, P., Jeppesen, E., Mischke, U., Moe, S. J., Pasztaleniec, A., Søndergaard, M., & Carvalho, L. (2018). Effects of multiple stressors on cyanobacteria abundance vary with lake type. *Global Change Biology*, *24*(11), 5044–5055. https://doi.org/10.1111/gcb.14396

Roegner, A. F., Brena, B., González-Sapienza, G., & Puschner, B. (2013). Microcystins in potable surface waters: toxic effects and removal strategies: Persistence of microcystins in drinking water. *Journal of Applied Toxicology*, *34*(5), 441–457. https://doi.org/10.1002/jat.2920

Rouquerol, J., Avnir, D., Fairbridge, C. W., Everett, D. H., Haynes, J. M., Pernicone, N., Ramsay, J. D. F., Sing, K. S. W., & Unger, K. K. (1994). Recommendations for the characterization of porous solids (Technical Report). *Pure and Applied Chemistry*, *66*(8), 1739–1758. https://doi.org/10.1351/pac199466081739

Rueden, C. T., Schindelin, J., Hiner, M. C., DeZonia, B. E., Walter, A. E., Arena, E. T., & Eliceiri, K. W. (2017). ImageJ2: ImageJ for the next generation of scientific image data. *BMC Bioinformatics*, *18*(1), 529. https://doi.org/10.1186/s12859-017-1934-z

Salmaso, N., Bernard, C., Humbert, J.-F., Akçaalan, R., Albay, M., Ballot, A., Catherine, A., Fastner, J., Häggqvist, K., Horecká, M., Izydorczyk, K., Köker, L., Komárek, J., Maloufi, S., Mankiewicz-Boczek, J., Metcalf, J. S., Quesada, A., Quiblier, C., & Yéprémian, C. (2016). *Handbook of Cyanobacterial Monitoring and Cyanotoxin Analysis*. 46–69. https://doi.org/10.1002/9781119068761.ch6

Sam, V. (2012). *THE OCCURRENCE AND REMOVAL OF CYANOBACTERIAL METABOLITES MICROYCSTIN - LR AND GEOSMIN FROM SOURCE WATERS WITH POWDERED ACTIVATED CARBON.*

Shimabuku, K. K., Cho, H., Townsend, E. B., Rosario-Ortiz, F. L., & Summers, R. S. (2014). Modeling nonequilibrium adsorption of MIB and sulfamethoxazole by powdered activated carbon and the role of

dissolved organic matter competition. *Environmental Science & Technology*, *48*(23), 13735–13742. https://doi.org/10.1021/es503512v

Song, Y., Dong, B., Gao, N., & Ma, X. (2015). Powder Activated Carbon Pretreatment of a Microfiltration Membrane for the Treatment of Surface Water. *International Journal of Environmental Research and Public Health*, *12*(9), 11269–11277. https://doi.org/10.3390/ijerph120911269

Stoquart, C., Rodríguez, G., Servais, P., Sauvé, S., & Barbeau, B. (2016). Micropollutant Removal Potential by Aged Powdered Activated Carbon. *Journal of Environmental Engineering*, *142*(11), 04016058. https://doi.org/10.1061/(asce)ee.1943-7870.0001125

Sukenik, A., Viner-Mozzini, Y., Tavassi, M., & Nir, S. (2017). Removal of cyanobacteria and cyanotoxins from lake water by composites of bentonite with micelles of the cation octadecyltrimethyl ammonium (ODTMA). *Water Research*, *120*, 165–173. https://doi.org/10.1016/j.watres.2017.04.075

Summers, S. R. (1986). *Activated carbon adsorption of humic substances: Effect of molecular size and heterodispersity*.

Svrcek, C., & Smith, D. W. (2004). Cyanobacteria toxins and the current state of knowledge on water treatment options: a review. *Journal of Environmental Engineering and Science*, *3*(3), 155–185. https://doi.org/10.1139/s04-010

Szlag, D., Sinclair, J., Southwell, B., & Westrick, J. (2015). Cyanobacteria and Cyanotoxins Occurrence and Removal from Five High-Risk Conventional Treatment Drinking Water Plants. *Toxins*, *7*(6), 2198–2220. https://doi.org/10.3390/toxins7062198

Takaesu, H., Matsui, Y., Nishimura, Y., Matsushita, T., & Shirasaki, N. (2019). Micro-milling Super-fine Powdered Activated Carbon Decreases Adsorption Capacity by Introducing Oxygen/hydrogen-Containing Functional Groups on Carbon Surface from Water. *Water Research*, *155*(Environmental Science Technology 28 11 1994), 66–75. https://doi.org/10.1016/j.watres.2019.02.019

Tinke, A. P., Vanhoutte, K., Vanhoutte, F., Smet, M. D., & Winter, H. D. (2005). Laser diffraction and image analysis as a supportive analytical tool in the pharmaceutical development of immediate release direct compression formulations. *International Journal of Pharmaceutics*, *297*(1–2), 80–88. https://doi.org/10.1016/j.ijpharm.2005.03.009

Vlad, S., Anderson, W. B., Peldszus, S., & Huck, P. M. (2014). Removal of the cyanotoxin anatoxin-a by drinking water treatment processes: a review. *Journal of Water and Health*, *12*(4), 601–617. https://doi.org/10.2166/wh.2014.018

Wang, H., Ho, L., Lewis, D. M., Brookes, J. D., & Newcombe, G. (2007). Discriminating and assessing adsorption and biodegradation removal mechanisms during granular activated carbon filtration of microcystin toxins. *Water Research*, *41*(18), 4262–4270. https://doi.org/10.1016/j.watres.2007.05.057

Waskom, M. (2021). seaborn: statistical data visualization. *Journal of Open Source Software*, *6*(60), 3021. https://doi.org/10.21105/joss.03021

Weber, W. J., Voice, T. C., & Jodellah, A. (1983). Adsorption of humic substances: the effects of heterogeneity and system characteristics. *Journal - American Water Works Association*, *75*(12), 612–619. https://doi.org/10.1002/j.1551-8833.1983.tb05246.x

Wedd, M. W. (2001). Procedure for Predicting a Minimum Volume or Mass of Sample to Provide a Given Size Parameter Precision. *Particle & Particle Systems Characterization*, *18*(3), 109–113. https://doi.org/10.1002/1521-4117(200110)18:3<109::aid-ppsc109>3.0.co;2-b

Westrick, J. A., Szlag, D. C., Southwell, B. J., & Sinclair, J. (2010). A review of cyanobacteria and cyanotoxins removal/inactivation in drinking water treatment. *Analytical and Bioanalytical Chemistry*, *397*(5), 1705–1714. https://doi.org/10.1007/s00216-010-3709-5

Worch, E. (2012). *Adsorption Technology in Water Treatment Fundamentals, Processes, and Modeling*. De Gruyter.

Yang, S., Chen, L., Wen, C., Zhang, X., Feng, X., & Yang, F. (2017). MicroRNA expression profiling involved in MC-LR-induced hepatotoxicity using high-throughput sequencing analysis. *Journal of Toxicology and Environmental Health. Part A*, *81*(5), 1–9. https://doi.org/10.1080/15287394.2017.1415580

Yoshida, H., Mori, Y., Masuda, H., & Yamamoto, T. (2009). Particle size measurement of standard reference particle candidates and theoretical estimation of uncertainty region. *Advanced Powder Technology*, *20*(2), 145–149. https://doi.org/10.1016/j.apt.2008.05.002

Zastepa, A., Watson, S. B., Kling, H., & Kotak, B. (2017). Spatial and temporal patterns in microcystin toxins in Lake of the Woods surface waters. *Lake and Reservoir Management*, *33*(4), 433–443. https://doi.org/10.1080/10402381.2017.1384415

Zhu, S., Yin, D., Gao, N., Zhou, S., Wang, Z., & Zhang, Z. (2016). Adsorption of two microcystins onto activated carbon: equilibrium, kinetic, and influential factors. *Desalination and Water Treatment*, *57*(50), 23666–23674. https://doi.org/10.1080/19443994.2015.1137492

Zietzschmann, F., Aschermann, G., & Jekel, M. (2016). Comparing and modeling organic micro-pollutant adsorption onto powdered activated carbon in different drinking waters and WWTP effluents. *Water Research*, *102*, 190–201. https://doi.org/10.1016/j.watres.2016.06.041

Zoschke, K., Engel, C., Börnick, H., & Worch, E. (2011). Adsorption of geosmin and 2-methylisoborneol onto powdered activated carbon at non-equilibrium conditions: influence of NOM and process modelling. *Water Research*, *45*(15), 4544–4550. https://doi.org/10.1016/j.watres.2011.06.006

Appendix A

Additional Information for chapter 3

Appendix A.1 Polydisperse particle standard certification

Appendix A.2 Polydisperse particle size analysis certification
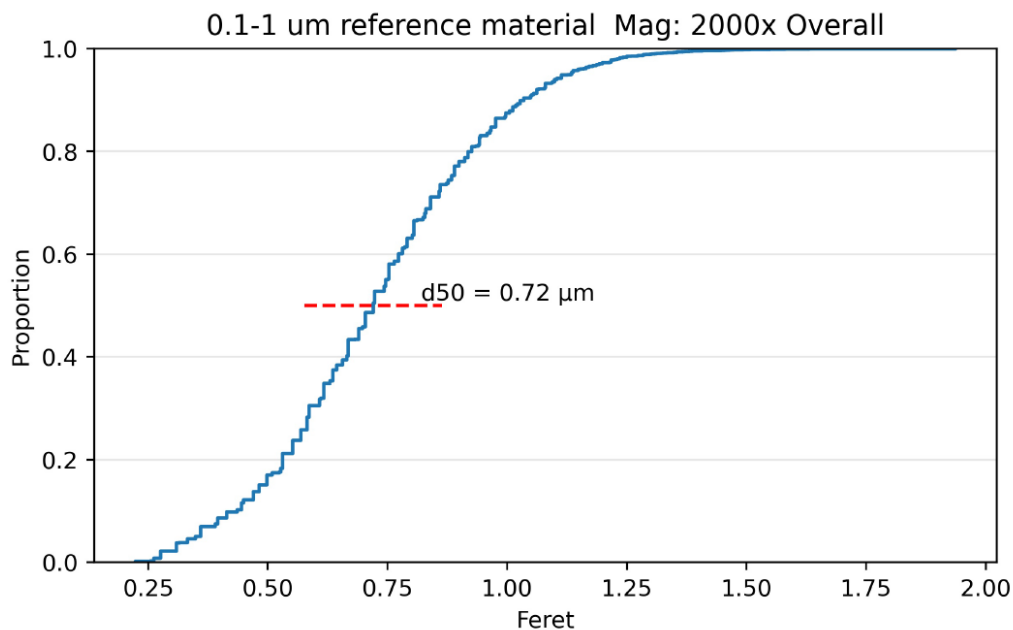
Figure A.1 Cumulative distribution of the polydisperse particle standard determined by the developed SEM method

Table A.1 PSD analysis statistics of the polydisperse particle standard of 0.1-1 μm

Image	Particle count	mean	std	Distribution				
				min	25%	50%	75%	max
1	256	0.75	0.22	0.28	0.59	0.75	0.89	1.36
2	354	0.73	0.23	0.26	0.57	0.72	0.89	1.58
3	274	0.74	0.24	0.26	0.57	0.72	0.91	1.41
4	109	0.70	0.25	0.22	0.53	0.69	0.86	1.29
5	149	0.75	0.25	0.26	0.55	0.75	0.96	1.35
6	158	0.70	0.22	0.28	0.56	0.69	0.83	1.33
7	152	0.72	0.23	0.26	0.58	0.70	0.86	1.31
8	173	0.72	0.23	0.22	0.57	0.69	0.84	1.49
9	217	0.75	0.27	0.22	0.55	0.72	0.92	1.94
10	161	0.76	0.27	0.22	0.58	0.75	0.97	1.55
11	167	0.71	0.24	0.26	0.53	0.70	0.91	1.23
12	184	0.74	0.25	0.26	0.58	0.75	0.89	1.51
13	321	0.71	0.20	0.22	0.58	0.70	0.84	1.28
14	424	0.71	0.21	0.26	0.57	0.70	0.84	1.46

Appendix A.3 SPAC particle size distribution via SEM imaging
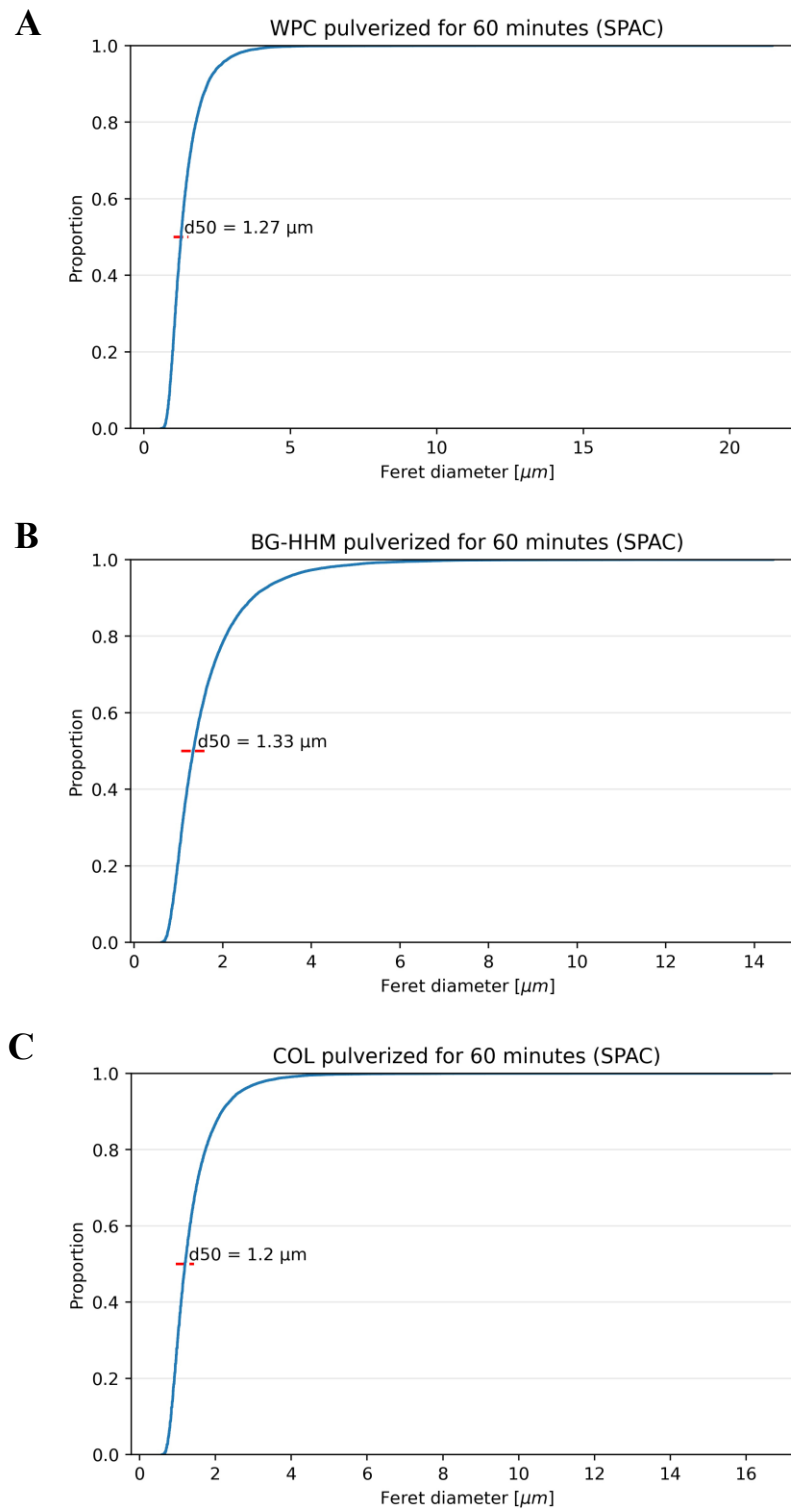
Figure A.2 Cumulative size distribution of SPACs determined by SEM imaging method; (A) Cumulative distribution of coconut-based (WPC) SPAC; (B) Cumulative distribution of wood-based (BG-HHM) SPAC; (C) Cumulative distribution of coal-based (COL-PL60-800) SPAC

Appendix A.4 PAC particle size distribution via laser diffraction (Malvern Mastersizer3000)

Table A.2 WPC (coconut-based) PAC particle size distribution

Record Number	Sample Name	Dx (10)	Dx (50)	Dx (90)	Uniformity	D [3,2]	D [4,3]
1	wpc - 1st	7.09	28.8	76.8	0.747	13.9	36.4
2	wpc - 1st	7.24	30.3	88.4	1.704	14.3	67.1
3	wpc - 1st	7.67	34	689	3.686	15.5	142
4	wpc - 1st	7.97	37.1	847	5.154	16.5	209
5	wpc - 1st	8.33	41.1	973	6.287	17.6	278
6	wpc - 1st	8.78	45.6	1020	6.762	19.3	330
7	wpc - 1st	9.17	52.2	1060	6.745	20.5	375
8	wpc - 1st	9.24	55.4	1110	7.001	20.9	412
9	wpc - 1st	9.05	55.3	1080	6.734	20.1	396
10	wpc - 1st	9.54	68.9	1100	6.065	22.1	445
11	wpc - 1st	9.71	85.7	1040	4.729	22.6	434
12	wpc - 1st	9.54	82.4	1060	4.849	22.2	428
13	wpc - 1st	8.98	65.7	1070	5.947	20.5	417
14	wpc - 1st	9.37	411	1050	0.986	21.7	436
15	wpc - 1st	9.16	83.1	1050	4.856	21.3	432
16	wpc - 1st	8.85	74.2	1060	5.457	20.6	432
17	wpc - 1st	8.57	67.8	1040	5.753	20	417
18	wpc - 1st	8.26	63.9	1060	6.08	19	414
19	wpc - 1st	8.16	64.6	1070	6.157	18.9	424
20	wpc - 1st	7.35	51.8	1040	6.9	16.9	380
21	Average of wpc - 1st	8.60	74.95	929.21	5.13	19.22	345.23
22	wpc - 2nd	5.19	26.7	71.3	0.758	11.4	33.1
23	wpc - 2nd	5.53	33.3	96.7	0.84	12.4	43.3
24	wpc - 2nd	5.67	38	97.6	0.748	12.7	45.7
25	wpc - 2nd	5.67	43.1	106	0.719	12.7	50.2
26	wpc - 2nd	5.58	46.1	103	0.65	12.5	50.6
27	wpc - 2nd	5.45	48.9	105	0.624	12.1	52.6
28	wpc - 2nd	6.28	58.3	129	0.635	13.2	63.9
29	wpc - 2nd	5.43	56.7	116	0.586	12	59.7
30	wpc - 2nd	5.58	61.1	118	0.54	11.9	62.6
31	wpc - 2nd	5.36	61	113	0.506	11.4	61.5
32	wpc - 2nd	5.6	66.1	123	0.501	11.5	67.2
33	wpc - 2nd	3.97	62.5	109	0.465	9.52	61.6
34	wpc - 2nd	3.63	69.8	125	0.477	9.13	70
35	wpc - 2nd	5.3	73	124	0.417	10.7	73.1

36	wpc - 2nd	2.71	72.3	118	0.408	7.64	70.2
37	wpc - 2nd	2.6	74	118	0.387	7.63	71.7
38	wpc - 2nd	1.94	73.6	117	0.402	6.27	70.4
39	wpc - 2nd	1.97	74.8	118	0.399	6.22	71.2
40	wpc - 2nd	1.62	82	134	0.419	5.55	78.5
41	wpc - 2nd	0.922	46.9	145	0.943	3.21	60.2
42	Average of wpc - 2nd	4.30	58.41	114.33	0.57	9.98	60.87
43	Average total	6.45	66.68	521.77	2.85	14.60	203.05

Table A.3 BG-HHM (wood-based) PAC particle size distribution

Record Number	Sample Name	Dx (10)	Dx (50)	Dx (90)	Uniformity	D [3,2]	D [4,3]
1	BG - 1st	6.8	25.7	70.6	0.761	14.5	33.2
2	BG - 1st	6.73	25.3	69.7	0.788	14.3	33.4
3	BG - 1st	6.69	25.2	72.7	1.052	14.3	39.9
4	BG - 1st	6.64	24.9	71.9	1.067	14.2	39.8
5	BG - 1st	6.55	24.5	70.4	1.113	14	40.3
6	BG - 1st	6.49	24.3	69.8	1.102	13.9	39.6
7	BG - 1st	6.39	23.9	68	1.087	13.6	38.6
8	BG - 1st	6.38	23.8	68.3	1.081	13.6	38.3
9	BG - 1st	6.19	22.7	59.7	0.739	13.1	29
10	BG - 1st	6.14	22.5	59.6	0.742	13	28.7
11	BG - 1st	6.08	22.1	57	0.714	12.8	27.6
12	BG - 1st	6.03	21.9	56.3	0.711	12.7	27.3
13	BG - 1st	5.98	21.7	55.3	0.703	12.6	26.9
14	BG - 1st	6.03	22.1	56.8	0.722	12.8	27.8
15	BG - 1st	5.83	21.1	51.7	0.675	12.3	25.5
16	BG - 1st	5.8	21	52.7	0.699	12.2	25.9
17	BG - 1st	5.72	20.6	49.6	0.662	12	24.6
18	BG - 1st	5.68	20.4	49	0.656	11.9	24.3
19	BG - 1st	5.53	19.8	45	0.616	11.6	22.8
20	BG - 1st	5.54	19.6	44.9	0.622	11.6	22.7
21	Average of 'BG - 1st'	6.11	22.5	58.7	0.834	13	30.8
22	BG - 2nd	4.21	13.3	27	0.531	8.53	14.6
23	BG - 2nd	4.12	12.5	23.6	0.481	8.25	13.3
24	BG - 2nd	4.13	12.2	22.9	0.474	8.19	12.9
25	BG - 2nd	4.18	12	23	0.482	8.21	12.9
26	BG - 2nd	4.16	11.5	21	0.45	8.06	12.1
27	BG - 2nd	4.18	11.1	19.8	0.43	7.98	11.6
28	BG - 2nd	4.36	11.4	21	0.449	8.55	12.1
29	BG - 2nd	4.37	11.2	20.4	0.438	8.52	11.9
30	BG - 2nd	4.37	11	19.8	0.428	8.44	11.6
31	BG - 2nd	4.39	10.8	19.2	0.418	8.38	11.4

32	BG - 2nd	4.45	10.6	18.6	0.407	8.37	11.2
33	BG - 2nd	4.5	10.5	18.1	0.395	8.36	11
34	BG - 2nd	4.55	10.2	17.4	0.384	8.26	10.6
35	BG - 2nd	4.6	10.6	18.8	0.411	8.54	11.2
36	BG - 2nd	4.64	10.4	18.2	0.398	8.49	11
37	BG - 2nd	4.69	10.3	17.9	0.392	8.5	10.9
38	BG - 2nd	4.71	10.2	17.3	0.379	8.43	10.6
39	BG - 2nd	4.78	10.1	16.9	0.37	8.45	10.5
40	BG - 2nd	4.87	10.8	20.1	0.434	8.93	11.7
41	BG - 2nd	4.91	10.7	19.5	0.42	8.89	11.5
42	Average of 'BG - 2nd'	4.49	11	20.1	0.44	8.41	11.7
43	Total Average	5.3	16.75	39.4	0.637	10.705	21.25

Table A.4 COL-PL60-800 (coal-based) PAC particle size distribution

Record Number	Sample Name	Dx (10)	Dx (50)	Dx (90)	Uniformity	D [3,2]	D [4,3]
1	COL-1st	5.63	24.3	71.3	0.843	13.1	32.1
2	COL-1st	5.42	24.6	73.9	0.863	12.9	32.9
3	COL-1st	5.38	25	74.3	0.857	12.8	33.2
4	COL-1st	5.39	25.4	75.8	0.862	12.9	33.8
5	COL-1st	5.42	25.7	77.2	0.864	13	34.3
6	COL-1st	5.44	25.9	78.1	0.867	13.1	34.6
7	COL-1st	5.48	26.4	80.6	0.879	13.2	35.6
8	COL-1st	5.49	26.5	79.8	0.867	13.2	35.3
9	COL-1st	5.58	27	83.9	0.893	13.4	36.8
10	COL-1st	5.63	27.1	86.1	0.912	13.5	37.4
11	COL-1st	5.7	27.8	87.2	0.904	13.7	38
12	COL-1st	5.74	28	86.7	0.893	13.8	38
13	COL-1st	5.78	28.3	89	0.907	13.9	38.9
14	COL-1st	5.82	28.6	93	0.932	14	40
15	COL-1st	5.86	28.8	92	0.916	14.1	39.8
16	COL-1st	5.93	29.4	93.1	0.911	14.3	40.4
17	COL-1st	5.98	29.9	97.1	0.935	14.4	41.8
18	COL-1st	6.05	30.6	100	0.94	14.6	42.9
19	COL-1st	6.11	31.1	102	0.942	14.8	43.5
20	COL-1st	6.11	31.2	102	0.939	14.8	43.6
21	Average of 'COL-1st'	5.68	27.5	86	0.905	13.7	37.6
22	COL-2nd	4.25	18.6	60.7	0.927	10.1	26.3
23	COL-2nd	4.33	19	62.4	0.927	10.3	27
24	COL-2nd	4.02	16.2	52.5	0.943	9.36	23.5
25	COL-2nd	3.78	14.3	35.3	0.751	8.57	18.2
26	COL-2nd	3.72	13.6	31.1	0.71	8.32	17
27	COL-2nd	3.64	12.9	26.9	0.558	8	14.2
28	COL-2nd	3.67	12.4	23.4	0.49	7.91	13.1
29	COL-2nd	3.66	12.1	22.1	0.467	7.82	12.6
30	COL-2nd	3.48	11.4	20.3	0.449	7.46	11.7
31	COL-2nd	3.51	11.2	19.3	0.428	7.45	11.4
32	COL-2nd	3.46	10.8	18.2	0.409	7.3	10.9
33	COL-2nd	3.53	10.7	17.8	0.399	7.34	10.8
34	COL-2nd	3.63	10.7	18	0.401	7.38	10.9
35	COL-2nd	3.65	10.5	17.3	0.384	7.38	10.6
36	COL-2nd	3.74	10.6	17.5	0.387	7.47	10.7
37	COL-2nd	3.83	10.4	16.9	0.373	7.48	10.5
38	COL-2nd	4.01	10.7	17.7	0.384	7.71	10.8
39	COL-2nd	4.13	10.5	17.2	0.369	7.75	10.7
40	COL-2nd	4.25	10.2	16.3	0.354	7.71	10.3

41	COL-2nd	4.4	10	15.8	0.343	7.62	10.1
42	Average of 'COL-2nd'	3.8	11.5	23.8	0.626	7.94	14.1
43	Total Average	4.74	19.5	54.9	0.7655	10.82	25.85

Appendix A.5 SPAC N2 hysteresis plots
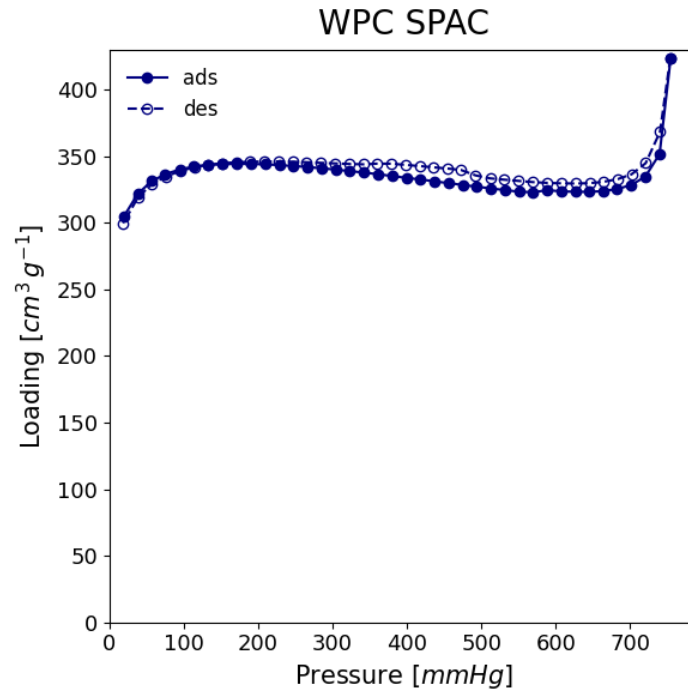
Figure A.3 N$_2$ hysteresis plot for WPC (coconut-based) SPAC
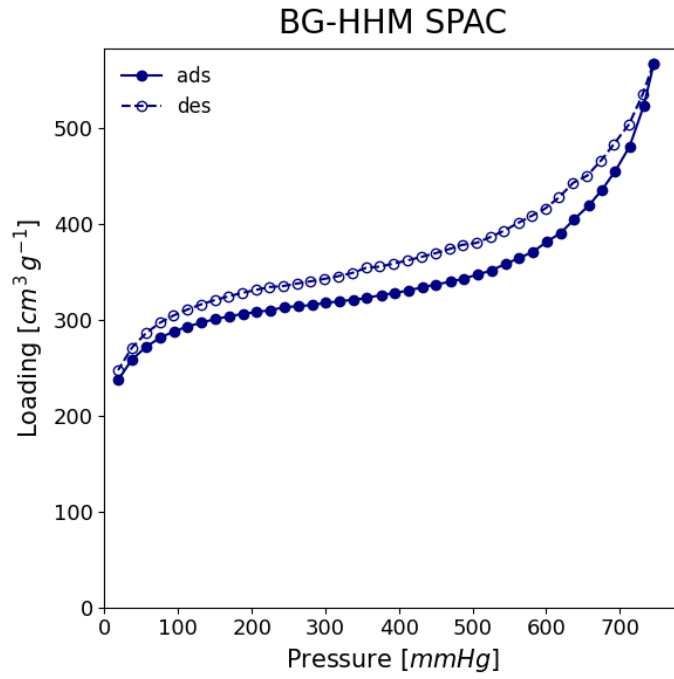
Figure A.2 N$_2$ hysteresis plot for BG-HHM (wood-based) SPAC
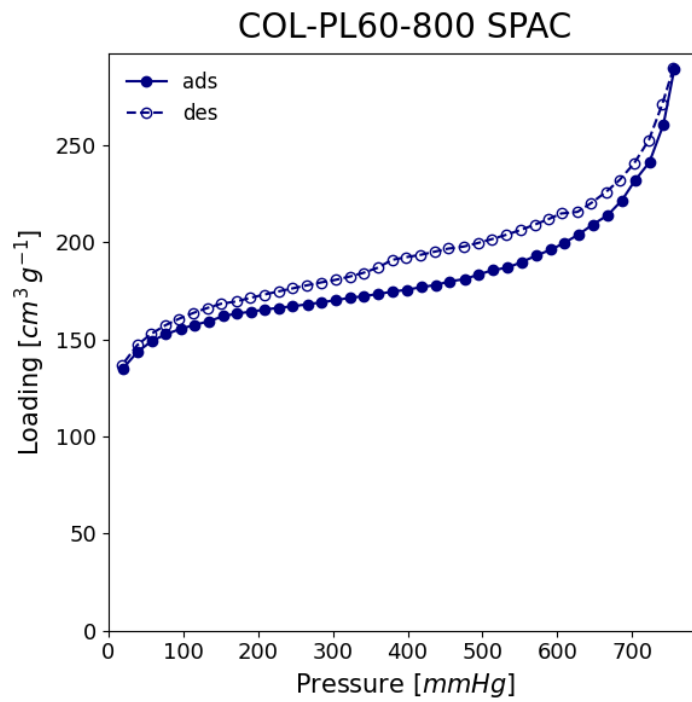
Figure A.3 N$_2$ hysteresis plot for COL-PL60-800 (coal-based) SPAC
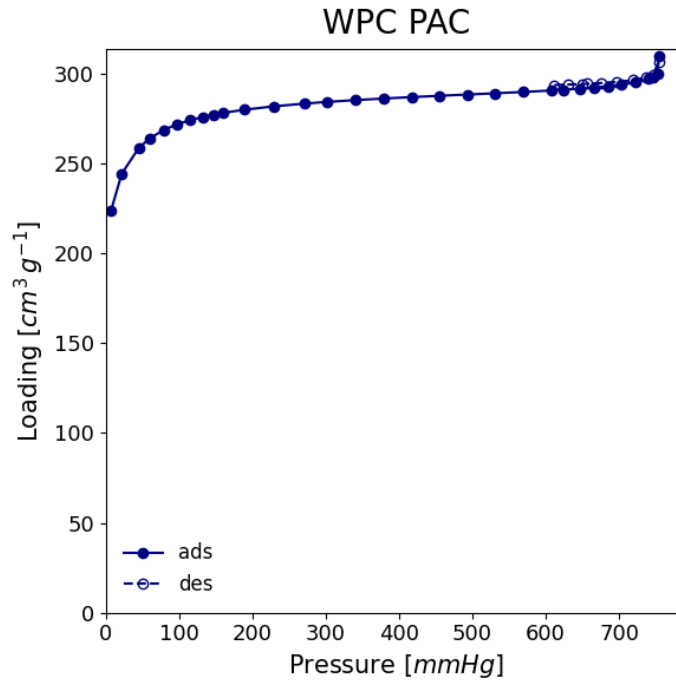
Figure A.4 N_2 hysteresis plot for WPC (coconut-based) PAC
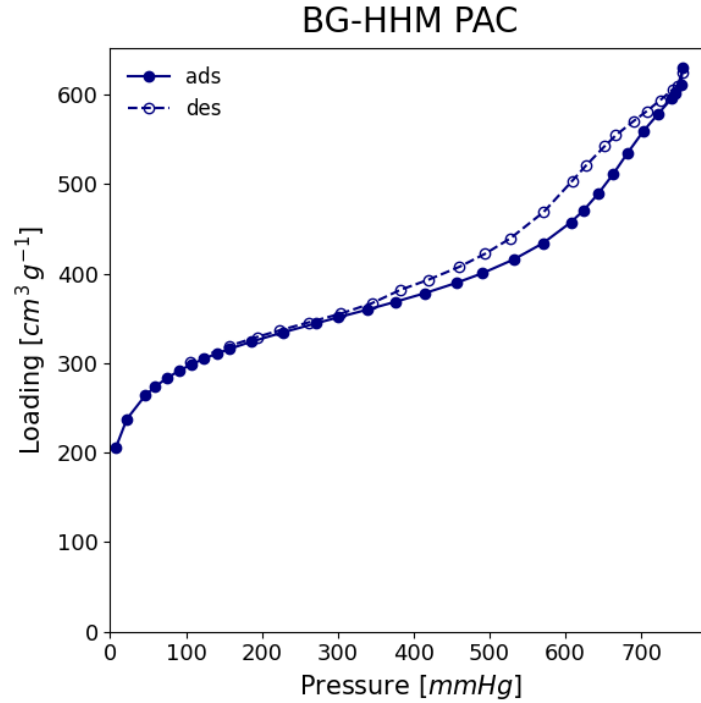
Figure A.5 N_2 hysteresis plot for BG-HHM (wood-based) PAC
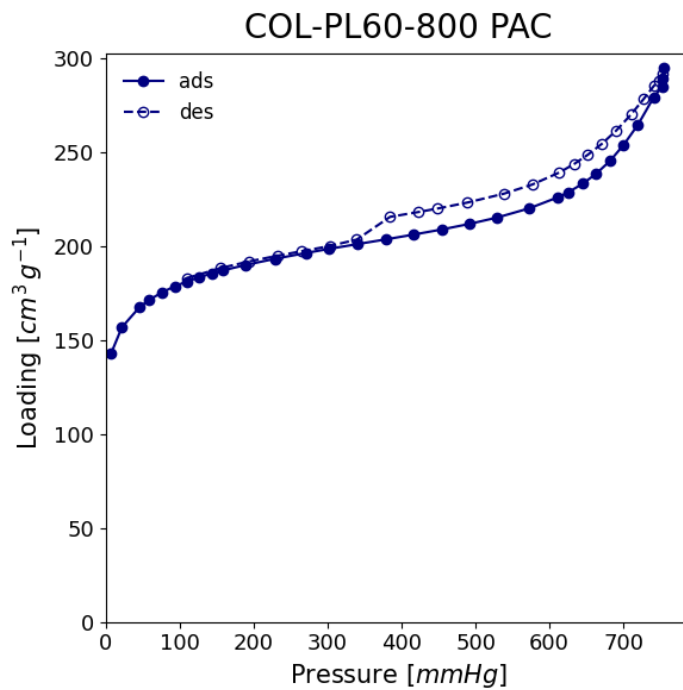
Figure A.6 N_2 hysteresis plot for COL-PL60-800 (coal-based) PAC

Appendix A.6 DFT fittings for PACs and SPACs

DFT kernel used for fitting:

- **Adsorbate:** N_2
- **Temp:** 77°K
- **Adsorbate material:** Carbon
- **Pore model:** Slit
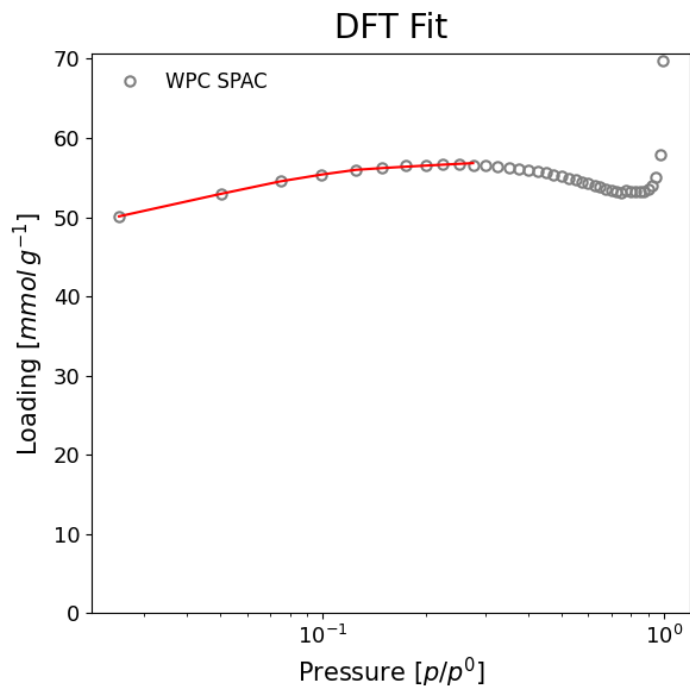
Figure A.7 DFT kernel fitting for WPC (coconut) SPAC, Pressure range: $0 - 0.3$ p/p^0
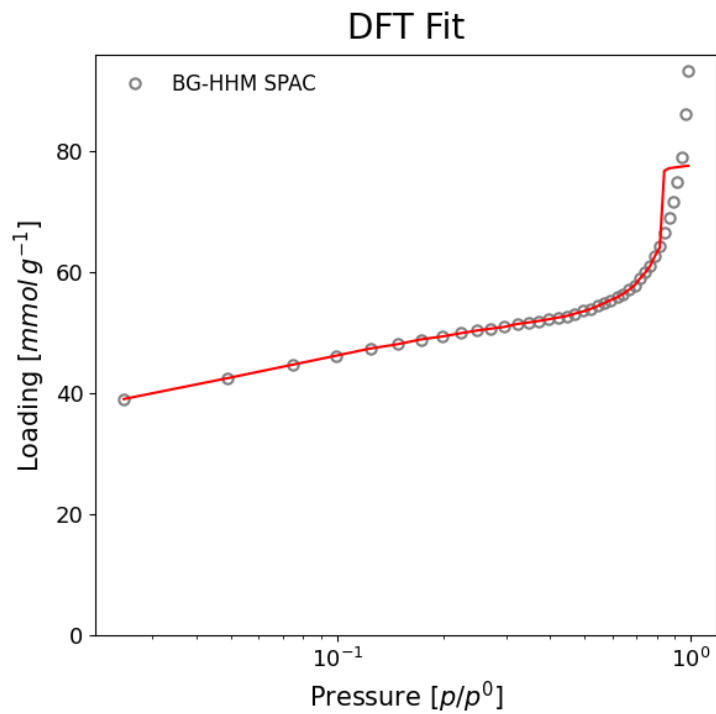
Figure A.8 DFT kernel fitting for BG-HHM (wood) SPAC, Pressure range: $0 - 1$ p/p^0
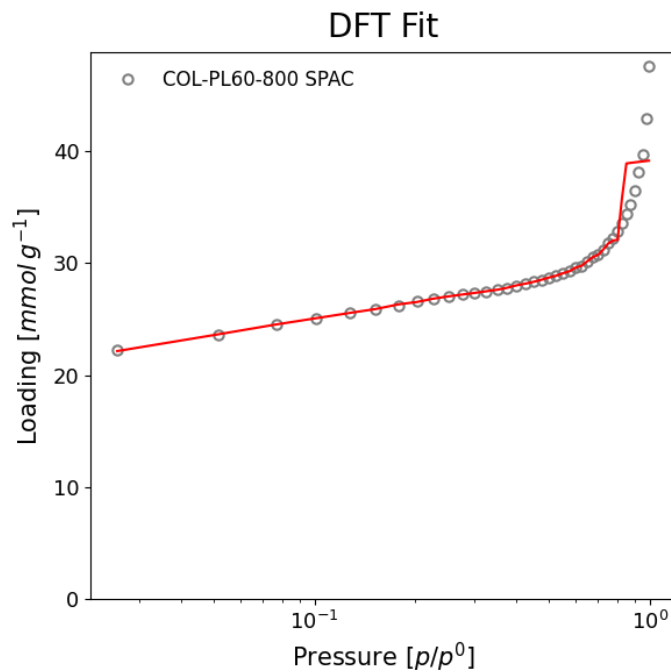
Figure A.9 DFT kernel fitting for COL-PL60-800 (coal) SPAC, Pressure range: $0 - 1$ p/p^0
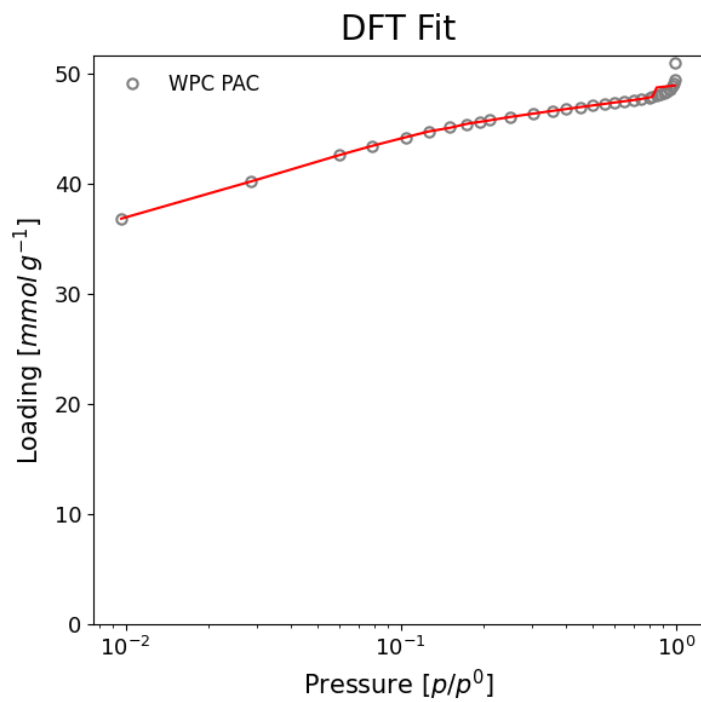
Figure A.10 DFT kernel fitting for WPC (coconut) PAC, Pressure range: $0 - 1$ p/p^0
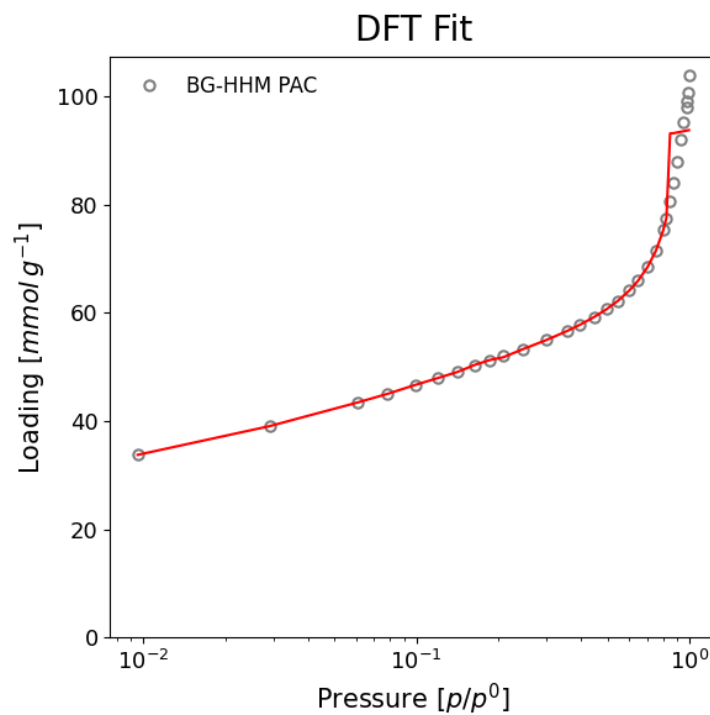
Figure A.11 DFT kernel fitting for BG-HHM (wood) PAC, Pressure range: $0 - 1$ p/p^0
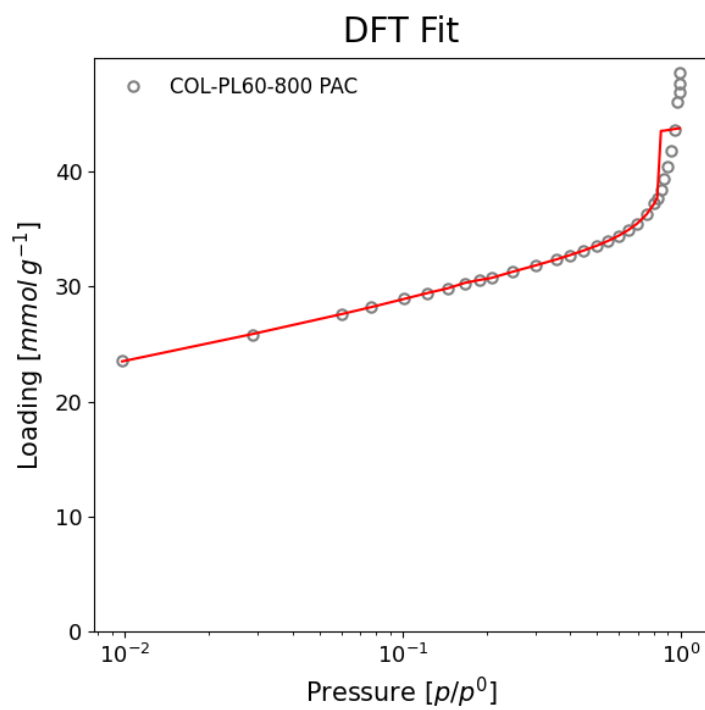
Figure A.12 DFT kernel fitting for COL-PL60-800 (coal) PAC, Pressure range: $0 - 1$ p/p^0

Appendix A.7 DFT pore size distribution
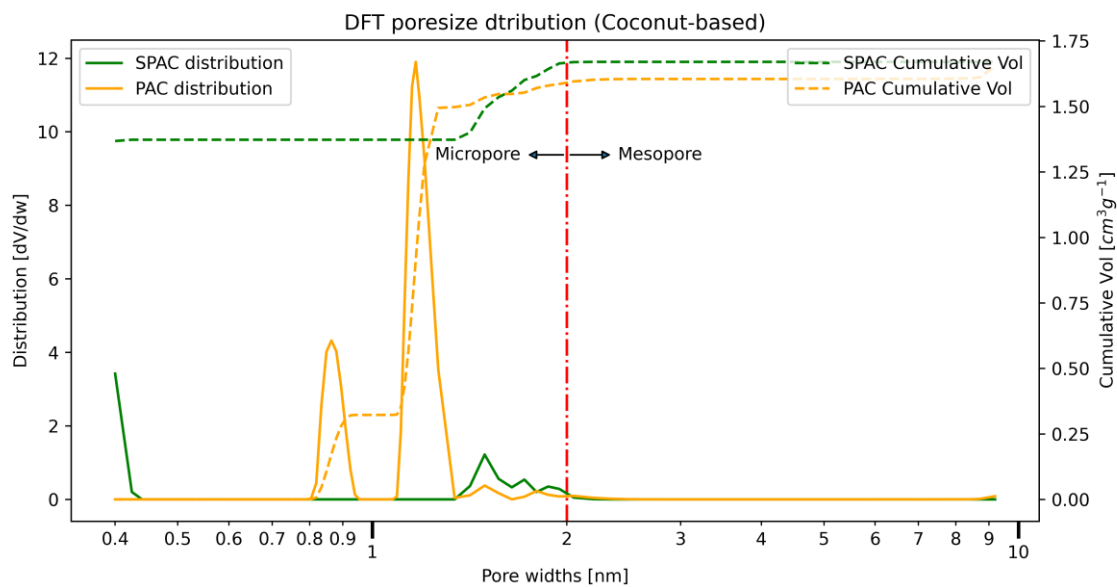
Figure A.13 pore size distribution for WPC (coconut) PAC and SPAC
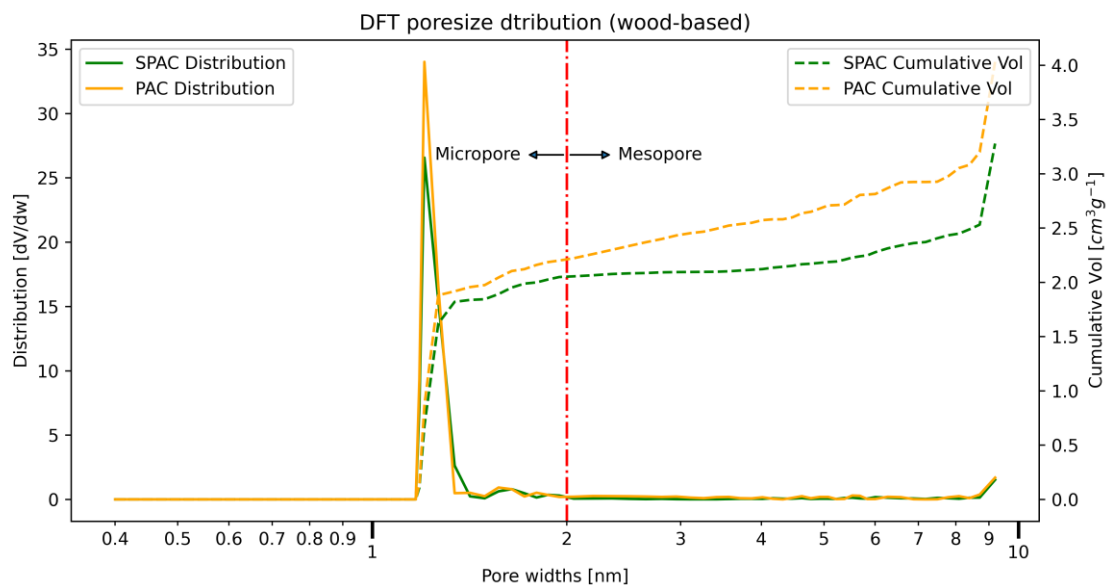
Figure A.14 Pore size distribution for BG-HHM (wood) PAC and SPAC
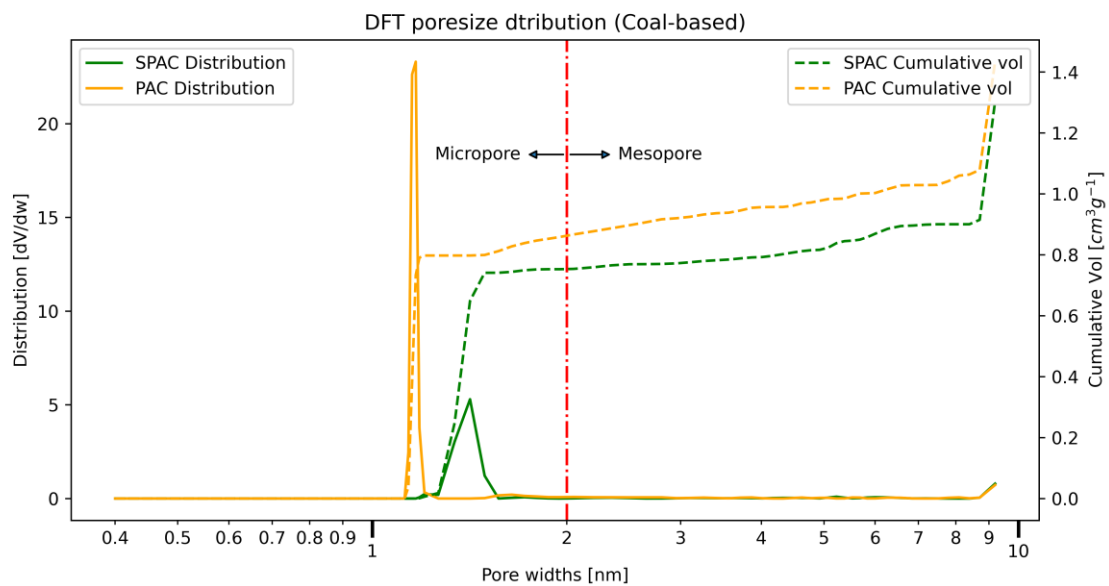
Figure A.15 Pore size distribution for COL-PL60-800 (coal) PAC and SPAC

Appendix A.8 pH$_{pzc}$ data from (Partlan et al., 2016)

Table A.5 pHpzc data from (Partlan et al., 2016)

Carbon	Milling time	pH$_{pzc}$
Watercarb-800 (bituminous coal-based) PAC	as-received PAC	10.37
	1 pass (45 second)	9.31
	15 min	9.09
	30 min	8.92
	1 hour	8.07
	2 hour	8.10
	6 hour	7.75
Aqua Nuchar (wood-based) PAC	as-received PAC	6.20
	1 pass (45 second)	6.25
	5 min	6.03
	10 min	5.72
	20 min	5.82
	1 hour	5.11
	6 hour	4.95
Aquacarb 1230C (coconut shell-based) PAC	as-received PAC	10.79
	1 pass (45 second)	10.73
	2 pass (90 second)	10.44
	5 min	10.57
	10 min	10.47
	20 min	10.33
	4 h	8.00

Calculation of estimated pH$_{pzc}$ for SPACs based on data above

SPAC	Similar SPAC from Partlan et al. (2016)	Difference of pH$_{pzc}$ after 60 minute of pulverization (from Table A.14)	Estimated pH$_{pzc}$
COL-PL60-800 (coal-based)	Watercarb-800 (bituminous coal-based)	$10.37 - 8.07 = 2.3$	$11.30 - 2.30 = 9$
BG-HHM (wood-based)	Aqua Nuchar (wood-based)	$6.20 - 5.11 = 1.09$	$4.10 - 1.09 = 3.01$
WPC (coconut-based)	Aquacarb 1230C (coconut shell-based)	60 min pH$_{pzc}$ was linearly interpolated for this SPAC $10.79 - 9.90 = 0.89$	$11.12 - 0.89 = 10.23$

Appendix B

Additional information for Chapter 4

Appendix B.1 LC-MS/MS Gradient

The gradient used for the LC-MS/MS method developed for measurement of MC-LR is as follows: The acidified acetonitrile (phase B) starts as 4% of the total eluent at beginning of the each run, at 1.5 minute the concentration starts to increase to 70% over 1.5 minutes and keep increasing to 80% by minute 5 of the run and stay at that concentration till minute 8, when it starts decreasing back to 4% over 1 minute. The column then reconditions for another 2.5 minutes before the run ends.

Table B.1 LC-MS/MS gradient

Time (minute)	Acetonitrile (Phase B) concentration (volume %)	Column status
0-1.5	4%	Wash
1.5–3	4% -> 70%	Elution
3-5	70% -> 80%	Elution
5-8	80%	Elution
8-9	80% -> 4%	Reconditioning
9-12.5	4%	Reconditioning

Appendix B.2 Removal rates of MC-LR via the SPACs at different doses in ultrapure water
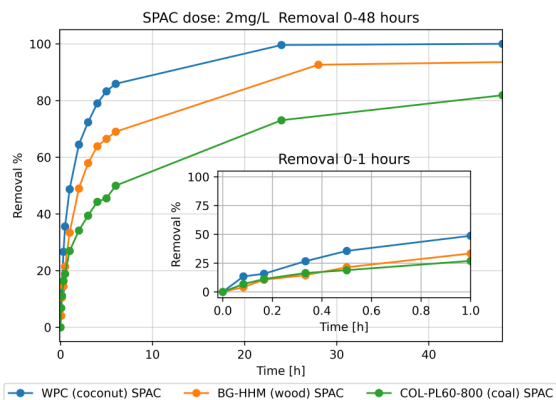
Figure B.1 Removal of MC-LR in ultrapure water via the prepared SPACs at the dose of 2mg/L
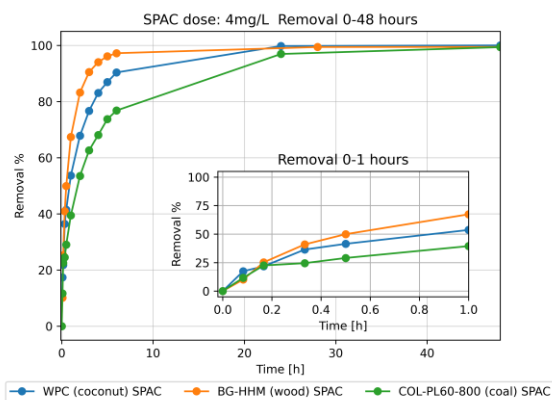
Figure B.2 Removal of MC-LR in ultrapure water via the prepared SPACs at the dose of 4mg/L
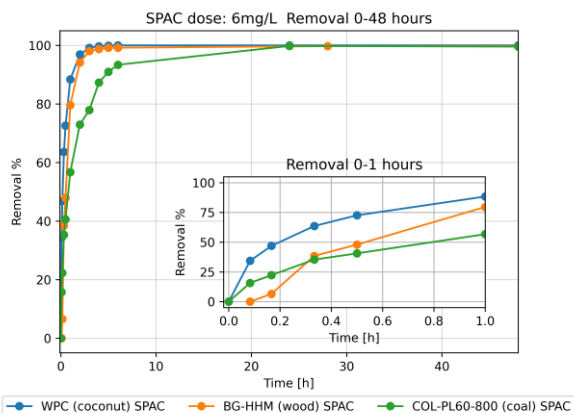
Figure B.3 Removal of MC-LR in ultrapure water via the prepared SPACs at the dose of 6mg/L
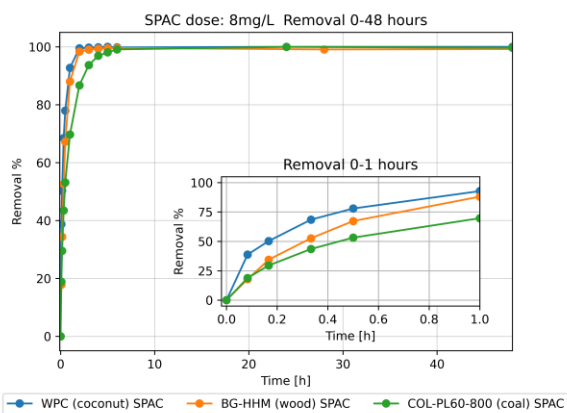
Figure B.4 Removal of MC-LR in ultrapure water via the prepared SPACs at the dose of 8mg/L
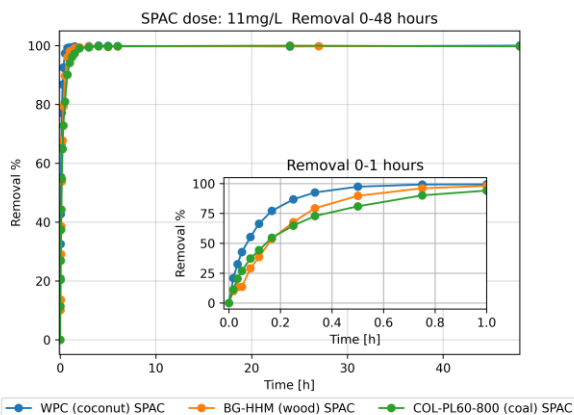
Figure B.5 Removal of MC-LR in ultrapure water via the prepared SPACs at the dose of 11mg/L
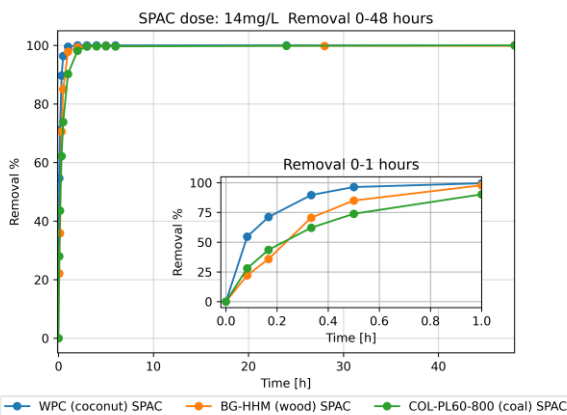
Figure B.6 Removal of MC-LR in ultrapure water via the prepared SPACs at the dose of 14mg/L
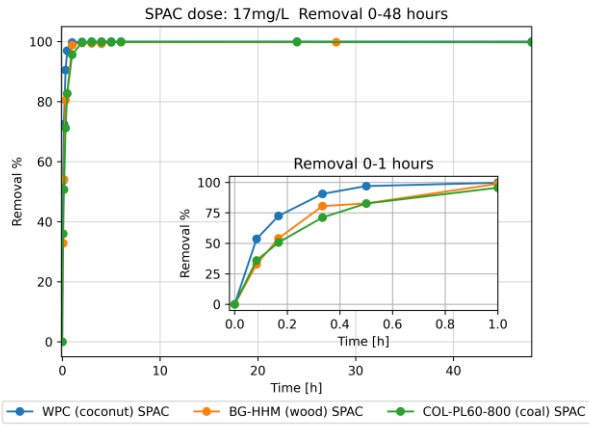
Figure B.7 Removal of MC-LR in ultrapure water via the prepared SPACs at the dose of 17mg/L
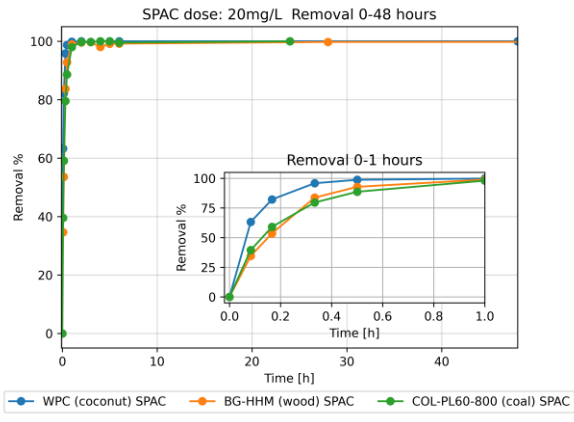
Figure B.8 Removal of MC-LR in ultrapure water via the prepared SPACs at the dose of 20mg/L
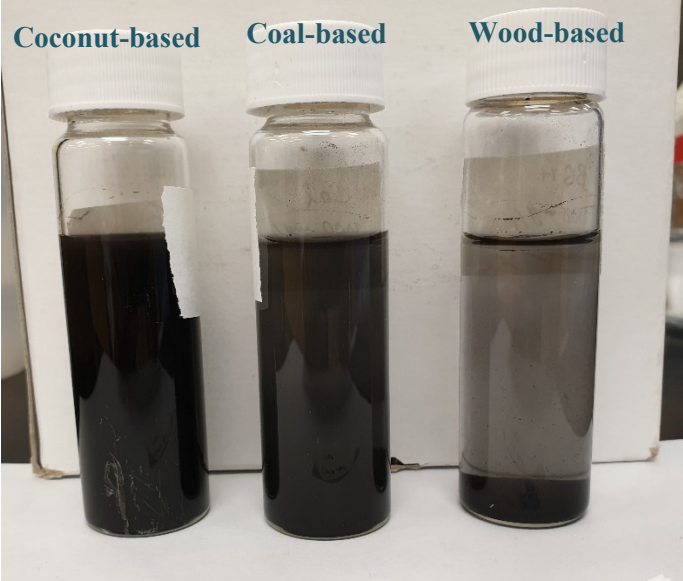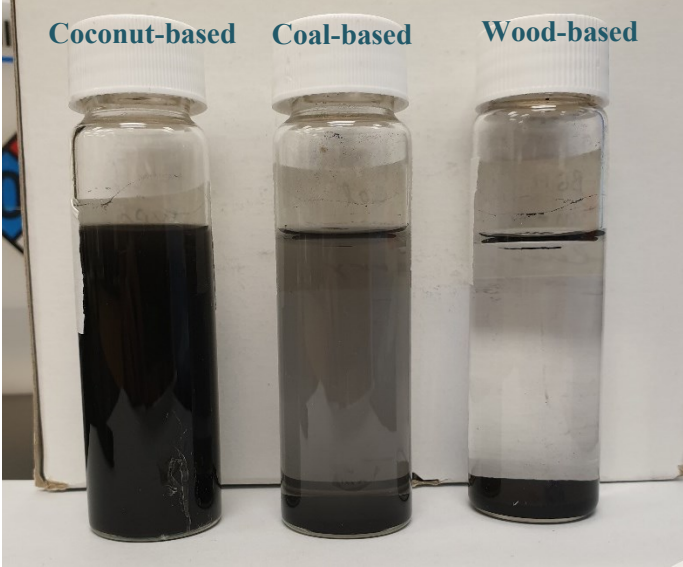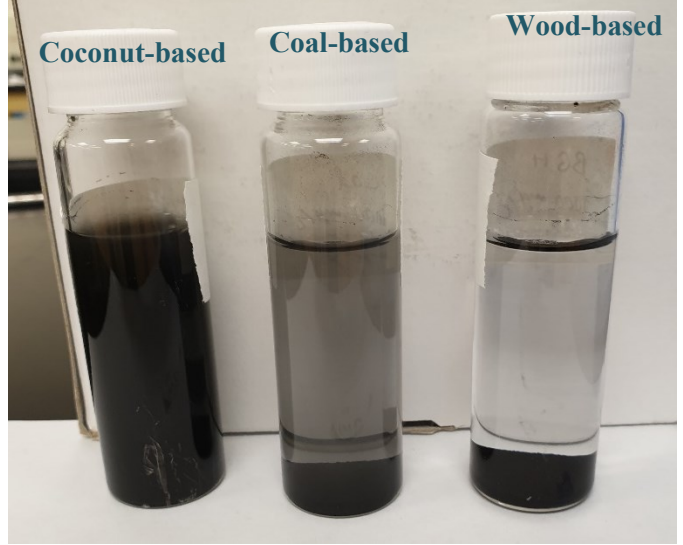
Appendix B.3 Image of bottle with carbon deposit on the rim after continuous shaking on orbital shaker

Figure B.9 Carbon buildup at bottle rim with dry powder dosing

Appendix B.4 Dispersion test of SPAC slurries

Day 1		

Day 2	
Day 4	
Day 6	

Appendix B.5 Pseudo-first-order fitting for SPACs (SPAC dose: 11mg/L)
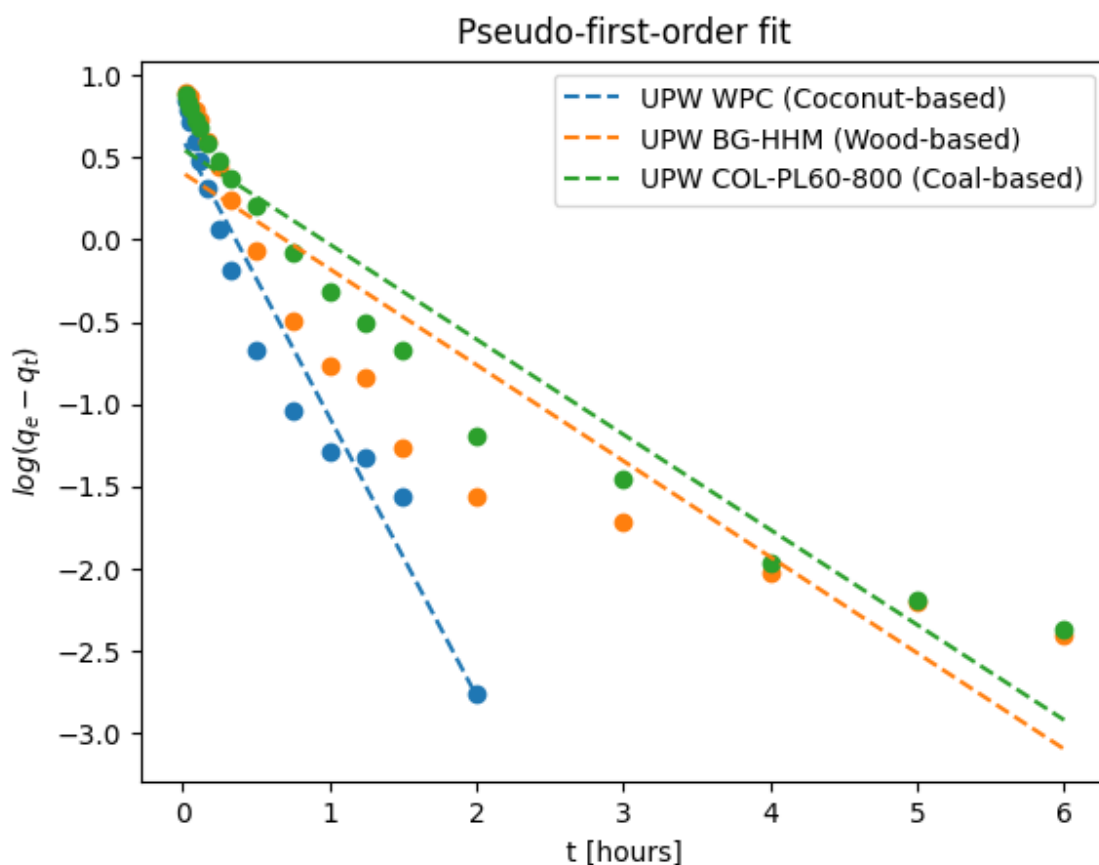
Figure B.10 Pseudo-first-order fitting to the MC-LR adsorption rate by SPACs at dose of 11mg/L

Table B.2 Pseudo-first-order kinetic model parameters for SPACs in ultrapure water

Carbon	q_e experimental ($\mu g/mg$)	q_e predicted ($\mu g/mg$)	K_1 (h^{-1})	R^2
WPC (Coconut-based)	8.97	4.09	3.89	0.948
BG-HHM (Wood-based)	8.61	2.55	1.34	0.831
COL-PL60-800 (Coal-based)	8.61	3.55	1.33	0.926
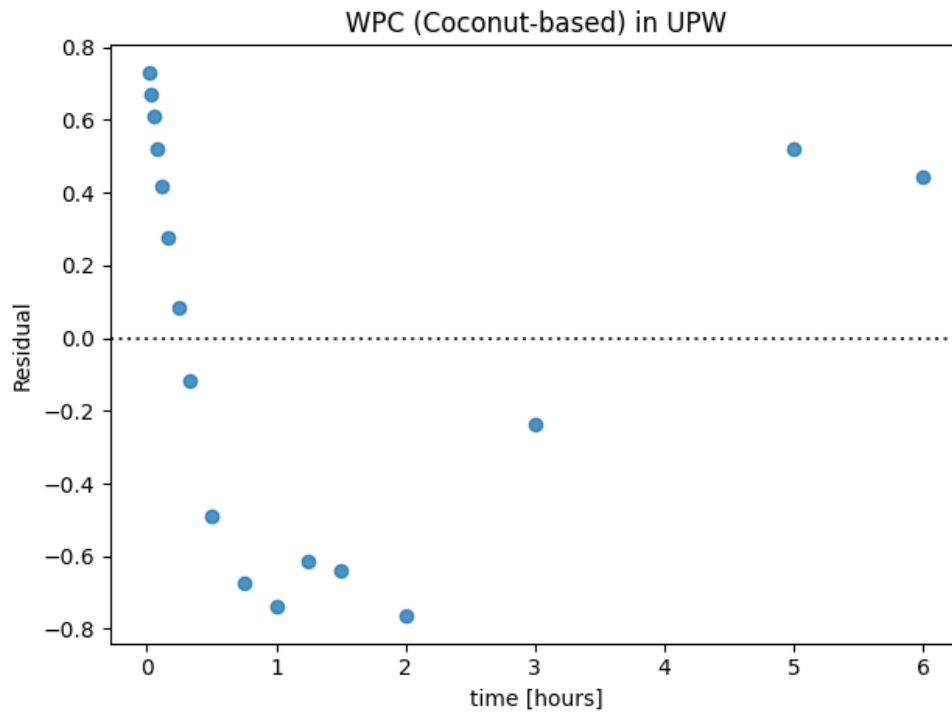
Figure B.11 Residual plot for pseudo-first-order fit of MC-LR adsorption by WPC (coconut) SPAC
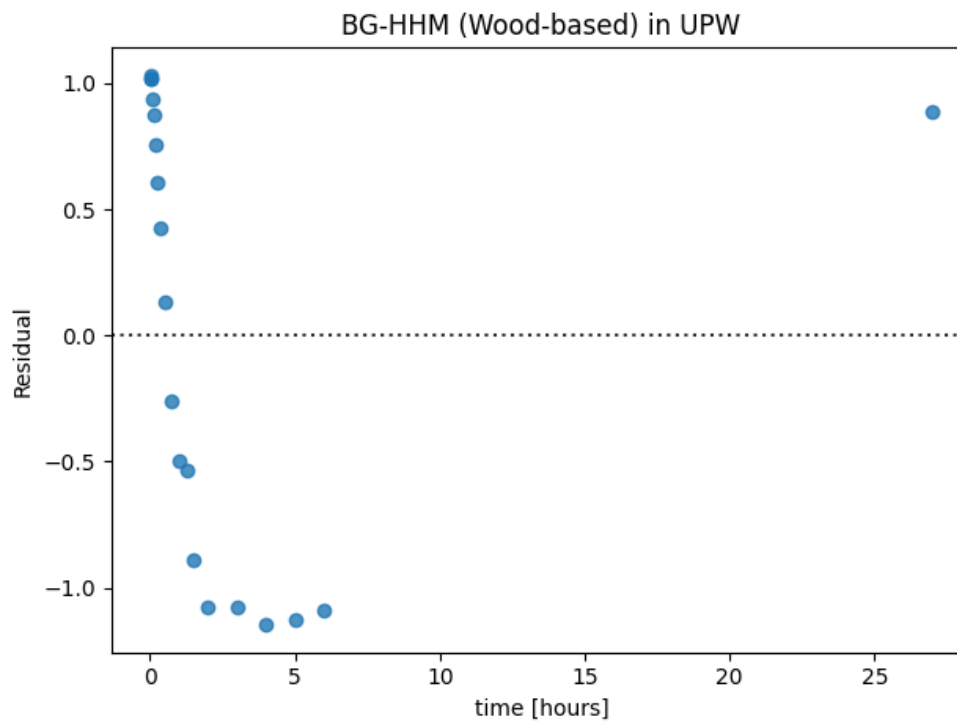
Figure B.12 Residual plot for pseudo-first-order fit of MC-LR adsorption by BG-HHM (wood) SPAC
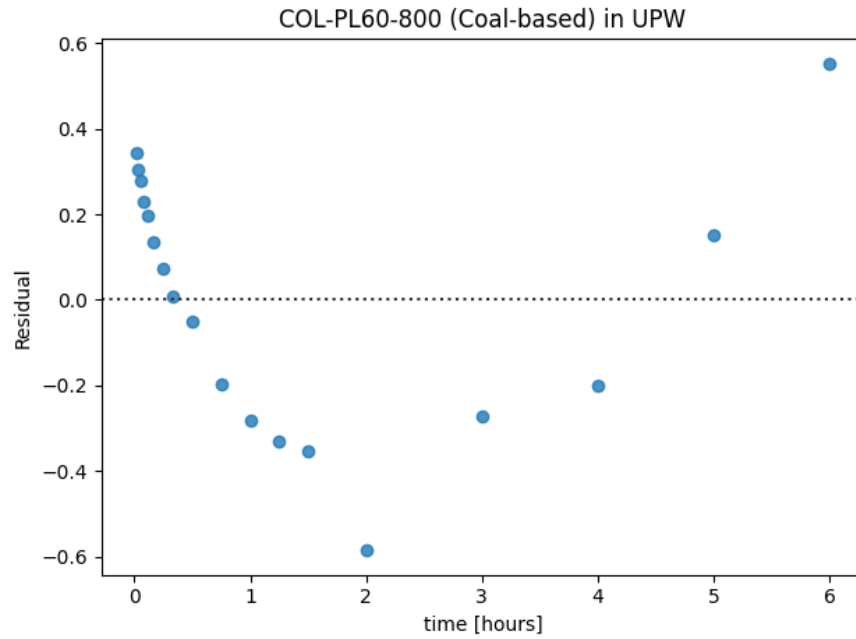
Figure B.12 Residual plot for pseudo-first-order fit of MC-LR adsorption by COL-PL60-800 (coal) SPAC

Appendix B.6 Pseudo-second-order fitting for SPACs (SPAC dose: 11mg/L)
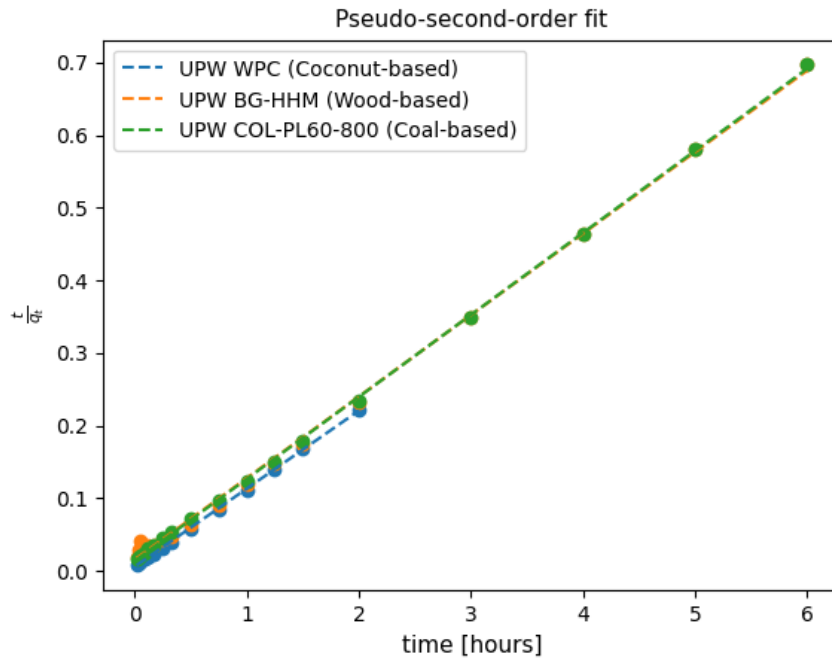
Figure B.14 Pseudo-second-order fitting to the MC-LR adsorption rate by SPACs at dose of 11mg/L

Table B.3 Pseudo-second-order kinetic model parameters for SPACs in ultra-pure water

Carbon	q_e experimental ($\mu g/mg$)	q_e predicted ($\mu g/mg$)	K_2 ($mg/\mu g/h$)	R^2
WPC (Coconut-based)	8.97	9.31	1.87	0.999
BG-HHM (Wood-based)	8.61	8.91	0.79	0.998
COL-PL60-800 (Coal-based)	8.61	8.85	0.91	0.999
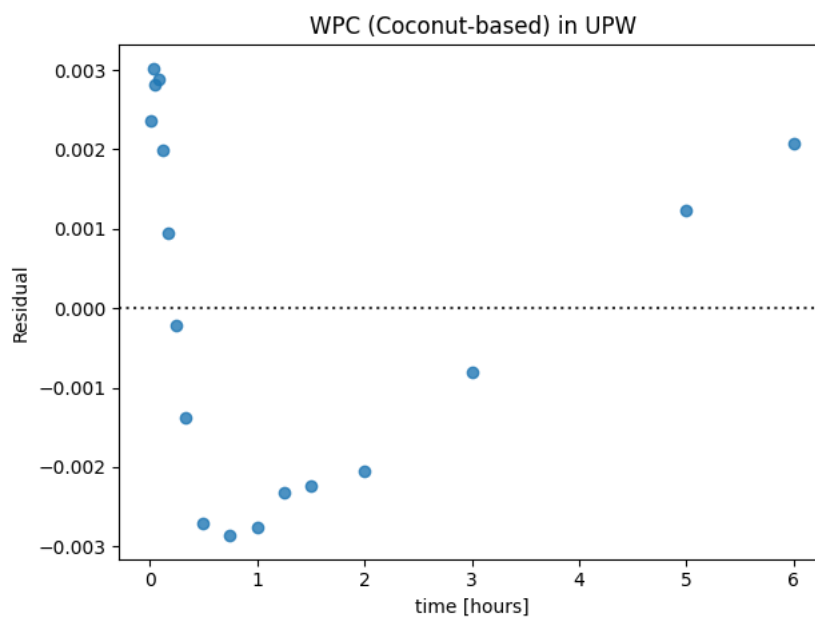
Figure B.14 Residual plot for pseudo-second-order fit of MC-LR adsorption by WPC (coconut) SPAC
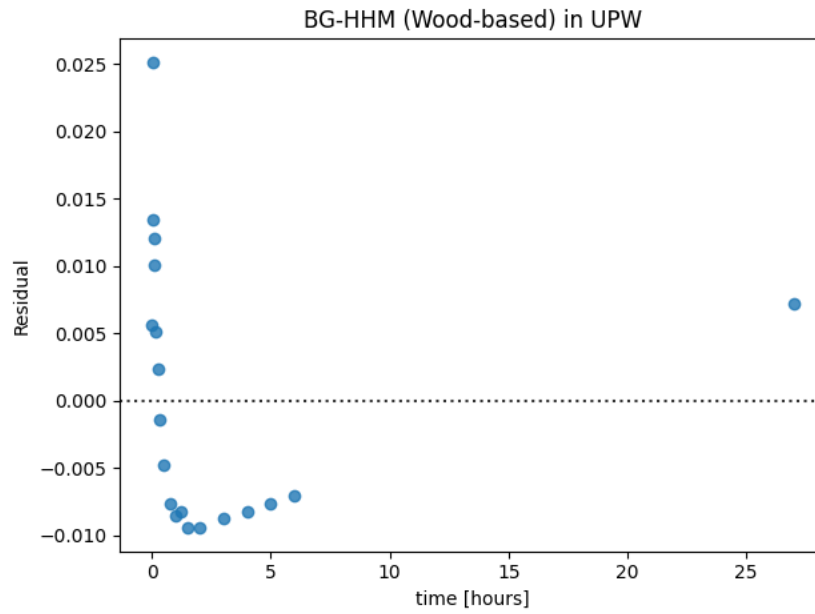
Figure B.15 Residual plot for pseudo-second-order fit of MC-LR adsorption by BG-HHM (wood) SPAC
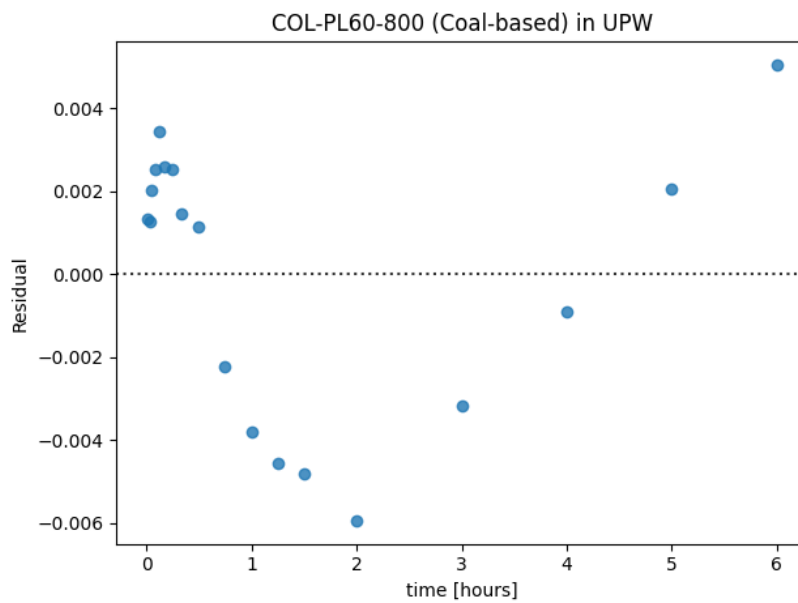
Figure B.16 Residual plot for pseudo-second-order fit of MC-LR adsorption by COL-PL60-800 (coal) SPAC

Comparison with parent PACs from Liu (2017)
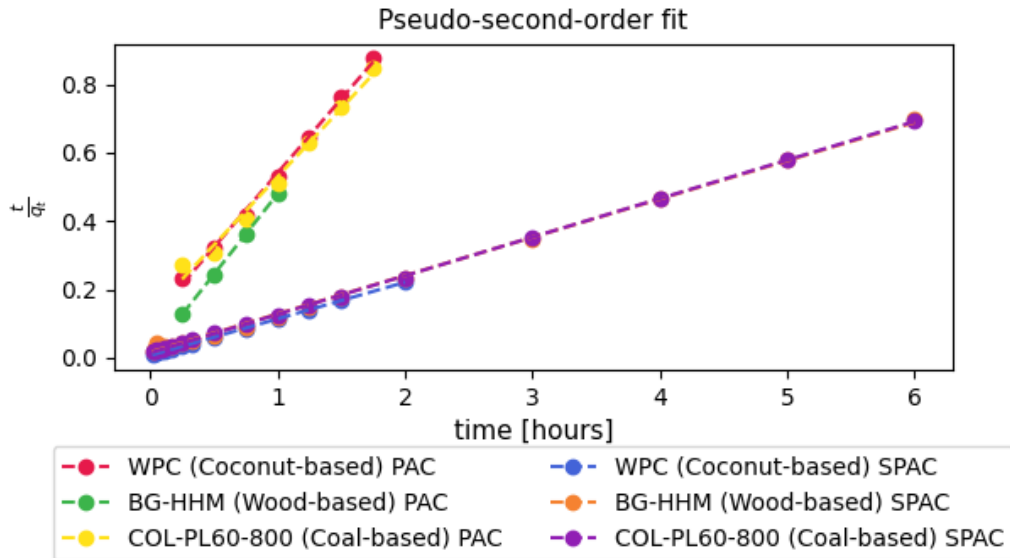
Figure B.17 Pseudo-second-order fitting to the MC-LR adsorption rate by SPACs at dose of 11mg/L compared with PAC results from Liu (2017) at dose of 50mg/L

Table B.4 Pseudo-second-order kinetic model parameters for SPACs and PACs (Liu, 2017) in ultra-pure water

Carbon	carbon type - dose	qe experimental ($\mu g/mg$)	qe predicted ($\mu g/mg$)	k_2 ($mg/\mu g/min$)	R^2
WPC (Coconut-based)	PAC dose: 50 mg/L	2.02	2.30	1.77	0.997
BG-HHM (Wood-based)	PAC dose: 50 mg/L	2.08	2.12	27.36	0.999
COL-PL60-800 (Coal-based)	PAC dose: 50 mg/L	2.07	2.49	1.24	0.987
WPC (Coconut-based)	SPAC dose: 11 mg/L	8.97	9.31	1.87	0.999
BG-HHM (Wood-based)	SPAC dose: 11 mg/L	8.61	8.91	0.79	0.998
COL-PL60-800 (Coal-based)	SPAC dose: 11 mg/L	8.61	8.85	0.91	0.999

Appendix B.7 Ultrapure water at equilibrium (vial point method) isotherms

Table B.5 Equilibrium (48hr) carbon loading data for MC-LR adsorption by BG-HHM (wood) in ultrapure water

Sample	SPAC dose (mg/L)	Equilibrium MC-LR concentration (µg /L)	Equilibrium capacity, q$_e$ (µg /mg)
1	1	122.7	27.2
2	2	24.4	32.0
3	3	1.19	38.9
4	4	0.48	49.6
5	5.5	0.26	68.1
6	7	0.26	90.6
7	8.5	0.49	124.3
8	10	0.46	150.3
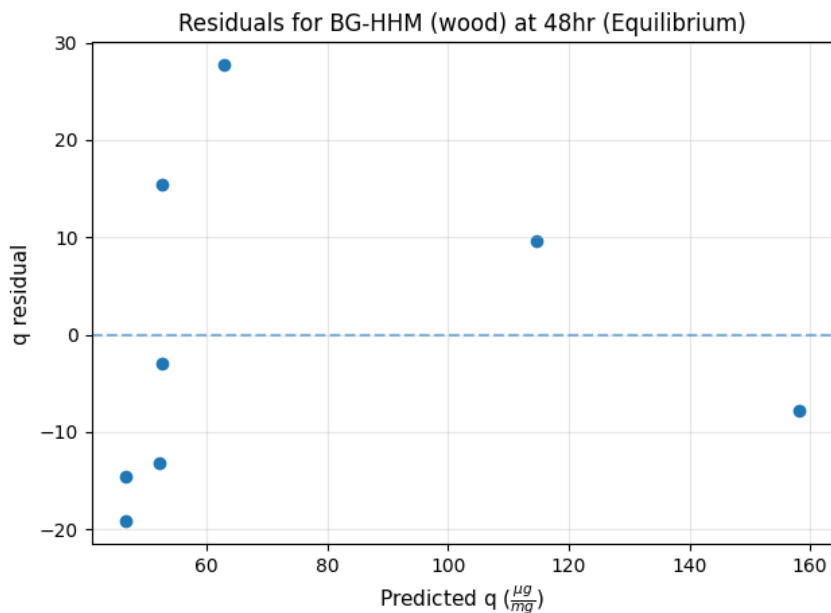
Figure B.17 Residual plot for Equilibrium (48h) isotherm of MC-LR adsorption by the BG-HHM (wood)

Table B.6 Equilibrium (96h) carbon loading data for MC-LR adsorption by BG-HHM (wood) in ultrapure water

Sample	SPAC dose (mg/L)	Equilibrium MC-LR concentration (µg /L)	Equilibrium capacity, qe (µg /mg)
1	1	126.6	27.3

2	2	19.7	39.0
3	3	0.8	68.2
4	4	0.4	90.7
5	7	0.2	126.6
6	10	0.3	146.4
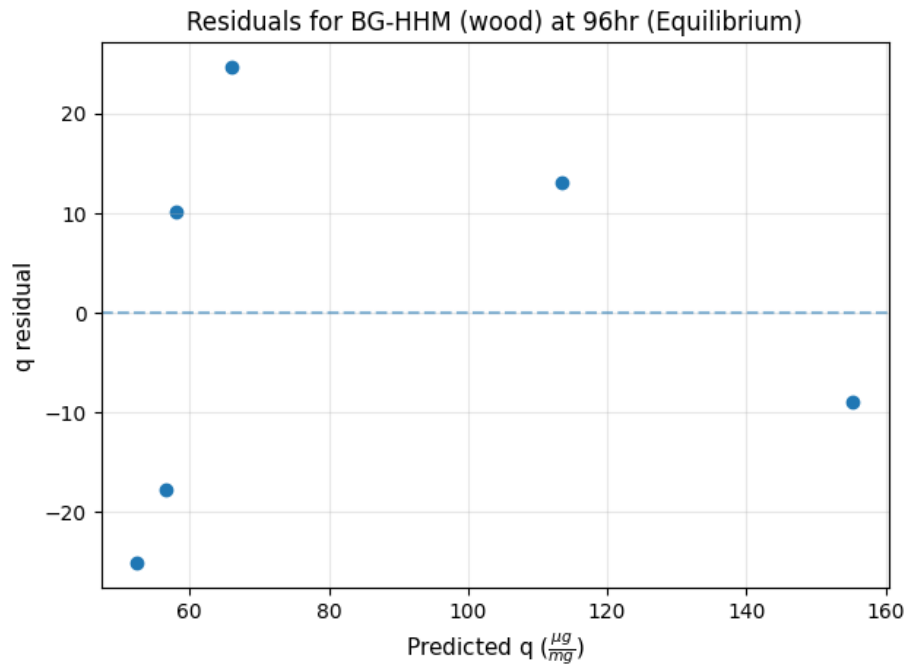
Figure B.18 Residual plot for Equilibrium (96h) isotherm of MC-LR adsorption by the BG-HHM (wood)

Table B.7 Equilibrium (48h) carbon loading data for MC-LR adsorption by COL-PL60-800 (coal) in ultrapure water

Sample	SPAC dose (mg/L)	Equilibrium MC-LR concentration (µg /L)	Equilibrium capacity, qe (µg/mg)
1	1	204.34	27.16
2	2	113.01	32.04
3	3	28.03	38.91
4	4	2.27	49.51
5	5.5	0.7	67.68
6	7	0.65	68.66
7	8.5	0.66	79.99

8	10	1.37	81.66
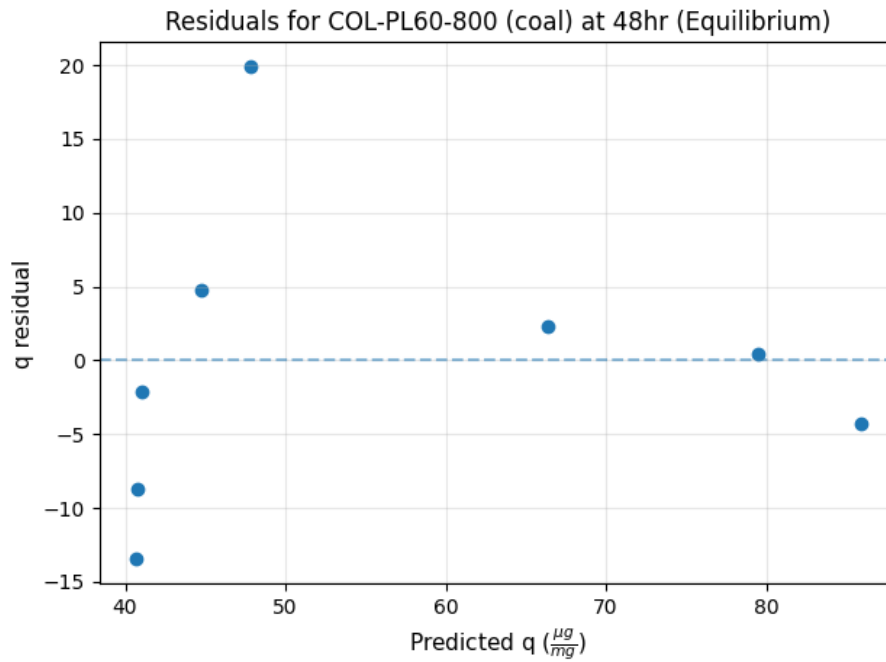
Figure B.19 Residual plot for Equilibrium (48h) isotherm of MC-LR adsorption by the COL-PL60-800 (coal)

Table B.8 Equilibrium (96h) carbon loading data for MC-LR adsorption by COL-PL60-800 (coal) in ultrapure water

Sample	SPAC dose (mg/L)	Equilibrium MC-LR concentration (µg/L)	Equilibrium capacity, qe (µg /mg)
1	1	207.54	27.26
2	2	107.44	32.01
3	3	18.94	38.97
4	4	0.92	49.51
5	5.5	0.7	65.46
6	7	0.23	68.02
7	8.5	0.88	82.78
8	10	0.42	84.69
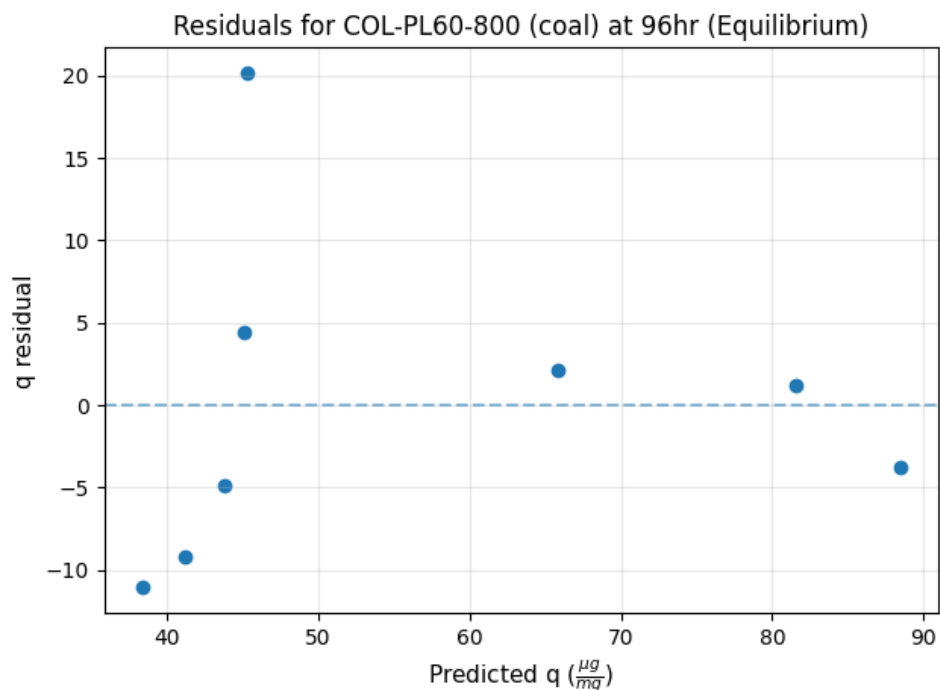
Figure B.20 Residual plot for Equilibrium (96h) isotherm of MC-LR adsorption by the COL-PL60-800 (coal)

Table B.9 Equilibrium (48h) carbon loading data for MC-LR adsorption by WPC (coconut) in ultrapure water

Sample	SPAC dose (mg/L)	Equilibrium MC-LR concentration (µg /L)	Equilibrium capacity, qe (µg /mg)
1	1	232.76	27.23
2	2	164.75	32.05
3	3	104.02	38.96
4	4	27.2	40.24
5	5.5	0.83	49.49
6	7	0.28	54.12
7	8.5	0.59	56.33
8	10	0.74	61.45
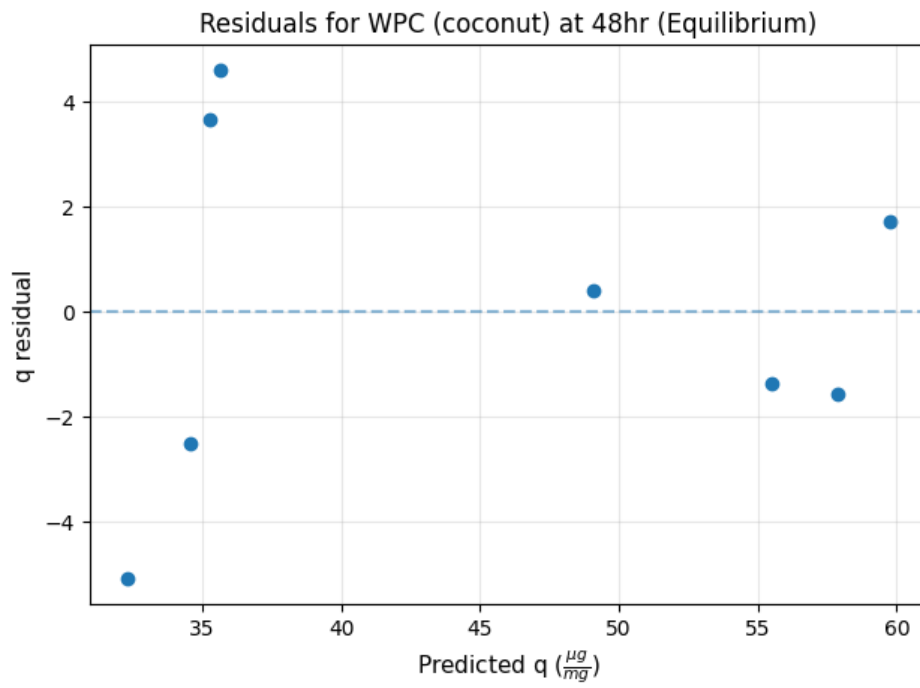
Figure B.21 Residual plot for Equilibrium (48h) isotherm of MC-LR adsorption by the WPC (coconut)

Table B.10 Equilibrium (96h) carbon loading data for MC-LR adsorption by WPC (coconut) in ultrapure water

Sample	SPAC dose (mg/L)	Equilibrium MC-LR concentration (µg/L)	Equilibrium capacity, qe (µg /mg)
1	1	232.02	27.26
2	2	157.73	32.05
3	3	88.44	38.9
4	4	13.04	40.98
5	5.5	0.31	49.58
6	7	0.72	57.63
7	8.5	0.55	61.52
8	10	0.36	64.99
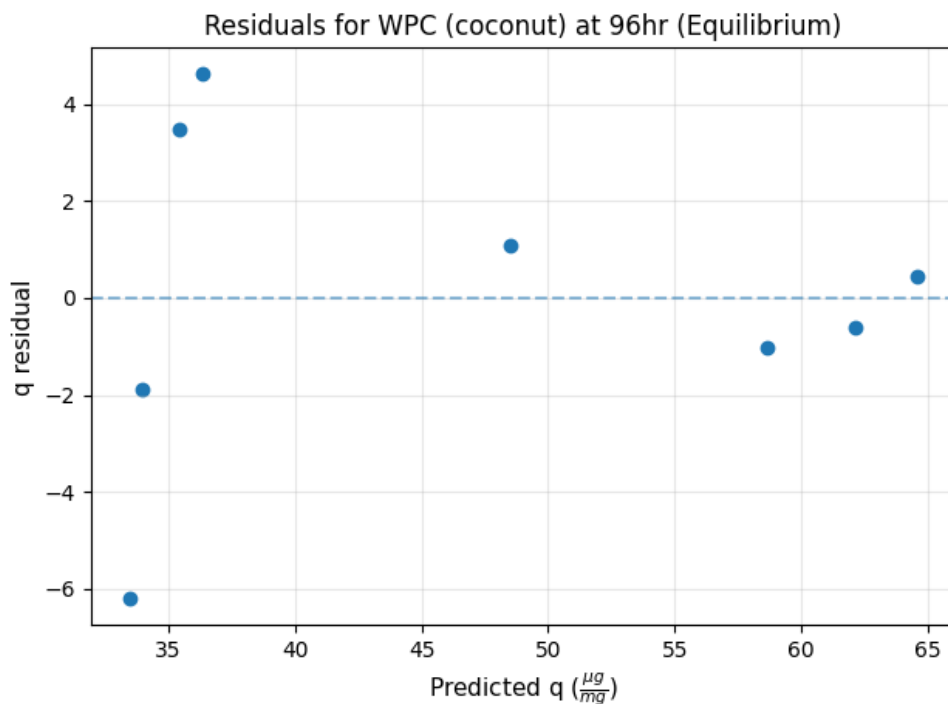
Figure B.22 Residual plot for Equilibrium (96h) isotherm of MC-LR adsorption by the WPC (coconut)

Appendix B.8 Python code for non-linear fitting and calculation of JCRs

#Python code for Freundlich model fitting via non-linear fitting and regression statistics by Sina Golchi

#Note: The indents are necessary for code to run properly

#importing the dependencies (required packages)

import numpy as np

import scipy as sp

from scipy import stats

from scipy.optimize import curve_fit

import matplotlib.pyplot as plt

from matplotlib.lines import Line2D

#Defining a custom function to apply to data for simultaneous fitting and statistics calculations

#x,y: data points, in this case Ce and qe

#alpha: uncertainty degree, for 95% confidence > alpha=0.05

#m: number of points for sum of squared error (SSE) matrix, defines the resolution of JCR contours

#p0: initial guess for model parameters, the default is set to zero

def joint_conf(x,y,alpha,m,p0=[0,0]):

  #defining the mathematical expression of Freundlich model for fitting

  #a is Kf and b is 1/n

  def f(x, a, b):

    return a * (x**b)

  #fiiting the data to the defined function (Freundlich model)

  #popt is an array containing optimal estimates for parameters in form of [a,b]

  #pcov is the covariance matrix for the fit, is used for the calculation of standard deviations and variances

  popt, pcov = curve_fit(f,x,y,p0=p0,maxfev=10000)

  a = popt[0]

```
b = popt[1]


#calculating standard deviations for parameters

s_a = np.sqrt(pcov[0,0])

s_b = np.sqrt(pcov[1,1])


#calculating R2 of the fit,

#Note: R2 is not a necessarily valid indicator for goodness of fit for non-linear fitting

r2 = 1.0 - (sum((y - f(x, a, b)) ** 2) / ((len(y) - 1.0) * np.var(y, ddof=1)))


#Calcualtion of upper and lower limits for parameters confidence intervals

#1.96 times standard deviation for 95% CIs

aL = a - 1.96 * s_a

aU = a + 1.96 * s_a

bL = b - 1.96 * s_b

bU = b + 1.96 * s_b


#calculate 8sigma interval for plotting the JCRs (limits of the SSE matrix)

a8L = a - 8.0 * s_a

a8U = a + 8.0 * s_a

b8L = b - 8.0 * s_b

b8U = b + 8.0 * s_b


m = m #number for creating the mesh grid (matrix) for sum of squared errors


#dimensions of the SSE meshgrid in range of 8sigma from the point estimate

i1 = np.linspace(a8L, a8U , m)

i2 = np.linspace(b8L, b8U , m)

a_grid, b_grid = np.meshgrid(i1, i2)

n = len(y)  # number of data points
```

```
p = 2  # number of parameters


# sum of squared errors

sse = np.empty((m, m))

for i in range(m):

    for j in range(m):

        at = a_grid[i, j]

        bt = b_grid[i, j]

        sse[i, j] = np.sum((y - f(x, at, bt)) ** 2)


# normalize to the optimal solution

best_sse = np.sum((y - f(x, a, b)) ** 2)

fsse = (sse - best_sse) / best_sse


# compute f-statistic for the f-test

alpha = 0.05  # alpha, confidence

# alpha=0.05 is 95% confidence

fstat = sp.stats.f.isf(alpha, p, (n - p)) #survival function of the f distribution for limits of JCR

flim = fstat * p / (n - p) #limit of JCR

obj_lim = flim * best_sse + best_sse #calculated distance limit from the point estimate


# Create a contour plot

fig = plt.figure()

ax = fig.add_subplot(111)

ax.set_ylabel('Slope (a)')

ax.set_xlabel('Intercept (b)')

# solid line to show confidence region

CS = ax.contour(a_grid, b_grid, sse, [obj_lim], colors='orange', linewidths=[2.0])

ax.clabel(CS, inline=1, fontsize=10)

ax.scatter(a, b, s=10, c='red', marker='o', label='Optimal Solution') #scatter for optimal point estimate
```

```python
#Custom legend handles for the contour plots

legend_elements = [Line2D([0], [0], color='Orange', linestyle='-', label='Joint confidence region'),

          Line2D([0], [0], color='w', linestyle='-',marker='o', markerfacecolor='r',label='Optimum point')]

plt.legend(handles=legend_elements, loc='upper left', fontsize=15)


#returning some of the parameters for later use and comparison

#fig: The JCR contour for later demonstration

#a, b: best fit model parameters, a is Kf and b is 1/n

#[a_grid, b_grid, sse,obj_lim]: values requred to generate JCRs (for later plotting and comparison)

#[[aL,aU],[bL,bU]]: lower and upper limit of parameters' confidence intervals

#r2: coefficient of determination (for reference only)

#len(y): number of data points used for fitting

#[x,y]: raw Ce and qe values for reference

return [fig,a,b,[a_grid, b_grid, sse,obj_lim],[[aL,aU],[bL,bU]],r2,len(y),[x,y]]
```

Appendix B.10 Ultrapure water at short contact times (Bottle point method) isotherms

Table B.11 Carbon loading data for MC-LR adsorption by BG-HHM (wood) in ultrapure water at 5 minutes of contact

Sample	SPAC dose (mg/L)	Equilibrium MC-LR concentration (ug/L)	Equilibrium capacity, qe (ug/mg)
1	20.4	62.11	0.52
2	17.2	63.83	1.89
3	14.2	73.99	1.9
4	11	67.4	2.15
5	7.6	78.09	2.99
6	6	97.64	3.03
7	3.9	85.39	3.95
8	2.2	91.13	4.39
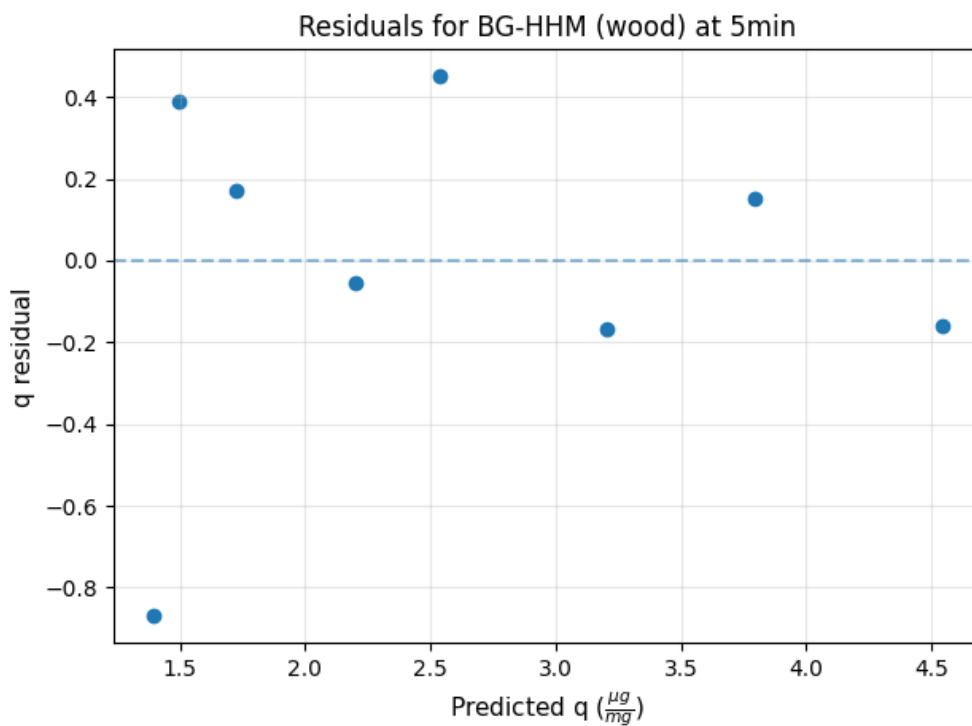
Figure B.23 Residual plot of Freundlich fitting for 5 min contact of MC-LR adsorption by the BG-HHM (wood)

Table B.12 Carbon loading data for MC-LR adsorption by BG-HHM (wood) in ultrapure water at 10 minutes of contact
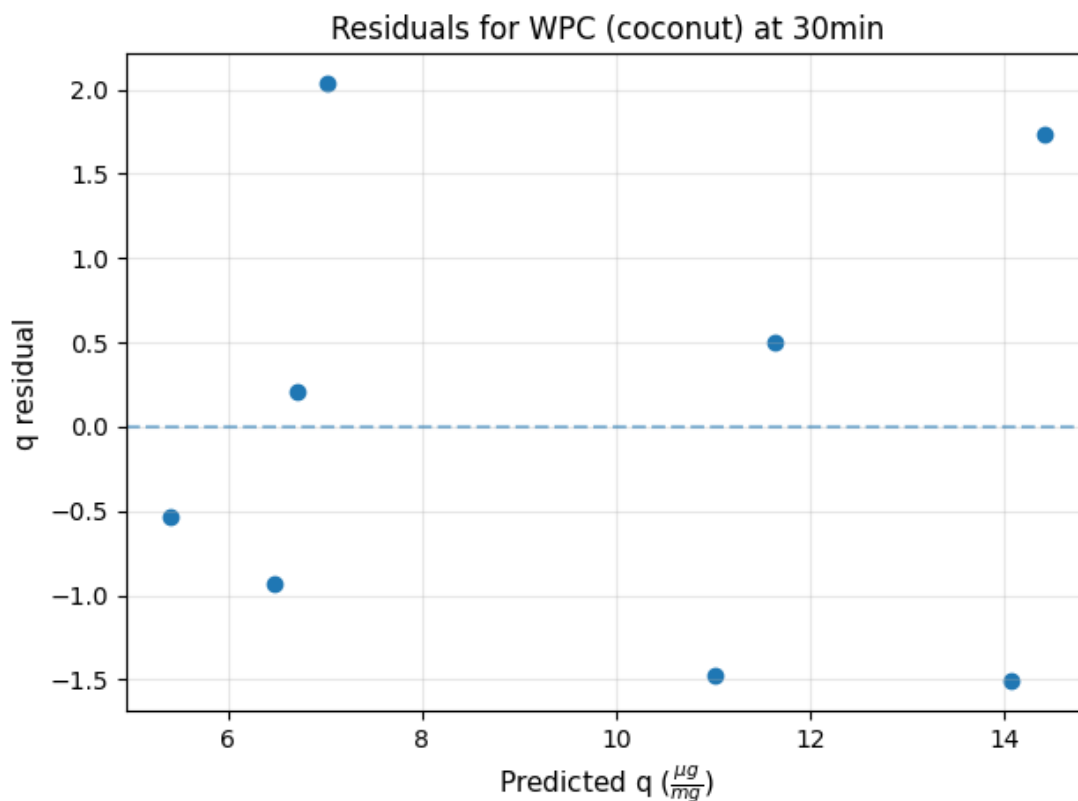
Sample	SPAC dose (mg/L)	Equilibrium MC-LR concentration (ug/L)	Equilibrium capacity, qe (ug/mg)
1	20.4	44.11	1.58
2	17.2	43.65	2.78
3	14.2	60.94	2.81
4	11	43.93	3.32
5	7.6	62.32	5.06
6	6	91.28	5.17
7	3.9	71.04	7.16
8	2.2	85.02	7.63
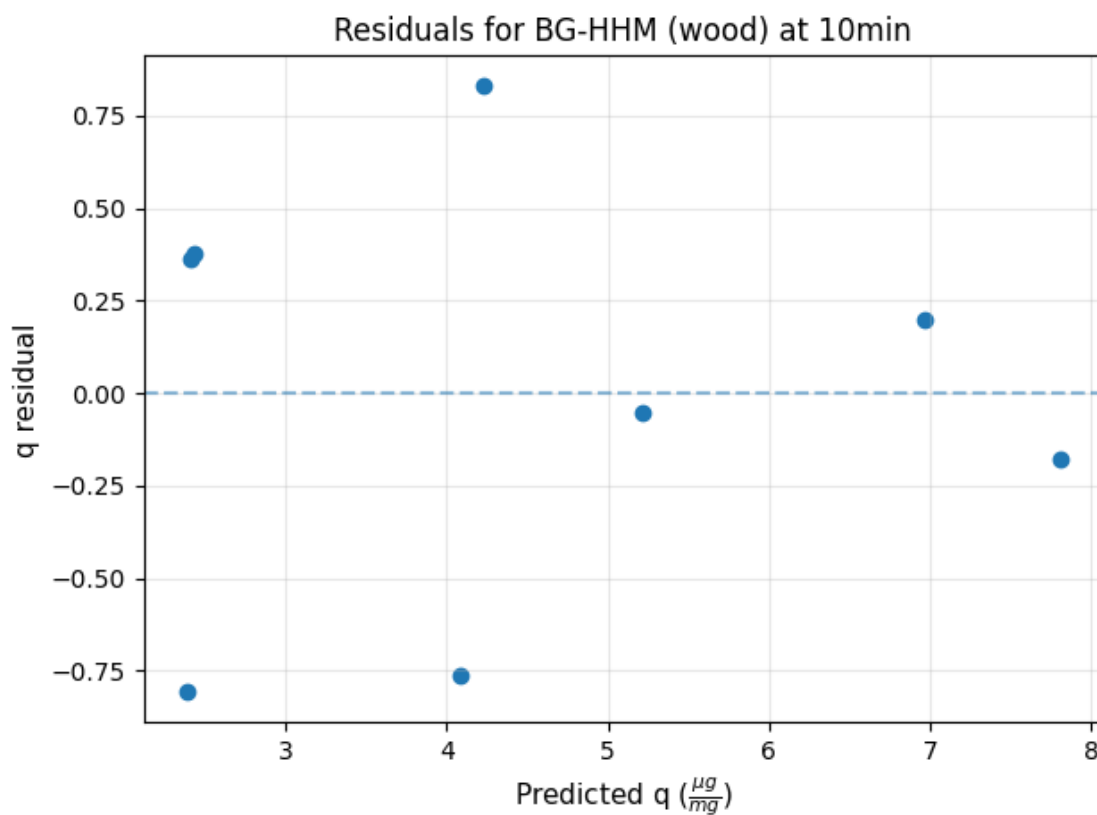
Figure B.24 Residual plot of Freundlich fitting for 10 min contact of MC-LR adsorption by the BG-HHM (wood)

Table B.13 Carbon loading data for MC-LR adsorption by BG-HHM (wood) in ultrapure water at 20 minutes of contact
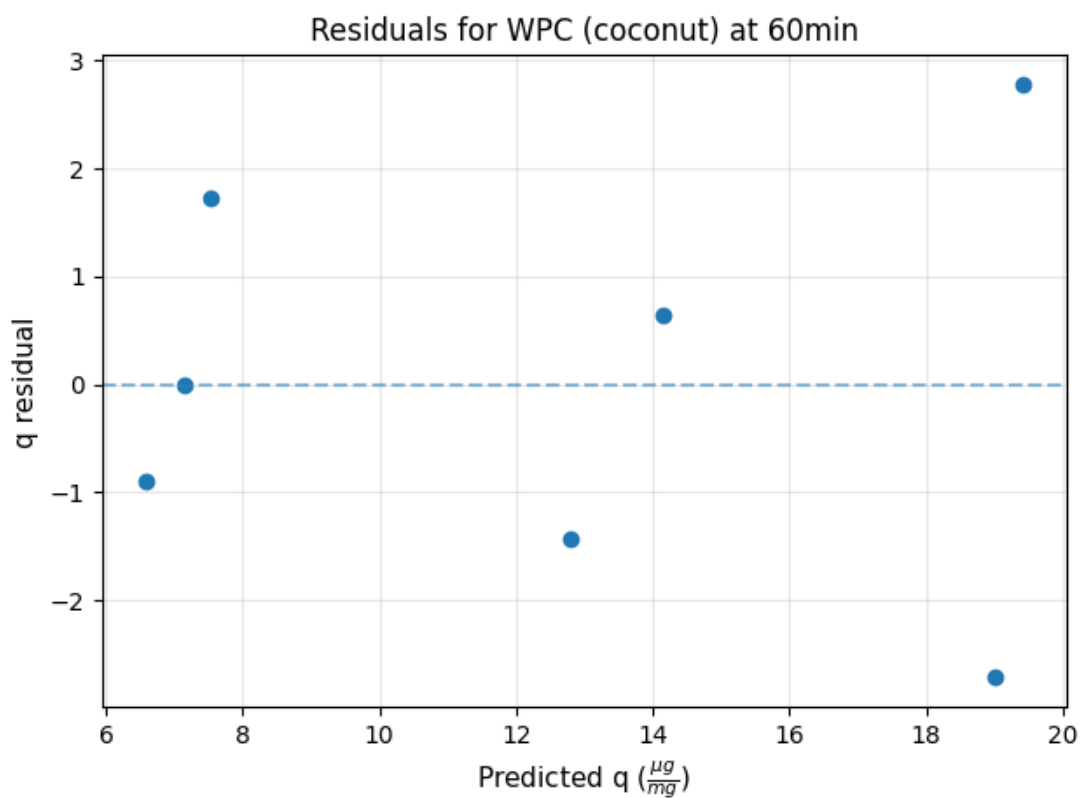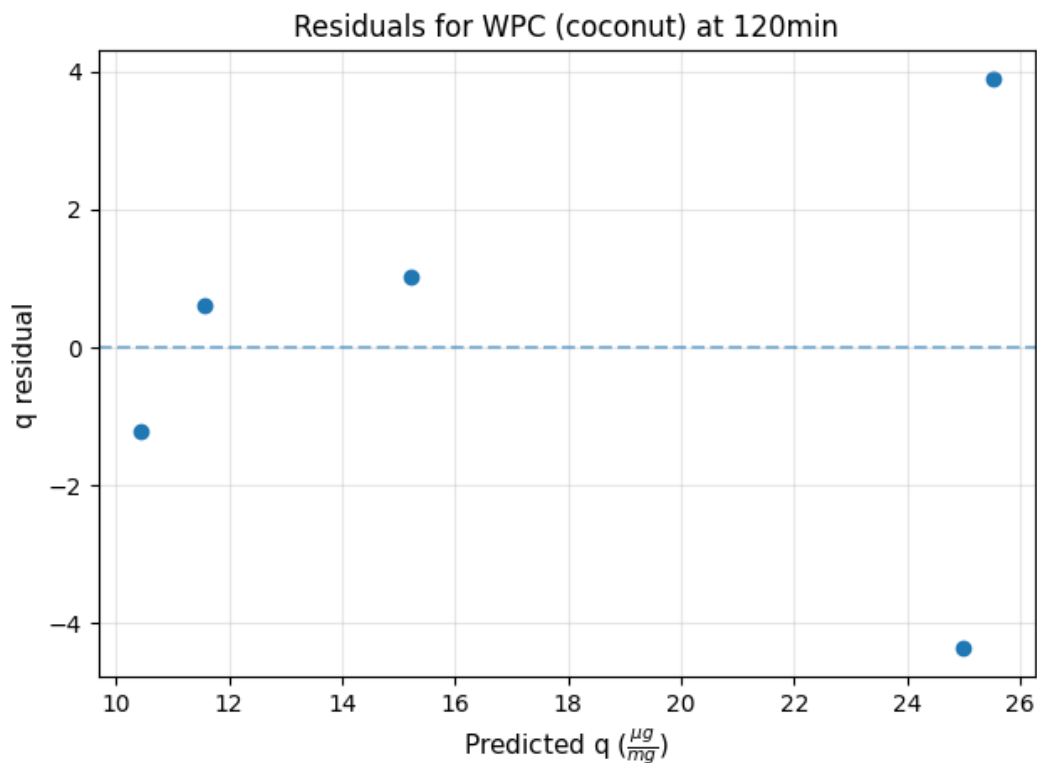
Sample	SPAC dose (mg/L)	Equilibrium MC-LR concentration (ug/L)	Equilibrium capacity, qe (ug/mg)
1	20.4	15.51	4.18
2	17.2	18.53	4.78
3	14.2	27.97	5.13
4	11	19.63	6.78
5	7.6	45.02	7.34
6	6	60.12	7.38
7	3.9	56.13	8.88
8	2.2	81.24	11.45
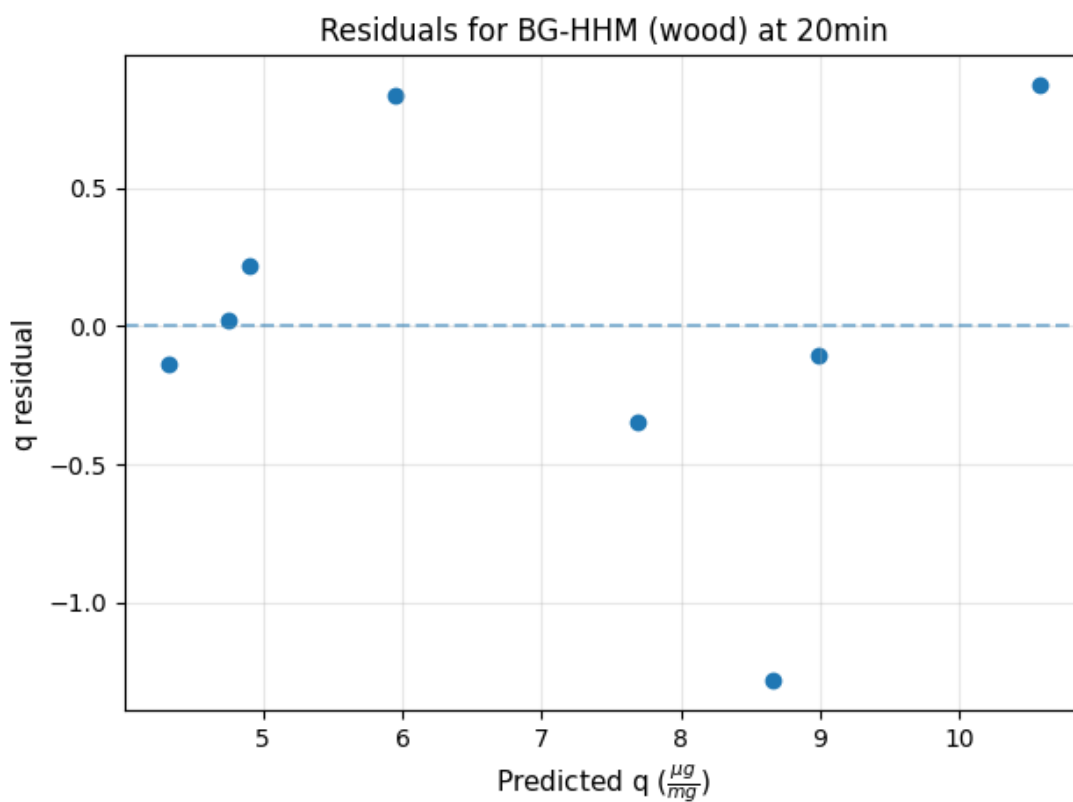
Figure B.25 Residual plot of Freundlich fitting for 20 min contact of MC-LR adsorption by the BG-HHM (wood)

**Table B.14 Carbon loading data for MC-LR adsorption by BG-HHM (wood) in ultrapure water at 30 minutes of contact**

Sample	SPAC dose (mg/L)	Equilibrium MC-LR concentration (ug/L)	Equilibrium capacity, qe (ug/mg)
1	20.4	6.84	4.6
2	17.2	16.38	4.91
3	14.2	14.25	6.09
4	11	9.78	8.27
5	7.6	31.11	8.33
6	6	50.81	9.17
7	3.9	47.59	11.85
8	2.2	74.71	13.64
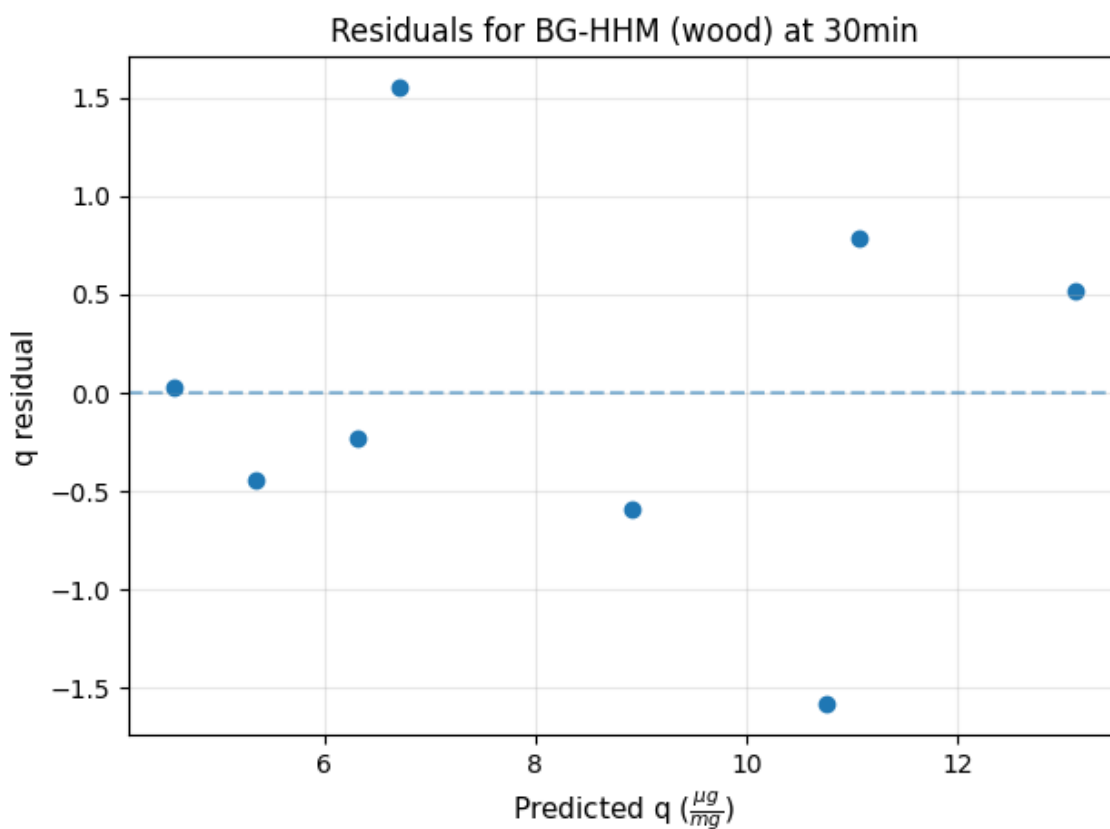
Figure B.26 Residual plot of Freundlich fitting for 30 min contact of MC-LR adsorption by the BG-HHM (wood)

**Table B.15 Carbon loading data for MC-LR adsorption by BG-HHM (wood) in ultrapure water at 60 minutes of contact**

Sample	SPAC dose (mg/L)	Equilibrium MC-LR concentration (ug/L)	Equilibrium capacity, qe (ug/mg)
1	20.4	1.01	4.89
2	17.2	1.14	5.79
3	14.2	2.09	6.95
4	11	1.83	9
5	7.6	11.38	11.76
6	6	19.95	13.47
7	3.9	31.01	17.04
8	2.2	63.29	17.89
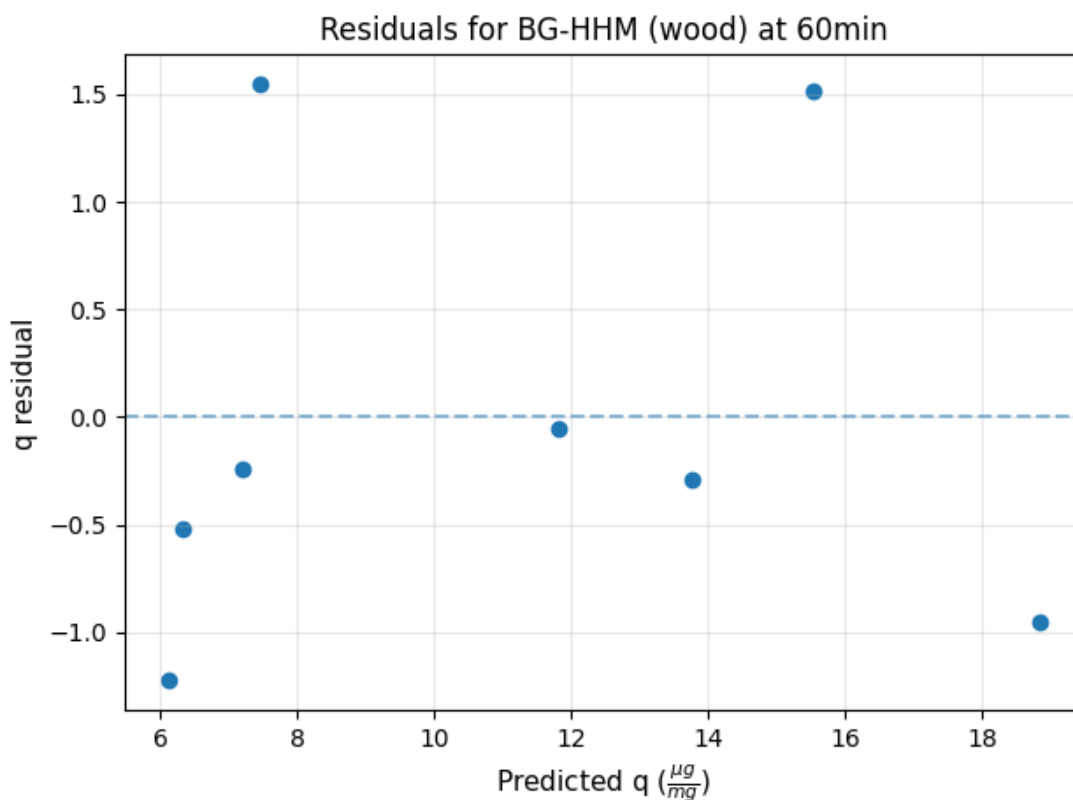
Figure B.27 Residual plot of Freundlich fitting for 60 min contact of MC-LR adsorption by the BG-HHM (wood)

Table B.16 Carbon loading data for MC-LR adsorption by BG-HHM (wood) in ultrapure water at 120 minutes of contact

Sample	SPAC dose (mg/L)	Equilibrium MC-LR concentration (ug/L)	Equilibrium capacity, qe (ug/mg)
1	20.4	0.38	4.92
2	17.2	0.44	5.83
3	14.2	0.64	7.05
4	11	0.52	9.11
5	7.6	1.58	13.05
6	6	5.73	15.84
7	3.9	15.96	21.75
8	2.2	48.5	23.76
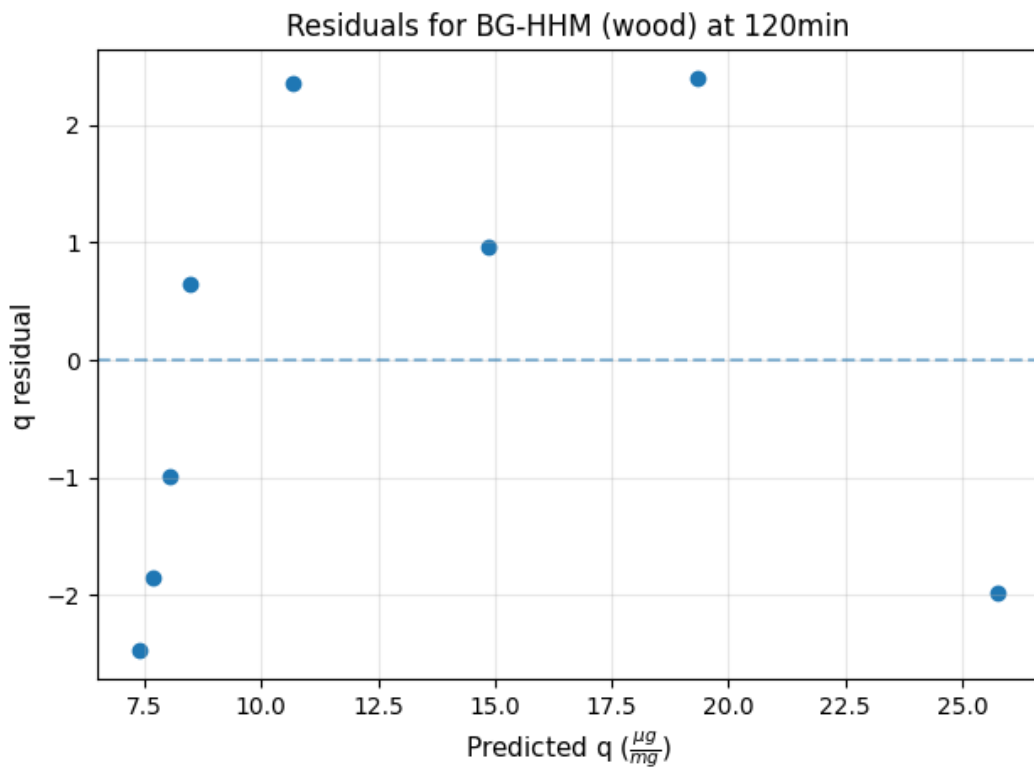
Figure B.28 Residual plot of Freundlich fitting for 120 min contact of MC-LR adsorption by the BG-HHM (wood)

Table B.17 Carbon loading data for MC-LR adsorption by BG-HHM (wood) in ultrapure water at 180 minutes of contact

Sample	SPAC dose (mg/L)	Equilibrium MC-LR concentration (ug/L)	Equilibrium capacity, qe (ug/mg)
1	20.4	0.3	4.93
2	17.2	0.59	5.82
3	14.2	0.33	7.07
4	11	0.33	9.13
5	7.6	0.93	13.14
6	6	1.92	16.48
7	3.9	9.04	23.52
8	2.2	40.02	27.62
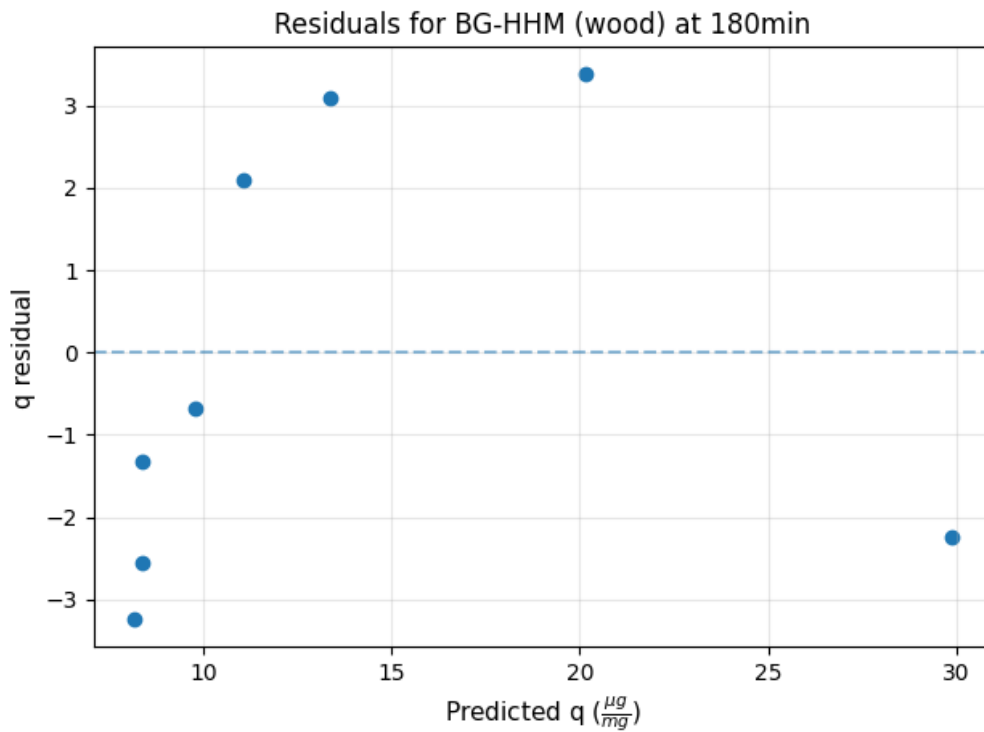
Figure B.29 Residual plot of Freundlich fitting for 180 min contact of MC-LR adsorption by the BG-HHM (wood)

Table B.18 Carbon loading data for MC-LR adsorption by COL-PL60-800 (coal) in ultrapure water at 5 minutes of contact

Sample	SPAC dose (mg/L)	Equilibrium MC-LR concentration (ug/L)	Equilibrium capacity, qe (ug/mg)
1	2.1	91.8	1.89
2	4	87	2.02
3	6.2	83	2.06
4	8.2	79.9	2.26
5	11.4	61.71	2.49
6	13.6	70.92	2.86
7	17.2	63.05	3.17
8	20.6	59.55	3.22
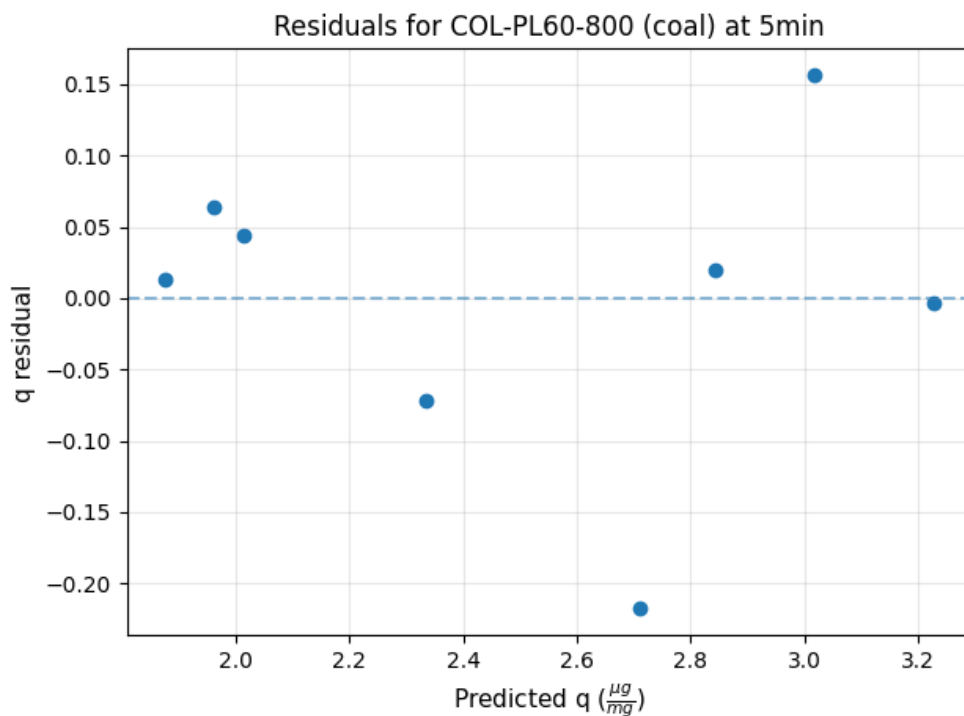
Figure B.30 Residual plot of Freundlich fitting for 5 min contact of MC-LR adsorption by the COL-PL60-800 (coal)

Table B.19 Carbon loading data for MC-LR adsorption by COL-PL60-800 (coal) in ultrapure water at 10 minutes of contact

Sample	SPAC dose (mg/L)	Equilibrium MC-LR concentration (ug/L)	Equilibrium capacity, qe (ug/mg)
1	2.1	87.48	2.82
2	4	76.32	2.9
3	6.2	76.55	3.15
4	8.2	69.41	3.53
5	11.4	44.65	3.54
6	13.6	55.59	4.72
7	17.2	48.53	5.23
8	20.6	40.28	5.54
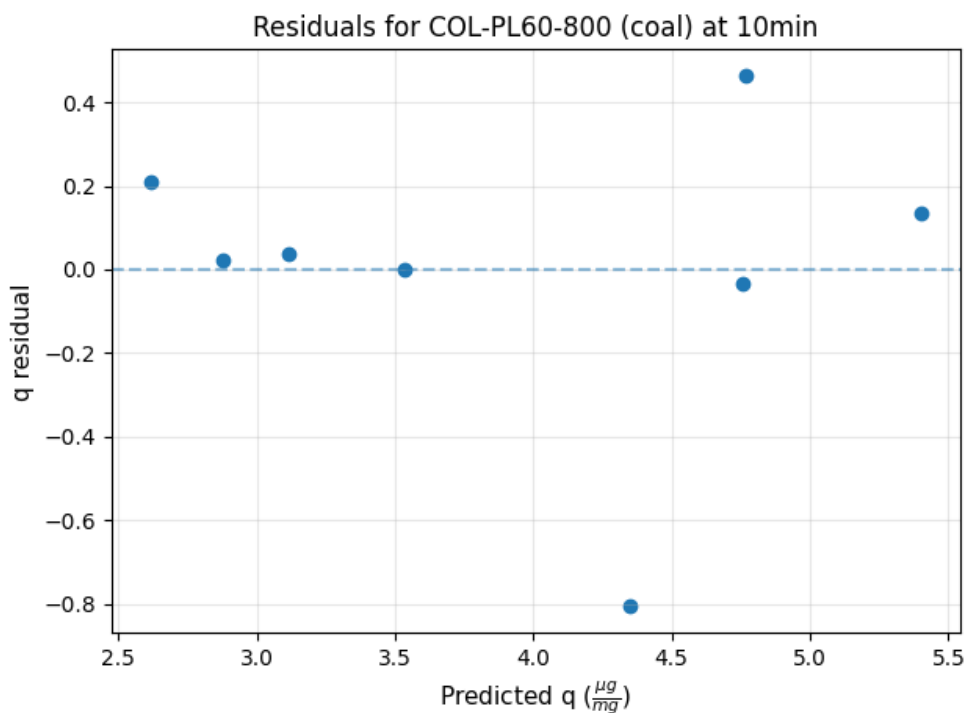
Figure B.31 Residual plot of Freundlich fitting for 10 min contact of MC-LR adsorption by the COL-PL60-800 (coal)

Table B.20 Carbon loading data for MC-LR adsorption by COL-PL60-800 (coal) in ultrapure water at 20 minutes of contact

Sample	SPAC dose (mg/L)	Equilibrium MC-LR concentration (ug/L)	Equilibrium capacity, qe (ug/mg)
1	2.1	82.34	3.8
2	4	74.36	4.07
3	6.2	63.7	4.5
4	8.2	55.66	5.22
5	11.4	26.78	5.61
6	13.6	37.28	6.03
7	17.2	28.38	6.29
8	20.6	20.14	7.68
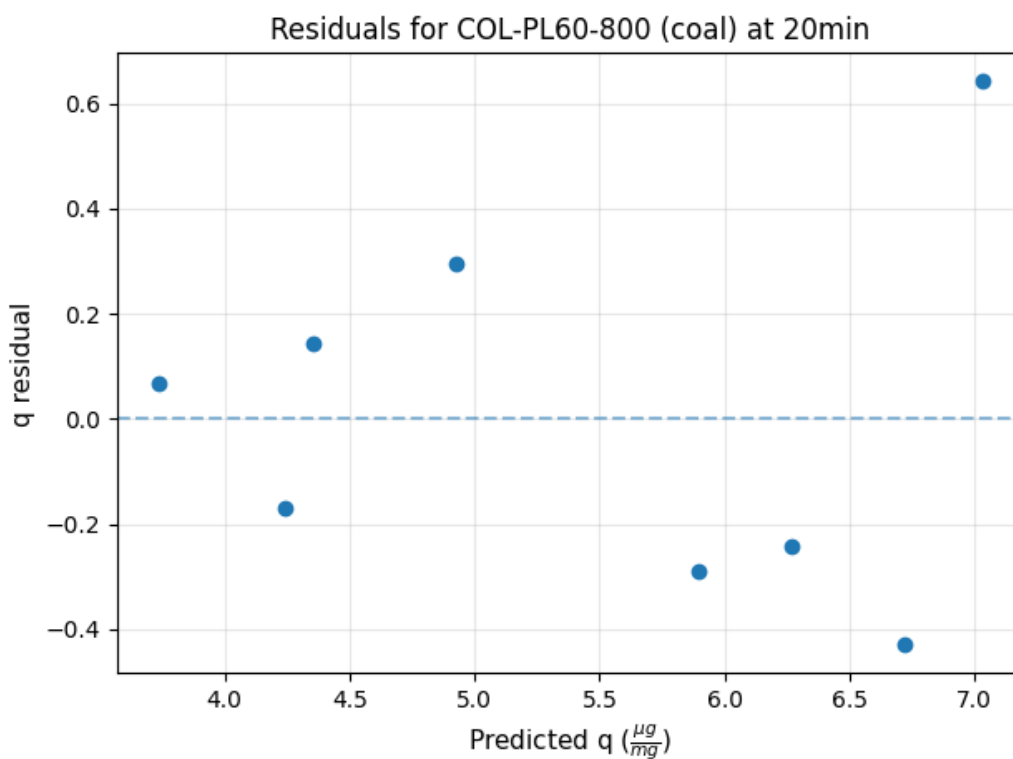
Figure B.32 Residual plot of Freundlich fitting for 20 min contact of MC-LR adsorption by the COL-PL60-800 (coal)

Table B.21 Carbon loading data for MC-LR adsorption by COL-PL60-800 (coal) in ultrapure water at 30 minutes of contact

Sample	SPAC dose (mg/L)	Equilibrium MC-LR concentration (ug/L)	Equilibrium capacity, qe (ug/mg)
1	2.1	79.9	4.24
2	4	69.87	4.73
3	6.2	58.51	5.35
4	8.2	46.12	6.38
5	11.4	18.76	6.44
6	13.6	25.76	6.99
7	17.2	17.09	7.15
8	20.6	11.21	8.84
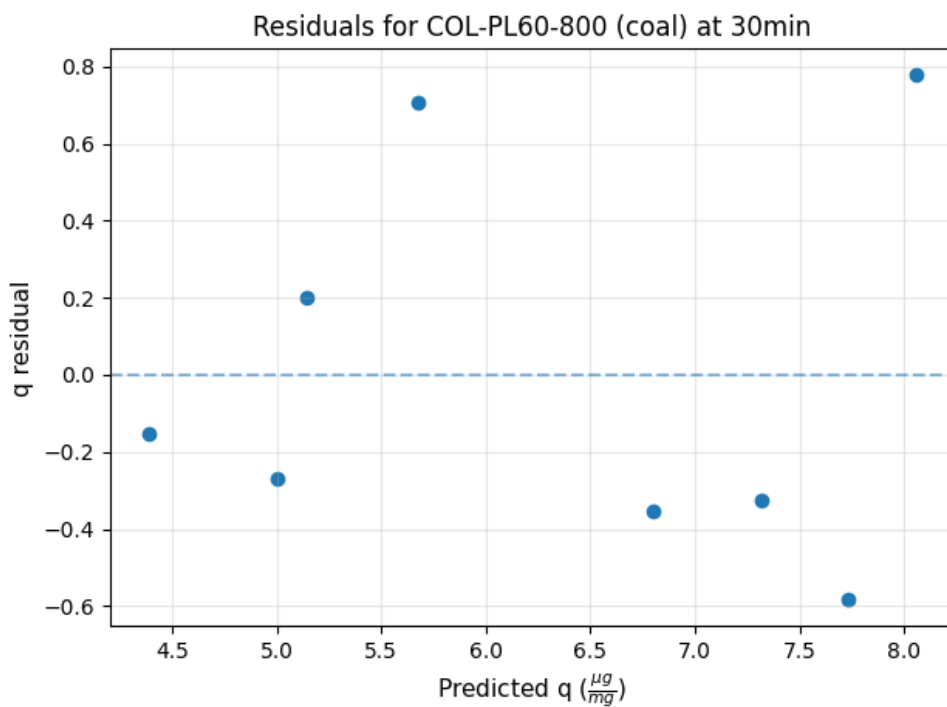
Figure B.33 Residual plot of Freundlich fitting for 30 min contact of MC-LR adsorption by the COL-PL60-800 (coal)

Table B.22 Carbon loading data for MC-LR adsorption by COL-PL60-800 (coal) in ultrapure water at 60 minutes of contact

Sample	SPAC dose (mg/L)	Equilibrium MC-LR concentration (ug/L)	Equilibrium capacity, qe (ug/mg)
1	2.1	71.95	4.68
2	4	59.61	5.47
3	6.2	42.64	6.53
4	8.2	29.84	8.13
5	11.4	5.8	8.37
6	13.6	9.65	9
7	17.2	4.33	9.71
8	20.6	1.96	12.63
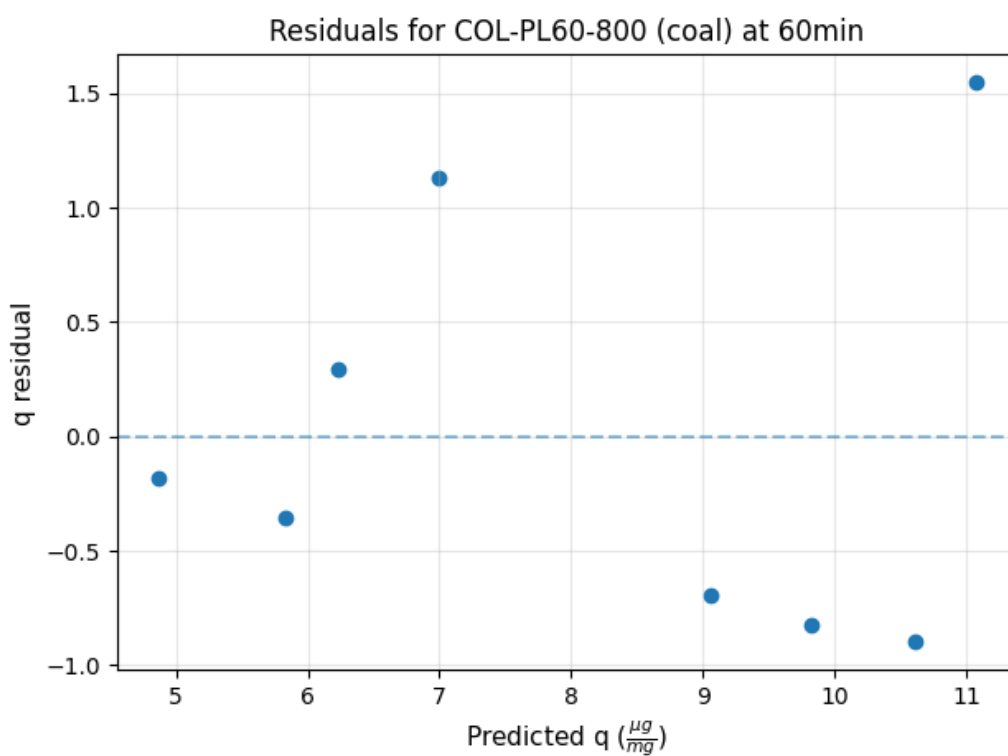
Figure B.34 Residual plot of Freundlich fitting for 30 min contact of MC-LR adsorption by the COL-PL60-800 (coal)

Table B.23 Carbon loading data for MC-LR adsorption by COL-PL60-800 (coal) in ultrapure water at 120 minutes of contact

Sample	SPAC dose (mg/L)	Equilibrium MC-LR concentration (ug/L)	Equilibrium capacity, qe (ug/mg)
1	2.1	64.87	4.77
2	4	45.8	5.7
3	6.2	26.65	7.1
4	8.2	13.11	8.55
5	11.4	0.95	10.41
6	13.6	1.84	11.58
7	17.2	0.37	13.16
8	20.6	0.25	15.99
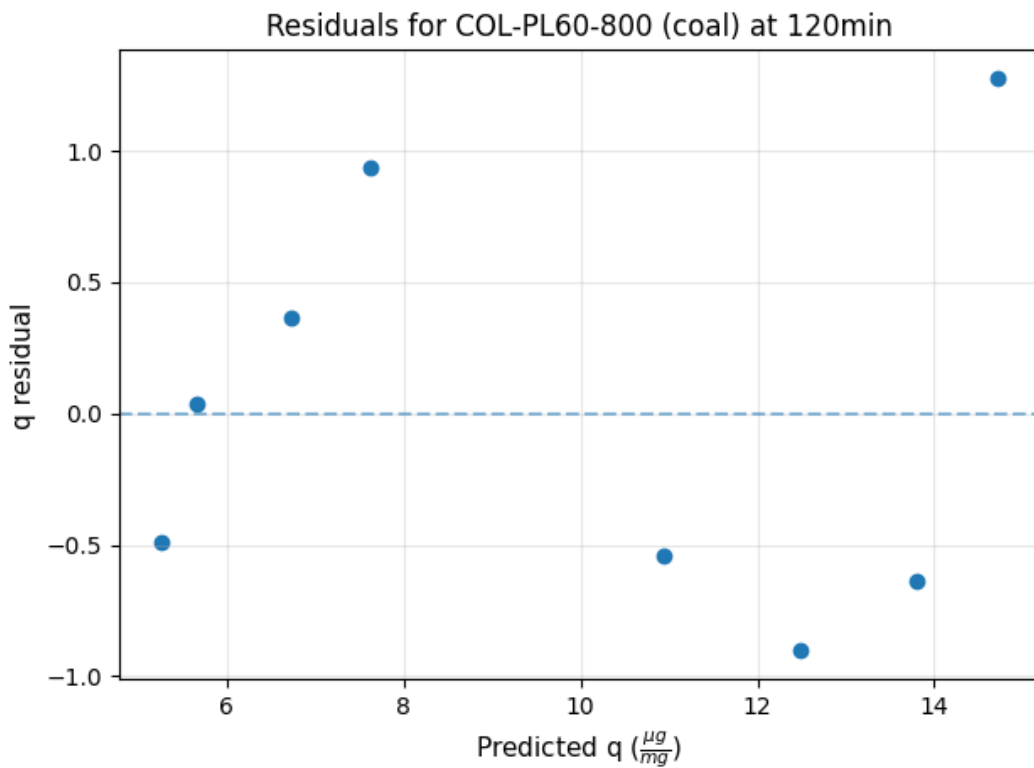
Figure B.35 Residual plot of Freundlich fitting for 120 min contact of MC-LR adsorption by the COL-PL60-800 (coal)

Table B.24 Carbon loading data for MC-LR adsorption by COL-PL60-800 (coal) in ultrapure water at 180 minutes of contact

Sample	SPAC dose (mg/L)	Equilibrium MC-LR concentration (ug/L)	Equilibrium capacity, qe (ug/mg)
1	2.1	59.66	4.77
2	4	36.83	7.21
3	6.2	21.79	8.58
4	8.2	6.23	11.25
5	11.4	0.61	12.37
6	13.6	0.41	15.41
7	20.6	0.21	18.48
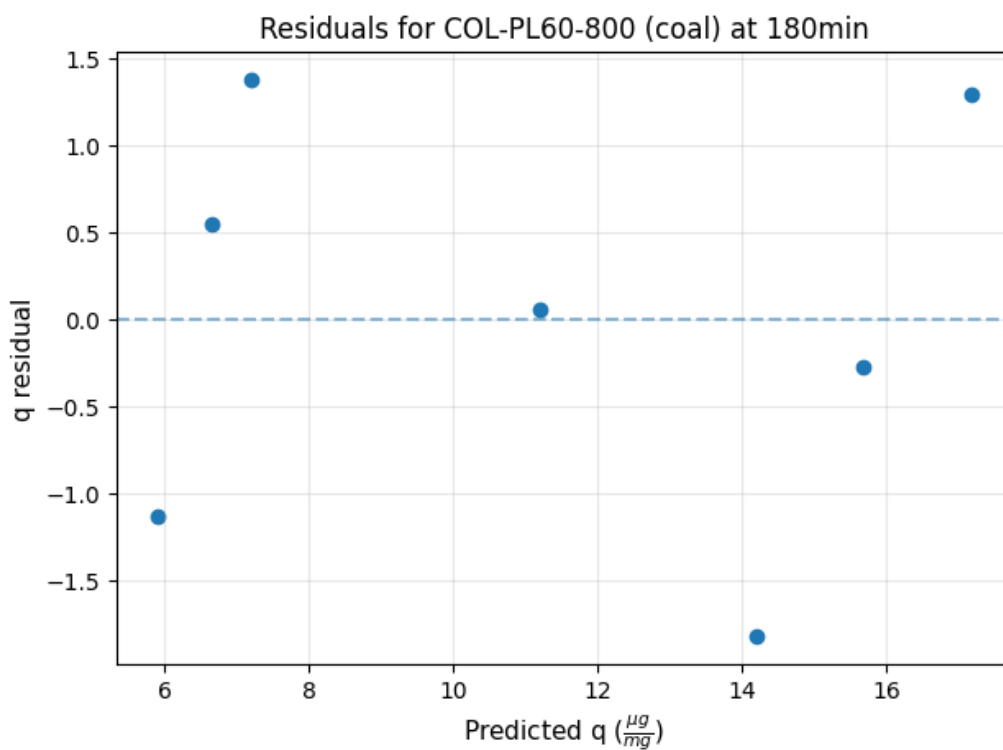
Figure B.36 Residual plot of Freundlich fitting for 180 min contact of MC-LR adsorption by the COL-PL60-800 (coal)

Table B.25 Carbon loading data for MC-LR adsorption by WPC (coconut) in ultrapure water at 5 minutes of contact

Sample	SPAC dose (mg/L)	Equilibrium MC-LR concentration (ug/L)	Equilibrium capacity, qe (ug/mg)
1	2.2	87.27	3.05
2	3.3	83.28	3.11
3	6	66.17	3.91
4	8.2	61.75	4.72
5	10.8	45.1	5.13
6	14	45.71	5.22
7	17.6	46.73	5.72
8	20.4	37.04	6.01
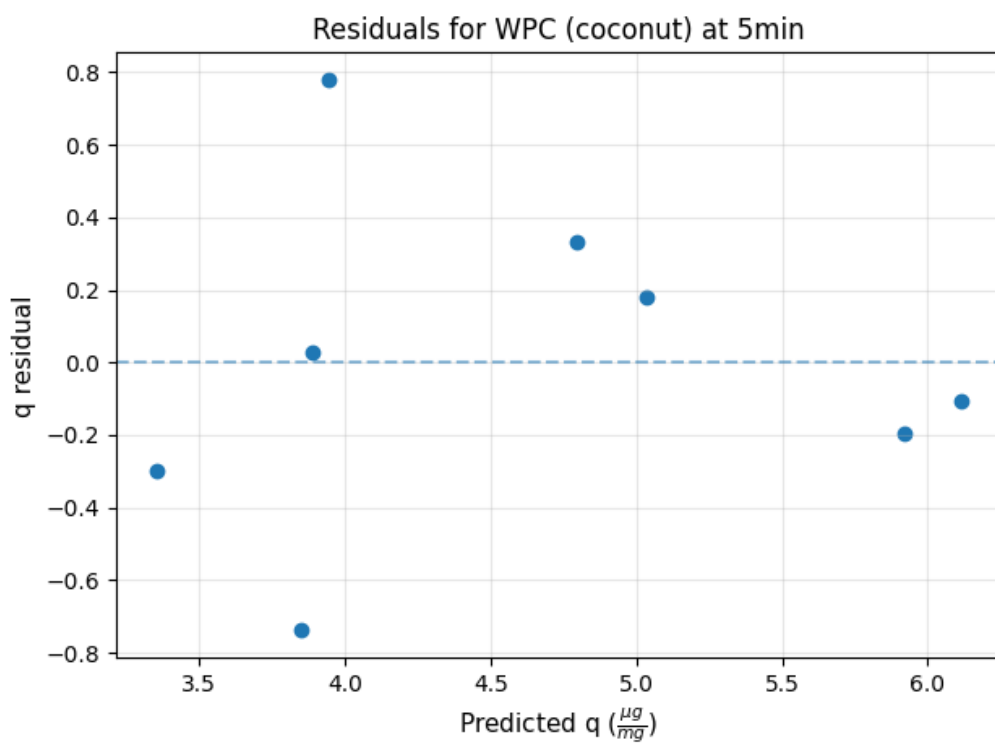
Figure B.37 Residual plot of Freundlich fitting for 5 min contact of MC-LR adsorption by the WPC (coconut)

Table B.26 Carbon loading data for MC-LR adsorption by WPC (coconut) in ultrapure water at 10 minutes of contact

Sample	SPAC dose (mg/L)	Equilibrium MC-LR concentration (ug/L)	Equilibrium capacity, qe (ug/mg)
1	2.2	84.93	4.05
2	3.3	78.86	4.13
3	6	53.53	5.1
4	8.2	50.11	6.14
5	10.8	23.03	6.56
6	14	29.1	7.07
7	17.6	27.73	7.17
8	20.4	17.95	7.83
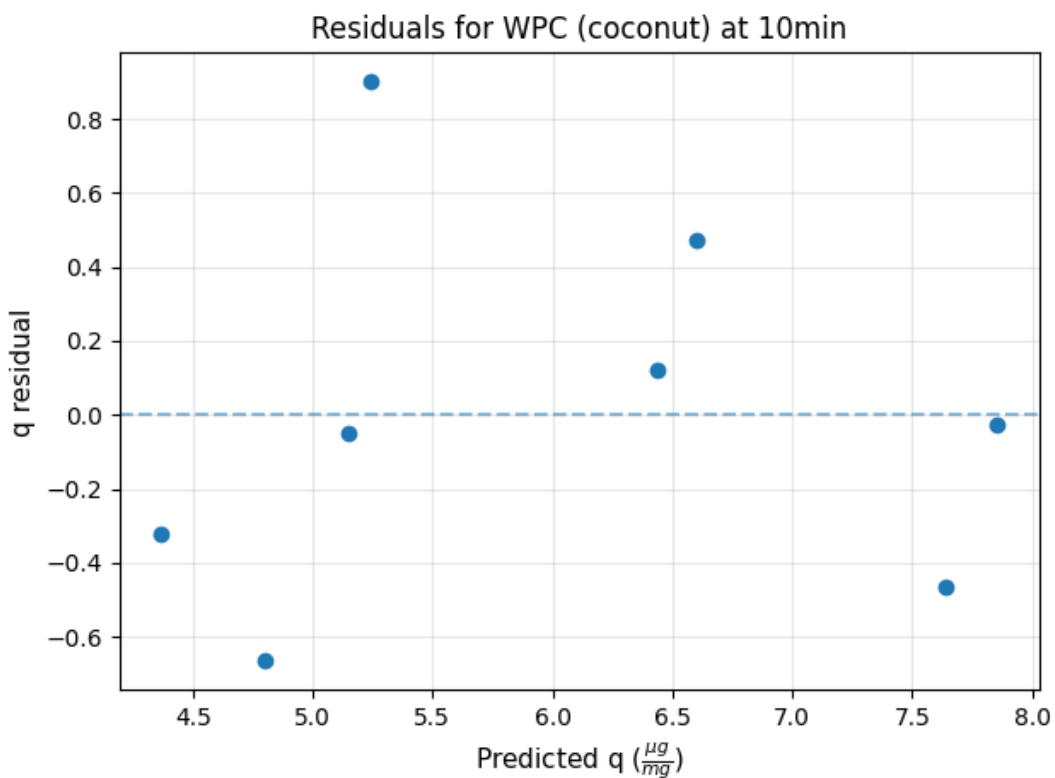
Figure B.38 Residual plot of Freundlich fitting for 10 min contact of MC-LR adsorption by the WPC (coconut)

Table B.27 Carbon loading data for MC-LR adsorption by WPC (coconut) in ultrapure water at 20 minutes of contact

Sample	SPAC dose (mg/L)	Equilibrium MC-LR concentration (ug/L)	Equilibrium capacity, qe (ug/mg)
1	2.2	73.93	4.72
2	3.3	64.1	5.17
3	6	36.7	6.43
4	8.2	31.8	8.38
5	10.8	7.55	8.61
6	14	10.44	10.63
7	17.6	9.55	11.03
8	20.4	4.21	12.07
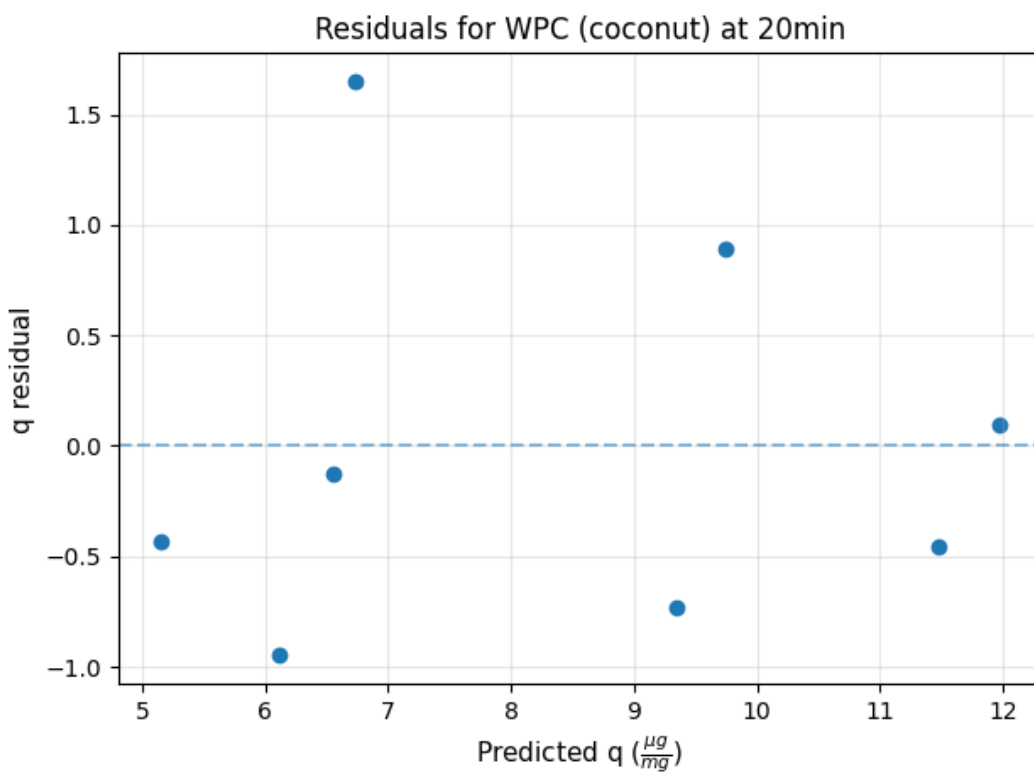
Figure B.39 Residual plot of Freundlich fitting for 20 min contact of MC-LR adsorption by the WPC (coconut)

Table B.28 Carbon loading data for MC-LR adsorption by WPC (coconut) in ultrapure water at 30 minutes of contact

Sample	SPAC dose (mg/L)	Equilibrium MC-LR concentration (ug/L)	Equilibrium capacity, qe (ug/mg)
1	2.2	64.94	4.86
2	3.3	59.01	5.54
3	6	27.65	6.91
4	8.2	22.23	9.06
5	10.8	2.66	9.54
6	14	3.69	12.14
7	17.6	3.07	12.57
8	20.4	1.29	16.16

Figure B.40 Residual plot of Freundlich fitting for30 min contact of MC-LR adsorption by the WPC (coconut)

Table B.29 Carbon loading data for MC-LR adsorption by WPC (coconut) in ultrapure water at 60 minutes of contact

Sample	SPAC dose (mg/L)	Equilibrium MC-LR concentration (ug/L)	Equilibrium capacity, qe (ug/mg)
1	2.2	51.68	5.69
2	3.3	46.75	7.14
3	6	11.72	9.25
4	8.2	7.31	11.36
5	10.8	0.61	14.79
6	14	0.48	16.29
7	17.6	0.32	22.18

Figure B.41 Residual plot of Freundlich fitting for 60 min contact of MC-LR adsorption by the WPC (coconut)

Table B.30 Carbon loading data for MC-LR adsorption by WPC (coconut) in ultrapure water at 120 minutes of contact

Sample	SPAC dose (mg/L)	Equilibrium MC-LR concentration (ug/L)	Equilibrium capacity, qe (ug/mg)
1	2.2	35.81	9.22
2	3.3	32.46	12.19
3	6	3.14	16.22
4	8.2	0.53	20.62
5	10.8	0.87	29.4

Figure B.42 Residual plot of Freundlich fitting for 120 min contact of MC-LR adsorption by the WPC (coconut)

Table B.31 Carbon loading data for MC-LR adsorption by WPC (coconut) in ultrapure water at 180 minutes of contact

Sample	SPAC dose (mg/L)	Equilibrium MC-LR concentration (ug/L)	Equilibrium capacity, qe (ug/mg)
1	2.2	27.9	4.91
2	3.3	23.51	12.22
3	6	0.85	16.61
4	8.2	0.28	23.33
5	20.4	0.28	33
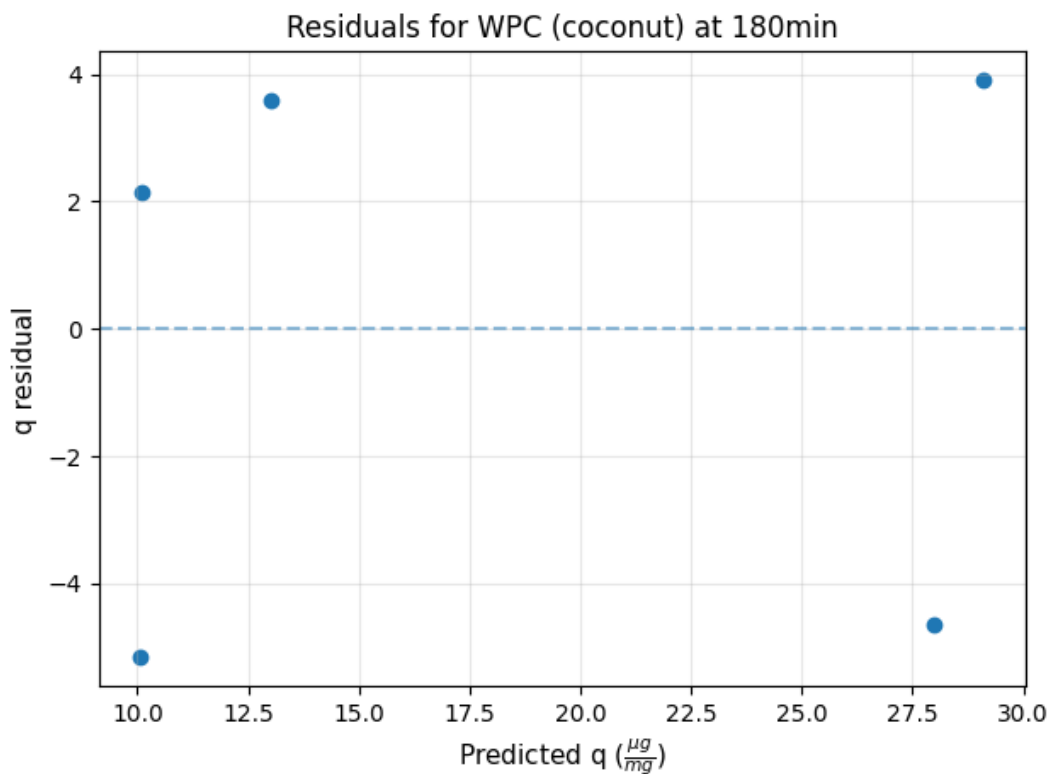
Figure B.43 Residual plot of Freundlich fitting for 180 min contact of MC-LR adsorption by the WPC (coconut)
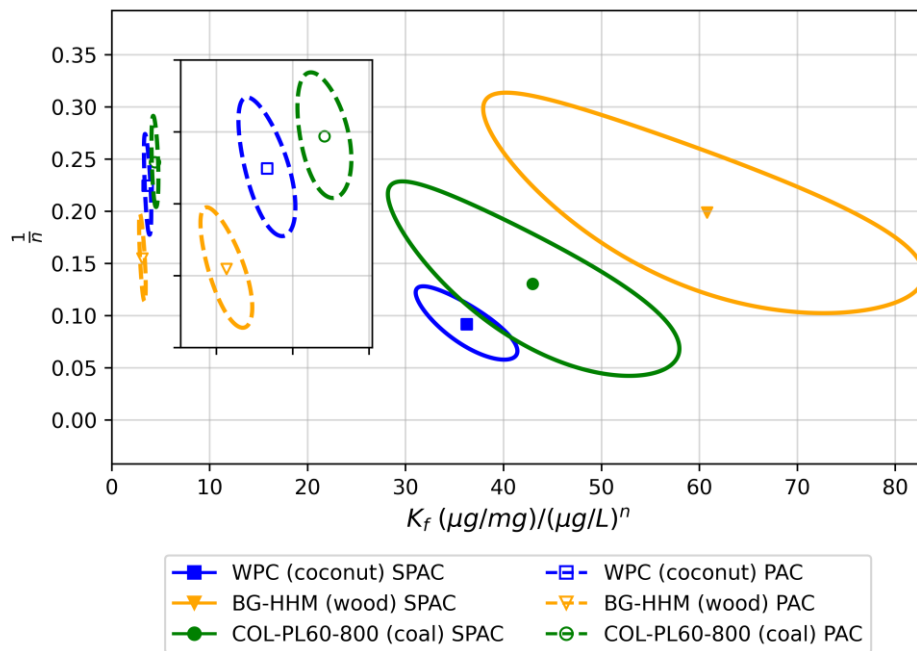
Figure B.44 Comparison of JCRs of prepared SPACs (solid regions) and parent PACs (dashed regions) at equilibrium

Appendix B.12 Comparison of JCRs for SPACs and parent PACs at short contact times of 30 and 60 minutes
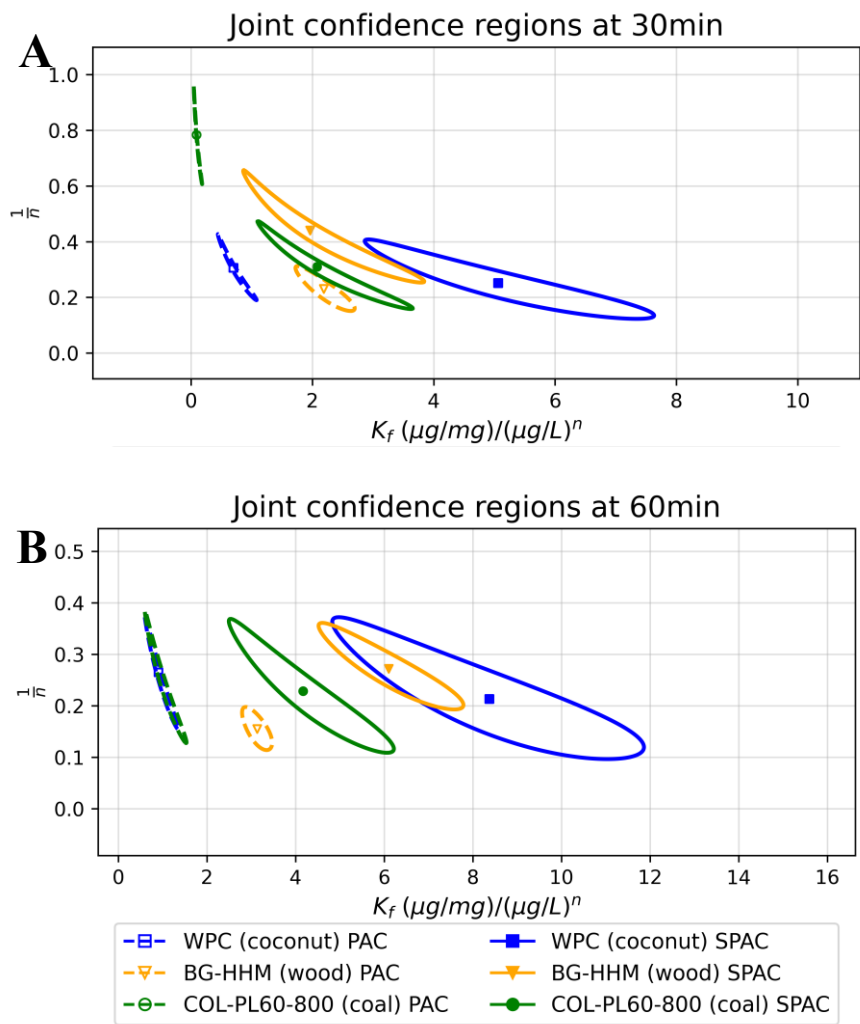
Figure B.45 JCRs for adsorption of MC-LR onto the three PACs (dashed regions) and SPACs (solid regions) at three different contact time of (A) 30 minutes and (B) 60 minutes

Appendix C

Additional Information for Chapter 5

Appendix C.1 Removal plots of the three SPACs in Lake Erie water at doses of 2-20 mg/L
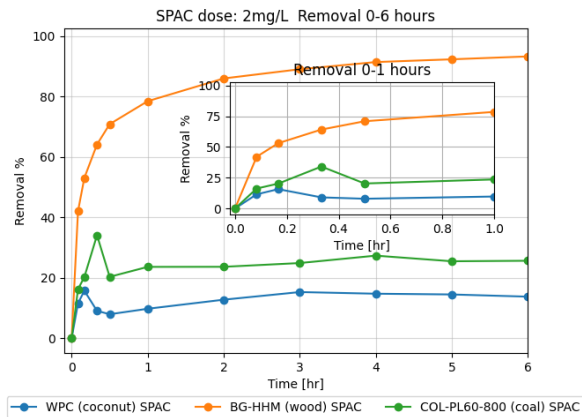
Figure C.1 Removal of MC-LR via SPACs at dose of 2 mg/L with respect to time
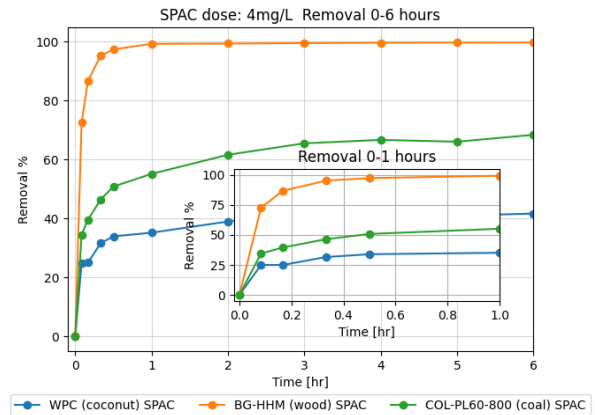
Figure C.2 Removal of MC-LR via SPACs at dose of 4 mg/L with respect to time
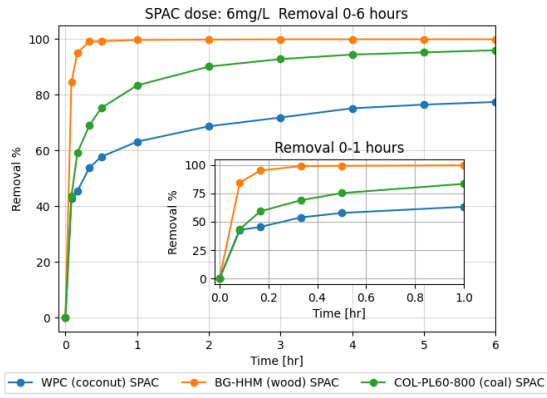
Figure C. 3 Removal of MC-LR via SPACs at dose of 6 mg/L with respect to time
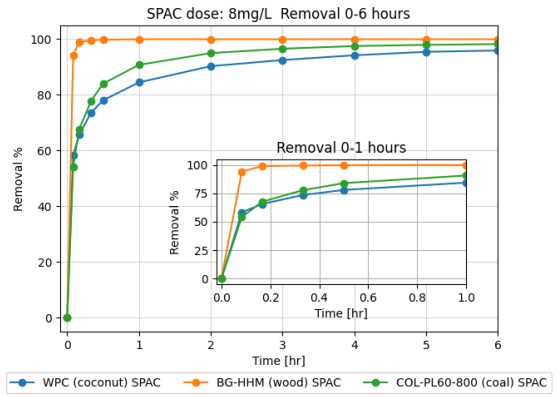
Figure C. 4 Removal of MC-LR via SPACs at dose of 8 mg/L with respect to time
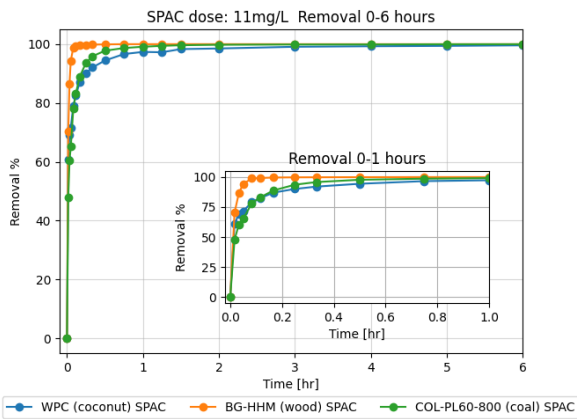
Figure C.5 Removal of MC-LR via SPACs at dose of 11 mg/L with respect to time
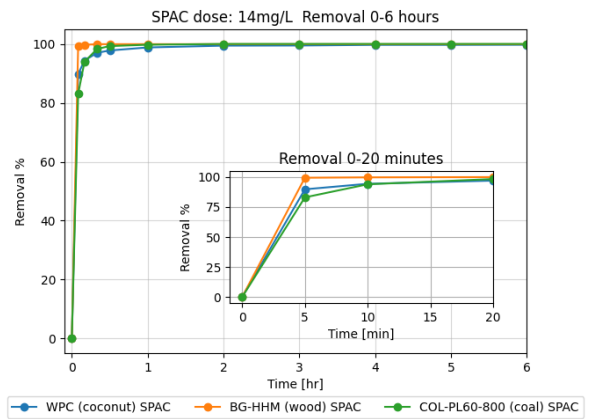
Figure C.6 Removal of MC-LR via SPACs at dose of 14 mg/L with respect to time
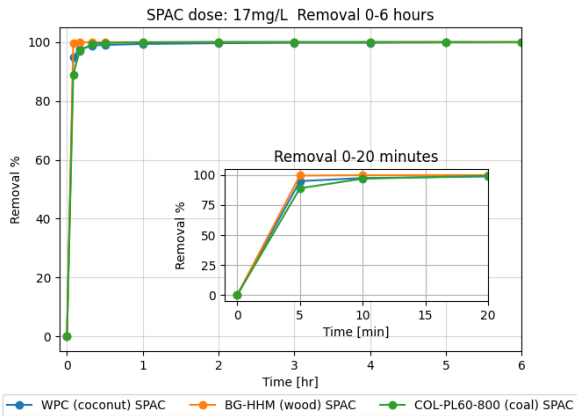
Figure C.7 Removal of MC-LR via SPACs at dose of 17 mg/L with respect to time
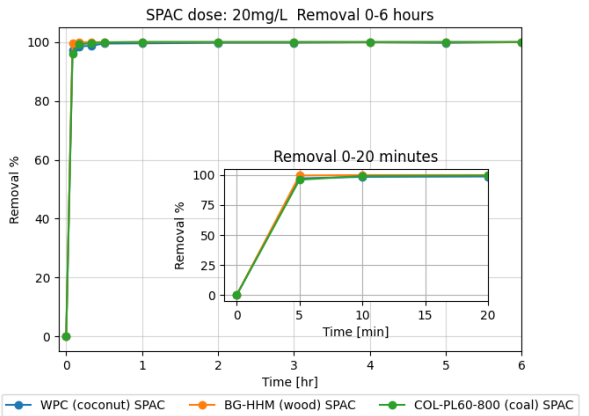
Figure C.8 Removal of MC-LR via SPACs at dose of 20 mg/L with respect to time

Appendix C.2 Pseudo-first-order fitting results and residual plots
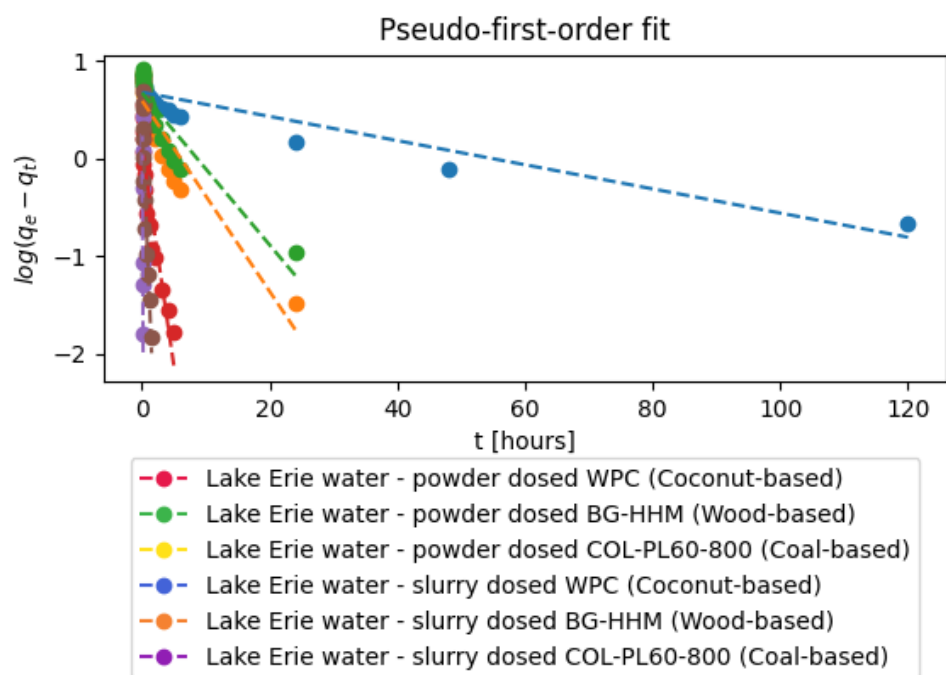
Figure C.9 Pseudo-first-order fitting plots in Lake Erie water for dry powder and slurry dosed SPACs

Table C.1 Pseudo-first-order fitting results in Lake Erie water for dry powder and slurry dosed SPACs

Carbon	Water – dosing method	q_e experimental $(\mu g/mg)$	q_e predicted $(\mu g/mg)$	$K_1(min^{-1})$	R^2
WPC (Coconut-based)	Lake Erie water - powder dosed	7.89	4.72	0.03	0.8673
BG-HHM (Wood-based)	Lake Erie water - powder dosed	7.76	3.88	0.23	0.8530
COL-PL60-800 (Coal-based)	Lake Erie water - powder dosed	8.16	4.65	0.18	0.8271
WPC (Coconut-based)	Lake Erie water - slurry dosed	9.13	1.28	1.03	0.8610
BG-HHM (Wood-based)	Lake Erie water - slurry dosed	9.14	3.19	34.44	0.9496
COL-PL60-800 (Coal-based)	Lake Erie water - slurry dosed	9.38	2.45	3.66	0.9351
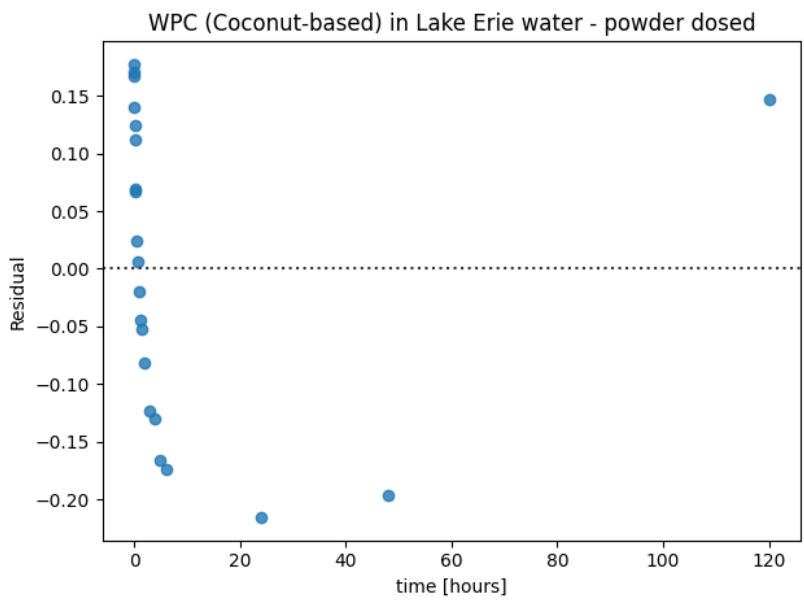
Figure C.10 Pseudo-first-order fitting residuals for dry powder dosed WPC (coconut-based) SPAC in Lake Erie water
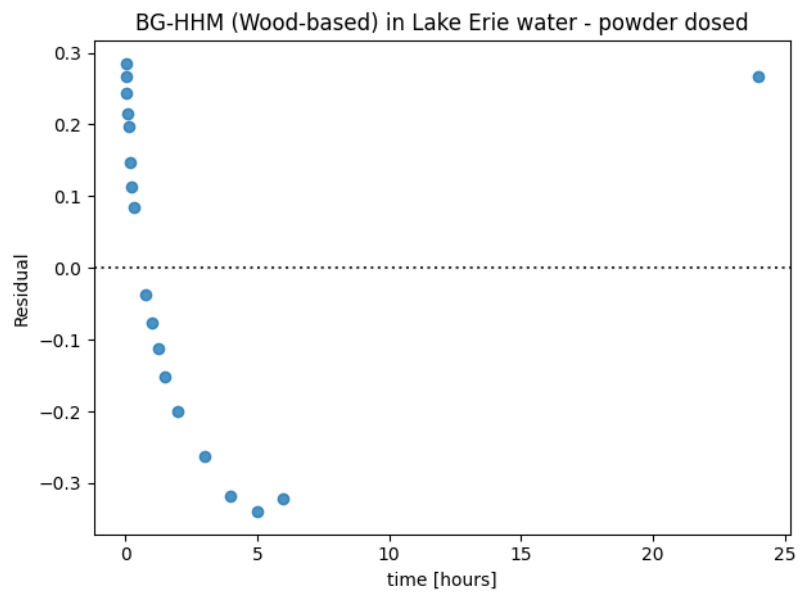
Figure C.11 Pseudo-first-order fitting residuals for dry powder dosed BG-HHM (wood-based) SPAC in Lake Erie water
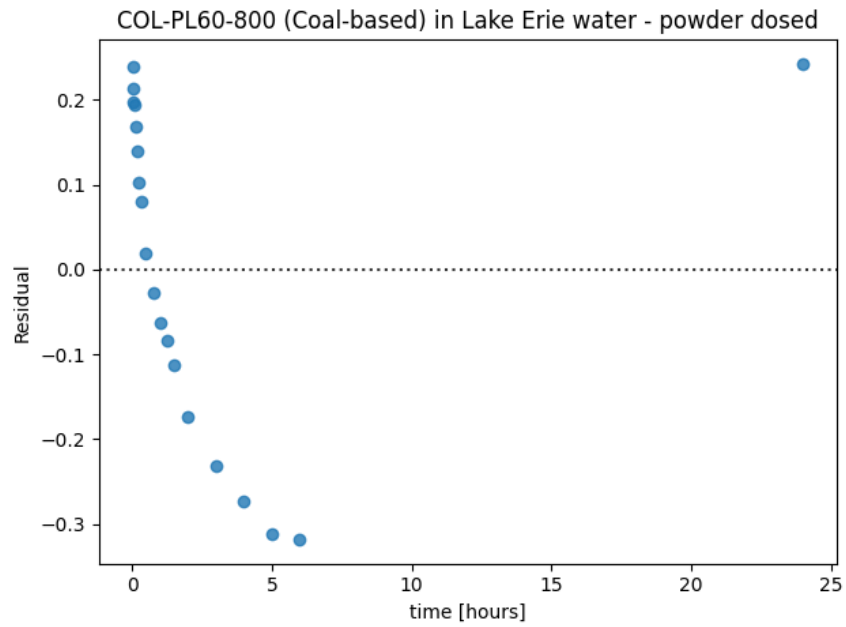
Figure C.12 Pseudo-first-order fitting residuals for dry powder dosed COL-PL60-800 (coal-based) SPAC in Lake Erie water
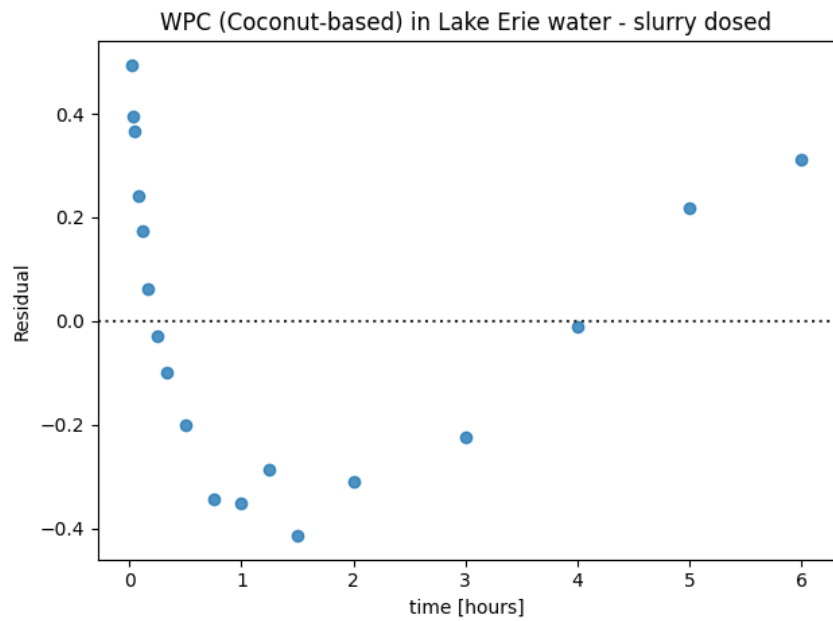
Figure C.13 Pseudo-first-order fitting residuals for slurry dosed WPC (coconut-based) SPAC in Lake Erie water
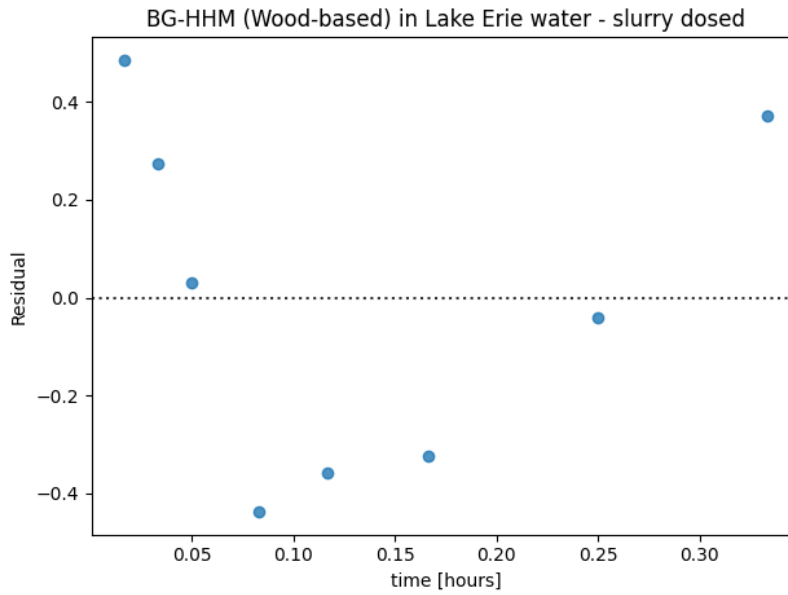
Figure C.14 Pseudo-first-order fitting residuals for slurry dosed BG-HHM (wood-based) SPAC in Lake Erie water
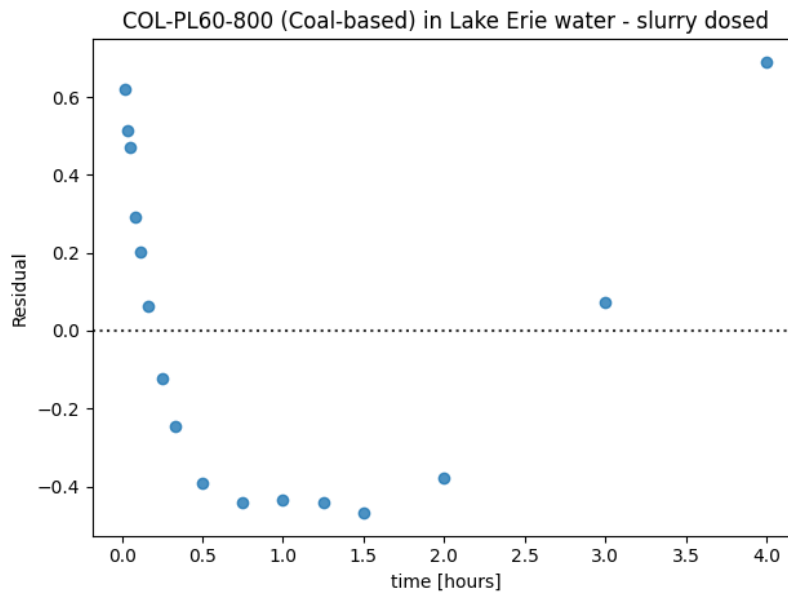
Figure C.15 Pseudo-first-order fitting residuals for slurry dosed COL-PL60-800 (coal-based) SPAC in Lake Erie water

Appendix C.3 Pseudo-second-order residuals at 11 mg/L for both dry powder and slurry dosing methods.
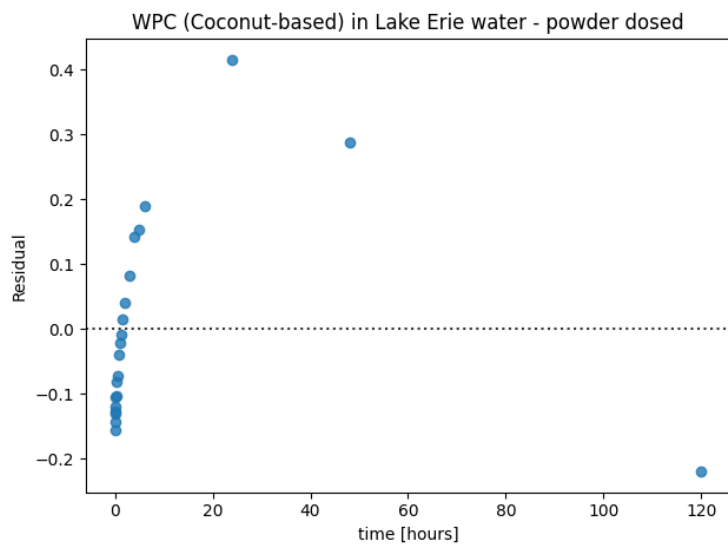
Figure C.16 Pseudo-second-order fitting residuals for dry powder dosed WPC (coconut-based) SPAC in Lake Erie water
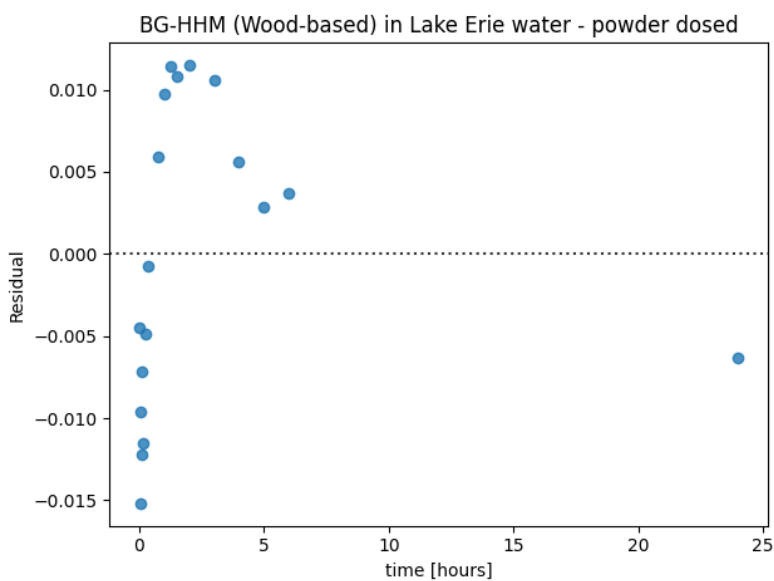
Figure C.17 Pseudo-second-order fitting residuals for dry powder dosed BG-HHM (wood-based) SPAC in Lake Erie water
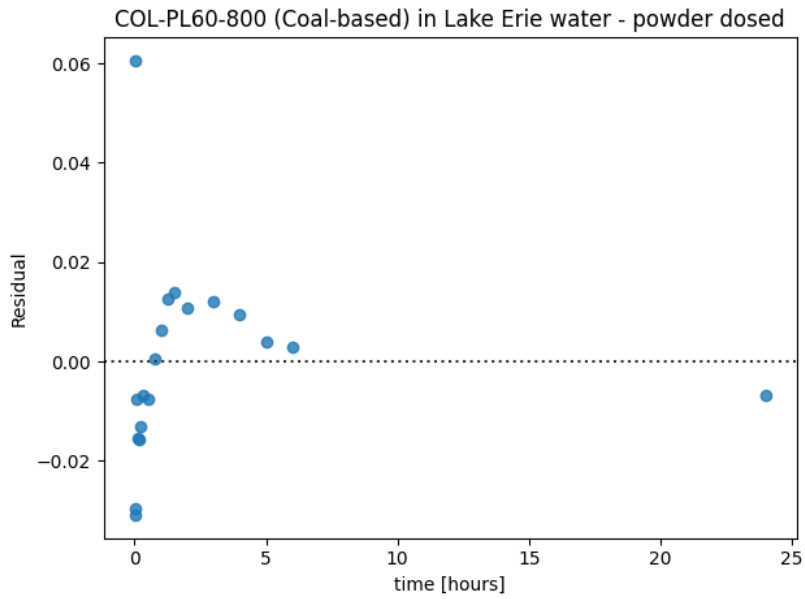
Figure C.18 Pseudo-second-order fitting residuals for dry powder dosed COL-PL60-800 (coal-based) SPAC in Lake Erie water
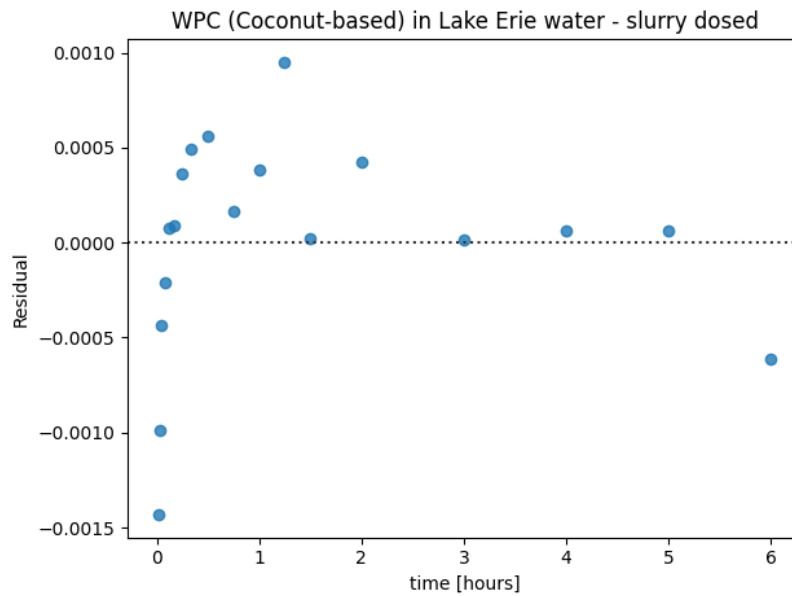
Figure C.19 Pseudo-second-order fitting residuals for slurry dosed WPC (coconut-based) SPAC in Lake Erie water
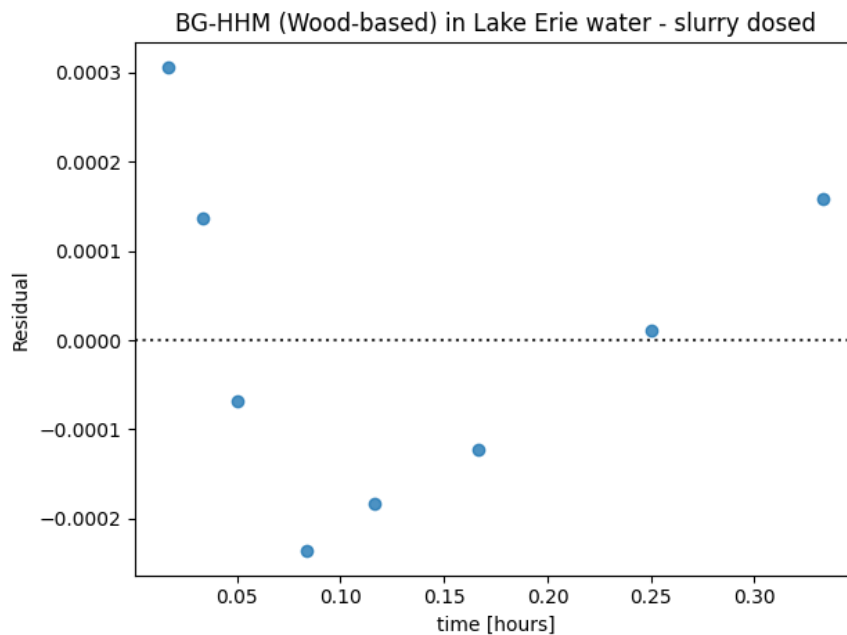
Figure C.20 Pseudo-second-order fitting residuals for slurry dosed BG-HHM (wood-based) SPAC in Lake Erie water
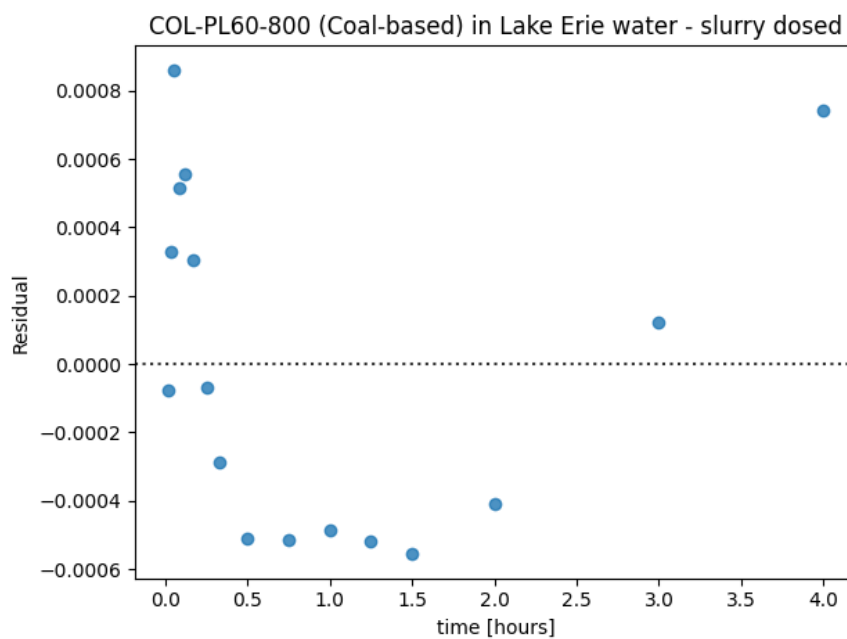
Figure C.21 Pseudo-second-order fitting residuals for slurry dosed COL-PL60-800 (coal-based) SPAC in Lake Erie water

Appendix C.4 Joint confidence regions at 48hr and 96hr (equilibrium)
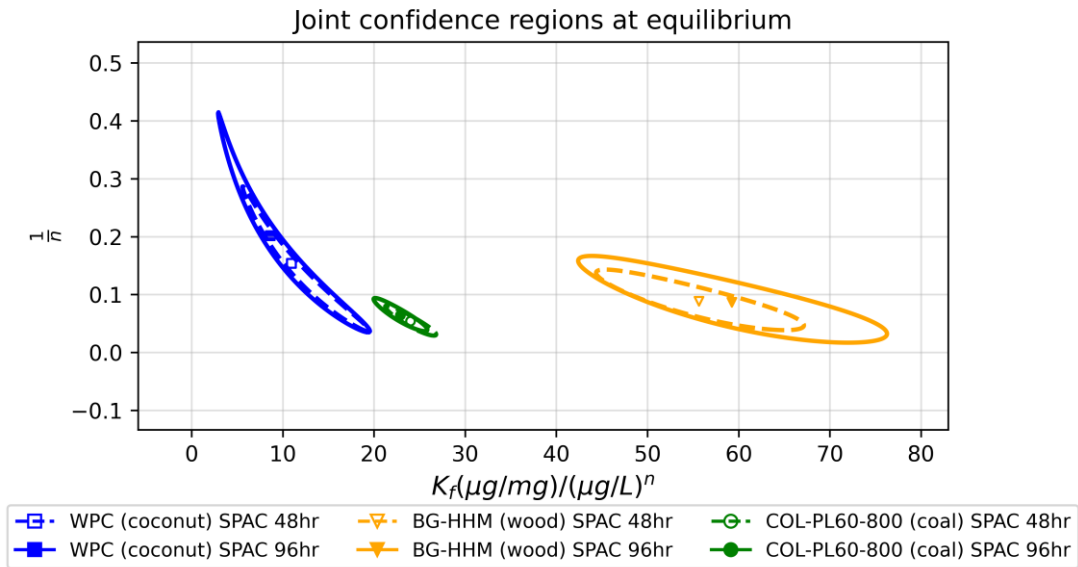
Figure C.22 JCRs of Freundlich parameters for adsorption of MC-LR onto SPACs at 48h and 96h of contact time (equilibrium)

Appendix C.5 Best-fit Freundlich curves at 48hr and 96hr (equilibrium)
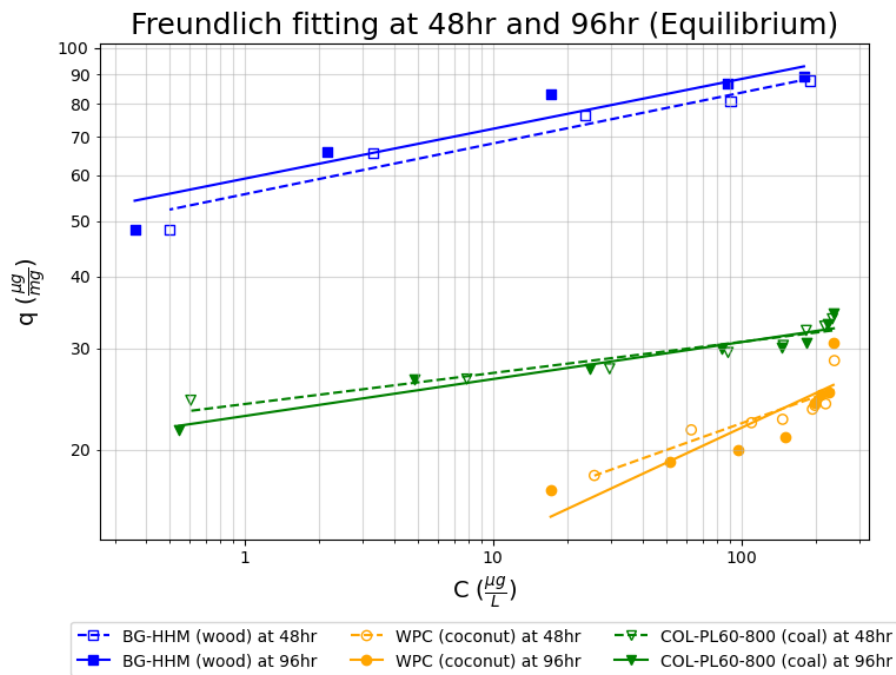
Figure C.23 Best-fit Freundlich curves for adsorption of MC-LR onto SPACs at 48h and 96h of contact time (equilibrium)

Appendix C.6 Joint confidence regions for SPACs at 96h (Equilibrium) in ultrapure water and Lake Erie water
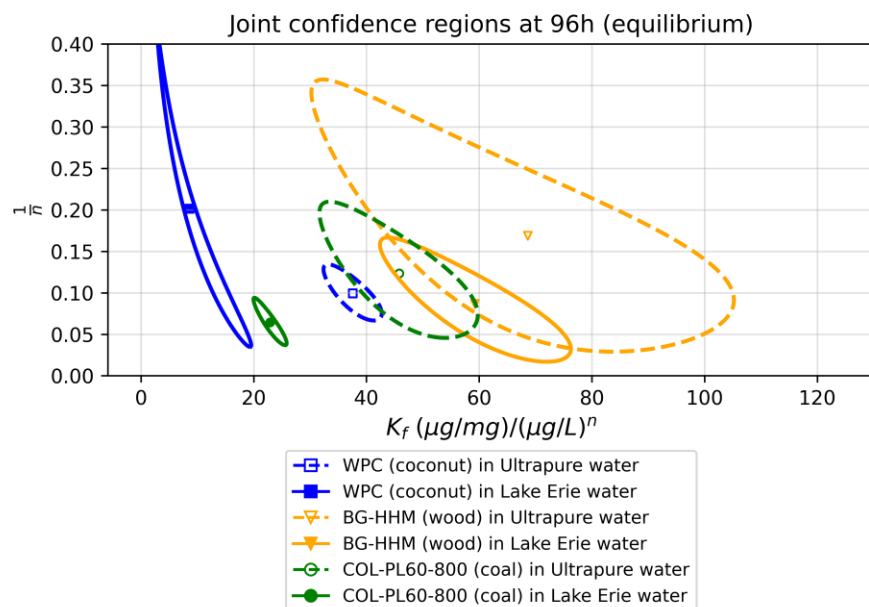
Figure C.24 JCRs of Freundlich parameters for adsorption of MC-LR onto SPACs at 96h of contact time (equilibrium) in Lake Erie water and ultrapure water

Appendix C.7 Joint confidence regions for SPACs and parent PACs at equilibrium in Lake Erie water
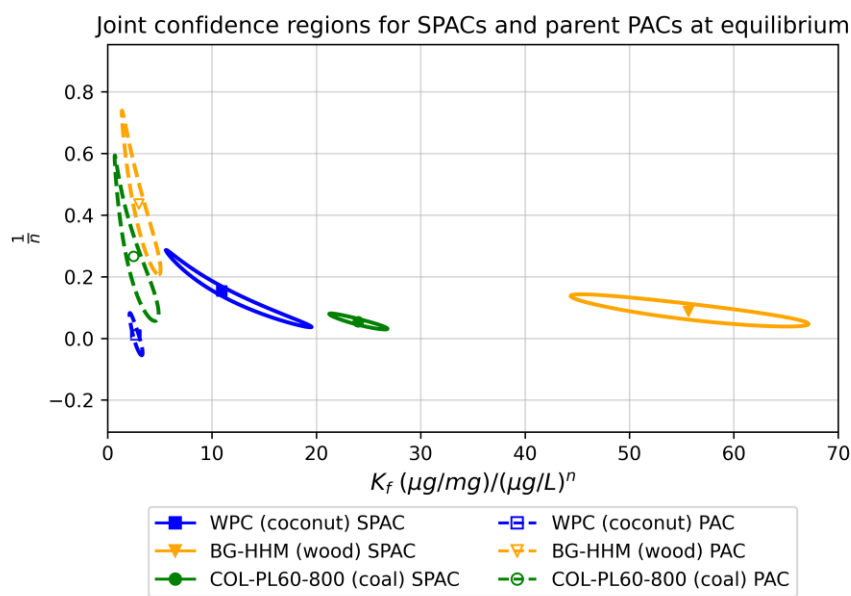
Figure C.25 JCRs of Freundlich parameters for adsorption of MC-LR onto SPACs and parent PACs at equilibrium in Lake Erie water

Appendix C.8 Best-fit Freundlich curves for SPACs and parent PACs at equilibrium in Lake Erie water
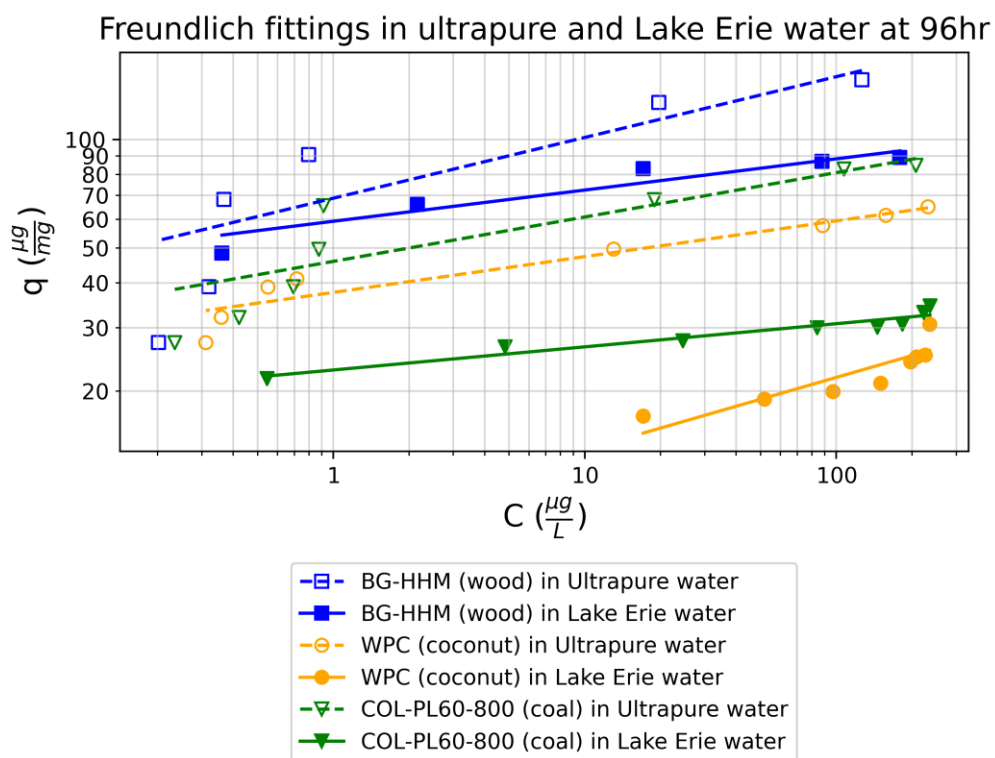
Figure C.26 Best-fit Freundlich curves for adsorption of MC-LR onto SPACs at 96h of contact time (equilibrium) in Lake Erie water compared with the curves for parent PACs at equilibrium

Appendix C.9 Lake Erie water at equilibrium (vial point method) isotherms

Table C.2 Equilibrium (48hr) carbon loading data for MC-LR adsorption by BG-HHM (wood) in Lake Erie water

Sample	SPAC dose (mg/L)	Equilibrium MC-LR concentration (µg/L)	Equilibrium capacity, qe (µg/mg)
1	1	189.7	48.27
2	2	90.5	65.67
3	3	23.46	76.3
4	4	3.3	80.85
5	5.5	0.5	87.75
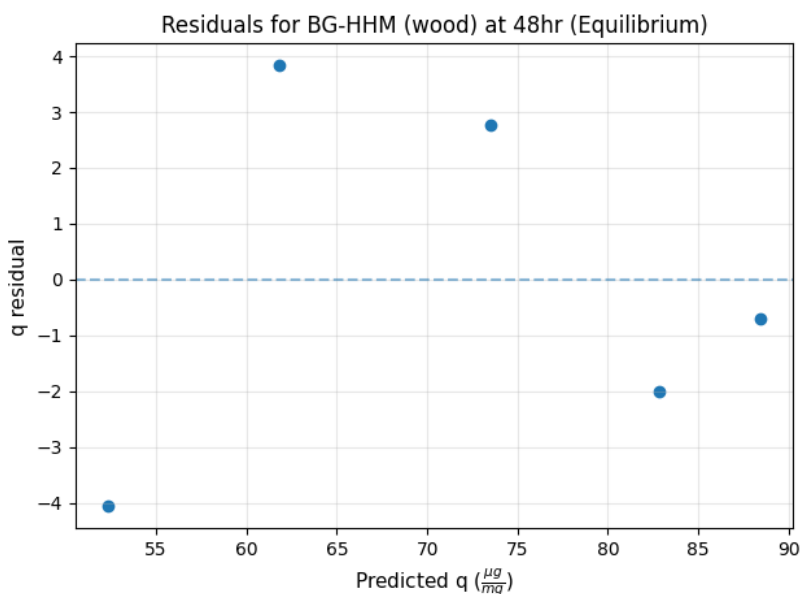
Figure C.3 Residual plot for Equilibrium (48h) isotherm of MC-LR adsorption by the BG-HHM (wood)

Table C.26 Equilibrium (96hr) carbon loading data for MC-LR adsorption by BG-HHM (wood) in Lake Erie water

Sample	SPAC dose (mg/L)	Equilibrium MC-LR concentration (µg/L)	Equilibrium capacity, qe (µg/mg)
1	1	179.1	48.3
2	2	87.9	65.96
3	3	17.07	82.98
4	4	2.16	86.9
5	5.5	0.36	89.05
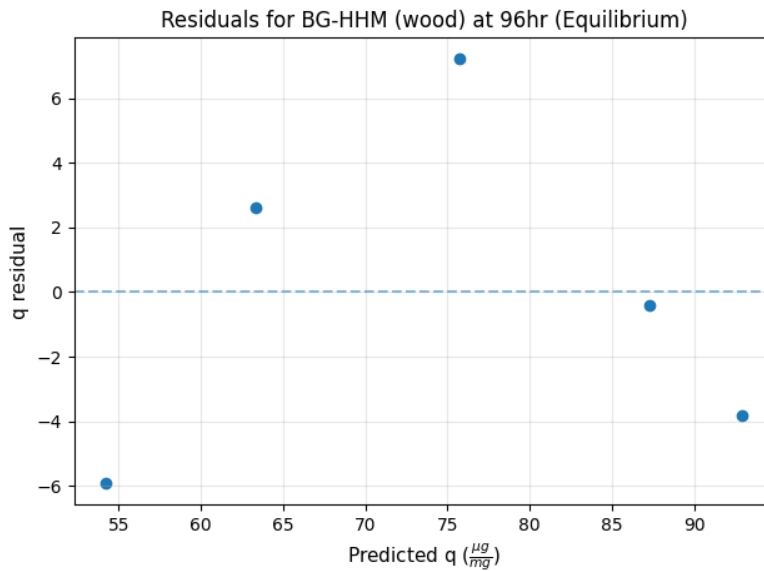
Figure C.28 Residual plot for Equilibrium (96h) isotherm of MC-LR adsorption by the BG-HHM (wood)

Table C.4 Equilibrium (48hr) carbon loading data for MC-LR adsorption by COL-PL60-800 (coal) in Lake Erie water

Sample	SPAC dose (mg/L)	Equilibrium MC-LR concentration (µg/L)	Equilibrium capacity, qe (µg/mg)
1	1	233.19	24.38
2	2	217.25	26.54
3	3	183.03	27.66
4	4	147.91	29.52
5	5.5	88.62	30.37
6	7	29.53	32.25
7	8.5	7.86	32.81
8	10	0.61	33.78
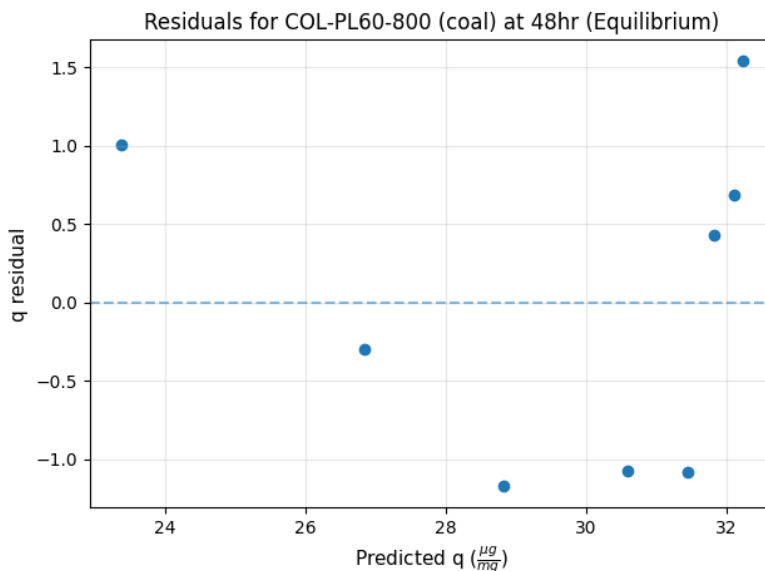
Figure C.29 Residual plot for Equilibrium (48h) isotherm of MC-LR adsorption by the COL-PL60-800 (coal)

Table C.4 Equilibrium (96hr) carbon loading data for MC-LR adsorption by COL-PL60-800 (coal) in Lake Erie water

Sample	SPAC dose (mg/L)	Equilibrium MC-LR concentration (µg/L)	Equilibrium capacity, qe (µg/mg)
1	1	235.99	21.67
2	2	222.65	26.55
3	3	183.17	27.61
4	4	145.54	30.01
5	5.5	83.85	30.12
6	7	24.53	30.73
7	8.5	4.82	33.12
8	10	0.55	34.5
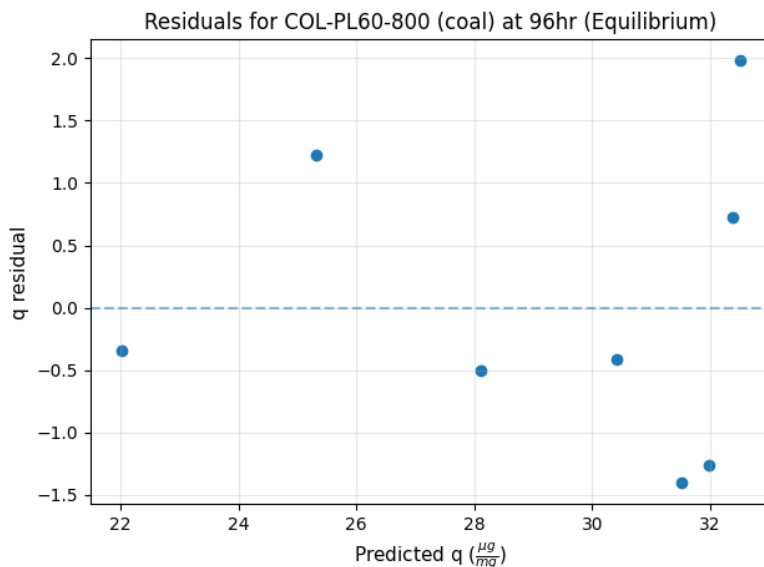
Figure C.30 Residual plot for Equilibrium (96h) isotherm of MC-LR adsorption by the COL-PL60-800 (coal)

Table C.5 Equilibrium (48hr) carbon loading data for MC-LR adsorption by WPC (coconut) in Lake Erie water

Sample	SPAC dose (mg/L)	Equilibrium MC-LR concentration (ug/L)	Equilibrium capacity, qe (µg/mg)
1	1	237.42	18.04
2	2	218.95	21.65
3	3	198.24	22.28
4	4	193.86	22.59
5	5.5	146.92	23.53
6	7	110.03	23.88
7	8.5	62.99	24.04
8	10	25.63	28.58
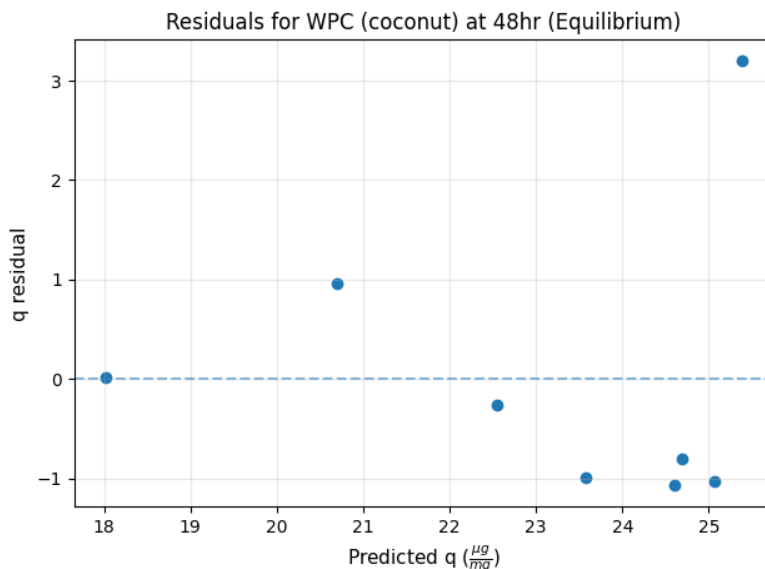
Figure C.31 Residual plot for Equilibrium (48h) isotherm of MC-LR adsorption by the WPC (coconut)

Table C.6 Equilibrium (96hr) carbon loading data for MC-LR adsorption by WPC (coconut) in Lake Erie water

Sample	SPAC dose (mg/L)	Equilibrium MC-LR concentration (µg/L)	Equilibrium capacity, q_e (µg/mg)
1	1	235.35	17.04
2	2	226.09	19.01
3	3	208.98	19.96
4	4	197.82	21.03
5	5.5	150.31	24.13
6	7	97.09	24.89
7	8.5	51.81	25.2
8	10	17.1	30.65
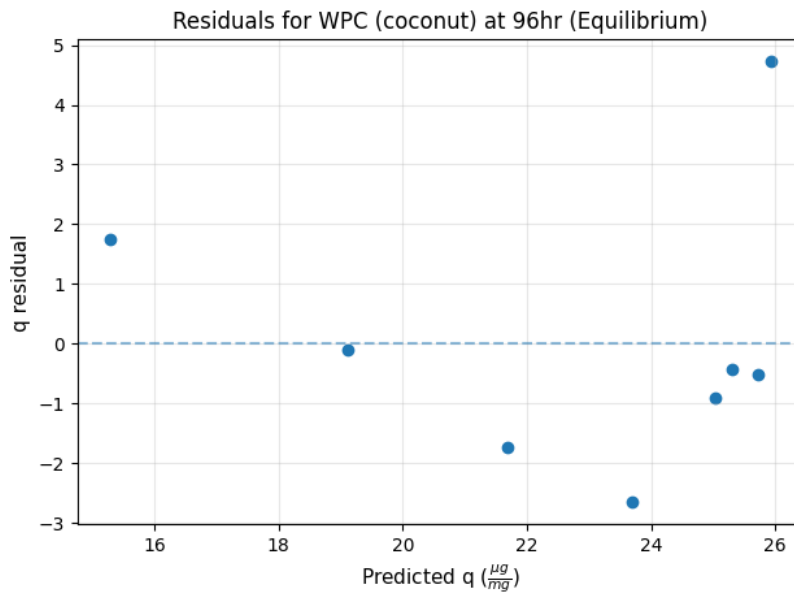
Figure C.32 Residual plot for Equilibrium (96h) isotherm of MC-LR adsorption by the WPC (coconut)
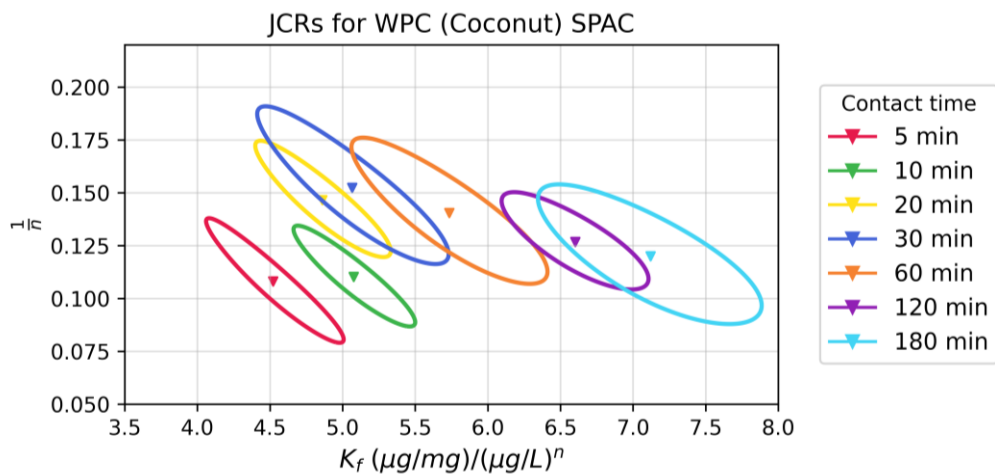
Figure C.33 JCRs at short contact times for WPC (coconut) in Lake Erie water
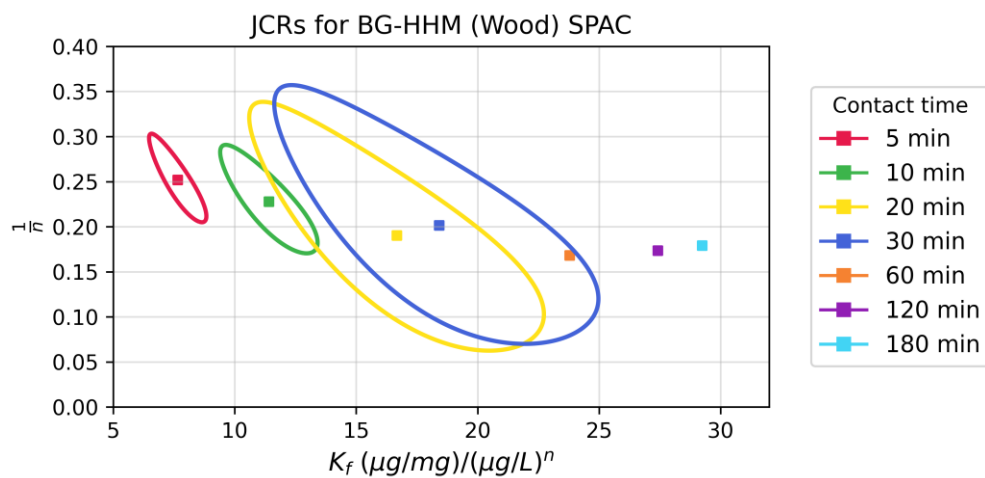
Figure C.34 JCRs at short contact times for BG-HHM (wood) in Lake Erie water
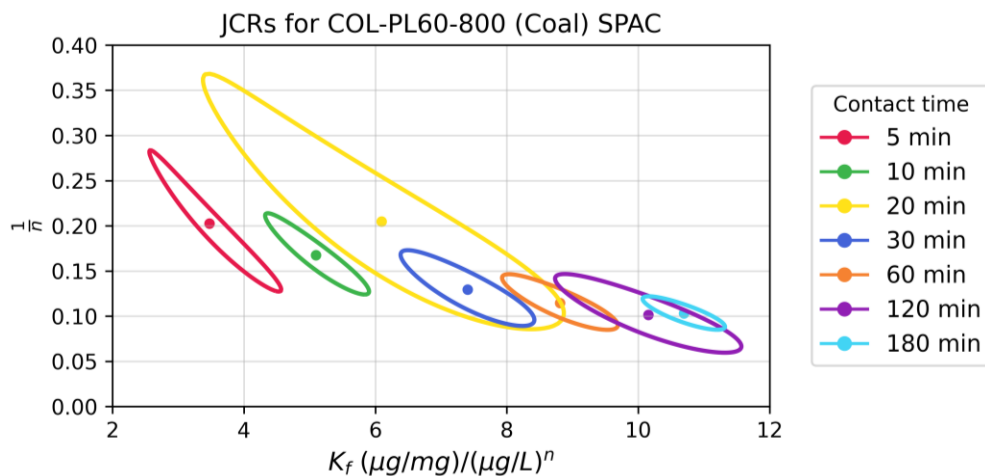
Figure C.35 JCRs at short contact times for COL-PL60-800 (coal) in Lake Erie water
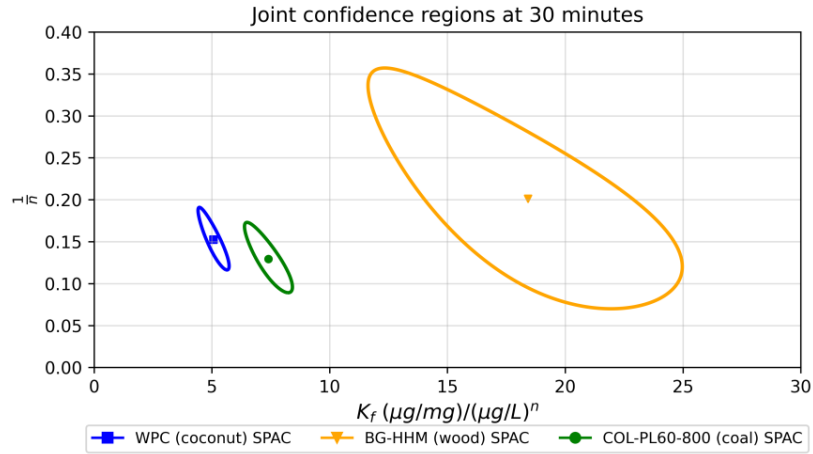
Figure C.36 Comparison of JCRs at contact time of 30 minutes
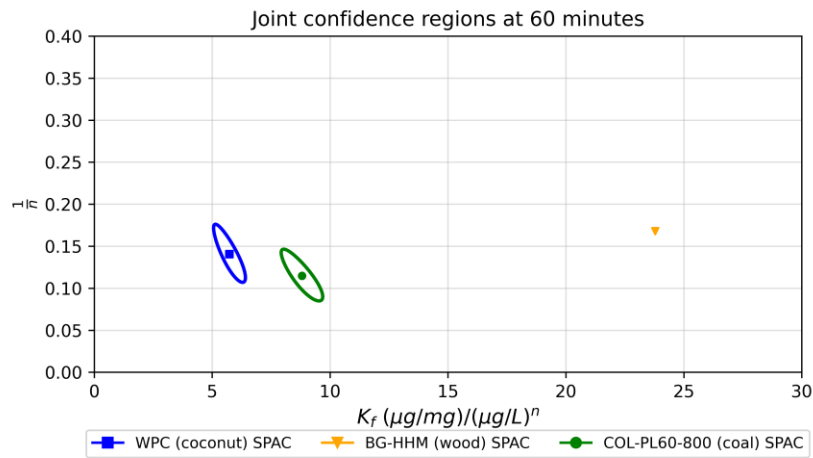
Figure C.37 Comparison of JCRs at contact time of 60 minutes
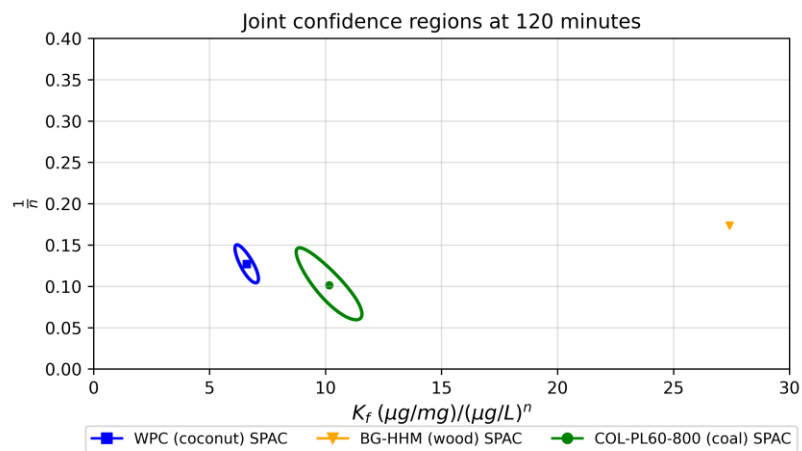
Figure C.38 Comparison of JCRs at contact time of 120 minutes

Appendix C.12 Best-fit Freundlich curves for SPACs in Lake Erie water compared to each other in contact times in range of 5-180 minutes
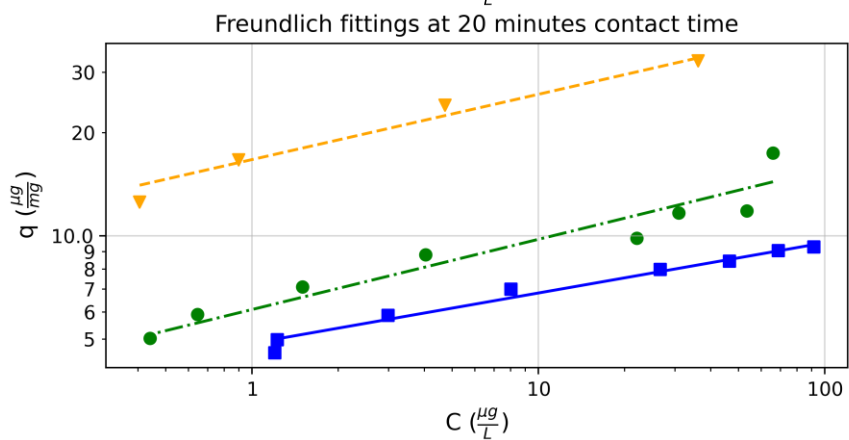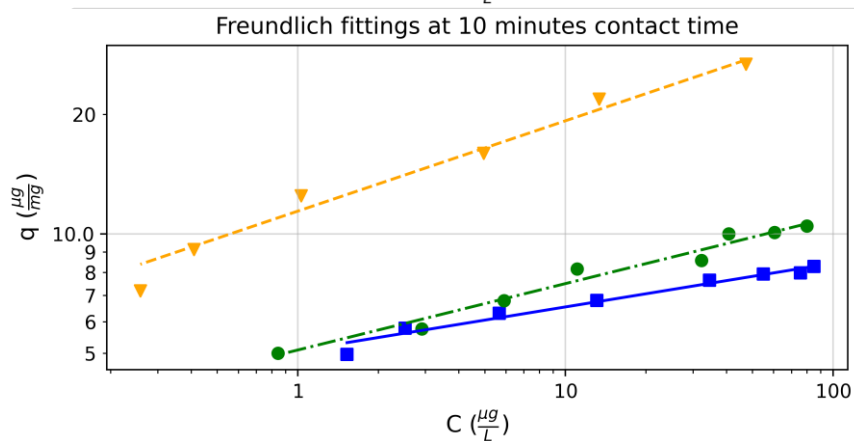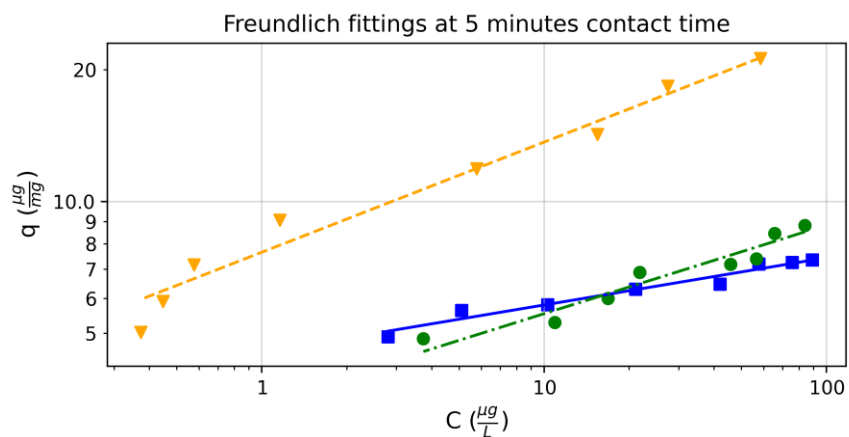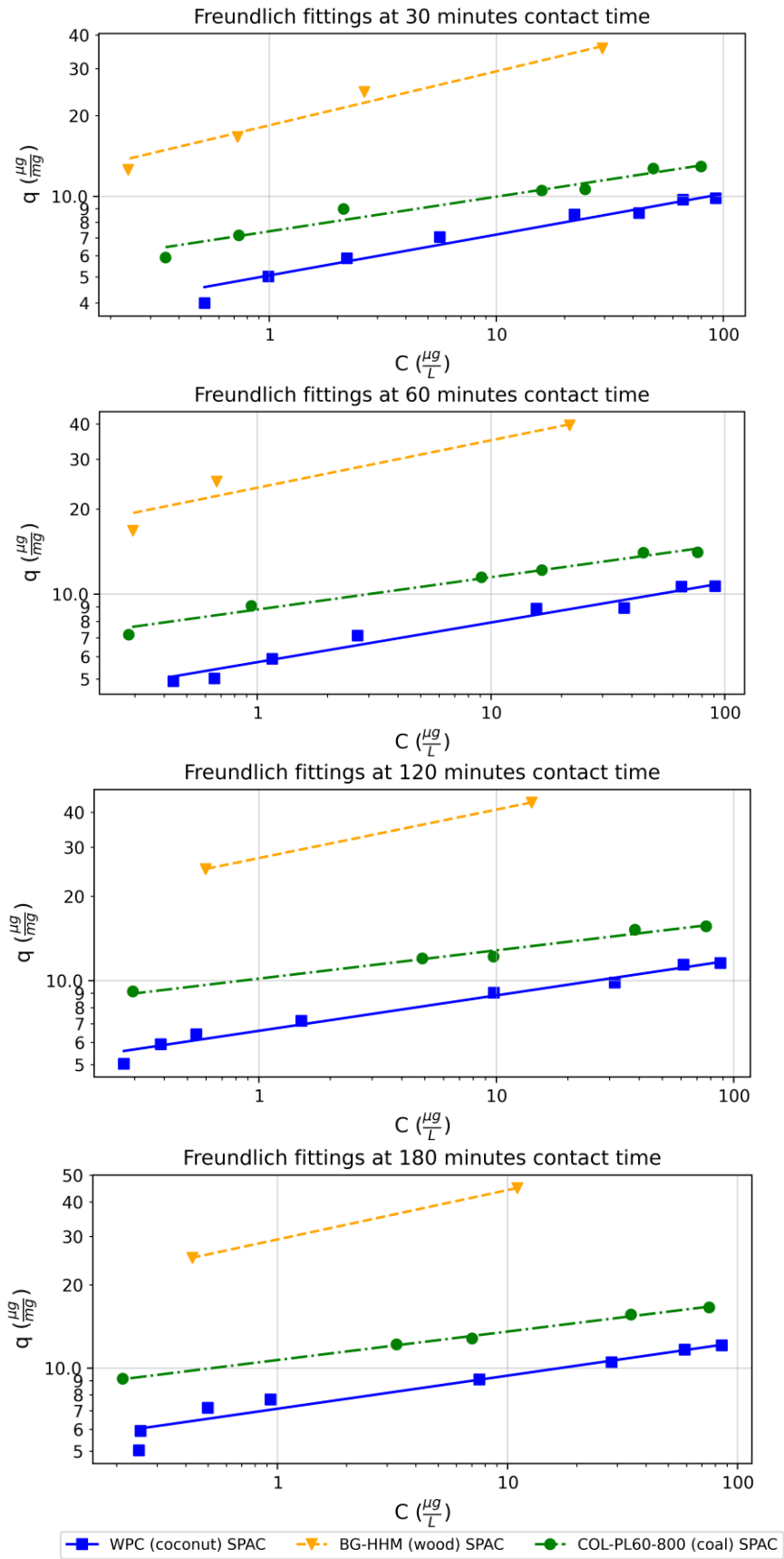
Figure C.39 Comparison of Freundlich fittings at contact times in range of 5 to 180 minutes

Appendix C.13 Isotherms in Lake Erie water at short contact times and residual plots

Table C.6 Carbon loading data for MC-LR adsorption by BG-HHM (wood) in ultrapure water at 5 minutes of contact

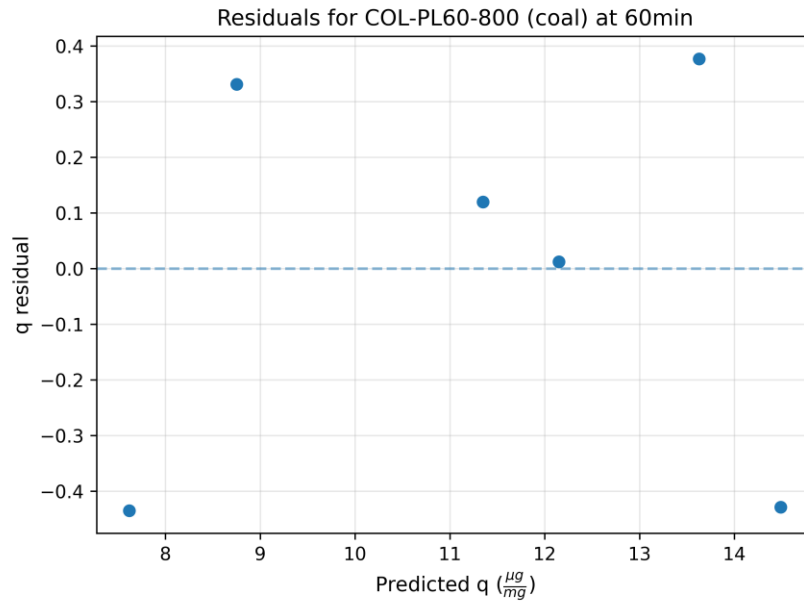| Sample	SPAC dose (mg/L)	Equilibrium MC-LR concentration (µg/L)	Equilibrium capacity, qe (µg/mg)
1	2	58.41	5.02
2	4	27.47	5.91
3	6	15.46	7.16
4	8	5.78	9.06
5	11	1.16	11.89
6	14	0.58	14.23
7	17	0.45	18.35
8	20	0.37	21.23
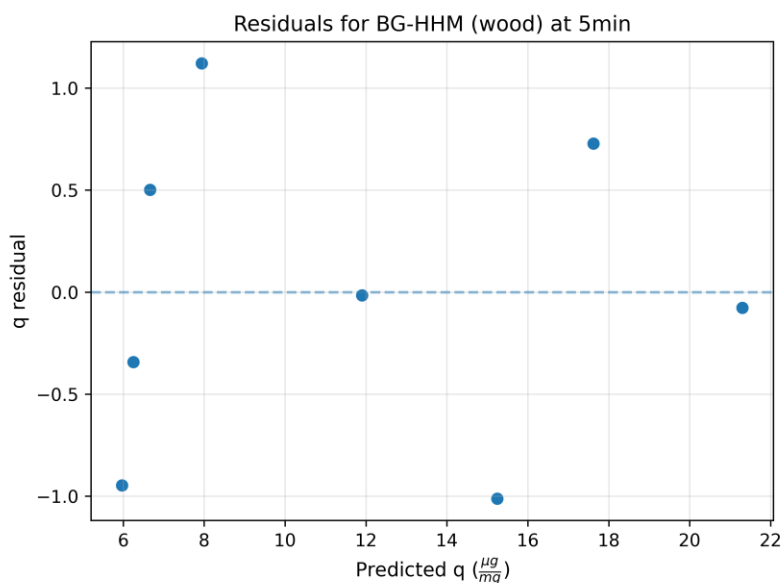
Figure C.40 Residual plot of Freundlich fitting for 5 min contact of MC-LR adsorption by the BG-HHM (wood)

228

Table C.7 Carbon loading data for MC-LR adsorption by BG-HHM (wood) in ultrapure water at 10 minutes of contact

Sample	SPAC dose (mg/L)	Equilibrium MC-LR concentration (µg/L)	Equilibrium capacity, qe (µg/mg)
1	2	47.29	7.19
2	4	13.39	9.13
3	6	4.95	12.48
4	8	1.03	15.98
5	11	0.41	21.87
6	14	0.26	26.78
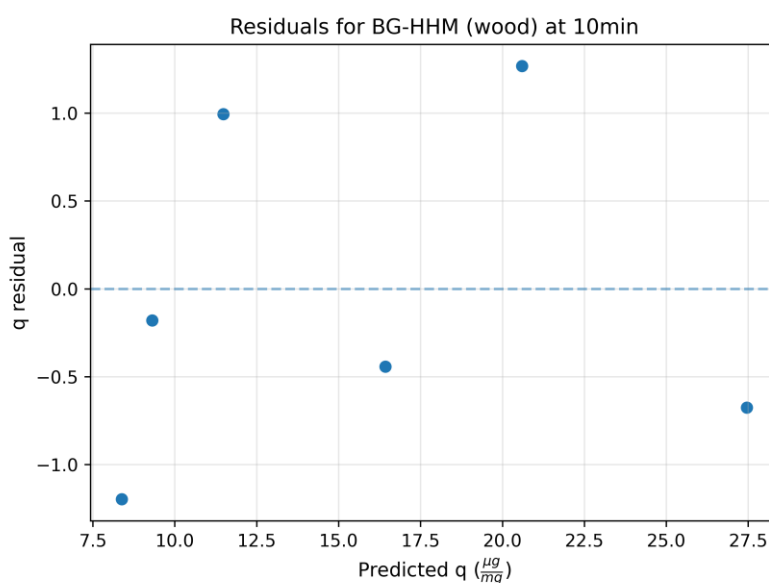
Figure C.41 Residual plot of Freundlich fitting for 10 min contact of MC-LR adsorption by the BG-HHM (wood)

Table C.8 Carbon loading data for MC-LR adsorption by BG-HHM (wood) in ultrapure water at 20 minutes of contact

Sample	SPAC dose (mg/L)	Equilibrium MC-LR concentration (µg/L)	Equilibrium capacity, qe (µg/mg)
1	2	36.12	12.56
2	4	4.72	16.66
3	6	0.9	24.04
4	8	0.41	32.37
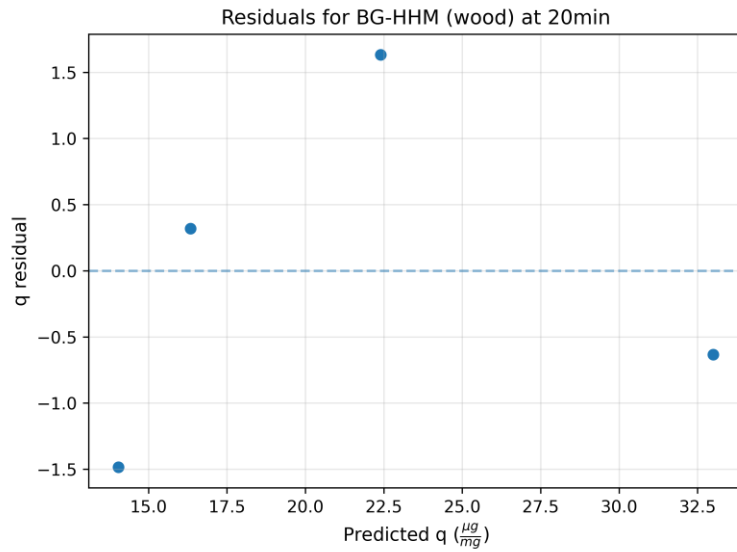
Figure C.42 Residual plot of Freundlich fitting for 20 min contact of MC-LR adsorption by the BG-HHM (wood)

Table C.9 Carbon loading data for MC-LR adsorption by BG-HHM (wood) in ultrapure water at 30 minutes of contact

Sample	SPAC dose (mg/L)	Equilibrium MC-LR concentration (µg/L)	Equilibrium capacity, qe (µg/mg)
1	2	29.34	12.58
2	4	2.62	16.69
3	6	0.73	24.56
4	8	0.24	35.76
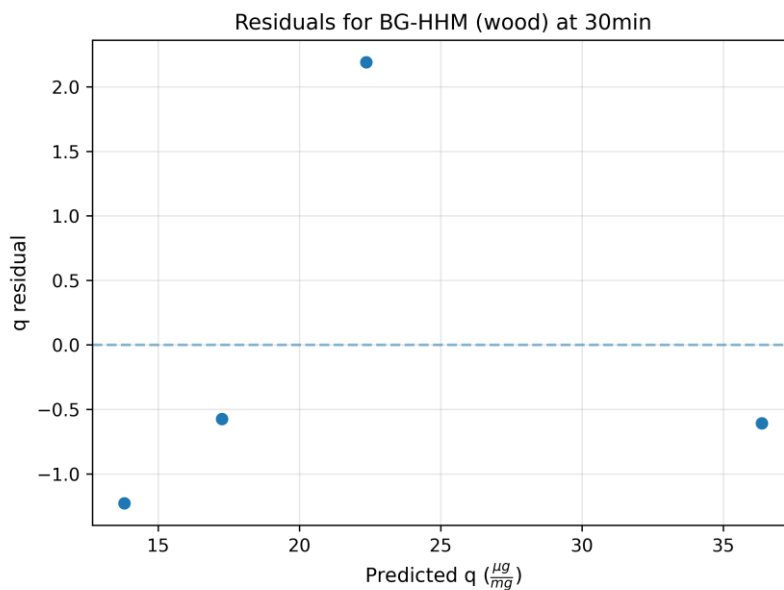
Figure C.43 Residual plot of Freundlich fitting for 30 min contact of MC-LR adsorption by the BG-HHM (wood)

Table C.10 Carbon loading data for MC-LR adsorption by BG-HHM (wood) in ultrapure water at 60 minutes of contact

Sample	SPAC dose (mg/L)	Equilibrium MC-LR concentration (µg/L)	Equilibrium capacity, qe (µg/mg)
1	2	21.68	16.76
2	4	0.67	25.05
3	6	0.29	39.59
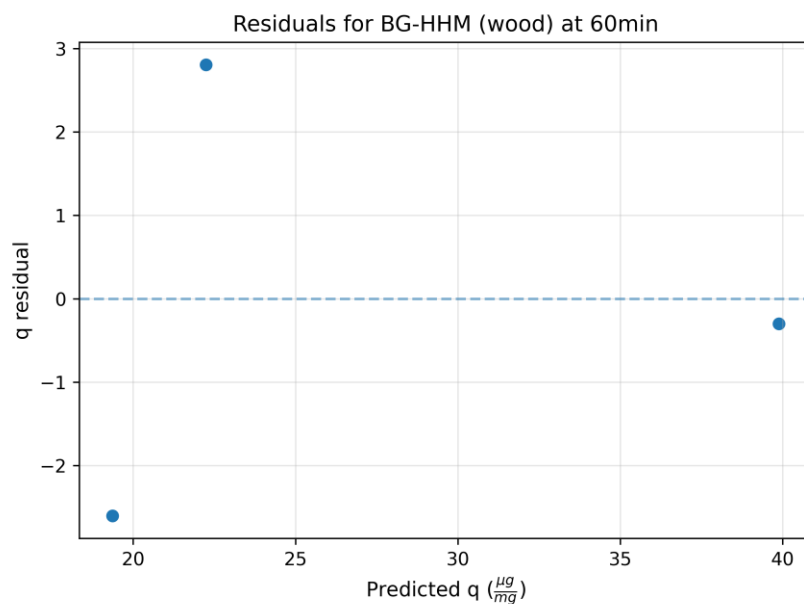
Figure C.44 Residual plot of Freundlich fitting for 60 min contact of MC-LR adsorption by the BG-HHM (wood)

Table C.11 Carbon loading data for MC-LR adsorption by BG-HHM (wood) in ultrapure water at 120 minutes of contact

Sample	SPAC dose (mg/L)	Equilibrium MC-LR concentration (µg/L)	Equilibrium capacity, qe (µg/mg)
1	2	14.1	25.07
2	4	0.6	43.38
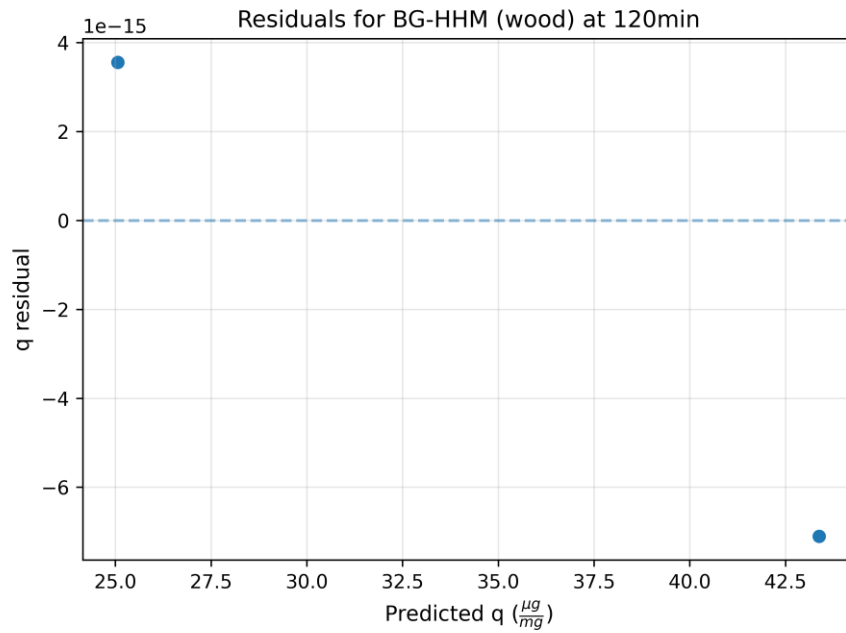
Figure C.45 Residual plot of Freundlich fitting for 120 min contact of MC-LR adsorption by the BG-HHM (wood)

Table C.12 Carbon loading data for MC-LR adsorption by BG-HHM (wood) in ultrapure water at 180 minutes of contact
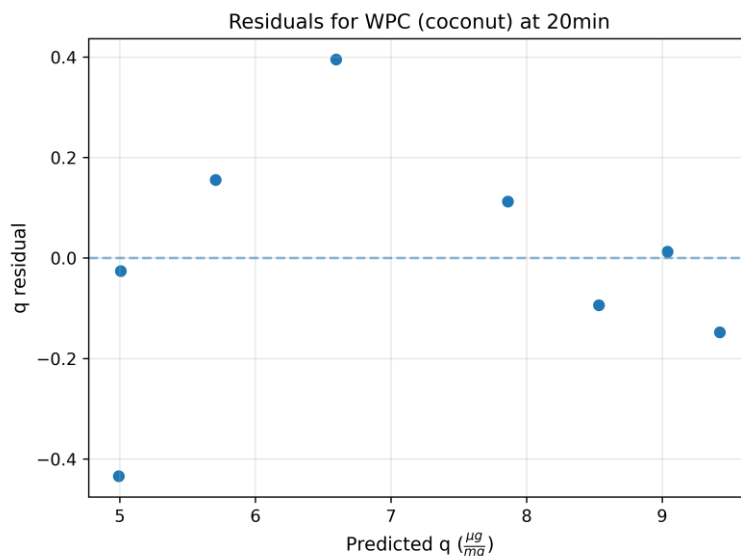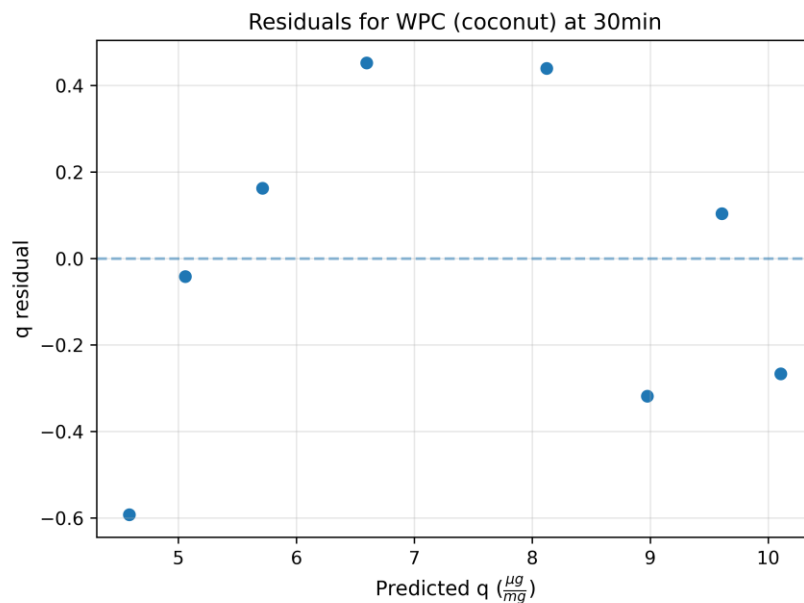
Sample	SPAC dose (mg/L)	Equilibrium MC-LR concentration (µg/L)	Equilibrium capacity, qe (µg/mg)
1	2	11.02	25.11
2	4	0.43	44.92
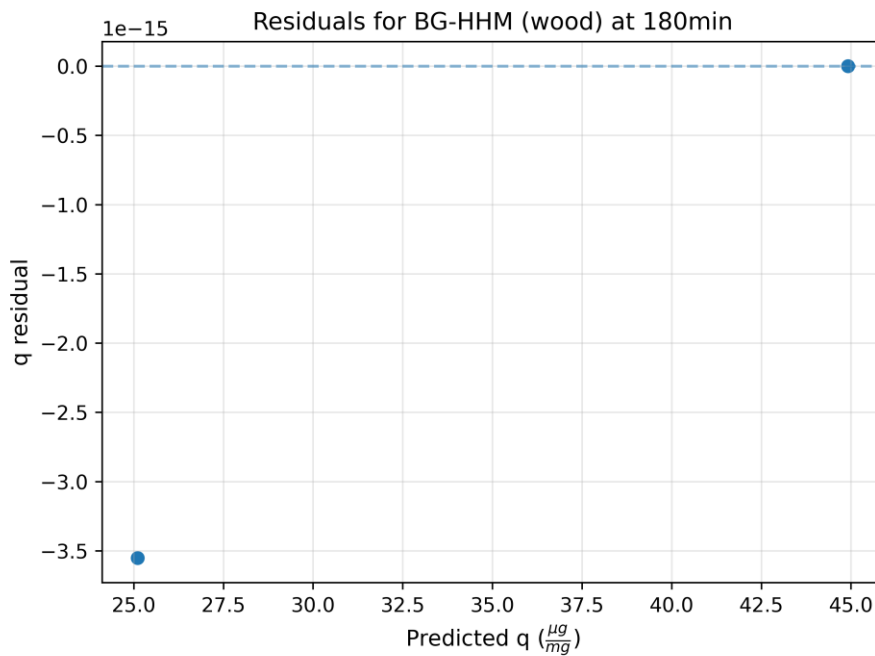
Figure C.46 Residual plot of Freundlich fitting for 180 min contact of MC-LR adsorption by the BG-HHM (wood)

232

Table C.13 Carbon loading data for MC-LR adsorption by COL-PL60-800 (coal) in ultrapure water at 5 minutes of contact

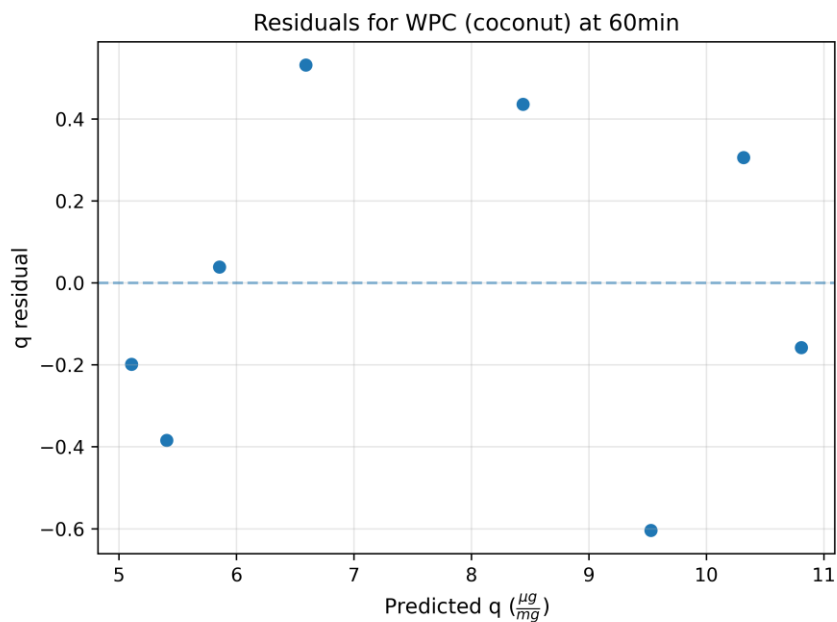| Sample	SPAC dose (mg/L)	Equilibrium MC-LR concentration (µg/L)	Equilibrium capacity, qe (µg/mg)
1	2	83.96	4.86
2	4	65.6	5.29
3	6	56.5	6
4	8	45.79	6.88
5	11	21.83	7.18
6	14	16.85	7.39
7	17	10.91	8.45
8	20	3.74	8.82
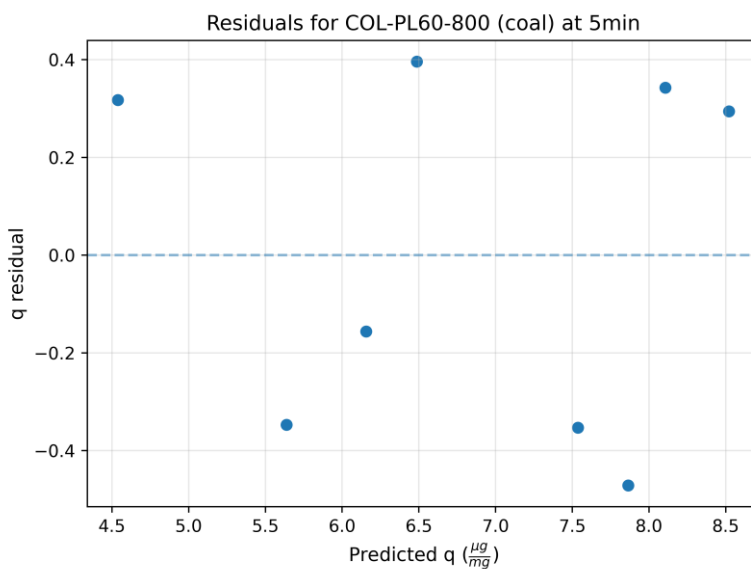
Figure C.47 Residual plot of Freundlich fitting for 5 min contact of MC-LR adsorption by the COL-PL60-800 (coal)

Table C.14 Carbon loading data for MC-LR adsorption by COL-PL60-800 (coal) in ultrapure water at 10 minutes of contact

Sample	SPAC dose (mg/L)	Equilibrium MC-LR concentration (µg/L)	Equilibrium capacity, qe (µg/mg)
1	2	79.92	5
2	4	60.52	5.76

233

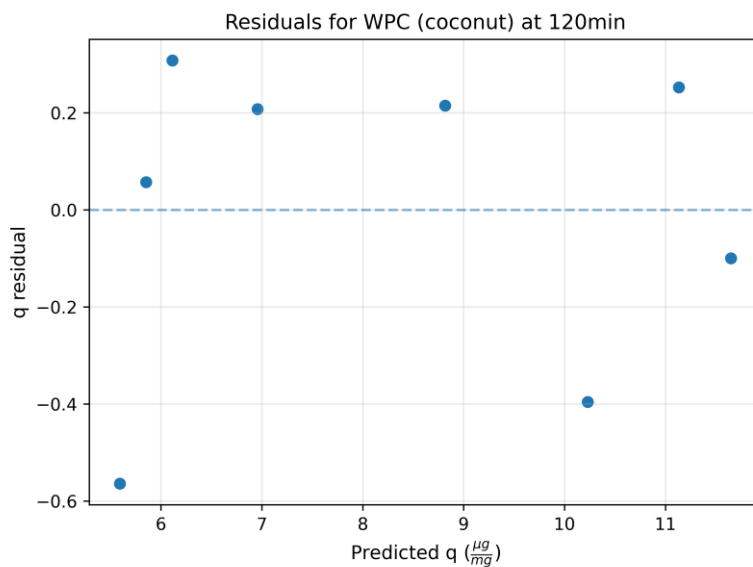|			
3	6	40.82	6.78
4	8	32.28	8.16
5	11	11.07	8.57
6	14	5.91	10.01
7	17	2.91	10.09
8	20	0.84	10.47

Residuals for COL-PL60-800 (coal) at 10min
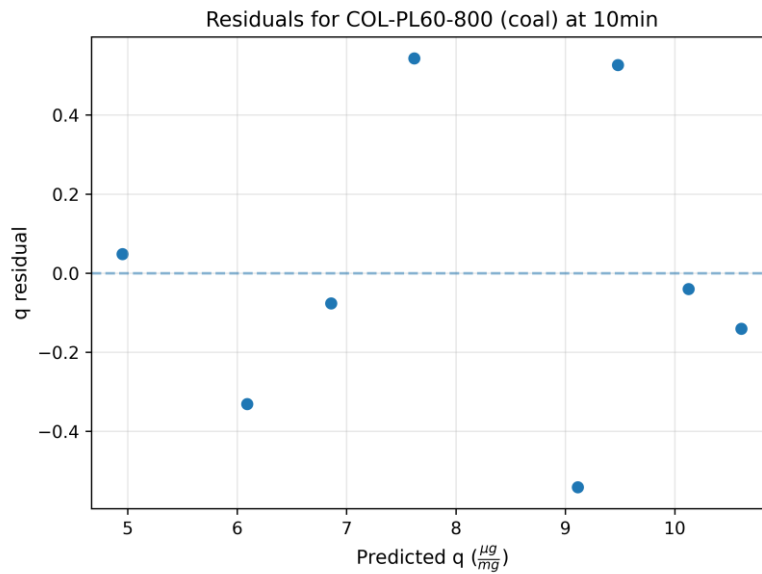
Figure C.48 Residual plot of Freundlich fitting for 10 min contact of MC-LR adsorption by the COL-PL60-800 (coal)

Table C.15 Carbon loading data for MC-LR adsorption by COL-PL60-800 (coal) in ultrapure water at 20 minutes of contact

Sample	SPAC dose (mg/L)	Equilibrium MC-LR concentration (µg/L)	Equilibrium capacity, qe (µg/mg)
1	2	66.02	5.02
2	4	53.57	5.89
3	6	30.97	7.1
4	8	22.11	8.8
5	11	4.04	9.84
6	14	1.50	11.65
7	17	0.65	11.82
8	20	0.44	17.42
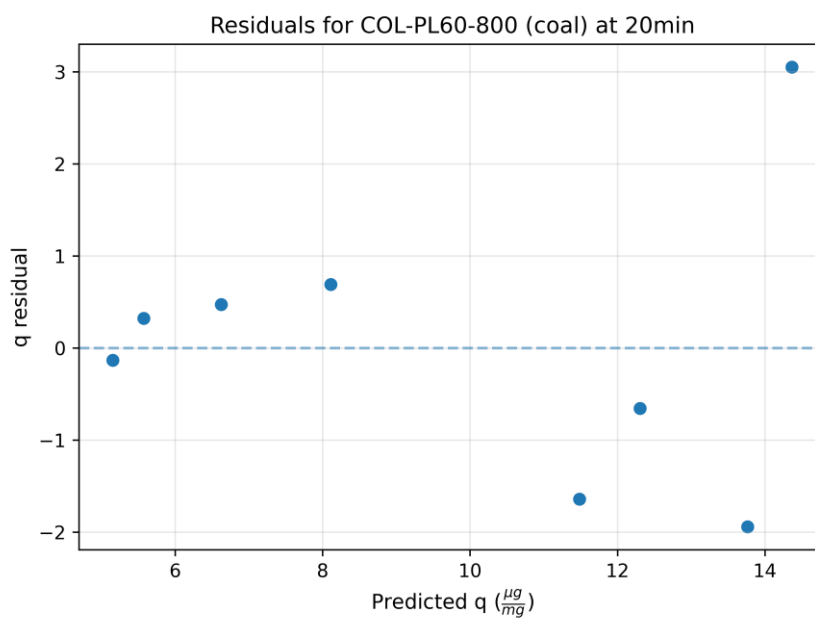
Figure C.49 Residual plot of Freundlich fitting for 20 min contact of MC-LR adsorption by the COL-PL60-800 (coal)

Table C.16 Carbon loading data for MC-LR adsorption by COL-PL60-800 (coal) in ultrapure water at 30 minutes of contact

Sample	SPAC dose (mg/L)	Equilibrium MC-LR concentration (µg/L)	Equilibrium capacity, qe (µg/mg)
1	2	79.83	5.91
2	4	49.17	7.15
3	6	24.65	8.98
4	8	15.88	10.51
5	11	2.13	10.62
6	14	0.73	12.7
7	17	0.35	12.92
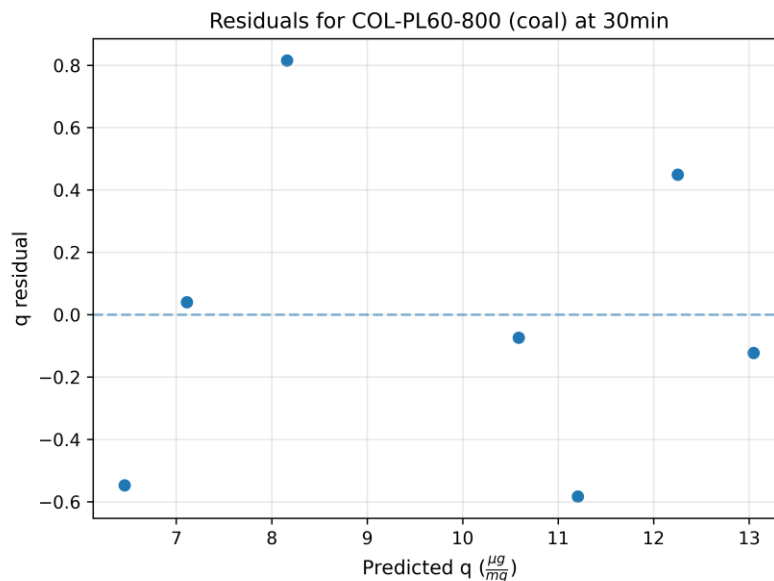
Figure C.50 Residual plot of Freundlich fitting for 30 min contact of MC-LR adsorption by the COL-PL60-800 (coal)

Table C.17 Carbon loading data for MC-LR adsorption by COL-PL60-800 (coal) in ultrapure water at 60 minutes of contact

Sample	SPAC dose (mg/L)	Equilibrium MC-LR concentration (µg/L)	Equilibrium capacity, qe (µg/mg)
1	2	76.53	7.18
2	4	44.84	9.08
3	6	16.5	11.47
4	8	9.11	12.16
5	11	0.94	14
6	14	0.28	14.06

Figure C.51 Residual plot of Freundlich fitting for 60 min contact of MC-LR adsorption by the COL-PL60-800 (coal)

Table C.18 Carbon loading data for MC-LR adsorption by COL-PL60-800 (coal) in ultrapure water at 120 minutes of contact

Sample	SPAC dose (mg/L)	Equilibrium MC-LR concentration (μg/L)	Equilibrium capacity, qe (μg/mg)
1	2	76.51	9.14
2	4	38.34	12
3	6	9.73	12.18
4	8	4.88	15.19
5	11	0.29	15.63
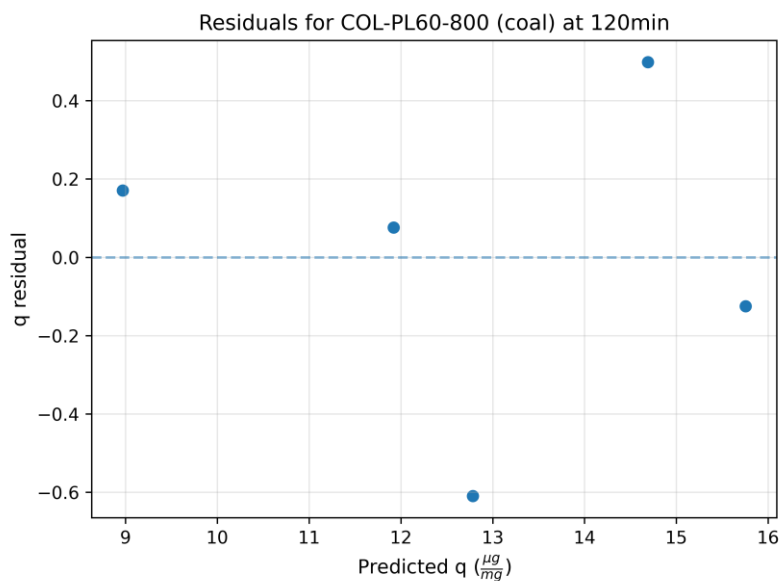
Figure C.52 Residual plot of Freundlich fitting for 120 min contact of MC-LR adsorption by the COL-PL60-800 (coal)

Table C.19 Carbon loading data for MC-LR adsorption by COL-PL60-800 (coal) in ultrapure water at 180 minutes of contact

Sample	SPAC dose (mg/L)	Equilibrium MC-LR concentration (μg/L)	Equilibrium capacity, qe (μg/mg)
1	2	75.26	9.15
2	4	34.43	12.2
3	6	7.02	12.8
4	8	3.29	15.64
5	11	0.21	16.61
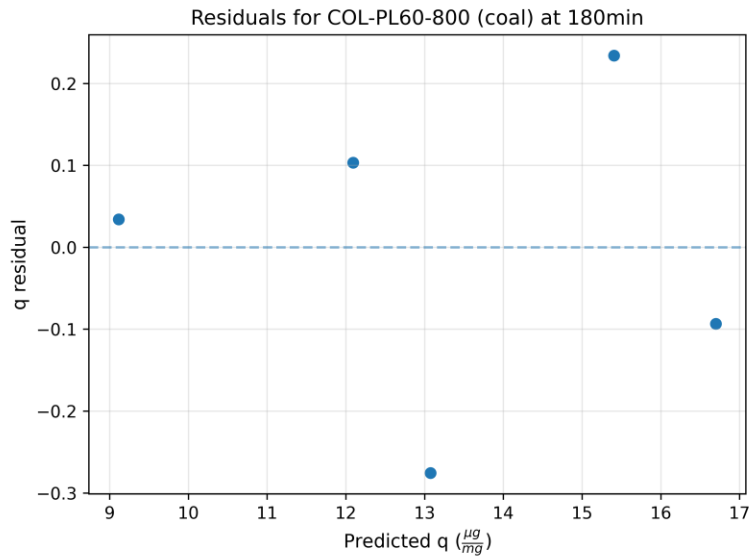
Figure C.53 Residual plot of Freundlich fitting for 180 min contact of MC-LR adsorption by the COL-PL60-800 (coal)

Table C.20 Carbon loading data for MC-LR adsorption by WPC (coconut) in ultrapure water at 5 minutes of contact

Sample	SPAC dose (mg/L)	Equilibrium MC-LR concentration (µg/L)	Equilibrium capacity, qe (µg/mg)
1	2	89.25	4.9
2	4	75.67	5.63
3	6	57.71	5.8
4	8	42.05	6.3
5	11	21.09	6.47
6	14	10.31	7.19
7	17	5.11	7.25
8	20	2.81	7.35
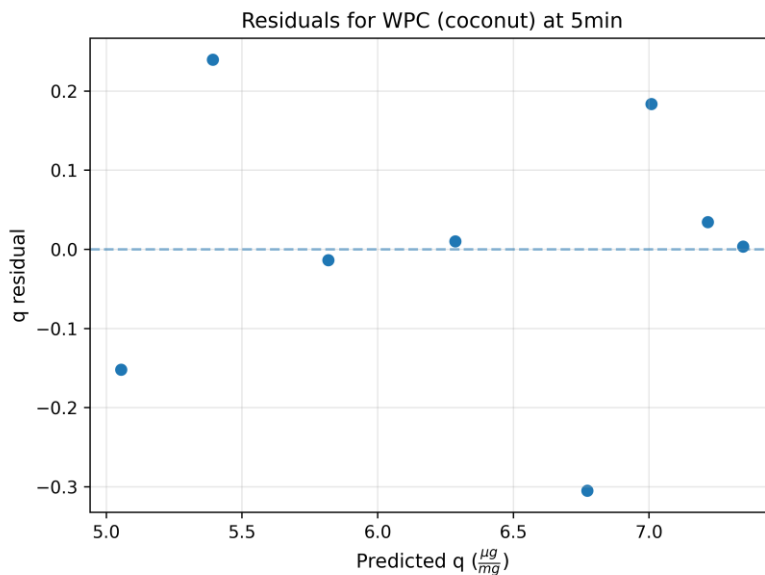
Figure C.54 Residual plot of Freundlich fitting for 5 min contact of MC-LR adsorption by the WPC (coconut)

Table C.21 Carbon loading data for MC-LR adsorption by WPC (coconut) in ultrapure water at 10 minutes of contact

Sample	SPAC dose (mg/L)	Equilibrium MC-LR concentration (µg/L)	Equilibrium capacity, qe (µg/mg)
1	2	85.02	4.97
2	4	75.62	5.78
3	6	55.02	6.31
4	8	34.61	6.8
5	11	13.11	7.64
6	14	5.67	7.92
7	17	2.52	7.98
8	20	1.53	8.28
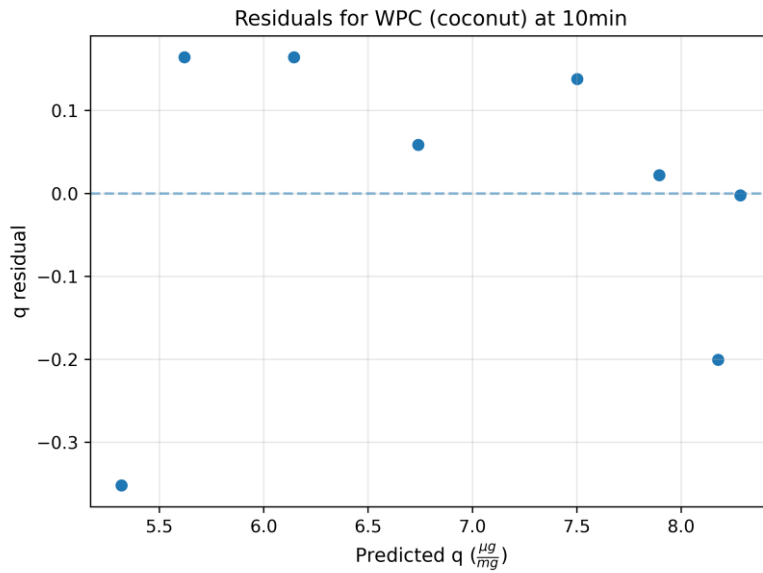
Figure C.55 Residual plot of Freundlich fitting for 10 min contact of MC-LR adsorption by the WPC (coconut)

Table C.22 Carbon loading data for MC-LR adsorption by WPC (coconut) in ultrapure water at 20 minutes of contact

Sample	SPAC dose (mg/L)	Equilibrium MC-LR concentration (µg/L)	Equilibrium capacity, qe (µg/mg)
1	2	91.74	4.56
2	4	68.96	4.98
3	6	46.55	5.86
4	8	26.64	6.99
5	11	8.03	7.98
6	14	2.99	8.44
7	17	1.2	9.05
8	20	1.23	9.28

Figure C.56 Residual plot of Freundlich fitting for 20 min contact of MC-LR adsorption by the WPC (coconut)

Table C.23 Carbon loading data for MC-LR adsorption by WPC (coconut) in ultrapure water at 30 minutes of contact

Sample	SPAC dose (mg/L)	Equilibrium MC-LR concentration (µg/L)	Equilibrium capacity, qe (µg/mg)
1	2	92.88	3.99
2	4	66.61	5.02
3	6	42.6	5.87
4	8	22.15	7.05
5	11	5.65	8.56
6	14	2.2	8.66
7	17	0.99	9.71
8	20	0.52	9.84

Figure C.57 Residual plot of Freundlich fitting for 30 min contact of MC-LR adsorption by the WPC (coconut)

Table C.24 Carbon loading data for MC-LR adsorption by WPC (coconut) in ultrapure water at 60 minutes of contact

Sample	SPAC dose (mg/L)	Equilibrium MC-LR concentration (µg/L)	Equilibrium capacity, qe (µg/mg)
1	2	91.05	4.91
2	4	65.36	5.02
3	6	37.12	5.89
4	8	15.66	7.12
5	11	2.69	8.88
6	14	1.16	8.92
7	17	0.66	10.62
8	20	0.44	10.65

Figure C.58 Residual plot of Freundlich fitting for 60 min contact of MC-LR adsorption by the WPC (coconut)

Table C.25 Carbon loading data for MC-LR adsorption by WPC (coconut) in ultrapure water at 120 minutes of contact

Sample	SPAC dose (mg/L)	Equilibrium MC-LR concentration (µg/L)	Equilibrium capacity, qe (µg/mg)
1	2	88.02	5.03
2	4	61.53	5.91
3	6	31.56	6.42
4	8	9.78	7.17
5	11	1.51	9.03
6	14	0.55	9.83
7	17	0.39	11.38
8	20	0.27	11.55

Figure C.59 Residual plot of Freundlich fitting for 120 min contact of MC-LR adsorption by the WPC (coconut)

Table C.26 Carbon loading data for MC-LR adsorption by WPC (coconut) in ultrapure water at 180 minutes of contact

Sample	SPAC dose (mg/L)	Equilibrium MC-LR concentration (µg/L)	Equilibrium capacity, qe (µg/mg)
1	2	85.47	5.03
2	4	58.91	5.92
3	6	28.38	7.17
4	8	7.55	7.69
5	11	0.93	9.08
6	14	0.5	10.49
7	17	0.25	11.66
8	20	0.25	12.08
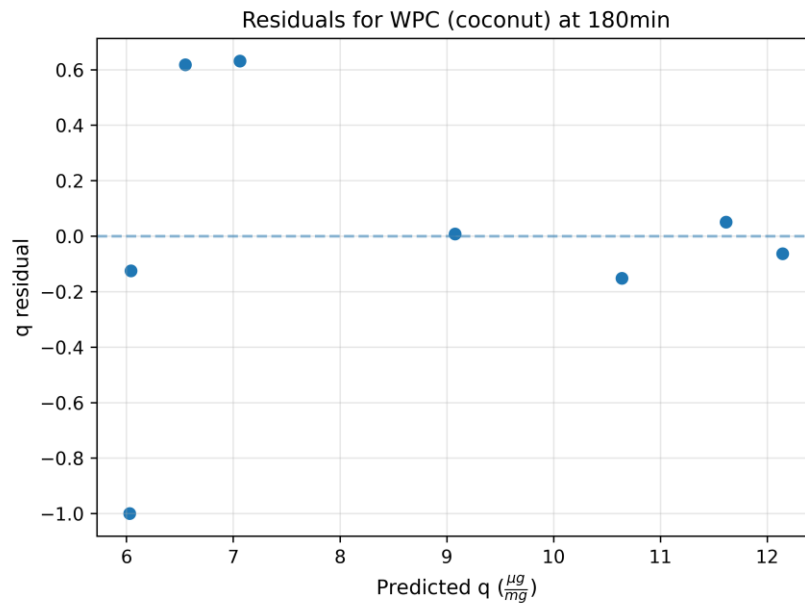
Figure C.60 Residual plot of Freundlich fitting for 180 min contact of MC-LR adsorption by the WPC (coconut)

Appendix C.14 Joint confidence regions for SPACs and parent PACs at 30 and 60 minutes of contact time in Lake Erie water
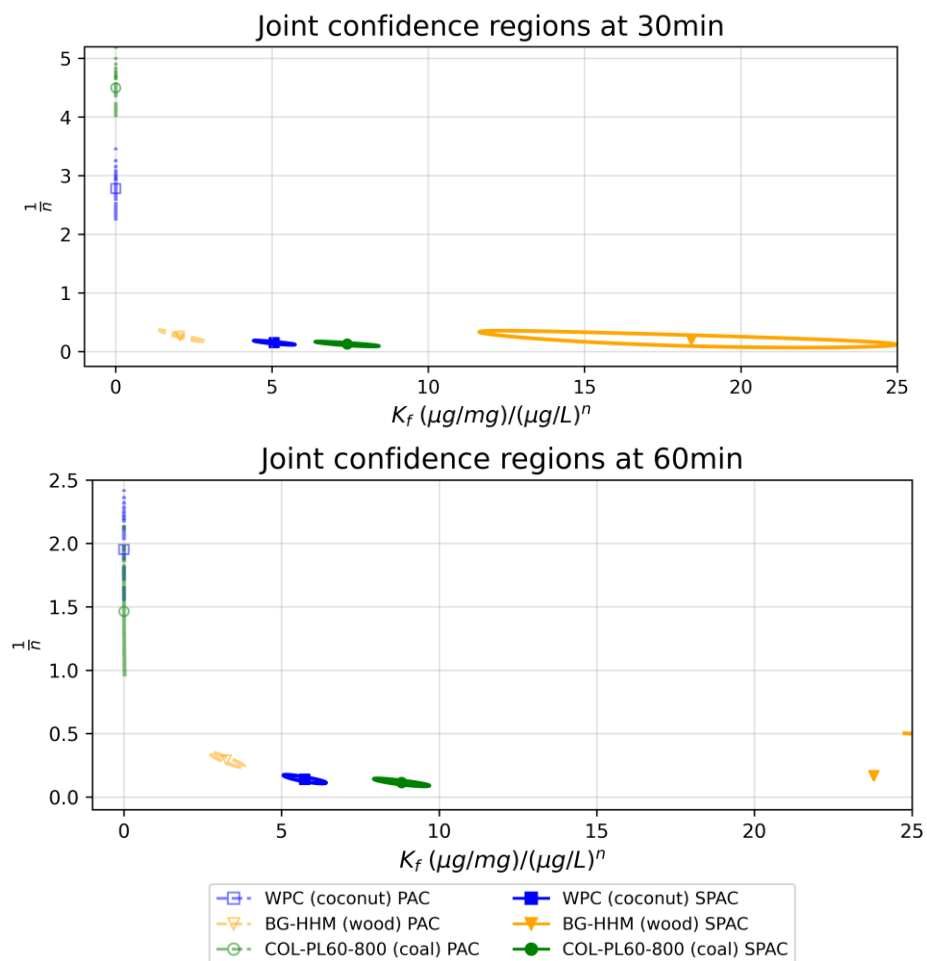
Figure C.61 JCRs of SPACs compared with parent PACs (Liu, 2017) at contact times of 30 and 60 minutes

Appendix C.15 DOC value before and after adsorption, SPAC dose: 20 mg/L
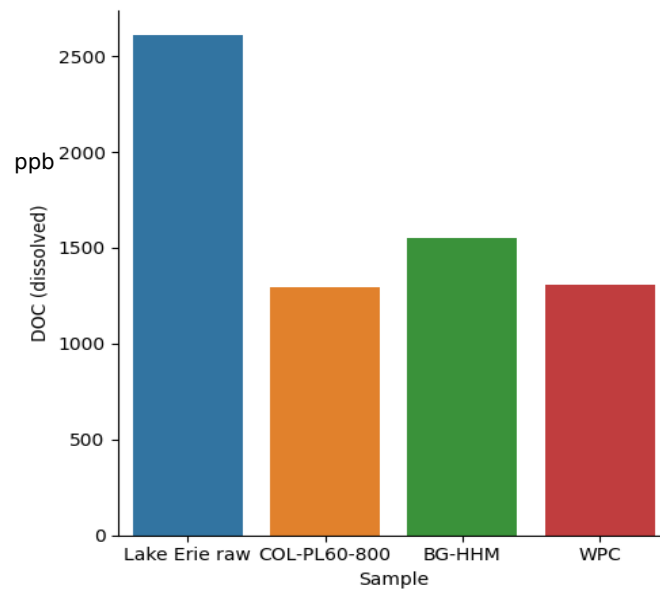
Figure C.62 DOC concentration before and after adsorption with SPAC dose of 20 mg/L

Appendix C.16 SEBCM at contact times of 60 and 120 minutes
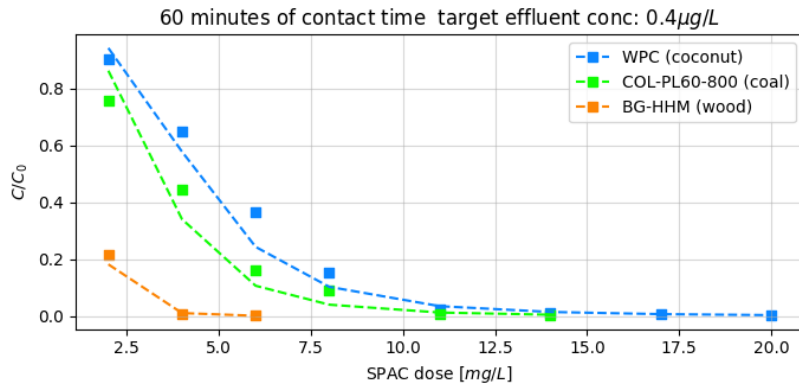
Figure C.63 SEBCM goodness of fit at 60 minutes of contact time
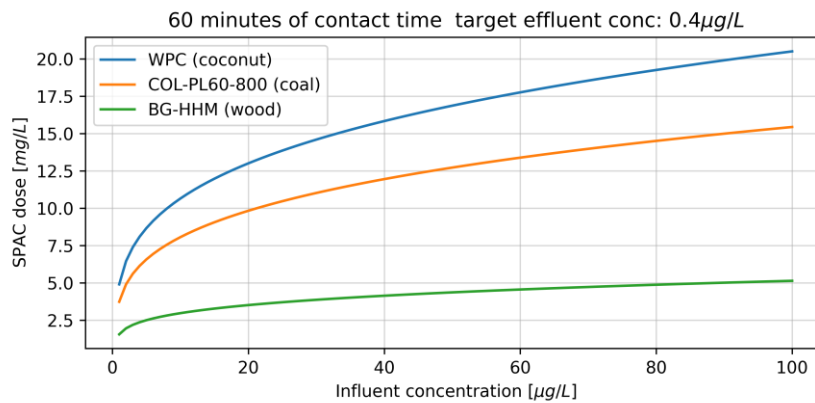
Figure C.64 Predicted SPAC doses for reduction of MC-LR influent concentration to the target concentration of 0.4 µg/L at 60 minutes of contact time
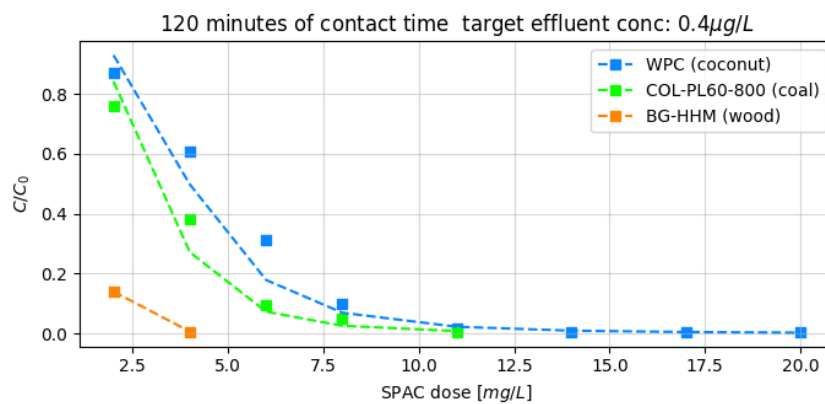
Figure C.65 SEBCM goodness of fit at 120 minutes of contact time
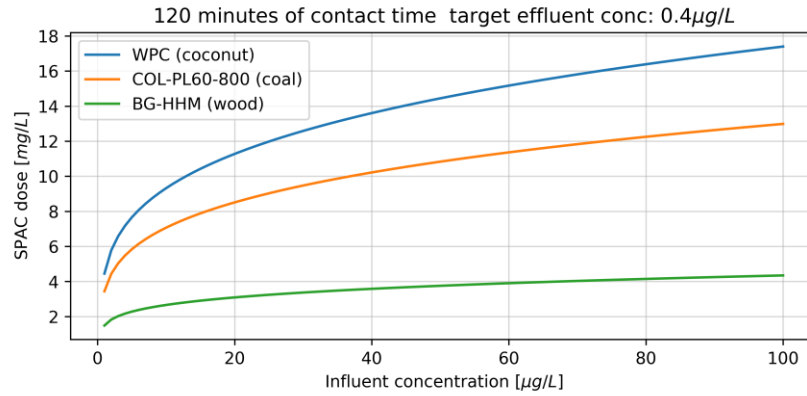
Figure C.66 Predicted SPAC doses for reduction of MC-LR influent concentration to the target concentration of 0.4 µg/L at 120 minutes of contact time

Table C.27 SEBCM parameters for the SPACs in Lake Erie water at contact times of 60 and 120 minutes

SPAC	Contact time	Number of data points	A	$1/n$	R^2
WPC (coconut-based)	60 minutes	8	193.15	3.57	0.989
	120 minutes	8	179.27	3.75	0.986
BG-HHM (wood-based)	60 minutes	3	4.29	4.26	0.980
	120 minutes	2	4.44	4.77	1.000
COL-PL60-800 (coal-based)	60 minutes	6	75.88	3.60	0.967
	120 minutes	5	77.03	3.85	0.964

Appendix C.17 SEBCM results at equilibrium
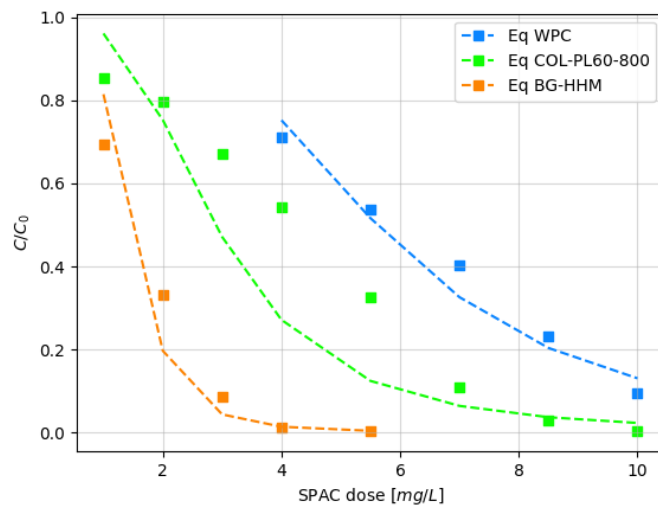
Figure C.67 SEBCM goodness of fit at equilibrium
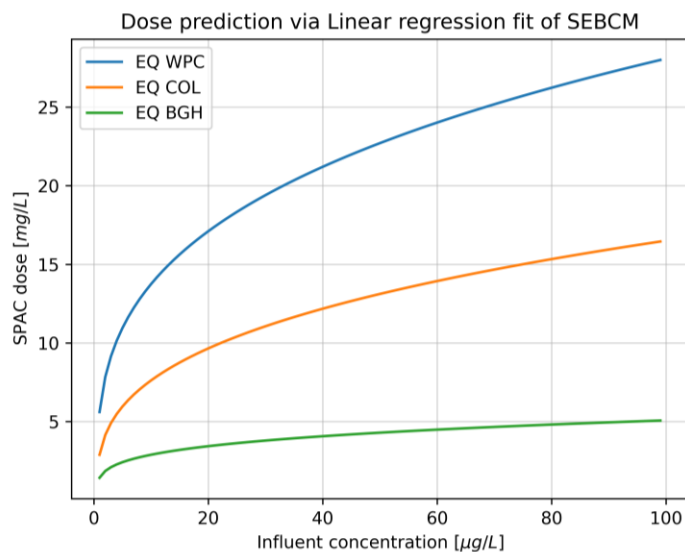
Figure C.68 Predicted SPAC doses for reduction of MC-LR influent concentration to the target concentration of 0.4 μg/L at 120 minutes of contact time

Table C.28 SEBCM parameters for the SPACs in Lake Erie water at equilibrium (96h contact)

SPAC	Contact time	Number of data points	A	$1/n$	R^2
WPC (coconut-based)	96 h	5	13.29	1.78	0.89
BG-HHM (wood-based)	96 h	5	3.79	4.31	0.967
COL-PL60-800 (coal-based)	96h	8	27.05	3.18	0.887

251

Appendix D

Additional information for chapter 6

Appendix D.1 G-curves for B-KER and Phips & Bird Jar tester apparatus
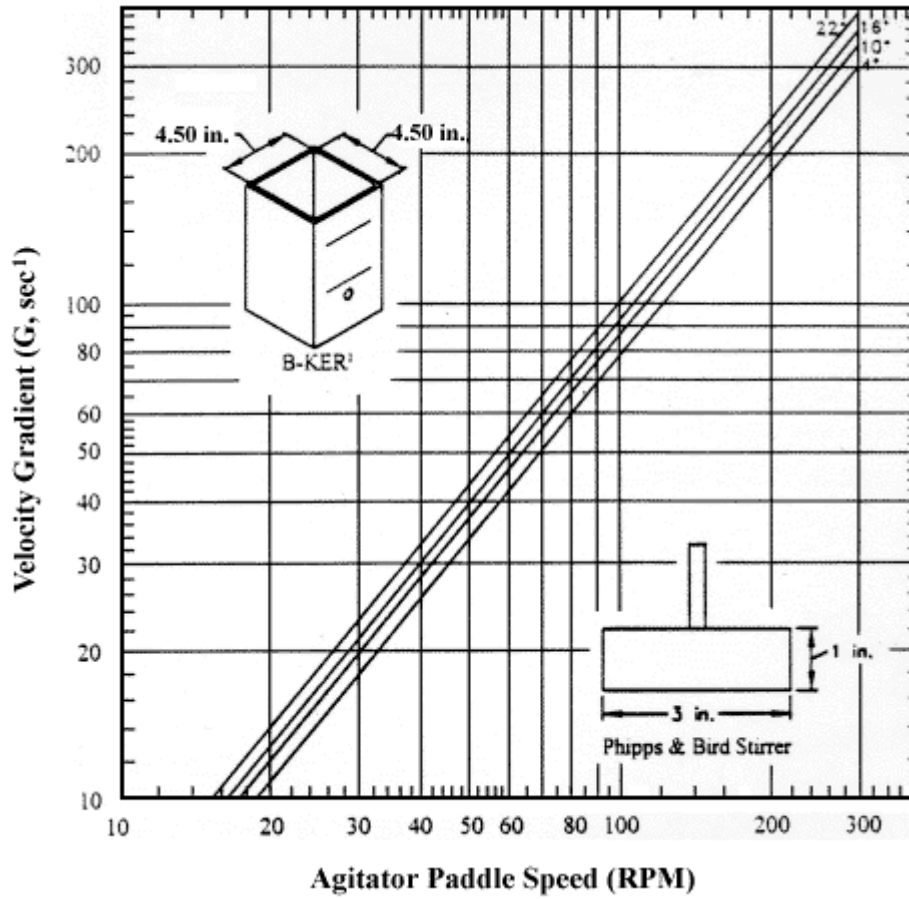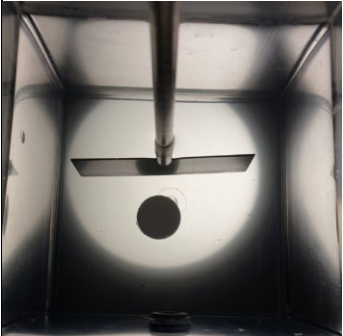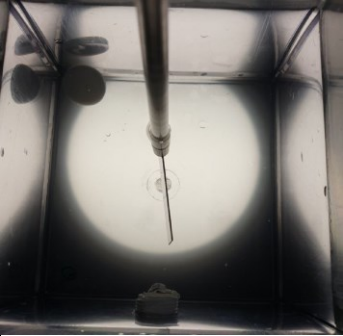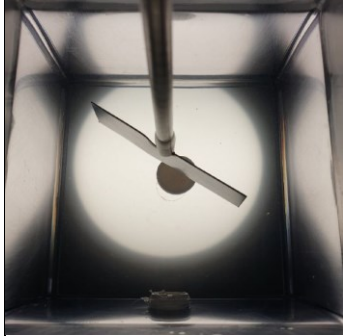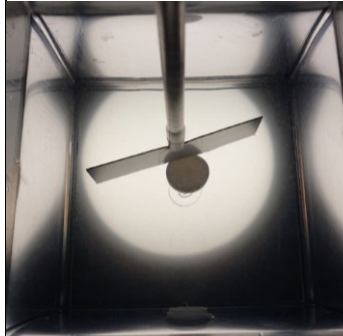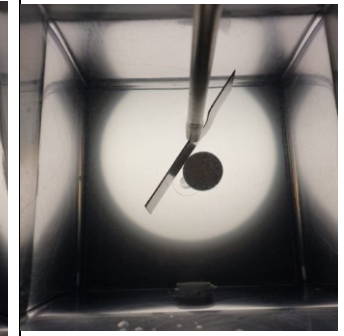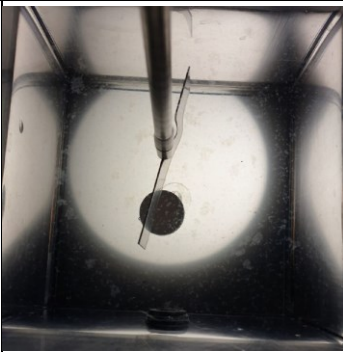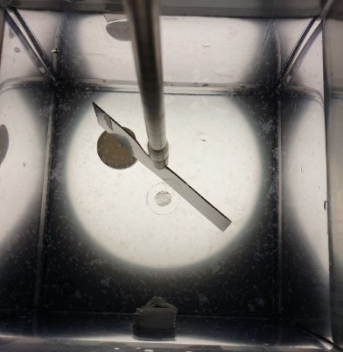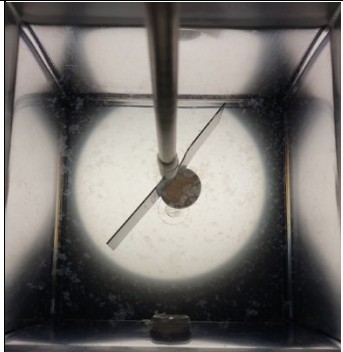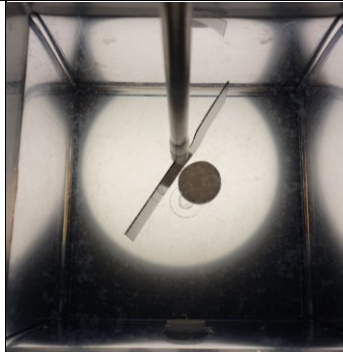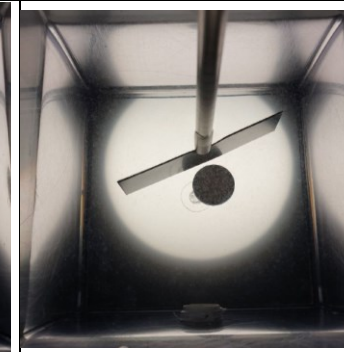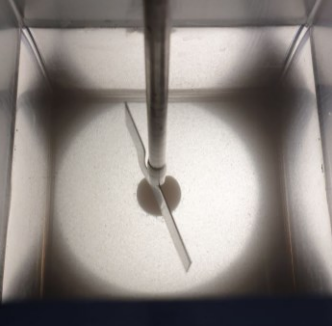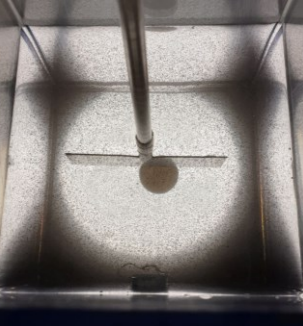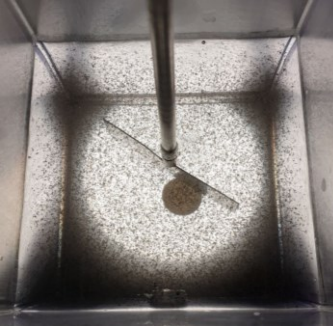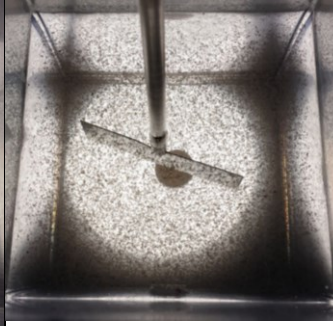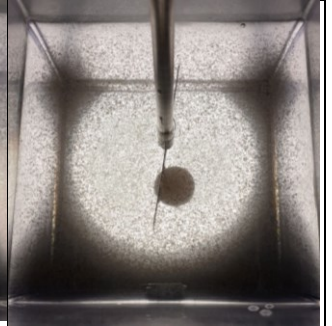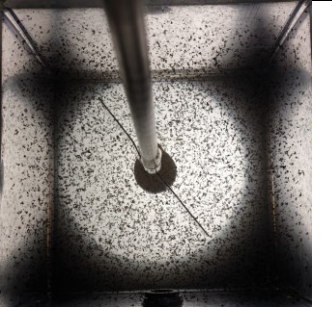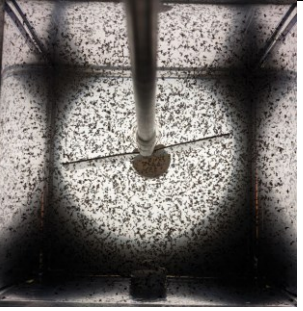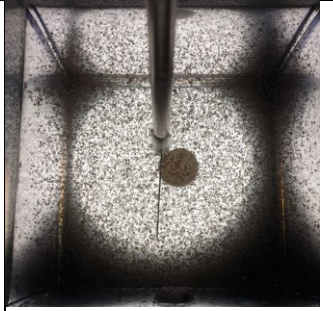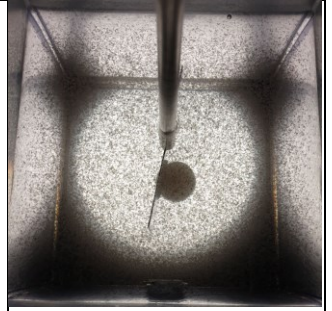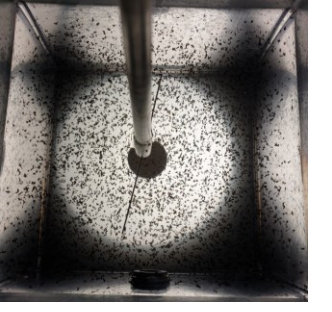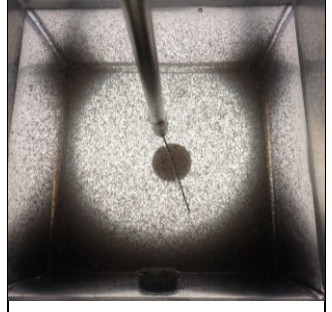
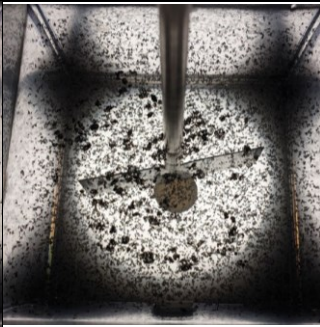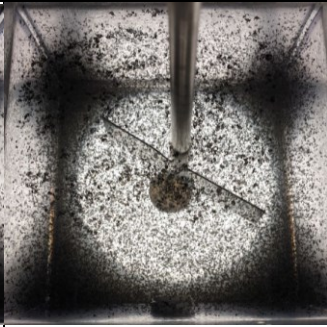**Figure D.1 G-Curves for B-KER while used with Phipps & Bird jar tester apparatus**
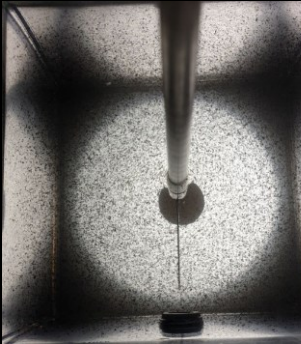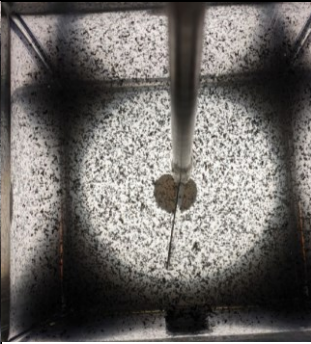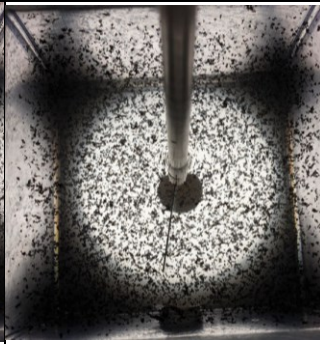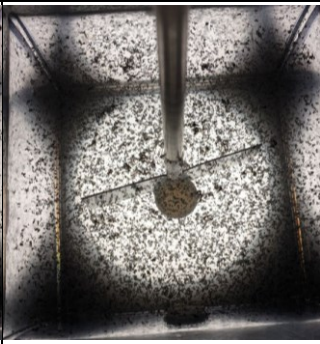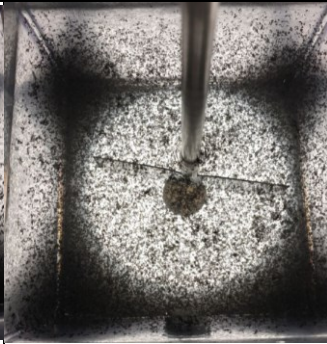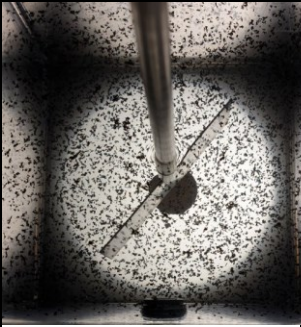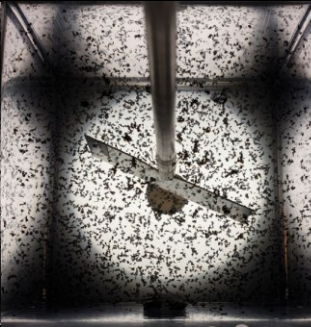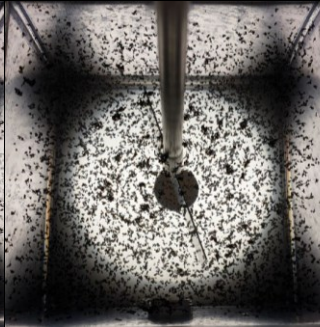
Appendix D.2 Floc formation in Lake Erie water without SPAC at different alum doses

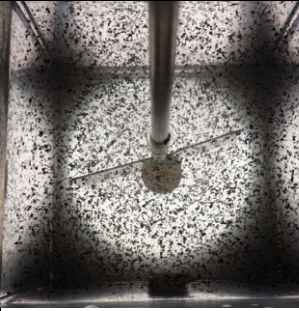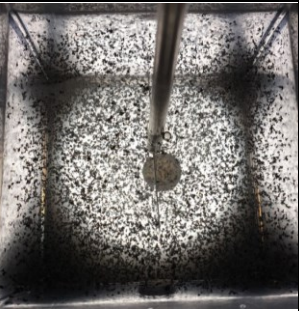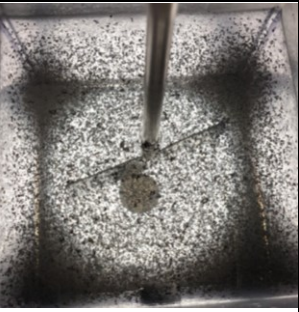| Time	10 mg/L	15 mg/L	20 mg/L	30 mg/L	45 mg/L
5 min flocculation					
15 min flocculation					

Appendix D.3 Floc formation of WPC (coconut-based) SPAC in Lake Erie water at different alum doses

Time\Al dose	10 mg/L	15 mg/L	20 mg/L	30 mg/L	45 mg/L
5 min flocculation					
10 min flocculation					
15 min flocculation					

Appendix D.4 Floc formation of COL-PL60-800 (coal-based) SPAC in Lake Erie water at different alum doses

time	10 mg/L	15 mg/L	20 mg/L	30 mg/L	45 mg/L
5 min flocculation					
15 min flocculation					

Appendix D.5 Floc formation of BG-HHM (wood-based) SPAC in Lake Erie water at different alum doses

time	10 mg/L	15 mg/L	20 mg/L	30 mg/L	45 mg/L
5 min flocculation					
15 min flocculation					